DISSERTATION

PHARMACOLOGICAL CHARACTERIZATION OF LOSARTAN AS A *CCR2* ANTAGONIST AND PRE-CLINICAL AND PHARMACODYNAMIC ASSESSMENT AS A POTENTIAL ANTI-METASTATIC THERAPY

Submitted by

Daniel P. Regan

Department of Microbiology, Immunology, and Pathology

In partial fulfillments of the requirements

For the Degree of Doctor of Philosophy

Colorado State University

Fort Collins, Colorado

Summer 2017

Doctoral Committee:

Advisor: Steven Dow

Alan Schenkel
Douglas Thamm
Jill Slansky
Randall Basaraba

ABSTRACT

PHARMACOLOGICAL CHARACTERIZATION OF LOSARTAN AS A *CCR2* ANTAGONIST AND PRE-CLINICAL AND PHARMACODYNAMIC ASSESSMENT AS A POTENTIAL ANTI-METASTATIC THERAPY

Metastasis is the leading cause of cancer-related mortality, and remains a major hurdle in improving patient outcomes. Initial first line therapies in cancer patients, such as curative-intent surgery and adjuvant chemotherapy, are often highly successful, with excellent 5-year survival rates for the majority of patients. Despite this, many of these individuals are still at an elevated lifetime risk for the eventual development of metastasis. For example, 5-year survival rates for patients who present with localized breast or colorectal cancer are ~ 99% and 90%, respectively, yet 30-50% of these individuals eventually go on to develop disseminated disease. Thus, there remains a critical need for the development of therapies which target the metastatic process.

Inflammatory monocytes (IMs), and their derivatives, metastasis-associated macrophages (MAMs), have been shown to play key roles in cancer metastasis through promotion of tumor cell extravasation, growth, and angiogenesis, in numerous pre-clinical mouse models. Furthermore, substantial clinical data demonstrating the prognostic importance of monocytes and tumor-associated macrophages in various human malignancies have validated these pre-clinical findings. Migration of IMs to sites of metastasis is mediated primarily via the action of the CCL2-CCR2 chemotactic axis. Thus, disruption of this axis represents an attractive therapeutic target for the treatment

of metastatic disease. Losartan, an angiotensin II type 1 receptor (AT1R) antagonist, has been previously reported to have immunomodulatory properties in models of atherosclerosis and autoimmune encephalomyelitis, via suppression of monocyte and macrophage mediated inflammation; however, the exact mechanism of this effect has not been fully elucidated. In addition, the potential anti-metastatic effects of losartan, via modulation of monocyte and macrophage responses to tumors, has not been evaluated.

To this point, and based on preliminary results of an in silico CCR2 homology model used to screen for small molecule antagonists, we undertook studies to pharmacologically characterize losartan as a potential CCR2 antagonist, and assess its ability to inhibit CCL2-CCR2 mediated monocyte recruitment, which are described in Chapter 2. Results of these studies demonstrated that both losartan and its primary metabolite (EXP-3174) potently inhibit CCL2-CCR2 dependent human and murine monocyte recruitment at clinically relevant doses. Furthermore, using G-protein coupled receptor function assays, we characterized the effects of losartan and EXP-3174 on CCL2 ligand binding and post-receptor signal transduction pathways stimulated by CCL2. Our findings suggest that both losartan and EXP-3174 function as noncompetitive antagonists of human, canine, and mouse CCR2. Based on its CCR2 antagonist properties, we also assessed the potential of losartan to be re-purposed as an anti-metastatic therapy in experimental metastasis models of breast and colon cancer, which showed that losartan significantly slowed metastatic progression in a process that was associated with blockade of inflammatory monocyte recruitment and reduction in metastasis-associated macrophages. Taken together, these studies suggest that losartan and its primary metabolite might represent a novel class of safe

and already-FDA approved, noncompetitive CCR2 antagonists, with potential to be rapidly repurposed for the treatment of metastatic disease.

While recent developments in human oncology have dramatically increased the relevance of immunotherapy as a new treatment modality, further progress in this field would be greatly accelerated by the ability to assess immune-based therapies in the more translationally relevant spontaneous canine cancer model. However, even a basic knowledge of the immune landscape of common canine tumor types is currently lacking, and to date, there has been little investigation into the role of monocytes in the regulation of canine tumor metastasis. This lack of foundational descriptive studies critically hinders appropriate tumor-type (target) selection, potentially precluding informed clinical evaluation of these drugs, such as losartan.

Therefore, in the studies presented in Chapter 3, we investigated the potential role of CCL2-CCR2 mediated monocyte recruitment in the regulation of tumor metastasis in dogs. To address this question, we performed immunohistochemistry for detection of CD18+ mononuclear cells to determine the degree of monocyte infiltration in pulmonary metastases of several common biologically aggressive and highly metastatic tumors of dogs, including hemangiosarcoma (HSA), osteosarcoma (OSA), melanoma, and transitional cell carcinoma. We found that compared to other tumor types, HSA and OSA metastases had significantly greater infiltration of CD18+ myeloid cells. In vitro assays confirmed that HSA and OSA cells were among the strongest at stimulating monocyte migration, and were also found to be the highest producers of the monocyte chemoattractant CCL2. Antibody-mediated neutralization of CCL2 in tumor-conditioned media significantly reduced the monocyte recruiting ability of HSA and OSA

cells in vitro. In addition, HSA and OSA metastases were found to produce large amounts of CCL2, compared to other tumor metastases, and CCL2 was found to be significantly elevated in the serum of hemangiosarcoma-bearing dogs as compared to healthy control dogs. Our results implicate a potential unique role for CCL2-CCR2 mediated monocyte recruitment in promoting hemangiosarcoma, and to a lesser degree, osteosarcoma metastasis in dogs. These findings are consistent therefore with the hypothesis that overexpression of CCL2 and recruitment of large numbers of monocytes may explain in part the highly aggressive metastatic nature of these canine tumor types. Furthermore, these results provide a rational basis for the assessment of monocyte-targeted therapies in dogs with these cancers.

Lastly, in Chapter 4, we assessed the clinical effects of losartan, based on its demonstrated inhibitory activity against CCL2-CCR2 monocyte recruitment, together with toceranib (Palladia), a drug known to deplete T regulatory cells (Tregs) in dogs, as a novel immunotherapy combination in a Phase I/II trial in dogs with spontaneous osteosarcoma pulmonary metastases. We initially screened this drug combination in a mouse osteosarcoma experimental metastasis model, which demonstrated synergistic activity of these drugs in combination. Utilizing in vitro monocyte chemotaxis assays, we identified a target losartan dose predicted to inhibit canine monocyte migration. For the clinical studies, we performed losartan pharmacokinetic analysis for 3 separate dose cohorts of 1mg/kg, 2.5mg/kg, and 10mg/kg in healthy and tumor bearing dogs, as well as monitored pharmacodynamic responses via ex-vivo monocyte chemotaxis, changes in plasma CCL2 concentrations, and flow cytometric evaluation of pre- and post-treatment changes in peripheral blood Tregs and monocytes. In addition, we quantified

changes in serum cytokines associated with angiogenesis (VEGF), and effector T cell responses (IFNγ). Results of these studies identified a clinically achievable dose of losartan which effectively inhibited ex vivo CCL2-directed canine monocyte migration. This final dose (10mg/kg) was 10 times higher than the conventionally used dose for the treatment of glomerular disease in dogs, yet was found to be safe and well-tolerated in these dogs. The objective response rate (ORR) was greater for dogs in the 10mg/kg (n=8) vs 1mg/kg losartan cohorts (n=8), while median progression-free survival (PFS) and biological response rate were similar for both cohorts. In the 10 mg/kg cohort, 2/8 dogs experienced a partial response (PR), for an ORR of 25%, and a biologic response rate of 37.5% (including 1 dog with stable disease, SD). No objective responses were observed in the 1mg/kg cohort (0/8), while the biologic response rate was 37.5% (3 dogs with SD). Median PFS was 42.5 days in 10mg/kg cohort, and 61 days in the 1mg/kg cohort. Furthermore, we observed evidence of modulation of systemic tumor immune suppression in these dogs, with post-treatment increases in absolute numbers of peripheral blood CD4+ and CD8+ T cells, and reductions in peripheral blood myeloid cells, which were associated with longer progression-free survival.

In conclusion, these studies describe the pharmacological and pre-clinical characterization of losartan as a repurposed CCR2 antagonist and potential anti-metastatic therapy. Furthermore, through retrospective histopathological and immunohistochemical analyses, as well as in vitro assays utilizing canine tumor cell lines, we provide foundational descriptive data which provide a rational basis for the evaluation of monocyte-targeted therapies in distinct canine tumor types. In addition, we highlight the importance of pharmacokinetics and pharmacodynamics for dose

optimization in translational chemokine antagonist drug development, and utilized pK/pD studies to optimize losartan dosing for inhibition of canine monocyte migration and evaluation as a novel immunotherapy in dogs with spontaneous metastatic disease.

ACKNOWLEDGEMENTS

First, I would like to thank my advisor, Dr. Steve Dow, for his generosity with his time and valuable support in both my personal and professional development over the last 6 years of this training program. Steve afforded me an invaluable opportunity to work in an area of translational and comparative cancer research that provided me with an excellent foundation and start to my biomedical research career. From day one, without question, Steve gave me the freedom yet trust to investigate the research questions I was interested in, resulting in a strong sense of personal responsibility and intellectual ownership for my project. I am sure the mentorship of Dr. Dow and my time in the Dow laboratory will have a significant and long lasting impact on my further development as an independent biomedical investigator.

I would also like to thank my committee members, Drs. Alan Schenkel, Doug Thamm, Jill Slansky, and Randy Basaraba, especially Jill for always making the long trip up to Fort Collins for our meetings. This project would not have been possible without all of your guidance, insight, and valuable feedback along the way, which I truly appreciate. While not a part of my committee, my pathology residency mentor, Dr. EJ Ehrhart, was also instrumental in my training and personal and career development. When the stresses of research, life, or board exams were building, EJ was always around to talk, keep things light-hearted, and keep me focused on the important things in life. In addition, I would like to express a HUGE thank you to all the members of the Dow lab, but especially to Jade Kurihara, Jonathan Coy, and Amanda Guth who provided valuable input and assistance with the studies presented in this thesis.

I would also like to acknowledge Todd Bass of the CSU histology lab, as well as Brad Charles of the Molecular Pathology lab, for assistance with tissue processing and immunohistochemistry.

In addition, I owe a huge thank you to the clinical trials staff at the Flint Animal Cancer Center, especially Kara Wells and Nikki Roatch. The clinical trials team is fantastic and they provided invaluable assistance and expertise with patient and patients sample management for the losartan osteosarcoma clinical trial.

A very important thank you also goes to Dr. Ed Hoover for securing and maintaining the T32 grant for biomedical research training for veterinarians at CSU. The support of the T32 program was invaluable in my training, and provided me with a level of security and independence which was instrumental in facilitating the next steps of my development as an independent investigator.

Lastly, I owe my greatest debt of gratitude to my family, especially my wife Lisa, my two daughters Maeve and Eila, and my parents John and Sheila. It is without a doubt that I would not have made it this far without the love and support of these individuals, and it is something I will never forget.

DEDICATION

This dissertation is dedicated to my parents, John and Sheila Regan, but especially to you Dad.

TABLE OF CONTENTS

CHAPTER 1

Review of the literature

Monocyte and macrophage development and biology

Monocytes are an innate immune cell subset which under normal physiological conditions play key roles in tissue homeostasis and inflammatory responses. Monocytes are produced in the bone marrow from hematopoietic progenitor cells, and progress through a developmental pathway involving common myeloid progenitor cells (CMPs), granulocyte-macrophage progenitor cells (GMPs), and macrophage-dendritic cell progenitors (MDPs) (1). At each of these stages, loss of pluripotency and further myeloid lineage commitment occurs, and current knowledge suggests that these steps are governed by the Ets family transcription factor PU.1, as well as signaling through the macrophage colony stimulating factor receptor (M-CSFR, CD115) (1).

Following their development, monocytes exit the bone marrow and enter the bloodstream where they temporarily reside and circulate (2). Blood monocytes exist in primarily two distinct subsets, categorized based on their cell surface expression of chemokine receptors (3). The first subset, which in mice is defined by CD11b and $Ly6C^{++}$ expression, and in humans $CD14^{++}/CD16^{-}$ expression, are termed inflammatory or classical monocytes, respectively (hereinafter jointly referred to as inflammatory monocytes) (2). In both humans and mice, these inflammatory monocytes express high levels of the chemokine receptor CCR2 which mediates their emigration from the bone marrow and into sites of peripheral tissue inflammation (4). The other primary subset of blood monocytes, termed steady-state/patrolling monocytes in mice, or non-

classical/patrolling monocytes in humans (hereinafter jointly referred to as patrolling monocytes), are defined by Ly6C^{low} and CD16^{++} expression, respectively (2, 3). This patrolling monocyte subset expresses low levels of CCR2 but high levels of the chemokine receptor CX3CR1 (3, 5). Interestingly, Swirksi et al. have demonstrated that besides the blood and bone marrow, the spleen serves as a significant reservoir for both inflammatory and patrolling subsets of monocytes, which upon inflammation or tissue injury can be rapidly deployed to peripheral tissues (6).

Distinct signaling cues coordinated by interactions between chemoattractant cytokines (chemokines), and their aforementioned cognate receptors expressed on the surface of monocytes, induce their migration into tissues (2, 7). Monocyte migration into tissues occurs in both normal tissue homeostasis as well as in response to inflammation, whereby these cells differentiate into various macrophage and dendritic cell (DC) populations (2). Migration of inflammatory monocytes into peripheral sites of infection or tissue injury is primarily controlled by the chemokines CCL2 and CCL7, via signaling through the chemokine receptor CCR2 (8). CCL2 is produced by almost all nucleated cells in the body, and is typically upregulated in response to various pro-inflammatory cytokines or microbial or tissue-damage by products acting on innate immune receptors such as toll-like receptors (9, 10). In contrast, recruitment of patrolling monocytes into tissues is mediated by the chemokine CX3CL1 (11).

To maintain normal tissue homeostasis, these monocyte subsets migrate into peripheral tissues and serve to replenish depleted tissue macrophage and dendritic cell subsets, including microglial in the central nervous system, Langerhan’s cells in the skin, and interdigitating DCs of the intestinal lamina propria (2). In addition, at sites of

inflammation, depending on the inflammatory cytokine milieu and tissue danger signals present, monocytes can differentiate into what have conventionally been termed classically-activated (M1) macrophages, or alternatively-activated (M2) macrophages (12). For the sake of simplicity, in this review, I will describe the differences in macrophage subsets based on this conventional paradigm; however, recent advancements in our understanding of macrophage biology suggest that these cells maintain a far greater degree of plasticity and diversity in their functional responses than previously thought (12). Classically activated (M1) macrophages are predominately thought to develop in response to a combination of two inflammatory signals, IFN-γ and TNF-α (7, 12). This combination of cytokines has been demonstrated to result in a macrophage population with enhanced production of pro-inflammatory cytokines and increased microbicidal and tumoricidal capabilities (7, 13). Specifically, M1 macrophages produce abundant amounts of reactive oxygen species, as well as the cytokines IL-1, IL-6, TNF-α, IL-12, IL-17, and IL-23 (7, 13). Thus, in the inflammatory microenvironment, these M1 macrophage derived cytokines direct the differentiation of naïve T cells towards the more pro-inflammatory Th1 and Th17 subsets (7, 13).

Conversely, alternatively-activated M2 macrophages, are associated with functions of immune suppression and tissue healing, including promotion of fibrosis and angiogenesis (7, 12, 13). Differentiation of macrophages towards an M2 phenotype has been shown to occur in vitro through treatment with the Th2 related cytokines IL-4 and IL-13, engagement of Fcγ or toll-like receptors, or in response to the anti-inflammatory cytokines TGF-β and IL-10 (7, 13). Subsequently, these cells are characterized by a significantly skewed cytokine profile towards the production of anti-inflammatory

molecules like TGF-β and IL-10, pro-angiogenic cytokines like VEGF, and minimal production of the pro-inflammatory cytokines IL-12 and IL-23 (7, 13). Another important feature of M2 macrophages is the induction of significant arginase activity in these cells, allowing them to metabolize arginine into ornithine, an important pre-cursor for collagen synthesis, thus highlighting their critical role in extracellular matrix remodeling following inflammation-mediated tissue damage (12).

The role of monocytes, macrophages, and CCL2-CCR2 signaling in tumor progression and metastasis

It is now known that the tumor microenvironment is composed of highly heterogeneous populations of both stromal and immune cells, including monocytes and macrophages, whose diverse functions serve a collective purpose to predominately promote tumor growth and progression (14, 15). In addition, the multi-step process of tumor metastasis, in which tumor cells leave a primary tumor, invade and migrate through an extracellular matrix, intravasate into the bloodstream, and subsequently arrest, extravasate and grow at a metastatic site, is governed by intricate, overlapping interactions between tumor cells, immune cells, and their surrounding host environment (16). Recent studies have demonstrated that similar cellular components and secreted factors of the primary TME also play critical roles in conditioning secondary sites of metastasis, creating a favorable environment for both the recruitment of immune cells as well as subsequent colonization by disseminated tumors cells (15, 17).The CCL2-CCR2 signaling axis has been demonstrated to play numerous vital roles in both tumor cell intrinsic and extrinsic processes of the metastatic cascade (18). CCL2 is produced

by both tumor and stromal cells, including fibroblasts and endothelial cells, in both primary tumors and metastatic sites (19, 20). Autocrine CCL2-CCR2 signaling in multiple cancer cells types has been shown to stimulate their proliferation through PI3K/Akt signaling, as well as induce their migration and invasion, either directly through CCR2-induced activation of Rac GTPase, or indirectly through the induction of matrix metalloproteinase (MMP) production by tumor cells (21-23). More well documented are the extrinsic tumor-promoting effects of CCL2-CCR2 signaling in the tumor microenvironment. CCL2 production by tumor cells has been associated with the recruitment of CCR2-expressing inflammatory monocytes to primary tumors, as well as their subsequent polarization into a growth promoting (M2) tumor-associated macrophage (TAM) phenotype associated with immune suppression and promotion of angiogenesis and tumor cell intravasation (24, 25). In addition, the CCL2-CCR2 axis has been heavily implicated in the process of metastatic colonization. In pre-clinical mouse models of breast and colorectal cancer metastasis, it has been demonstrated that CCR2 expressing inflammatory monocytes are preferentially recruited early on to metastatic sites of the lung and liver, as early as 24 hours after the arrival of tumor cells, via tumor and stromal cell-mediated production of CCL2 (19, 26). Once present at metastases, these monocytes can differentiate into metastasis-associated macrophages (MAMs), which have been shown to play essential roles in metastatic colonization via promotion of tumor cell extravasation, growth, and angiogenesis through mechanisms associated with production of soluble factors such as VEGF, or the direct engagement of VCAM-1 on metastatic tumor cells (19, 27-29). More recently, it has been demonstrated that CCL2 signaling plays a critical role in the retention of

these MAMs within the metastatic site. CCL2 signaling through CCR2 expressed on MAMs induced their production of another chemokine CCL3, which through its interactions with its receptor CCR1, retains these cells within the metastatic lung (30).

Substantiating these seminal observations in mice, and providing direct clinical evidence supporting a role for inflammatory monocytes in tumor progression in humans are multiple studies demonstrating that pre-treatment elevations in peripheral blood monocyte count and serum CCL2 levels are both negative prognostic indicators for a variety of cancers in people, including melanoma, lymphoma, and carcinomas of the prostate, colon, pancreas, and kidney, among others (31-38). For example, in patients with pancreatic cancer, an increased ratio of blood to bone marrow monocytes as well as patients whose tumors demonstrated high CCL2 expression and low CD8+ T cell infiltrates, were both inversely correlated with survival (38). Similarly, in patients with renal cell carcinoma, high CCL2 and CCR2 expression in patient tumors, as identified by immunohistochemistry, was associated with decreased survival time and increased risk of recurrence (39).

Interestingly, hematopoietic stem/progenitor cells of a CD11b+ myelo-monocytic phenotype are also one of multiple cell types which preferentially accumulate at metastatic sites even *before* the arrival of tumor cells, a phenomenon known as the pre-metastatic niche (40-42). This phenomenon has been demonstrated experimentally in syngeneic mouse models of lung carcinoma and melanoma, as well as a human xenograft breast cancer model (40-42). In addition, elevated levels of these cells have been detected in human cancer patients and correlate with increased risk for metastatic progression (40). Once present at metastatic sites, these cells function to establish a

permissive niche for incoming tumor cells through mechanisms involving immune suppression, up-regulation of tumor cell chemoattractants, and promotion of tumor cell survival, both directly via secretion of molecules like S100A8 and A9, and indirectly via matrix metalloproteinase-mediated release of VEGF and c-KIT(40-42). Furthermore, the functional impact of these cells on metastatic progression has been confirmed experimentally, as antibody-mediated depletion of these cells completely prevented metastasis in mice bearing well-established tumors (42).

The role of inflammatory monocytes and macrophages in the regulation of tumor responses to chemotherapeutic drugs is also beginning to be defined. Recently, it has been demonstrated that conventional cytotoxic therapies such as doxorubicin can induce tumor and stromal cell production of CCL2 as well as other monocyte and macrophage chemoattractants such as M-CSF (20, 43). This therapy-induced inflammatory response was shown to lead to enhanced recruitment of CCR2+ monocytes and macrophage infiltration of primary tumors in a murine breast cancer model and in human breast cancer patients treated with neoadjuvant chemotherapy (20, 43). Importantly, the functional role of these recruited cells in mediating chemoresistance was demonstrated via concurrent macrophage depletion with chemotherapy, which significantly improved overall survival in mammary tumor bearing mice (20, 43). In addition, clinical evidence supporting a role for monocytes and macrophages in chemoresistance comes from multiple studies in human breast cancer patients. In one study, patients having a high tumor gene expression ratio of CD68+ macrophages to CD8+ T cells had a significantly lower rate of pathological complete response to neoadjuvant chemotherapy, and significantly reduced overall survival, while

another study demonstrated that breast cancer patients having lower pre-treatment levels of circulating monocytes and an increased lymphocyte to monocyte ratio had a significantly high probability of pathological complete response to neoadjuvant therapy, and subsequently improved disease-free intervals and overall survival (43, 44). In conclusion, these findings highlight the potential therapeutic value in targeting the CCL2-CCR2 axis for the prevention of tumor progression and metastasis.

GPCR biology and chemokine receptor signaling

G-protein coupled receptors (GPCRs) comprise the largest protein family in the mammalian genome, with an estimate of >800 GPCRs encoded in the human genome (45). As compared to other cell surface receptors, such as receptor tyrosine kinases (RTKs), GPCRs have a relatively complex molecular structure, consisting of a 7-transmembrance domain cell surface receptor, coupled to an intracellular signal-transducing effector molecule, which is typically a heterotrimeric G protein (45, 46). Reflective of their complex molecular structure is the significant variety of extracellular stimuli that can be transduced by GPCRs into an intracellular response. These stimuli range from photons, taste, and pheromones, to lipids, amino acids, peptides, and proteins such as chemokines (47). Chemokine receptors, including CCR2, are members of the Class A family of GPCRs, the most highly studied class of GPCRs, and which contains the greatest number of documented receptor structures (48). For simplicity, this review will focus on G protein receptor signaling through heterotrimeric proteins; however, it must be noted that other effector molecules have been associated with G-protein signaling, including G-protein coupled receptor kinases (GRKs) and β-arrestins

(48). To date, there are four known members of heterotrimeric G proteins, each made up of α, β, and γ subunits (46). These four members consist of G_s, which stimulates adenylate cyclase, G_i, which inhibits adenylate cyclase, G_q, which activates phospholipase C (PLC), and $G_{12/13}$, whose function is currently unknown (46).

Upon ligand-binding, GPCRs undergo activation and conformational change which catalyzes the exchange of GDP for GTP in the $G\alpha$ subunit (46). This exchange results in dissociation of the $G\alpha$ and $G\beta\gamma$ subunits, and subsequent activation of downstream signaling molecules, including adenylate cyclase, PLC, and PI3K, with resulting increases in second messengers such as Ca^{2+}, cAMP, IP3, and DAG leading to activation of further downstream signal transduction pathways such as the MAP kinase pathway (46, 48). Specifically, previous work by Myers et al. assessing the effects of pertussis toxin on CCL2 signaling have demonstrated that the chemokine receptor CCR2 is coupled to the G_i class of heterotrimeric proteins (49). Subsequent work by Ashida et al. investigating the signal transduction pathways specifically associated with monocyte chemotaxis demonstrated that in THP-1 cells, CCL2-induced integrin activation and monocyte chemotaxis was indeed mediated through the mitogen-activated protein kinase/extracellular signal-regulated kinase (MAPK/ERK) pathway (50). Building on these foundational studies, more recent work by Jimenez-Sainz et al. elegantly dissected the cascade of second messengers required for CCL2-induced activation of ERK1/2 following CCR2 stimulation (51). These studies showed clearly showed that ERK activation was in fact independent of CCR2 receptor internalization/β-arrestin recruitment, changes in cytosolic [Ca^{2+}], or transactivation by EGFR or other cytosolic tyrosine kinases, but required G_i proteins, protein kinase C (PKC), phospho-

inositide-3-kinase (PI3K), and RAS (51). Importantly, these results demonstrated that different signal transduction pathways, acting in parallel, were required for complete ERK activation in response to CCL2. Furthermore, these results suggest that cytosolic calcium flux assays, a conventionally used screening assay for identification of chemokine receptor antagonists, and likely still useful in broad hit to lead optimization of CCR2 inhibitors, may not be predictive of their actual biological efficacy.

CCL2-CCR2 targeted therapies in oncology

The initial discovery of G-protein coupled receptors functioning as chemokine receptors stimulated great excitement in the drug development industry, as GPCRs have been traditionally been a foundation for drug discovery in the pharmaceutical industry (52). However, almost two decades after many of these discoveries, only two small molecules chemokine receptor antagonists are approved for the treatment of HIV (CCR5 antagonist Maraviroc) and stem cell mobilization (CXCR4 antagonist Plerixafor) (52). While numerous large pharmaceutical companies have active programs for the development of small molecule CCR2 antagonists, their therapeutic targets are not predominately not focused on cancer, and instead primarily on inflammatory diseases such as rheumatoid arthritis and multiple sclerosis (53). Instead, initial clinical trials targeting the CCL2-CCR2 axis in human cancer patients have utilized biologic therapies with anti-human CCL2 monoclonal antibody (Carlumab, CNTO888), or the monoclonal CCR2 blocking antibody MLN1202 (ClinicalTrials.gov identifier: NCT01015560) (54, 55). Initial trials with CNTO88 showed that CNTO888 alone or in combination with standard

of care therapies was ineffective at reducing serum CCL2 levels or slowing tumor progression in patients with various solid tumors (54).

However, more recent and ongoing trials have shown that blockade of CCR2 via the monoclonal antibody MLN1202 has the potential to suppress tumor growth in patients with bone metastases (ClinicalTrials.gov identifier: NCT01015560). In addition, a small molecule CCR2 antagonist developed by Pfizer (PF-04136309) was recently evaluated in combination with FOLFIRINOX chemotherapy (5-fluorouracil, leucovorin, irinotecan, oxaliplatin) in a Phase 1B clinical trial in patients with locally advanced pancreatic cancer (ClinicalTrials.gov identifier: NCT01413022) (56). Results of this trial were promising and demonstrated an increased overall response rate as compared to patients receiving FOLFIRINOX alone, leading to a currently ongoing larger Phase II as a first line therapy in patients with stage IV pancreatic cancer (ClinicalTrials.gov identifier: NCT02732938). Interestingly, one of the secondary outcome measures of this study is ex vivo evaluation of CCL2-induced ERK phosphorylation. Combined, these clinical data suggest that inhibition of CCR2 might be a more valuable approach in the therapeutic targeting of the CCL2-CCR2 axis. However, while these recent early Phase I/II trials of CCR2 inhibitors are promising, they are not without hesitation, as recent data suggests that only 10% of agents entering clinical cancer trials make it to FDA approval (57, 58) . Furthermore, given that current estimations for the time and cost invested in new drugs is now a staggering 10 years and $2.6 billion dollars (59), alternative drug development programs which focus on re-purposing already approved drugs as potential anti-cancer therapies might offer greater promise, in terms of reduced cost and time, for getting more effective treatment options to patients with cancer (60).

AT1R antagonists and their immunomodulatory properties

Losartan, a type I angiotensin II receptor (AT1R) blocker (ARB) used in the treatment of hypertension, has been shown to have immunomodulatory and anti-inflammatory properties in models of vascular inflammation and multiple sclerosis (61-63). Interestingly, these anti-inflammatory properties were primarily associated with an observation of reduced monocyte and macrophage recruitment to inflammatory lesions such as atherosclerotic plaques. In these studies, losartan's blockade of monocyte and macrophage recruitment was attributed to an indirect effect on CCL2 and/or CCR2 signaling, secondary to primary inhibition of AT1R signaling. Specifically, in a model of myelin-oligodendrocyte glycoprotein (MOG)-induced inflammation of the central nervous system (CNS), losartan treatment reduced accumulation of CD11b+ and CD11c+ cells within the spleen and CNS inflammatory lesions, which was attributed to a reduction in CCL2 expression secondary to inhibition of enhanced AT1R signaling in macrophages and spinal cord tissues in response to vaccination with MOG (61). Additionally, in a model of macrophage-mediated aortic vessel wall inflammation in spontaneously hypertensive rats, treatment with losartan significantly decreased macrophage infiltration into vessels walls, which was associated with reduced expression of CCL2 and CCR2 (63). Again, these results were concluded to be an effect of inhibition of Angiotensin II-mediated inflammation; however, it was not definitively shown that losartan was not directly disrupting the CCL2-CCR2 axis, and in fact, molecular modeling studies of CCR2 suggest that losartan and other ARBs have a high affinity for and the potential to act as CCR2 antagonists (64).

Increasingly, a role for the renin-angiotensin system (RAS) in the promotion of tumor growth via both tumor cell intrinsic and extrinsic (stromal-mediated) actions has been described (65). Specifically, these studies have demonstrated that autocrine angiotensin II-AT1R signaling in tumor cells can stimulate their proliferation, invasion, migration, and growth (66, 67), while AngII-AT1R signaling within the tumor stroma can drive tumor-promoting inflammation (68, 69), as well as tumor angiogenesis (70). In line with these observations are several pre-clinical studies in mice which have demonstrated anti-tumor effects associated with losartan monotherapy. In these models, losartan's anti-tumor mechanism of action was primarily associated with either anti-angiogenic or anti-invasive properties, which were concluded to be the downstream result of primary inhibition of AngII-AT1R signaling, or secondary to anti-TGF-β signaling effects, as losartan has been demonstrated to reduce TGF-β expression, although again presumed (without direct supporting evidence) to be secondary to blockade of Angiotensin II-induced expression of the molecule. In a mouse model of pancreatic ductal adenocarcinoma, daily oral losartan treatment reduced aberrant TGF-β expression and prolonged overall survival of these mice (71). In the B16 mouse model of melanoma, pre-treatment with and continued daily dosing with losartan significantly reduced subcutaneous primary tumor growth and metastasis (72). In this model, the authors demonstrated expression of AT1R within B16 melanoma tumors and associated this anti-tumor effect of losartan to inhibition of angiogenesis (72). Cortez-Retamozo et. al have previously demonstrated a unique role for AngII-ATIR signaling in splenic myelopoiesis and subsequent $Ly6C^{Hi}$ monocyte recruitment to the lungs of tumor-bearing mice in the KRAS-p53 (KP) conditional model of NSCLC (73). In this model,

disruption of AT1R signaling via losartan or the angiotensin converting enzyme inhibitor (ACEi) enalapril, reduced the number of splenic monocytes; however, the impact of this effect on overall survival of mice with KP lung carcinomas was only evaluated for continuous enalapril treatment (and not for losartan therapy). Lastly, retrospective analyses of clinical data of patients being treated for hypertension have shown a correlation between the use of losartan, or other ARBs and ACE-inhibitors, with improved outcomes in patients with pancreatic, breast, or lung cancer (66, 74-76). Again, the therapeutic benefit in human cancer patients was presumed to be secondary to the effects of direct inhibition of AngII-AT1R signaling.

Translational and comparative oncology: Recent progress, remaining hurdles, and the value of the spontaneous canine cancer model

The last 10 years have witnessed significant progress in translational oncology research which has led to dramatic improvements in the treatment of primary tumors, with advances in molecular therapeutics such as drugs targeting receptor tyrosine kinases helping to make substantial gains in the survival of patients whose tumors harbor specific mutations (14, 77). Despite this, the inevitable clinical reality is that tumor metastasis remains the single greatest contributor to cancer patient mortality (14, 77), accounting for up to 90% of all cancer-related deaths (78, 79). To frame the clinical significance of this problem, at the time of diagnosis, distant metastases are present in 6-21% of breast and colorectal cancer patients, respectively, two tumor types whose incidence remains in the top three in the U.S. (80). Furthermore, although 5-year survival rates experienced by many patients treated for localized cancer, including

breast and colorectal cancer patients, these individuals are still considered to have a substantially increased lifetime risk for metastasis, with up to 30-50% of these patients eventually developing disseminated disease (81-83). Further compounding this situation are multiple independent analyses of clinical trial data for certain tumor types, such as those of the breast or pancreas, which demonstrate that in the established metastatic setting, survival of these patients has been unchanged for over 30 years (84-86). Thus, there remains a critical need for continued clinical development of anti-metastatic therapies, in both the context of preventing metastasis formation and treating established metastatic lesions.

One significant therapeutic advancement in human oncology over the last decade has been the use of immunotherapy as a new treatment modality (87). In the case of certain patients, such as those with melanoma, lung, or renal cancer, immunotherapeutic interventions have resulted in unprecedented responses in patients with advanced stage/metastatic disease that would have otherwise been fatal (88, 89). The approval and use of monoclonal antibodies targeting T cell checkpoint molecules such as programmed cell-death protein 1 (PD-1), or cytotoxic T-lymphocyte associated protein 4 (CTLA-4) (89, 90) have primarily accounted for these dramatic clinical responses. These recent developments in human oncology have substantially increased the relevance of immunotherapy as a new treatment modality, and were predominately the result of discoveries made during foundational pre-clinical studies in mice. While murine cancer models remain an invaluable tool for understanding basic cancer biology, the continued low rate of successful translation of therapies from pre-clinical studies to human cancer patients calls into question their predictive value (91)

As such, a growing community of scientists and clinicians recognize that further progress in immuno-oncology and anti-metastatic drug development would be greatly accelerated by the ability to assess immune-based therapies in the more translationally relevant spontaneous canine cancer model (92, 93).

Spontaneously occurring tumors in pet dogs represent a highly valuable intermediary animal model for evaluation of novel therapeutics and validation of pre-clinical findings, prior to assessment in expensive human clinical trials. Naturally occurring tumors in dogs co-evolve in the presence of an intact host immune system and complex tumor microenvironment, and share striking similarities on a clinical, biological, genetic, and histological basis (91, 94). Canine osteosarcoma (OSA) is a prime example of a naturally occurring canine cancer with significant potential to inform oncology drug development (77, 95). Dogs with OSA share many clinical similarities with human pediatric OSA including primary tumor location, response to conventional therapies, the presence of microscopic metastases at diagnosis, and unfortunately, a lack of significant improvement of survival times over the past 15 years (77, 95). In addition, dogs develop OSA at an ~10 times greater incidence than people, thus facilitating rapid patient recruitment for evaluation of novel therapeutics (95). Yet one significant hurdle to fully leveraging this drug development pathway is that even a basic knowledge of the immune response or immune-based mechanisms of promoting tumor growth and metastasis of common canine tumor types, including osteosarcoma, is currently lacking including minimal investigation into the role of monocytes and the CCL2-CCR2 axis in the regulation of canine OSA metastasis.

A handful of studies have retrospectively characterized the presence of tumor-associated myeloid cells/macrophages (TAMs) in primary canine tumor tissues of various histo-type including melanoma, mammary carcinoma, seminoma, glioma, meningioma, and nasal carcinoma (96-100). These studies were primarily small descriptive studies aimed at semi-quantitative assessment and characterization of tumor-infiltrating T cells, B cells, plasma cells, and myeloid cells, as well as expression of MHC class II antigen. Additionally, a single study of canine mammary tumors demonstrated an association between a high density of TAMs and significantly decreased overall survival time (99). The work of Biller et al. showed that elevated peripheral blood monocyte counts as well as a decrease in the ratio of CD8+ T cells to regulatory T cells are independently associated with decreased survival in dogs with OSA (101). Likewise, retrospective analyses by Sottnik et al. of clinical data from dogs with OSA demonstrated that higher numbers of circulating monocytes (> $0.4x10^3$ cells/μL) and lymphocytes (> $1 x 10^3$ cells/μL was associated with significantly shorter disease-free interval (102). In a separate but similar study of 26 dogs with lymphoma, Perry et al. demonstrated that serum CCL2 levels, and peripheral blood neutrophil and monocyte counts were significantly elevated in lymphoma-bearing dogs as compared to healthy controls, and that elevations in all three parameters were independently associated with significantly shorter disease free interval (103). In addition, serum CCL2 was also positively and significantly correlated with lymphoma disease stage in these patients.

More substantiating however, is the significant amount of clinical data in dogs with OSA, which suggest that this is one canine tumor type which is not immunologically

ignorant, and indeed appears to have a pre-existing anti-tumor immune response which is primed for immunomodulation and/or response to immunotherapy (104). One of the most striking clinical findings for this tumor type is that for dogs undergoing limb-salvage surgery, those patients which experience bacterial infection of their surgery site experience significantly increased survival times (105). In addition, some of the earliest clinical trials of immunotherapeutics in veterinary medicine were performed in dogs with osteosarcoma. For example, clinical trials evaluating the administration of non-specific innate immune stimulants (so-called biologic response modifiers) such as live, attenuated *Mycobacterium bovis* (strain Bacillus Calmette-Geurin, BCG) or later, a modified component of the mycobacterial cell wall, liposomal muramyl tripeptide (L-MTP) were initially performed in dogs with OSA (106, 107). Results of these studies demonstrated the activation and induction of tumoricidal activity of monocytes and macrophages, primarily in a mechanism dependent on TNF-α, and were associated with significantly improved median survival times and disease-free intervals in these dogs (104, 106-109). These data suggest that pre-existing host immune responses likely play a significant role in the progression of canine OSA, and that dogs with spontaneous OSA likely represent a valuable model for the assessment of novel immunotherapy combinations.

REFERENCES

1. Auffray C, Sieweke MH, & Geissmann F (2009) Blood monocytes: development, heterogeneity, and relationship with dendritic cells. *Annu Rev Immunol* 27:669-692.

2. Shi C & Pamer EG (2011) Monocyte recruitment during infection and inflammation. *Nat Rev Immunol* 11(11):762-774.

3. Geissmann F, Jung S, & Littman DR (2003) Blood monocytes consist of two principal subsets with distinct migratory properties. *Immunity* 19(1):71-82.

4. Palframan RT*, et al.* (2001) Inflammatory chemokine transport and presentation in HEV: a remote control mechanism for monocyte recruitment to lymph nodes in inflamed tissues. *J Exp Med* 194(9):1361-1373.

5. Cros J*, et al.* (2010) Human CD14dim monocytes patrol and sense nucleic acids and viruses via TLR7 and TLR8 receptors. *Immunity* 33(3):375-386.

6. Swirski FK*, et al.* (2009) Identification of splenic reservoir monocytes and their deployment to inflammatory sites. *Science* 325(5940):612-616.

7. Italiani P & Boraschi D (2014) From Monocytes to M1/M2 Macrophages: Phenotypical vs. Functional Differentiation. *Frontiers in Immunology* 5:514.

8. Tsou C-L*, et al.* (2007) Critical roles for CCR2 and MCP-3 in monocyte mobilization from bone marrow and recruitment to inflammatory sites. *The Journal of Clinical Investigation* 117(4):902-909.

9. Struyf S*, et al.* (1998) Synergistic induction of MCP-1 and -2 by IL-1beta and interferons in fibroblasts and epithelial cells. *J Leukoc Biol* 63(3):364-372.

10. Tsuboi N*, et al.* (2002) Roles of toll-like receptors in C-C chemokine production by renal tubular epithelial cells. *J Immunol* 169(4):2026-2033.

11. Auffray C*, et al.* (2007) Monitoring of blood vessels and tissues by a population of monocytes with patrolling behavior. *Science* 317(5838):666-670.

12. Mosser DM & Edwards JP (2008) Exploring the full spectrum of macrophage activation. *Nature reviews. Immunology* 8(12):958-969.

13. Koh TJ & DiPietro LA (2011) Inflammation and wound healing: The role of the macrophage. *Expert reviews in molecular medicine* 13:e23-e23.

14. Steeg PS (2016) Targeting metastasis. *Nat Rev Cancer* 16(4):201-218.

15. Hanahan D & Weinberg RA (2011) Hallmarks of cancer: the next generation. *Cell* 144(5):646-674.

16. Valastyan S & Weinberg RA (2011) Tumor metastasis: molecular insights and evolving paradigms. *Cell* 147(2):275-292.

17. Liu Y & Cao X (2016) Characteristics and Significance of the Pre-metastatic Niche. *Cancer Cell* 30(5):668-681.

18. Lim SY, Yuzhalin AE, Gordon-Weeks AN, & Muschel RJ (2016) Targeting the CCL2-CCR2 signaling axis in cancer metastasis. *Oncotarget* 7(19):28697-28710.

19. Qian BZ*, et al.* (2011) CCL2 recruits inflammatory monocytes to facilitate breast-tumour metastasis. *Nature* 475(7355):222-225.

20. Nakasone ES*, et al.* (2012) Imaging tumor-stroma interactions during chemotherapy reveals contributions of the microenvironment to resistance. *Cancer Cell* 21(4):488-503.

21. Chiu HY*, et al.* (2012) Autocrine CCL2 promotes cell migration and invasion via PKC activation and tyrosine phosphorylation of paxillin in bladder cancer cells. *Cytokine* 59(2):423-432.

22. Tang CH & Tsai CC (2012) CCL2 increases MMP-9 expression and cell motility in human chondrosarcoma cells via the Ras/Raf/MEK/ERK/NF-kappaB signaling pathway. *Biochemical pharmacology* 83(3):335-344.

23. Loberg RD*, et al.* (2006) CCL2 is a potent regulator of prostate cancer cell migration and proliferation. *Neoplasia (New York, N.Y.)* 8(7):578-586.

24. Roca H*, et al.* (2009) CCL2 and interleukin-6 promote survival of human CD11b+ peripheral blood mononuclear cells and induce M2-type macrophage polarization. *The Journal of biological chemistry* 284(49):34342-34354.

25. Low-Marchelli JM*, et al.* (2013) Twist1 induces CCL2 and recruits macrophages to promote angiogenesis. *Cancer Res* 73(2):662-671.

26. Piao C*, et al.* (2015) Complement 5a Enhances Hepatic Metastases of Colon Cancer via Monocyte Chemoattractant Protein-1-mediated Inflammatory Cell Infiltration. *The Journal of biological chemistry* 290(17):10667-10676.

27. Qian BZ*, et al.* (2015) FLT1 signaling in metastasis-associated macrophages activates an inflammatory signature that promotes breast cancer metastasis. *J Exp Med* 212(9):1433-1448.

28. Chen Q, Zhang XH, & Massague J (2011) Macrophage binding to receptor VCAM-1 transmits survival signals in breast cancer cells that invade the lungs. *Cancer Cell* 20(4):538-549.

29. Mazzieri R*, et al.* (2011) Targeting the ANG2/TIE2 axis inhibits tumor growth and metastasis by impairing angiogenesis and disabling rebounds of proangiogenic myeloid cells. *Cancer Cell* 19(4):512-526.

30. Kitamura T*, et al.* (2015) CCL2-induced chemokine cascade promotes breast cancer metastasis by enhancing retention of metastasis-associated macrophages. *J Exp Med* 212(7):1043-1059.

31. Feng J*, et al.* (2016) Effect of initial absolute monocyte count on survival outcome of patients with de novo non-M3 acute myeloid leukemia. *Leukemia & lymphoma*:1-7.

32. Izumi K*, et al.* (2016) Serum chemokine (CC motif) ligand 2 level as a diagnostic, predictive, and prognostic biomarker for prostate cancer. *Oncotarget* 7(7):8389-8398.

33. Lu X*, et al.* (2011) Serum CCL2 and serum TNF-alpha--two new biomarkers predict bone invasion, post-treatment distant metastasis and poor overall survival in nasopharyngeal carcinoma. *Eur J Cancer* 47(3):339-346.

34. Nishijima TF, Muss HB, Shachar SS, Tamura K, & Takamatsu Y (2015) Prognostic value of lymphocyte-to-monocyte ratio in patients with solid tumors: A systematic review and meta-analysis. *Cancer treatment reviews* 41(10):971-978.

35. Sasaki A*, et al.* (2007) Prognostic value of preoperative peripheral blood monocyte count in patients with colorectal liver metastasis after liver resection. *Journal of gastrointestinal surgery : official journal of the Society for Surgery of the Alimentary Tract* 11(5):596-602.

36. Schmidt H*, et al.* (2005) Elevated neutrophil and monocyte counts in peripheral blood are associated with poor survival in patients with metastatic melanoma: a prognostic model. *British journal of cancer* 93(3):273-278.

37. Vassilakopoulos TP*, et al.* (2016) Prognostic Implication of the Absolute Lymphocyte to Absolute Monocyte Count Ratio in Patients With Classical Hodgkin Lymphoma Treated With Doxorubicin, Bleomycin, Vinblastine, and Dacarbazine or Equivalent Regimens. *The oncologist* 21(3):343-353.

38. Sanford DE*, et al.* (2013) Inflammatory monocyte mobilization decreases patient survival in pancreatic cancer: a role for targeting the CCL2/CCR2 axis. *Clin Cancer Res* 19(13):3404-3415.

39. Wang Z*, et al.* (2016) CCL2/CCR2 axis is associated with postoperative survival and recurrence of patients with non-metastatic clear-cell renal cell carcinoma. *Oncotarget* 7(32):51525-51534.

40. Giles AJ*, et al.* (2016) Activation of Hematopoietic Stem/Progenitor Cells Promotes Immunosuppression Within the Pre-metastatic Niche. *Cancer Res* 76(6):1335-1347.

41. Hiratsuka S, Watanabe A, Aburatani H, & Maru Y (2006) Tumour-mediated upregulation of chemoattractants and recruitment of myeloid cells predetermines lung metastasis. *Nat Cell Biol* 8(12):1369-1375.

42. Kaplan RN*, et al.* (2005) VEGFR1-positive haematopoietic bone marrow progenitors initiate the pre-metastatic niche. *Nature* 438(7069):820-827.

43. DeNardo DG*, et al.* (2011) Leukocyte complexity predicts breast cancer survival and functionally regulates response to chemotherapy. *Cancer discovery* 1(1):54-67.

44. Ni XJ*, et al.* (2014) An elevated peripheral blood lymphocyte-to-monocyte ratio predicts favorable response and prognosis in locally advanced breast cancer following neoadjuvant chemotherapy. *PLoS One* 9(11):e111886.

45. Katritch V, Cherezov V, & Stevens RC (2013) Structure-function of the G protein-coupled receptor superfamily. *Annual review of pharmacology and toxicology* 53:531-556.

46. Hamm HE (1998) The many faces of G protein signaling. *The Journal of biological chemistry* 273(2):669-672.

47. Wettschureck N & Offermanns S (2005) Mammalian G proteins and their cell type specific functions. *Physiological reviews* 85(4):1159-1204.

48. Zweemer AJ, Toraskar J, Heitman LH, & AP IJ (2014) Bias in chemokine receptor signalling. *Trends Immunol* 35(6):243-252.

49. Myers SJ, Wong LM, & Charo IF (1995) Signal transduction and ligand specificity of the human monocyte chemoattractant protein-1 receptor in transfected embryonic kidney cells. *The Journal of biological chemistry* 270(11):5786-5792.

50. Ashida N, Arai H, Yamasaki M, & Kita T (2001) Distinct signaling pathways for MCP-1-dependent integrin activation and chemotaxis. *The Journal of biological chemistry* 276(19):16555-16560.

51. Jimenez-Sainz MC, Fast B, Mayor F, Jr., & Aragay AM (2003) Signaling pathways for monocyte chemoattractant protein 1-mediated extracellular signal-regulated kinase activation. *Molecular pharmacology* 64(3):773-782.

52. Garin A & Proudfoot AE (2011) Chemokines as targets for therapy. *Experimental cell research* 317(5):602-612.

53. Xia M & Sui Z (2009) Recent developments in CCR2 antagonists. *Expert opinion on therapeutic patents* 19(3):295-303.

54. Sandhu SK*, et al.* (2013) A first-in-human, first-in-class, phase I study of carlumab (CNTO 888), a human monoclonal antibody against CC-chemokine ligand 2 in patients with solid tumors. *Cancer chemotherapy and pharmacology* 71(4):1041-1050.

55. Pienta KJ*, et al.* (2013) Phase 2 study of carlumab (CNTO 888), a human monoclonal antibody against CC-chemokine ligand 2 (CCL2), in metastatic castration-resistant prostate cancer. *Investigational new drugs* 31(3):760-768.

56. Nywening TM*, et al.* (2016) Targeting tumour-associated macrophages with CCR2 inhibition in combination with FOLFIRINOX in patients with borderline resectable and locally advanced pancreatic cancer: a single-centre, open-label, dose-finding, non-randomised, phase 1b trial. *The Lancet. Oncology* 17(5):651-662.

57. DiMasi JA & Grabowski HG (2007) Economics of new oncology drug development. *J Clin Oncol* 25(2):209-216.

58. Kola I & Landis J (2004) Can the pharmaceutical industry reduce attrition rates? *Nature reviews. Drug discovery* 3(8):711-715.

59. Mullard A (2014) New drugs cost US[dollar]2.6 billion to develop. *Nature reviews. Drug discovery* 13(12):877-877.

60. Bertolini F, Sukhatme VP, & Bouche G (2015) Drug repurposing in oncology--patient and health systems opportunities. *Nature reviews. Clinical oncology* 12(12):732-742.

61. Stegbauer J*, et al.* (2009) Role of the renin-angiotensin system in autoimmune inflammation of the central nervous system. *Proc Natl Acad Sci U S A* 106(35):14942-14947.

62. Yang J*, et al.* (2015) Comparison of angiotensin-(1-7), losartan and their combination on atherosclerotic plaque formation in apolipoprotein E knockout mice. *Atherosclerosis* 240(2):544-549.

63. Dai Q, Xu M, Yao M, & Sun B (2007) Angiotensin AT1 receptor antagonists exert anti-inflammatory effects in spontaneously hypertensive rats. *British journal of pharmacology* 152(7):1042-1048.

64. Marshall TG, Lee RE, & Marshall FE (2006) Common angiotensin receptor blockers may directly modulate the immune system via VDR, PPAR and CCR2b. *Theoretical biology & medical modelling* 3:1.

65. George AJ, Thomas WG, & Hannan RD (2010) The renin-angiotensin system and cancer: old dog, new tricks. *Nat Rev Cancer* 10(11):745-759.

66. Rhodes DR*, et al.* (2009) AGTR1 overexpression defines a subset of breast cancer and confers sensitivity to losartan, an AGTR1 antagonist. *Proc Natl Acad Sci U S A* 106(25):10284-10289.

67. Suganuma T*, et al.* (2005) Functional expression of the angiotensin II type 1 receptor in human ovarian carcinoma cells and its blockade therapy resulting in suppression of tumor invasion, angiogenesis, and peritoneal dissemination. *Clin Cancer Res* 11(7):2686-2694.

68. Suzuki Y*, et al.* (2003) Inflammation and angiotensin II. *The international journal of biochemistry & cell biology* 35(6):881-900.

69. Chehl N*, et al.* (2009) Angiotensin II regulates the expression of monocyte chemoattractant protein-1 in pancreatic cancer cells. *Journal of gastrointestinal surgery : official journal of the Society for Surgery of the Alimentary Tract* 13(12):2189-2200.

70. Fujita M*, et al.* (2005) Angiotensin type 1a receptor signaling-dependent induction of vascular endothelial growth factor in stroma is relevant to tumor-associated angiogenesis and tumor growth. *Carcinogenesis* 26(2):271-279.

71. Arnold SA*, et al.* (2012) Losartan slows pancreatic tumor progression and extends survival of SPARC-null mice by abrogating aberrant TGFbeta activation. *PLoS One* 7(2):e31384.

72. Otake AH*, et al.* (2010) Inhibition of angiotensin II receptor 1 limits tumor-associated angiogenesis and attenuates growth of murine melanoma. *Cancer chemotherapy and pharmacology* 66(1):79-87.

73. Cortez-Retamozo V*, et al.* (2013) Angiotensin II drives the production of tumor-promoting macrophages. *Immunity* 38(2):296-308.

74. Chae YK*, et al.* (2011) Reduced risk of breast cancer recurrence in patients using ACE inhibitors, ARBs, and/or statins. *Cancer investigation* 29(9):585-593.

75. Miao L*, et al.* (2016) Impact of Angiotensin I-converting Enzyme Inhibitors and Angiotensin II Type-1 Receptor Blockers on Survival of Patients with NSCLC. *Scientific reports* 6:21359.

76. Nakai Y*, et al.* (2010) Inhibition of renin-angiotensin system affects prognosis of advanced pancreatic cancer receiving gemcitabine. *British journal of cancer* 103(11):1644-1648.

77. Khanna C*, et al.* (2014) Toward a drug development path that targets metastatic progression in osteosarcoma. *Clin Cancer Res* 20(16):4200-4209.

78. Mehlen P & Puisieux A (2006) Metastasis: a question of life or death. *Nat Rev Cancer* 6(6):449-458.

79. Monteiro J & Fodde R (2010) Cancer stemness and metastasis: therapeutic consequences and perspectives. *Eur J Cancer* 46(7):1198-1203.

80. Howlader N NA, Krapcho M, Miller D, Bishop K, Altekruse SF, Kosary CL, Yu M, Ruhl J, Tatalovich Z, Mariotto A, Lewis DR, Chen HS, Feuer EJ, Cronin KA (eds). SEER Cancer Statistics Review, 1975-2013, National Cancer Institute. Bethesda, MD, http://seer.cancer.gov/csr/1975_2013/, based on November 2015 SEER data submission, posted to the SEER web site, April 2016.

81. Weigelt B, Peterse JL, & van 't Veer LJ (2005) Breast cancer metastasis: markers and models. *Nat Rev Cancer* 5(8):591-602.

82. O'Shaughnessy J (2005) Extending survival with chemotherapy in metastatic breast cancer. *The oncologist* 10 Suppl 3:20-29.

83. Van Cutsem E & Oliveira J (2009) Advanced colorectal cancer: ESMO clinical recommendations for diagnosis, treatment and follow-up. *Annals of oncology : official journal of the European Society for Medical Oncology* 20 Suppl 4:61-63.

84. Tevaarwerk AJ*, et al.* (2013) Survival in Metastatic Recurrent Breast Cancer after Adjuvant Chemotherapy: Little Evidence for Improvement Over the Past Three Decades. *Cancer* 119(6):1140-1148.

85. Bernards N*, et al.* (2013) No improvement in median survival for patients with metastatic gastric cancer despite increased use of chemotherapy. *Annals of Oncology* 24(12):3056-3060.

86. Worni M*, et al.* (2013) Modest improvement in overall survival for patients with metastatic pancreatic cancer: a trend analysis using the surveillance, epidemiology, and end results registry from 1988 to 2008. *Pancreas* 42(7):1157-1163.

87. Khalil DN, Smith EL, Brentjens RJ, & Wolchok JD (2016) The future of cancer treatment: immunomodulation, CARs and combination immunotherapy. *Nature reviews. Clinical oncology* 13(5):273-290.

88. Robert C*, et al.* (2015) Pembrolizumab versus Ipilimumab in Advanced Melanoma. *N Engl J Med* 372(26):2521-2532.

89. Rizvi NA*, et al.* (2015) Activity and safety of nivolumab, an anti-PD-1 immune checkpoint inhibitor, for patients with advanced, refractory squamous non-small-cell lung cancer (CheckMate 063): a phase 2, single-arm trial. *The Lancet. Oncology* 16(3):257-265.

90. Hodi FS*, et al.* (2010) Improved survival with ipilimumab in patients with metastatic melanoma. *N Engl J Med* 363(8):711-723.

91. Gordon I, Paoloni M, Mazcko C, & Khanna C (2009) The Comparative Oncology Trials Consortium: using spontaneously occurring cancers in dogs to inform the cancer drug development pathway. *PLoS medicine* 6(10):e1000161.

92. Khanna C, London C, Vail D, Mazcko C, & Hirschfeld S (2009) Guiding the Optimal Translation of New Cancer Treatments From Canine to Human Cancer Patients. *Clinical Cancer Research* 15(18):5671.

93. LeBlanc AK*, et al.* (2016) Perspectives from man's best friend: National Academy of Medicine's Workshop on Comparative Oncology. *Science translational medicine* 8(324):324ps325.

94. Paoloni M & Khanna C (2008) Translation of new cancer treatments from pet dogs to humans. *Nat Rev Cancer* 8(2):147-156.

95. Fenger JM, London CA, & Kisseberth WC (2014) Canine osteosarcoma: a naturally occurring disease to inform pediatric oncology. *ILAR journal* 55(1):69-85.

96. Boozer LB*, et al.* (2012) Characterization of immune cell infiltration into canine intracranial meningiomas. *Veterinary pathology* 49(5):784-795.

97. Gregorio H, Raposo TP, Queiroga FL, Prada J, & Pires I (2016) Investigating associations of cyclooxygenase-2 expression with angiogenesis, proliferation, macrophage and T-lymphocyte infiltration in canine melanocytic tumours. *Melanoma research*.

98. Grieco V, Rondena M, Romussi S, Stefanello D, & Finazzi M (2004) Immunohistochemical characterization of the leucocytic infiltrate associated with canine seminomas. *Journal of comparative pathology* 130(4):278-284.

99. Raposo T, Gregorio H, Pires I, Prada J, & Queiroga FL (2014) Prognostic value of tumour-associated macrophages in canine mammary tumours. *Vet Comp Oncol* 12(1):10-19.

100. Vanherberghen M*, et al.* (2009) An immunohistochemical study of the inflammatory infiltrate associated with nasal carcinoma in dogs and cats. *Journal of comparative pathology* 141(1):17-26.

101. Biller BJ, Guth A, Burton JH, & Dow SW (2010) Decreased ratio of CD8+ T cells to regulatory T cells associated with decreased survival in dogs with osteosarcoma. *J Vet Intern Med* 24(5):1118-1123.

102. Sottnik JL*, et al.* (2010) Association of blood monocyte and lymphocyte count and disease-free interval in dogs with osteosarcoma. *J Vet Intern Med* 24(6):1439-1444.

103. Perry JA, Thamm DH, Eickhoff J, Avery AC, & Dow SW (2011) Increased monocyte chemotactic protein-1 concentration and monocyte count independently associate with a poor prognosis in dogs with lymphoma. *Vet Comp Oncol* 9(1):55-64.

104. Wycislo KL & Fan TM (2015) The immunotherapy of canine osteosarcoma: a historical and systematic review. *J Vet Intern Med* 29(3):759-769.

105. Lascelles BD*, et al.* (2005) Improved survival associated with postoperative wound infection in dogs treated with limb-salvage surgery for osteosarcoma. *Annals of surgical oncology* 12(12):1073-1083.

106. Owen LN & Bostock DE (1974) Effects of intravenous BCG in normal dogs and in dogs with spontaneous osteosarcoma. *Eur J Cancer* 10(12):775-780.

107. Kurzman ID*, et al.* (1995) Adjuvant therapy for osteosarcoma in dogs: results of randomized clinical trials using combined liposome-encapsulated muramyl tripeptide and cisplatin. *Clin Cancer Res* 1(12):1595-1601.

108. Betton GR, Gorman NT, & Owen LN (1979) Cell mediated cytotoxicity in dogs following systemic or local BCG treatment alone or in combination with allogeneic tumour cell lines. *Eur J Cancer* 15(5):745-754.

109. Kurzman ID, Shi F, & MacEwen EG (1993) In vitro and in vivo canine mononuclear cell production of tumor necrosis factor induced by muramyl peptides and lipopolysaccharide. *Vet Immunol Immunopathol* 38(1-2):45-56.

CHAPTER 2

Pharmacological characterization and pre-clinical assessment of losartan as a CCR2 antagonist and potential anti-metastatic therapy

Summary

Metastasis is the leading cause of cancer-related mortality, and remains a major hurdle in improving patient outcomes. Inflammatory monocytes (IMs) have been shown to play key roles in cancer metastasis through promotion of tumor cell extravasation, growth, and angiogenesis. Migration of IMs to sites of metastasis is mediated primarily via the action of the CCL2-CCR2 chemotactic axis. Thus, disruption of this axis represents an attractive therapeutic target for the treatment of metastatic disease. Losartan, an angiotensin II type 1 receptor (AT1R) antagonist, has been previously reported to have immunomodulatory properties via suppression of monocyte and macrophage-mediated inflammation; however, the exact mechanism of this effect has not been fully elucidated. Therefore, we characterized the direct effects of losartan and its EXP-3174 metabolite on CCL2-mediated monocyte recruitment and CCR2 receptor function. We show that losartan and its metabolite potently inhibit monocyte recruitment through inhibition of CCL2 induced ERK1/2 activation, and provide strong evidence which suggests that losartan is a non-competitive inhibitor of CCR2. Based on these observations, we conducted studies in murine breast (4T1) and colon (CT26) carcinoma experimental metastasis models, to determine if losartan exerted anti-metastatic activity via inhibition of CCL2-CCR2 mediated monocyte recruitment. We found that daily treatment with losartan prolonged survival, and significantly reduced metastatic burden,

percentages of $CD11b^+/Ly6C^+$ lung monocytes, and tumor microvessel density in mice with 4T1 and CT26 pulmonary metastases. Collectively, these results suggest that losartan, via inhibition of CCR2 signaling, has the potential for rapid repurposing as a novel anti-metastatic agent in humans at high risk for tumor metastasis.

Significance

Despite initial success with first-line therapies in cancer patients, many these patients still go on to develop metastasis. Significant progress has recently been made in our understanding of the tumor microenvironment, including how the host immune system can be co-opted by tumors to promote their growth and dissemination. CCR2-expressing monocytes are one immune cell type which has been shown to play a critical role in the promotion of tumor cell metastasis, yet to date, there are currently no approved therapies which target these cells. Here, we show that losartan, an already approved and known to be safe drug, has significant antagonistic activity against CCR2, and can suppress pulmonary metastasis growth via sustained inhibition of monocyte recruitment.

Introduction

Metastasis remains the greatest clinical challenge in cancer treatment, accounting for up to 90% of all cancer-related deaths (1, 2). Specifically, the incidence of breast and colorectal cancer remains in the top three in the U.S., and at time of diagnosis, distant metastases are present in 6 to 21% of these patients, respectively (3). Furthermore, although 5-year survival rates experienced by breast and colorectal

cancer patients with localized disease are typically excellent, these individuals are still considered to have a substantially increased lifetime risk for metastasis, with up to 30-50% of these patients eventually developing disseminated disease (4-6). While the success of cytotoxic and molecularly-targeted therapies in both the established and adjuvant disease setting is undeniable, the continued development of therapies that halt metastatic progression remains a critical hurdle in improving patient outcome. Conventionally, the track to FDA-approval of anti-cancer drugs is based on direct anti-tumor activity in pre-clinical models, followed by demonstration of responses in early phase clinical trials of patients with established gross metastases (7, 8). Yet, under this current paradigm, drugs designed to target micro-metastatic processes would often be predicted to fail in this established disease setting (8, 9) .Therefore, it is becoming more and more apparent that the disconnect often observed between preclinical and clinical efficacy is likely in part be due to a disregard for the impact of the tumor microenvironment (TME) on tumor progression and anti-cancer drug responses.

It is now known that the TME is composed of highly heterogeneous populations of both stromal and immune cells, whose diverse functions serve a collective purpose to predominately promote tumor growth and progression (9, 10). Recent studies have also demonstrated that the same cellular components and secreted factors of the primary TME also play critical roles in conditioning secondary sites of metastasis, creating a favorable environment for colonization by disseminated tumors cells (10, 11). Inflammatory monocytes (IMs) are a myeloid-derived immune cell subset, and one component of the TME which have recently been shown to play key roles in the metastatic process (12). In pre-clinical models, CCR2 expressing IMs are preferentially

recruited early on to metastatic sites such as the lung and liver via tumor and stromal cell-mediated production of the monocyte chemoattractant, CCL2 (13, 14). Once present at metastases, IMs, and their derivatives, metastasis-associated macrophages (MAMs), play key roles in promoting metastatic tumor cell extravasation and growth (13, 15-17). In these models, the importance of IMs and MAMs in the metastatic process was demonstrated through the pharmacologic or genetic manipulation of macrophages, their secreted factors, or the CCL2-CCR2 recruitment axis, which resulted in significantly slowed metastatic tumor growth and prolonged survival in mice. In addition, the translational relevance of these findings has also been validated by multiple clinical studies which have demonstrated a negative prognostic role for IMs and the CCL2-CCR2 axis in human patients with various malignancies, including those of the breast, colon, and pancreas (18-21). Thus, it is now apparent that IMs, macrophages, and the CCL2-CCR2 chemotactic axis represent an attractive therapeutic target for the treatment of cancer metastasis.

Initial clinical trials targeting the CCL2-CCR2 axis in human cancer patients evaluated an anti-human CCL2 monoclonal antibody (Carlumab, CNTO888), which showed that CNTO888 alone or in combination with standard of care therapies was ineffective at reducing serum CCL2 levels or slowing tumor progression in patients with various solid tumors (22). However, more recent and ongoing trials have shown that blockade of the CCL2 receptor, CCR2, has the potential to suppress tumor growth in patients with bone metastases and locally advanced pancreatic cancer, suggesting that inhibition of CCR2 might be a more valuable approach in the therapeutic targeting of the CCL2-CCR2 axis (23). While these recent early Phase I/II trials of CCR2 inhibitors are

promising, they are not without hesitation, as recent data suggests that only 10% of agents entering clinical cancer trials make it to FDA approval (24, 25) . Furthermore, given that current estimations for the time and cost invested in new drugs is now a staggering 10 years and $2.6 billion dollars (26), alternative drug development programs which focus on re-purposing already approved drugs as potential anti-cancer therapies might offer greater promise, in terms of reduced cost and time, for getting more effective treatment options to patients with cancer (27).

Losartan, a type I angiotensin II receptor (AT1R) blocker (ARB) used in the treatment of hypertension, has been shown to have immunomodulatory and anti-inflammatory properties in models of vascular inflammation and multiple sclerosis (28-30). Interestingly, these anti-inflammatory properties were primarily associated with an observation of reduced monocyte and macrophage recruitment to inflammatory lesions. In these studies, losartan's blockade of monocyte and macrophage recruitment was attributed to an indirect effect on CCL2 and/or CCR2, secondary to primary inhibition of AT1R signaling. However, it was not definitively shown that losartan was not directly disrupting the CCL2-CCR2 axis, and in fact, molecular modeling studies of CCR2 suggest that losartan and other ARBs have a high affinity for and the potential to act as CCR2 antagonists (31). Despite these observations, very few studies have evaluated the immunomodulatory properties and potential therapeutic efficacy of losartan in models of tumor metastasis, and to date, no one has evaluated the molecular pharmacology underlying losartan's interactions with CCR2, and its potential to act as a CCR2 antagonist.

To this point, we evaluated losartan's ability to directly inhibit monocyte recruitment using a diverse repertoire of in vitro and in vivo assays of monocyte chemotaxis, acute inflammation, and early tumor metastasis. Our results demonstrate that both losartan and its primary metabolite (EXP-3174) potently inhibit CCL2-CCR2 dependent human and murine monocyte recruitment at clinically relevant doses. Furthermore, using G-protein coupled receptor function assays, we characterized the effects of losartan and EXP-3174 on CCL2 ligand binding and post-receptor signal transduction pathways stimulated by CCL2. Our findings suggest that both losartan and EXP-3174 function as noncompetitive inhibitors of human CCR2. Based on its CCR2 antagonist properties, we assessed the potential of losartan to be re-purposed as an anti-metastatic therapy in experimental metastasis models of breast and colon cancer, which showed that losartan significantly slowed metastatic progression in a process that was associated with blockade of inflammatory monocyte recruitment and reduction in metastasis-associated macrophages. Taken together, these studies suggest that losartan and its primary metabolite might represent a novel class of safe and already-FDA approved, noncompetitive CCR2 antagonists, which could be rapidly repurposed for the treatment of metastatic disease.

Materials and Methods

Mice

6-8 week old, female BALB/c and ICR mice were purchased from Harlan laboratories (Denver, CO). *CCR2*$^{-/-}$ mice on the C57BL/6J background and wild-type C57BL/6J mice were purchased from The Jackson Laboratory (Bar Harbor, ME). *CCR2*$^{-}$

$^{-/-}$ mice on a BALB/c background were obtained from Dr. Cynthia Ju (University of Colorado, Denver). All animals were housed in microisolator cages in the laboratory animal facility at Colorado State University, and all procedures were approved by the Institutional Animal Care and Use Committee at Colorado State University.

Cell lines

4T1-luc, CT26, and CT26-luc cells were generously provided by Dr. Daniel Gustafson (Colorado State University, Fort Collins, CO). THP-1 cells were purchased from the ATCC. CT26-GFP cells were generated by transducing CT26 cells with lentivirus particles expressing GFP under the EF1A promoter (LVP425, GenTarget Inc. San Diego, CA). After 72 h cells were treated with G-418 (600 μg/mL; Invivogen, San Diego, CA) to select for successfully transduced cells, and GFP expression was subsequently confirmed by flow cytometry. Cells were maintained in MEM [4T1 and CT26] or RPMI1640 [THP1] media (Gibco, Grand Island, NY USA) supplemented with 10% fetal bovine serum (FBS; Atlas Biologicals, Fort Collins, CO USA), penicillin (100 U/mL), streptomycin (100 μg/mL), L-glutamine (2 mM), and non-essential amino acids (0.1 mM) (All obtained from Gibco). Cells were grown sterilely on standard plastic tissue culture flasks (Cell Treat, Shirley, MA), under standard conditions of 37 °C, 5% CO_2, and humidified air, and were confirmed Mycoplasma-free. *CCR2* expression by THP-1 cells was periodically confirmed by flow cytometry.

Losartan, losartan EXP3174 metabolite, and CCR2 antagonist drugs

50mg losartan potassium tablets (Cozaar) were obtained from the Veterinary Teaching Hospital pharmacy, ground using a mortar and pestle, and dissolved in water and sterile-filtered to obtain a stock concentration of 10 mg/mL. Losartan carboxylic acid (EXP3174 metabolite) was purchased as a powder from Santa Cruz Biotechnology (Dallas, TX), and reconstituted in DMSO at 10 mg/mL. INCB3284 and RS102895 powder stocks were obtained from Tocris Bioscience (Bristol, UK), and re-constituted in DMSO at 10 mg/mL. All drug stocks were aliquoted and stored at -20°C. For all animal experiments, losartan and losartan EXP3174 metabolite drug stocks were diluted in PBS, and administered by once daily intra-peritoneal (i.p.) injection of 60 mg/kg and 10 mg/kg, respectively, in a 100 μL volume.

Experimental lung metastasis models

Wild-type or *CCR2*$^{-/-}$ BALB/c mice were inoculated by I.V. tail vein injection of 1 x 10^5 4T1-luc cells, 2.5 x 10^5 CT26-luc cells, or 4 x 10^5 CT26-GFP cells in 100 μL PBS. Treatment with losartan (60 mg/kg, i.p.) was initiated 24h after tumor cell inoculation. For 72 h metastasis assays, mice were treated a total of three times (24, 48, and 72 h) prior to euthanasia and tissue collection. For long term tumor growth studies, mice were treated daily until study completion. To monitor the development and growth of luciferase-positive pulmonary metastases, bioluminescence imaging was performed thrice weekly using an IVIS100 imager (Perkin-Elmer, Waltham, MA). For imaging, mice were injected i.p. with 100 μL of 30 mg/mL luciferin (GoldBio, St. Louis, MO), followed

by isoflurane anesthesia and imaging 12 minutes post-luciferin injection (2 minute exposure, medium binning).

Analysis of lung inflammatory monocytes

Following study completion and animal euthanasia, lungs were collected from mice and stored in complete media on ice prior to processing. Right lung lobes were minced in 6-well plates, and then digested in 2x collagenase D (Roche) diluted in HBSS + 0.1% FBS/EDTA for 30 minutes at 37°C. Following digestion, tissues were triturated using an 18 g needle and filtered through 70 µm cell strainers (x2) (BD Biosciences). Lastly, red blood cells were lysed using ACK solution and remaining cells re-suspended in FACS buffer (PBS with 2% fetal bovine serum and 0.05% sodium azide) for immunostaining.

Flow cytometry analysis

Following plating of single cell suspensions of lung or LN in 96 well round-bottom plates, non-specific binding was blocked by adding normal mouse serum (Jackson Immunoresearch) and un-labeled anti-mouse CD16/32 (eBiosciences) to cells before immunostaining. Cells were then incubated with the following directly labeled rat monoclonal antibodies (eBioscience, San Diego, CA unless otherwise noted) directed against mouse CD11b (clone M1/70), mouse Ly6C (clone AL-21), mouse Ly6G (clone 1A8), mouse MHC II (clone M5/114.15.2), mouse Gr1 (clone RB6-8C5), mouse F4/80 (clone MCA497; AbD Serotec) mouse CD11c (clone N418), and mouse CCR2 (clone 475301; R&D Systems) for 25 min at room temperature (RT). Cells were washed in FACS buffer (PBS + 2% FBS and 1% sodium azide) and incubated with streptavidin conjugates

when necessary. Flow cytometry was conducted using either a Dako/CyanADP or Beckman Coulter Gallios flow cytometer. Analysis was done with FlowJo software (Ashland, OR).

Fluorescence microscopy

Immediately following euthanasia, left lung lobes were dissected and immersion fixed in 1% paraformaldehyde-lysine-periodate fixative (1% paraformaldehyde in 0.2 M lysine-HCL, 0.1 M anhydrous dibasic sodium phosphate, with 0.21% sodium periodate, pH 7.4) for 24 hours at 4°C. Following fixation, lungs were placed in a 30% w\v sucrose solution for 24 hours at 4°C, prior to embedding and freezing in O.C.T. compound (Tissue Tek). Embedded tissues were sectioned at 5 μm for immunostaining. Nonspecific binding was blocked by pre-incubation of sections with 5% donkey serum (Jackson ImmunoResearch, West Grove, PA) in 1% BSA for 30 min at RT. Primary antibody labeling (1:200 anti-GFP, Novus Biologicals; 1:100 anti-F4/80 clone BM8, eBiosciences, and 1:100 anti-Ly6C ab76975) was performed at RT for 1 hr in 1% BSA. After removal of the primary antibody, tissues were washed with PBS-T, followed by addition of the following secondary antibodies (diluted 1:200 in PBST) for 30 min at RT: AlexFluor488-conjugated donkey anti-rabbit IgG (GFP), AlexaFluor647-cojugated donkey anti-rat IgG (F4/80), and Cy3-conjugated donkey anti-rat IgG (Ly6C) (Jackson ImmunoResearch). Tissues were counter stained with DAPI, cover-slipped, and visualized using an Olympus IX83 confocal microscope and Hamamatsu digital camera. Figures were assembled using Adobe Photoshop (CC2016).

In vivo mouse footpad vaccination assay

The cationic liposome-poly I:C adjuvant was prepared in the laboratory as described previously. Using an insulin syringe (BD Biosciences), 50 μl of adjuvant was injected into the right rear footpad of mice while under isoflurane anesthesia. Following injection, mice were immediately treated i.p. with losartan or losartan EXP3174 metabolite (60 mg\kg, or 10 mg\kg, respectively), and again 24 hours later. Animals were euthanized ~2 hours following the second drug treatment, and right popliteal lymph nodes (LNs) were harvested and stored in complete media on ice until processing. Right popliteal LNs harvested from naïve, un-injected mice served as controls. LNs were mashed on 40 μM cell-strainers using a 3 ml syringe plunger, rinsed with 10 ml complete medium, centrifuged @1200 rpm for 5 min, and re-suspended in FACS buffer for immunostaining and flow cytometry analysis.

In vitro THP-1 and PBMC chemotaxis assays

Peripheral Blood Mononuclear Cells (PBMCs) were isolated from fresh, EDTA-treated human blood by lysing erythrocytes (x2) with ACK buffer solution (150 mM NH_4Cl, 10 mM $KHCO_3$, and 0.1 mM Na_2EDTA). PBMCs were washed into serum-free RPMI (sf-RPMI), and re-suspended at 2 x 10^6 cells/ml. Cultured THP-1 cells were washed into sf-RPMI and re-suspended at 6 x10^6 cells/ml. Drug stocks (losartan, losartan EXP3174 metabolite, or RS102895) were diluted to 2x in sf-RPMI. THP-1 cells or PBMCs were diluted 1:1 in media alone (positive and negative controls) or in media containing 2x drug dilutions. Cells were pre-treated @ 37°C in the incubator for 1 hour prior to plating. The chemotactic stimulus for positive control and drug treated wells

consisted of 50 ng/ml recombinant human CCL2 (Peprotech Inc. Rocky Hill, NJ). Negative control wells consisted of sf-RPMI only. THP-1 chemotaxis was conducted in 24-well plates containing 3 μM-pore diameter cell culture inserts (Falcon, Corning, NY). For these assays, 600μl of medium +/- *CCL2* was plated in the lower compartment of the plate, while 100 μL (3×10^5) THP-1 cells in medium +/- drug were plated in the upper compartment of the cell culture insert. For PBMC migration assays, 96 well chemotaxis plates (Corning, Corning, NY) with an 8 μM pore diameter were used, and 150 μl of media +/- CCL2 was plated in the lower compartment of the plate, while 50μl (5×10^4) PBMCs in media +/- drug were plated in the upper compartment of the cell culture insert. Cells were allowed to migrate for 4 h. Following migration, non-migrated cells were removed, wells washed, and membranes (THP-1 migration) or lower compartment wells (PBMCs) were fixed with 4% paraformaldehyde for 10 min on ice, stained with 3% crystal violet (Sigma-Aldrich, St. Louis, MO USA), rinsed with dH_20, and air-dried overnight. For analysis of THP-1 chemotaxis, membranes were cut from the cell culture inserts, and mounted “migrated-side” up on superfrost plus glass slides using immersion oil. A total of (5) 40x fields per membrane were counted to determine the Mean # of monocytes/40x field for each membrane. For PBMC migration assays, 4x4-tiled 10x magnification overviews of 96 well plates were obtained for each individual well, and total monocytes per/well counted using ImageJ (NIH).

***CCL2*-induced *ERK* phosphorylation**

Western blot. THP-1 cells (5×10^5 cells/ well) were plated in 24 well plates and serum starved overnight for ~20-24 hours in the incubator. The following morning,

losartan or losartan EXP3174 was added to cultures to achieve the indicated treatment concentrations, and cells were pre-treated for 2 hours prior to CCL2 stimulation. Samples were stimulated with CCL2 (10 nM; Peprotech, Rocky Hill, NJ) for 1 min, quickly pelleted, supernatant discarded, and re-suspended in ice-cold lysis buffer [M-PER reagent (ThermoFisher, Waltham, MA) containing 1mM sodium orthovanadate, 100 mM PMSF, 2% SDS, and 1x protease inhibitor cocktail (Roche, Basel, Switzerland)] for 10 min on ice. Lysates were then centrifuged at 13,000 rpm for 5 min and supernatant removed. For western analysis, 5 µg of THP-1 lysate was mixed 1:1 with 2x Laemelli sample buffer containing 5% 2-Mercaptoethanol (BioRad, Hercules, CA), boiled for 5 minutes, cooled on ice, and then loaded into a Mini-Protean TGX 4-20% pre-cast polyacrylamide gel (BioRad) for electrophoresis (150 V, 45 min). Protein was then transferred to nitrocellulose membranes (95 V, 50 min, at 4 °C), and membranes were blocked for 1 h at RT with 5% BSA in Tris-buffered saline Tween 20 solution (TBST). After washing in TBST, membranes were incubated with the primary antibody (monoclonal rabbit anti-Phospho p44/42 MAPK, clone D13.14.4E, Cell Signaling Technology, Danvers, MA) diluted in 5% BSA-TBST, overnight at 4 °C. The following day membranes were rinsed (x3 with TBST), incubated with the secondary antibody (HRP-linked goat anti-rabbit IgG; ThermoFisher, Waltham, MA) diluted 1: 20,000 in 5% BSA/TBST for 1 h at RT. Lastly, membranes were imaged with chemiluminescent substrate (Clarity Western ECL, BioRad) using a Chemi Doc XES + system (BioRad).

Flow cytometry. 2.5 x 10^5 THP-1 cells in serum-free RPMI +/- losartan or losartan EXP3174 metabolite at indicated concentrations were incubated for 1 h 37°C in

microcentrifuge tubes. Following drug pre-treatment, cells were stimulated with 20 nM human rCCL2 for 3 min at 37°C. Immediately following stimulation, the reaction was terminated by fixation of cells in an equal volume of 4% paraformaldehyde for 15 min at 37°C. Fixed cells were pelleted, washed twice in FACS buffer, and then permeabilized by re-suspension in 150μL of ice-cold 100% methanol for 15 min. Following permeabilization, cells were washed in FACS (x2), and then stained with monoclonal rabbit anti-human Phospho p44/42 MAPK-AlexaFluor 647 (clone1792G2, Cell Signaling Technology, Danvers, MA) at 1 μg/mL diluted in FACS for 30 min at RT. Following primary antibody labeling, cells were washed in FACS (x2), and then analyzed by flow cytometry.

CCR2 cell surface expression

THP-1 cells, human PBMCs, or mouse bone marrow cells were washed and re-suspended into sf-RPMI at 8 x 10^5 cells/mL. Drug stocks (10 mg/mL) were diluted to either 2x or 4x treatment concentrations for either single agent or combination therapy studies, respectively. 2 x 10^5 cells in 250 μL were plated in 24 well plates and diluted either 1:1 with media alone (control) or 2x drug stocks (single agent treatment), or 1:0.5:0.5 (4x drug stocks, combination treatment studies). Cells +/- drug treatment were then incubated under standard conditions of 37 °C, 5% CO_2, and humidified air for the indicated time periods (1-24 hr). Following drug treatment, cells were centrifuged @1800 rpm for 3 minutes, re-suspended in FACS buffer and stained for CCR2 using a monoclonal mouse anti-human CCR2 antibody (clone TG5/CCR2, Biolegend, San Diego, CA). For human PBMCs, cells were also labeled with mouse anti-human CD14

(clone TUK4, Bio-Rad, Hercules, CA). For mouse bone marrow, cells were stained with the following panel of rat monoclonal antibodies directed against: mouse CD11b (clone M1/70), mouse Ly6C (clone AL-21), mouse Ly6G (clone 1A8), and mouse CCR2 (clone 475301; R&D Systems). Data were expressed as CCR2 geometric mean fluorescence (gMFI) intensity as % of un-treated controls.

CCL2 ligand binding assays

THP-1 cells (2.5 x 10^5 cells/well) were plated in 96 well plates in chemokine-labeling buffer (RPMI + 20mM HEPES, 10% FBS, 1% L-glutamine, and 1% pen/strep) alone (positive control), or buffer containing either 30nM un-labeled human rCCL2 (cold-competition control), or losartan, losartan EXP3174 metabolite, or INCB3284 at the indicated concentrations. Human rCCL2-AlexFluor 647 (CAF-2, Almac, Souderton, PA) was then added to all wells to obtain a final concentration of 30nM. Cells were then incubated for 1h @ 37°C, and ligand binding subsequently analyzed by flow cytometry. Data were expressed as % inhibition of ligand binding as determined by differences in CCR2 gMFI between untreated and drug treated cells.

Intracellular *Ca^{2+}* signaling

Briefly, changes in cytoplasmic calcium levels in response to CCL2 stimulation (10 nM) was measured in THP-1 cells (2.5x10^5 cells/well) loaded with Fluo-3AM dye (1 μM for 45 min at 37°C; ThermoFisher, Waltham, MA). Following loading, cells were washed and re-suspended in buffer +/- losartan, losartan EXP3174 metabolite, or CCR2 antagonist at the indicated concentrations, and pre-treated for 1 hour at 37°C prior to

CCL2 stimulation. Analysis was performed on a BioTek Synergy HTX plate reader. Baseline fluorescence was collected over a 30 s interval prior to addition of CCL2, and then for 2 minutes after stimulation. The buffer for cell loading, drug treatment, and CCL2 stimulation consisted of Hanks' balanced salt solution containing 20 mM HEPES and 0.2 mM sulfinpyrazone.

Angiotensin II and CCL2 ELISA assays

Angiotensin II (AngII) and CCL2 production by tumor cell lines and in the serum of tumor bearing mice were measured using commercially available ELISA kits (For AngII: RAB0010, Sigma-Aldrich, St. Louis, MO; For CCL2: DY479, R&D Systems, Minneapolis, MN). Assays were performed according to kit instructions.

Losartan pharmacokinetics

Following two weeks of losartan dosing (60 mg/kg/day i.p.), blood samples were collected via cardiac venipuncture at 0.25, 0.5, 1, 2, 4, 6, 12, and 24 hours after the final dose on day 14. Samples were treated with EDTA anticoagulant, centrifuged, and plasma removed and stored at -80°C prior to analysis. Standard curve and QCs were prepared in the following manner: Initial 10 mg/ml stocks of losartan and losartan EXP3174 carboxylic acid metabolite were prepared in 1:1 acetonitrile(ACN)/Milli-Q water (1 mg/mL). A standard curve of losartan and EXP3174 metabolite was then prepared ranging from 5 to 25000 ng/mL in 1:1 ACN/Milli-Q water. 10 μl of each appropriate standard was then added to 100 μL of blank plasma collected from naïve ICR mice fortified with 10 μL internal standard (ENMD-2076 at 1000 ng/mL). 10 μL

internal standard, 10 µL 1:1 ACN/Milli-Q water, and 100 µL ACN were then added to 100 µL of each unknown plasma sample in 1.5mL micro centrifuge tubes. All samples were then vortexed for 5 min, centrifuged @ 13,300 rpm for 20 min, and 200 µL of the organic phase was transferred to fresh 2 mL micro-centrifuge tubes. Samples were concentrated to dryness on a speed vacuum then reconstituted in 200 µL of 85:15 [v:v], 0.1% formic acid: 50/50 ACN/methanol. Finally, samples were transferred to glass autosampler vials for injection onto the HPLC system. Mass spectra were obtained with a MDS Sciex 3200 Q-TRAP triple quadrupole mass spectrometer (Applied Biosystems, Inc., Foster City, CA) with a turbo ionspray source (operating in positive ion mode) interfaced to an Agilent 1200 Series Binary Pump SL HPLC system (Santa Clara, CA). Samples were chromatographed with Kinetix 2.6 □ C18 100 Å (Size 50 mm X 4.6 mm) Phenomenex, Torrance, CA). An LC gradient was employed with mobile phase A consisting of 0.1% formic acid and mobile phase B consisting of 50/50 ACN/methanol. Chromatographic resolution was achieved by increasing mobile phase B linearly from 15 to 98% from 1 to 1.5 min, maintaining at 98% from 1.5 to 3.75 min, decreasing linearly from 98 to 215% from 3.75 to 4 min, followed by re-equilibration of the column at 15% B from 4 to 5 min. The LC flow rate was 1.25 mL/min, the sample injection volume was 30 µL, and the analysis run time was 5 min.

Statistical analysis

All data expressed as means ± SD unless otherwise noted. Statistical significance was determined by a two-tailed, unpaired Student's *t* test, or One-way

ANOVA with Tukey's post-test for multiple group comparisons. All statistical analyses were performed using Graph Pad Prism software (La Jolla, CA, USA).

Results

Losartan and its primary metabolite (EXP3174) inhibit CCL2-mediated monocyte migration in vitro and in vivo in humans and mice

We first determined the effect of losartan and losartan's primary carboxylic acid metabolite (Los CA; EXP3174) on in vitro, CCL2-directed THP-1 migration using a trans-well chemotaxis assay (Fig. 2.1A). Both losartan and its EXP3174 metabolite significantly inhibited CCL2 directed THP-1 migration to ~10% of that observed for positive control wells (*$p<0.05$). Furthermore, the strength of this inhibition was comparable to that observed for the specific small molecule CCR2 antagonist RS102895 when evaluated at equimolar concentrations. To determine if this inhibitory effect of losartan was intrinsic only to THP-1 cells, we also evaluated losartan's ability to inhibit CCL2-mediated migration of human peripheral blood mononuclear cells (PBMCs) (Fig. 2.1B-F). These results demonstrated that losartan significantly inhibited human PBMC migration (by ~50%; *$p<0.04$) at a pharmacologically achievable and clinical relevant dose. Next, to evaluate the ability of losartan and EXP3174 to inhibit in vivo inflammatory monocyte recruitment, we utilized a murine footpad vaccination model. Using this model, we have previously demonstrated that vaccination with a lipsome-Toll like receptor (TLR) adjuvant induces recruitment of large numbers of Ly6C^{Hi} IMs to vaccine-draining lymph nodes (LNs), a process which is almost entirely dependent on CCL2-CCR2 signaling (Fig. 2.2). Both losartan and EXP3174 significantly reduced the

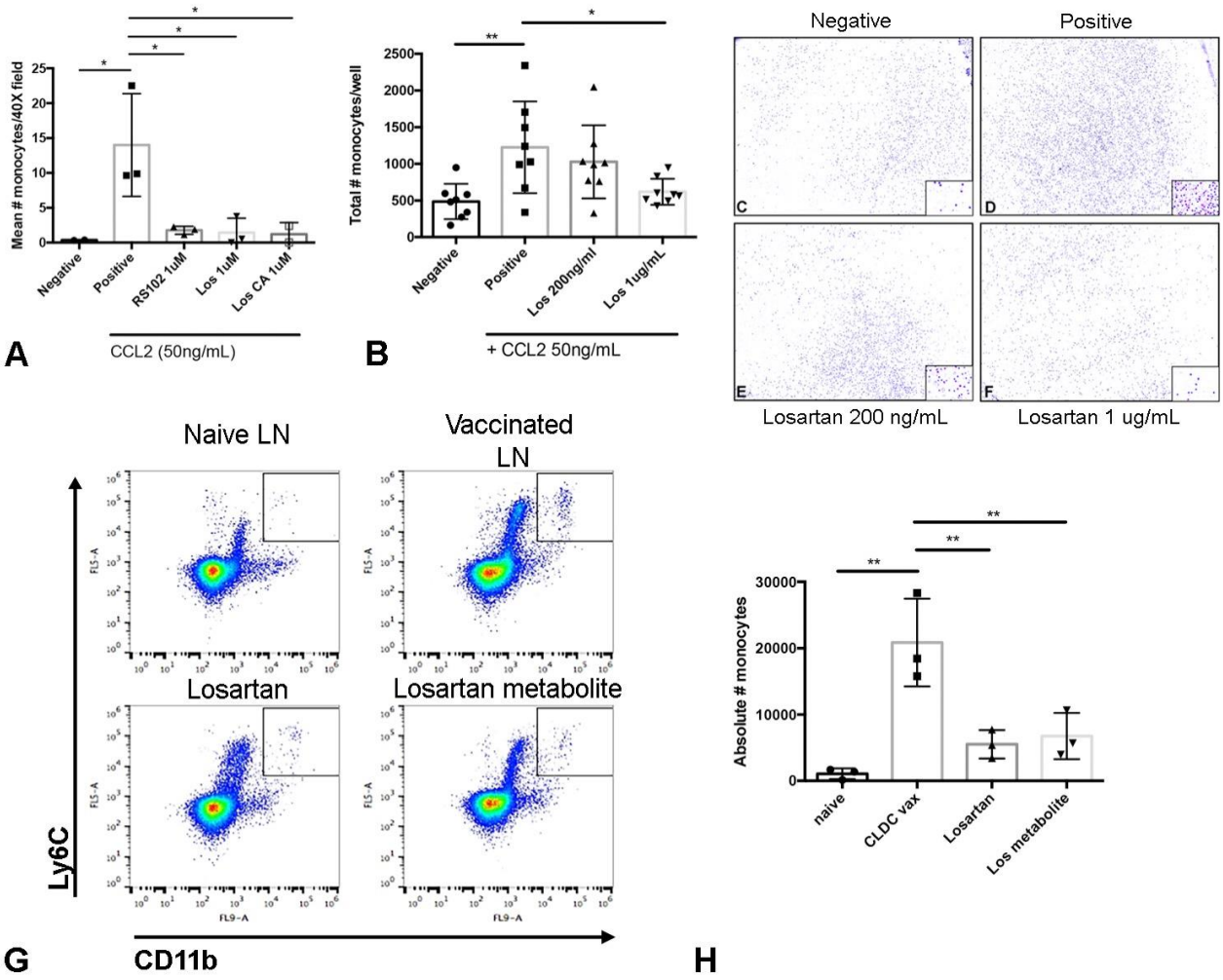

Figure 2.1 Losartan and its primary EXP3174 metabolite inhibit *CCL2-CCR2* mediated monocyte migration in vitro and in vivo in humans and mice at pharmacologically relevant concentrations and equimolar potency to a small molecule *CCR2* antagonist. *(A)* Graph depicting results of in vitro trans-well migration assays assessing the ability of losartan (Los) and its EXP3174 metabolite (losartan carboxylic acid, Los CA) to inhibit *CCL2*-directed THP-1 monocyte migration as compared to the specific small molecule *CCR2* antagonist RS102895 (RS102). *(B)* Graph showing inhibition of *CCL2*-mediated human PBMC migration by losartan at clinically relevant concentrations. *(C-F)* Representative whole well images (10x) and higher magnification (40x; inset) of human PBMC migration assays quantified in *(B)*. *(G)* Representative dot plots demonstrating the ability of losartan and it's metabolite to inhibit the recruitment of *Ly6G^{-} /CD11b^{+}/Gr1(Ly6C)^{Hi}* inflammatory monocytes (IMs) to vaccine-draining popliteal lymph nodes (LNs) of mice. This recruitment is almost entirely dependent on the CCL2-CCR2 axis (**Fig. 2.2**). Mice were treated at time of vaccination and 24h later with losartan

(60mg/kg), or EXP3174 losartan metabolite (10mg/kg). *(H)* Graph showing flow cytometric quantification of absolute numbers of IMs in vaccine-draining popliteal LNs of groups of mice in *(G)*. Data expressed as means ± SD, and were analyzed by One-way ANOVA, with Tukey's post-test comparisons (n= 3 mice per group, or 2-4 independent experiments representing the mean of technical replicates, each technical replicate being the average of (5) 40x fields (THP-1 migration) or (16) 10x fields (PBMC migration), $*p < 0.05$, $**p < 0.01$).

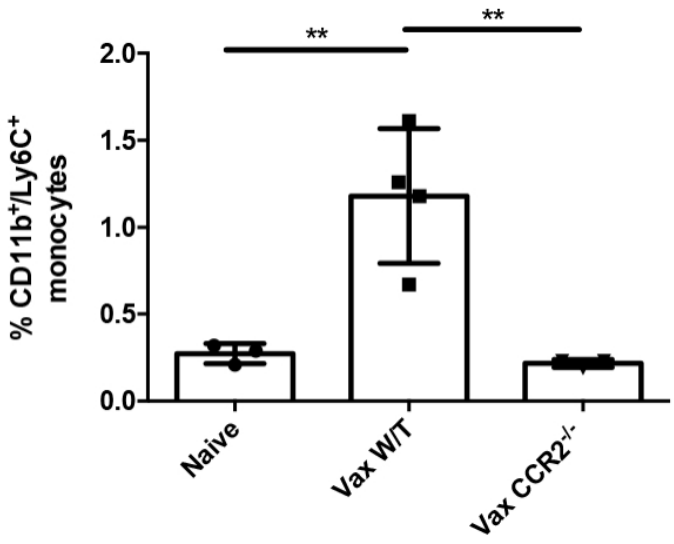

Figure 2.2 Recruitment of IMs to vaccine draining LNs is entirely dependent on the chemokine receptor *CCR2.* Graph showing results of flow cytometric quantification of *Ly6G^{-}/CD11b^{+}/Ly6C^{Hi}* IMs in naïve (un-injected) C57BL/6 w/t mice as compared to C57BL/B6 w/t (Vax W/T) or *CCR2$^{-/-}$* (VAX *CCR2$^{-/-}$*) mice injected in the right-rear footpad with 50μL of a liposome-TLR3 agonist adjuvant. Popliteal LNs were harvested 24 hours after injection and processed to single suspensions for flow cytometry. Data expressed as means ± SD, and were analyzed by One-way ANOVA, with Tukey's post-test comparisons (n= 3 mice per group, $^{**}p < 0.01$).

absolute number of IMs recruited to popliteal draining LNs of vaccinated mice by ~75% (**p<0.01) (Fig. 2.1 G-H). Thus, we next sought to evaluate losartan's ability to inhibit IM recruitment to tumor metastases using experimental lung colonization assays.

Losartan blocks early tumor-mediated inflammatory monocyte recruitment to the lungs and significantly reduces CT26 tumor cell colonization

To assess losartan's effect on monocyte recruitment in a model of early tumor lung colonization, we injected syngeneic wild-type BALB/c mice in the lateral tail vein with CT26-GFP colon carcinoma cells, which resulted in reliable lung colonization (Fig. 2.3F) and significantly increased (~ 4-fold) recruitment of $CD11b^{+}/Ly6C^{Hi}$ IMs to the lungs of tumor-injected as compared to naïve control mice (Fig. 2.3 A, B, & F) by 72 hours. In addition, injection of CT26-GFP cells into BALB/c-$CCR2^{-/-}$ mice demonstrated that this recruitment was entirely dependent on the presence of CCR2 (Fig. 2.3 D & E). To assess losartan's ability to inhibit CT26 mediated recruitment of IMs, mice were treated with losartan 60 mg • kg^{-1} • d^{-1} i.p. beginning 24 hours after tumor cell injection, and were sacrificed at 72h post-injection for flow cytometric and immunofluorescent quantification of $Ly6G^{-}/SiglecF^{-}/CD11c^{-}/CD11b^{+}/Ly6C^{Hi}$ lung IMs, and $F4/80^{+}$ metastasis-associated macrophages (MAMs), respectively. Losartan treatment significantly reduced the percentages of lung IMs and mean number of $F4/80^{+}$ MAMs by 70% and 36%, respectively, to levels near those observed in $CCR2^{-/-}$ and naïve un-injected mice (Fig. 2.3 C, E, F, & I). Similar results were also observed when IM recruitment was evaluated by Ly6C immunofluorescent staining of micrometastases (Fig. 2.4 A-C).

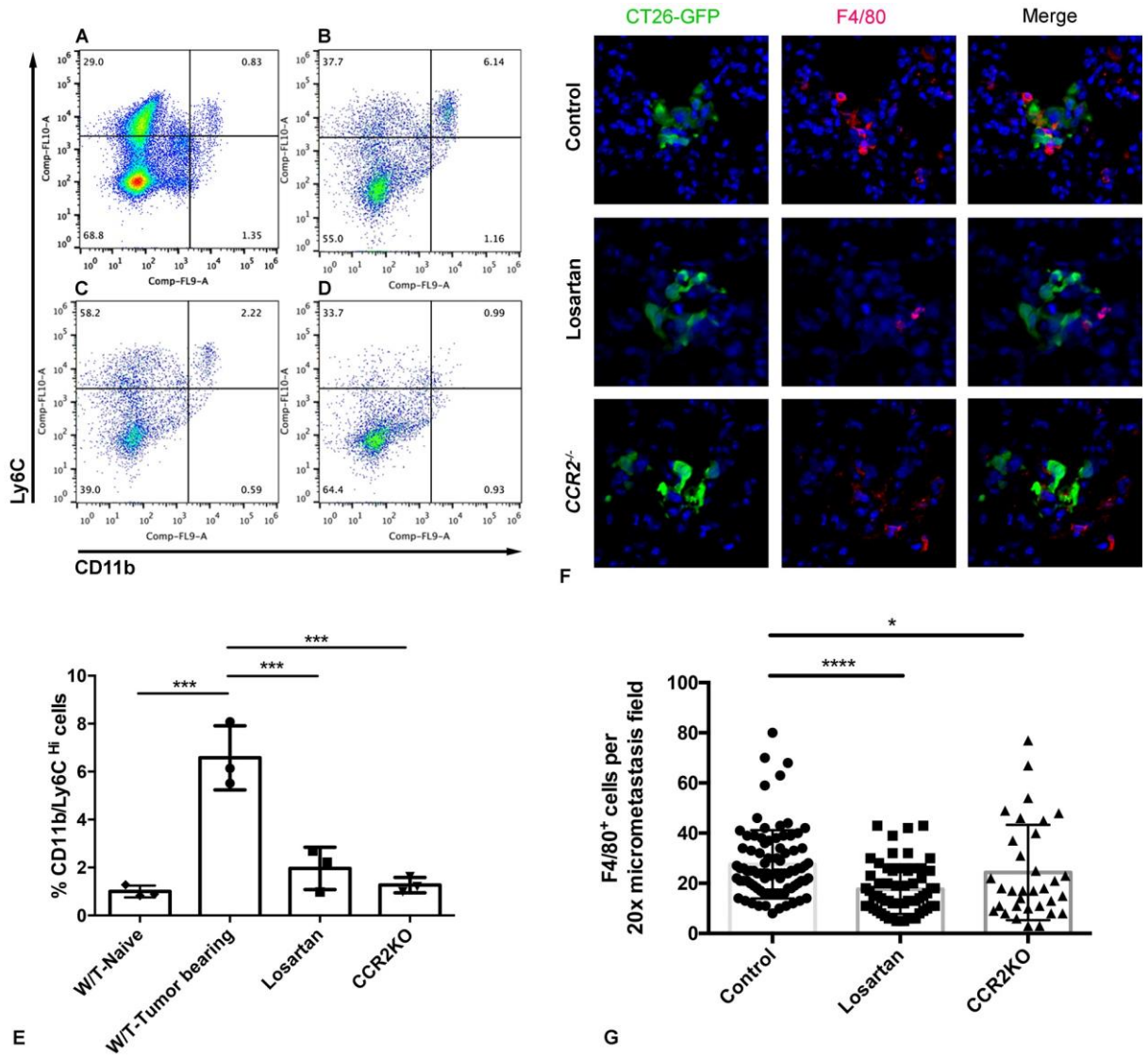

Figure 2.3. Losartan blocks IM recruitment to the lungs during early CT26 tumor cell engraftment. *(A-D)* Representative dot plots gated on *CD11b*$^{+}$*/Ly6C*^{Hi} IMs in the lungs of either naïve Balb/c mice *(A)*, or 72 hours post tail-vein injection of CT26-GFP tumor cells (4 x 10^5 cells) in control mice *(B)*, mice treated with Losartan 60mg/kg *(C)*, or *CCR2*$^{-/-}$ mice *(D)*. *(E)* Graph depicting the flow-cytometric quantification of IMs in the lungs of the groups of mice in *(A-D)*. *(F)* Corresponding immunofluorescent images of F4/80^{+} metastasis-associated macrophages (MAMs, red) surrounding CT26-GFP+ micrometastases (green) in control, losartan-treated, and *CCR2*$^{-/-}$ mice. (G) Graph of immunofluorescent quantification of F4/80+ MAM density in the lungs of the groups of mice in *(F)*. Data expressed as means ± SD, and were analyzed by One-way ANOVA, with Tukey's *(E)* or Kruskal-Wallis *(G)* post-test comparisons (n= 3 mice per group *(E and G)*, 10-46 micrometastases analyzed per mouse (G) ***$p < 0.001$).

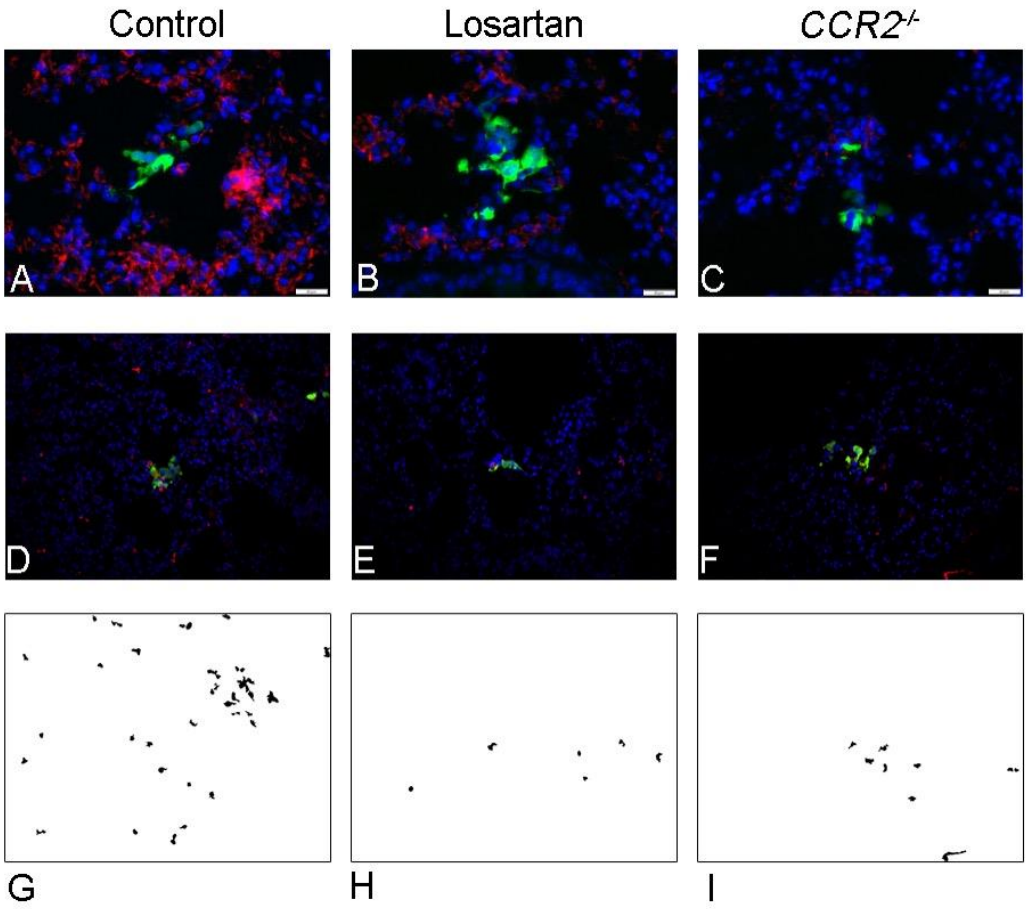

Figure 2.4. Immunofluorescent image analysis of IMs and MAMs surrounding early CT26-GFP micrometastases. *(A-C)* Immunofluorescent images of pulmonary micrometastases showing *Ly6C*$^+$ monocytes (red) also intimately surrounding early (72h) CT26-GFP pulmonary micrometastases (green). (D-F) Representative lower magnification *F4/80*$^+$ (red) immunofluorescent images of micrometastases used for ImageJ analysis, and (E-I) Corresponding *F4/80*$^+$ threshold masks of immunofluorescent images shown in (D-F), which were used to determine the *F4/80*$^+$ MAM cell count data shown in the graph in Fig. 2I. DAPI nuclear counterstain. 40x magnification (Ly6C), 20x magnification (F4/80).

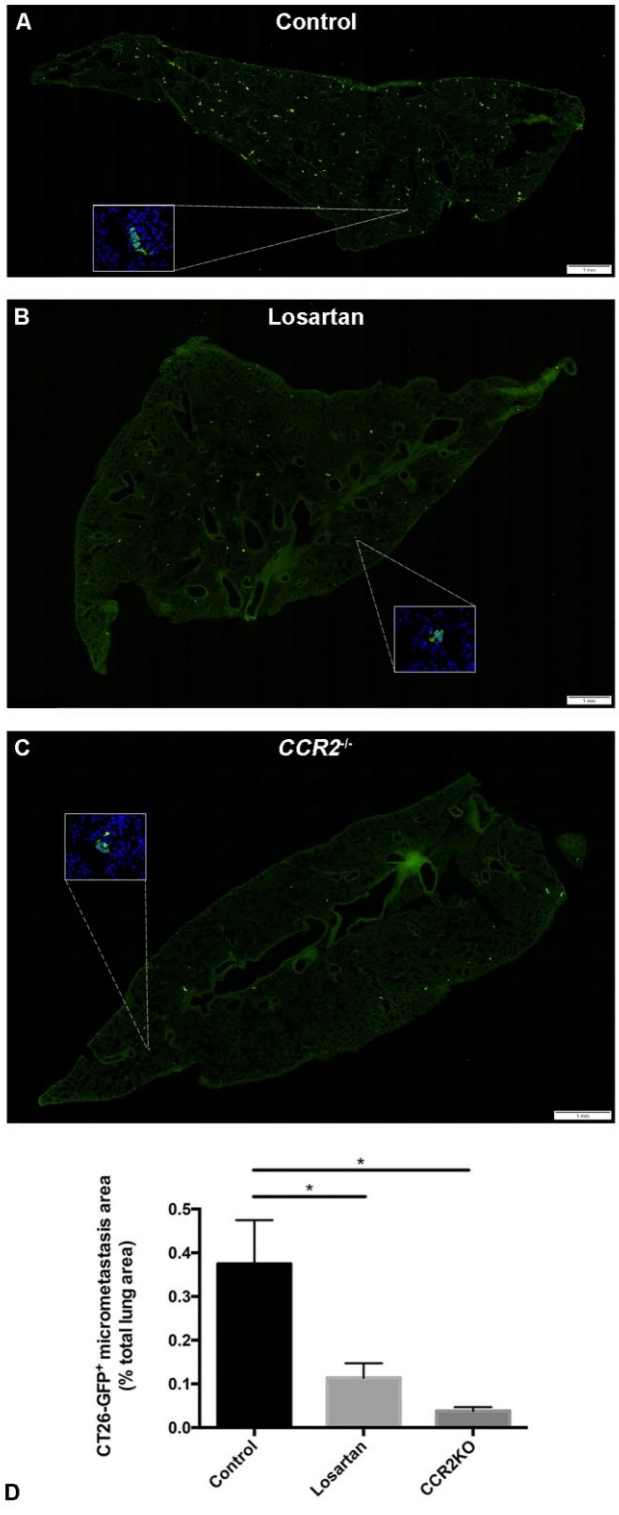

Figure 2.5. Losartan treatment significantly reduces the establishment of early CT26 pulmonary micrometastases to a density similar to that observed in *CCR2$^{-/-}$mice.* (A-C)

Representative 10x magnification whole left lung lobe immunofluorescent images demonstrating the density of CT26-GFP^{+} tumor cell clusters in control (A), losartan treated (B), and *CCR2*$^{-/-}$ mice (C). Insets are higher magnification (20x) images representing single CT26-GFP^{+} micrometastases chosen from the indicated region of the whole lung overview field. (D) Graph depicting quantification of micrometastatic burden (CT26-GFP+ tumor cell area as % of total lung area) for groups of mice shown in (A-C). Data expressed as means ± SD, and were analyzed by One-way ANOVA, with Tukey's post-test comparison (n= 3 mice per group, $*p < 0.05$).

Figure 2.6. (A-C) Corresponding ImageJ image analysis masks from the whole lung overview images in Fig 3. A-C, which demonstrate accurate thresholding for determination of total lung lobe area (black) and CT26-GFP+ tumor cell cluster area (overlaid in green), used in the quantification of pulmonary micrometastatic burden expressed in Fig 3D. (A) Control, (B) losartan-treated, and (C) $CCR2^{-/-}$.

In addition, when performing the image analysis for F4/80^{+} MAM density (Fig. 2.4 D-I), we also observed a striking reduction in the number of CT26-GFP^{+} colonies in the lungs of losartan-treated and CCR2$^{-/-}$ mice as compared to control mice. Using ImageJ (NIH), we quantified the area of all CT26-GFP micrometastases as a percentage of total lung lobe area, which was reduced by 70% and 90% in losartan-treated and CCR2$^{-/-}$ mice, respectively, as compared to un-treated control mice (Fig. 2.5 & 2.6). These results suggested that losartan-mediated blockade of IM recruitment was associated with decreased tumor cell engraftment of the lungs. Additional image analysis quantifying the average size (μm^2) of CT26-GFP micrometastases, as well as Ki67 immunoreactivity of CT26-GFP cells suggested that this reduction in total micrometastatic burden was predominately the result of decreased tumor cell extravasation/retention within the lungs, and not necessarily reduced tumor cell growth following colonization, as GFP+ tumor cells displayed positive nuclear immunoreactivity for Ki67, and no significant difference in the average size of CT26GFP micrometastases was observed between control and losartan treated mice (data not shown).

Losartan and its primary metabolite inhibit CCL2-induced ERK1/2 phosphorylation and reduce cell surface CCR2 expression in monocytes

While results of the in vitro chemotaxis and in vivo vaccine and tumor-elicited monocyte recruitment assays strongly suggested that losartan blocks CCL2-CCR2 directed monocyte migration, we still sought to determine whether or not this effect was due to direct inhibition of CCL2-induced CCR2 signaling by losartan or its EXP-3174 metabolite. Prior studies have demonstrated that CCL2-induced integrin activation and

monocyte chemotaxis is mediated through the mitogen-activated protein kinase/extracellular signal-regulated kinase (MAPK/ERK) pathway. Thus, we evaluated the inhibitory effect of losartan and EXP-3174 on CCL2-induced ERK1/2 activation in THP-1 cells, using western blot and intracellular flow cytometry assays to detect phospho-ERK1/2 (Fig. 2.7). For these assays, human THP-1 cells were pre-treated with losartan/EXP-3174 for various durations at pharmacologically relevant concentrations that resulted in drug exposure levels similar to those observed in our prior mouse studies (Fig. 2.13). Cells were then stimulated with 20nM CCL2, a concentration previously reported to induce strong and rapid activation (phosphorylation) of ERK1/2, and were subsequently fixed or lysed and analyzed by intracellular flow cytometry and western blot. Results of phospho-ERK1/2 flow cytometry demonstrated that both losartan and EXP-3174 significantly inhibited ERK activation in response to CCL2 to ~25% of that observed in un-treated cells (Fig. 2.7 A, B). Similarly, a dose-dependent inhibition of ERK1/2 phosphorylation by both losartan and EXP-3174 was also observed in human peripheral blood-derived CD14+ monocytes (Fig. 2.8 A, B). In addition, we evaluated ERK1/2 phosphorylation by western blot analysis of THP-1 cells following either acute (Fig. 2.7C) or chronic/prolonged (Fig. 2.7D) CCL2 stimulation (as would be expected in a tumor-bearing individual), which showed similar results. Both losartan and EXP-3174 inhibited ERK activation in response to CCL2 by 29% and 42% following acute stimulation, respectively, and 67% and 65%, following prolonged 24h CCL2 stimulation, respectively (Fig. 2.7 C, D).

As it is plausible that the observed effects of both losartan and EXP-3174 on CCL2-induced ERK stimulation and monocyte chemotaxis could be due to drug-induced

receptor down regulation, we evaluated cell surface CCR2 expression in losartan or EXP-3174 pre-treated THP-1 cells by flow cytometry. Indeed, flow cytometry demonstrated a moderate dose and time-dependent reduction in cell surface CCR2 expression following losartan or EXP-3174 treatment, an effect which appeared additive with combination treatment (Fig. 2.7 E, F). In addition, similar results of reduced CCR2 cell surface expression by losartan and EXP-3174 treatment were also observed in human peripheral blood CD14+ monocytes (Fig. 2.8 C, D) and murine bone-marrow derived $CD11b^{+}/Ly6C^{+}$ monocytes (Fig. 2.8 E, F). Thus, while these results suggest that losartan and EXP-3174's effects on CCL2-induced ERK activation could in part be secondary to drug-induced CCR2 receptor down regulation, the degree to which losartan or EXP-3174 reduced CCR2 expression was not concordant with the observed inhibitory effect of these drugs on CCL2-induced ERK1/2 phosphorylation. As it is known that CCR2 and other G-protein coupled receptors are internalized following ligand (chemokine or drug) binding, and that receptor internalization following agonist or antagonist binding has been demonstrated to be an accurate indirect measurement of beta-arresting recruitment, we felt that these results instead were more consistent with additional indirect evidence of binding of losartan and EXP-3174 to CCR2.

Pharmacological characterization of losartan, EXP-3174, and CCR2 interactions

Based on the above results, we hypothesized that losartan and its metabolite were in fact directly antagonizing CCR2 signaling, and decided to conduct additional experiments to better pharmacologically characterize this interaction. Using the THP-1 cell line, which was confirmed to express high levels of CCR2 by flow cytometry, we

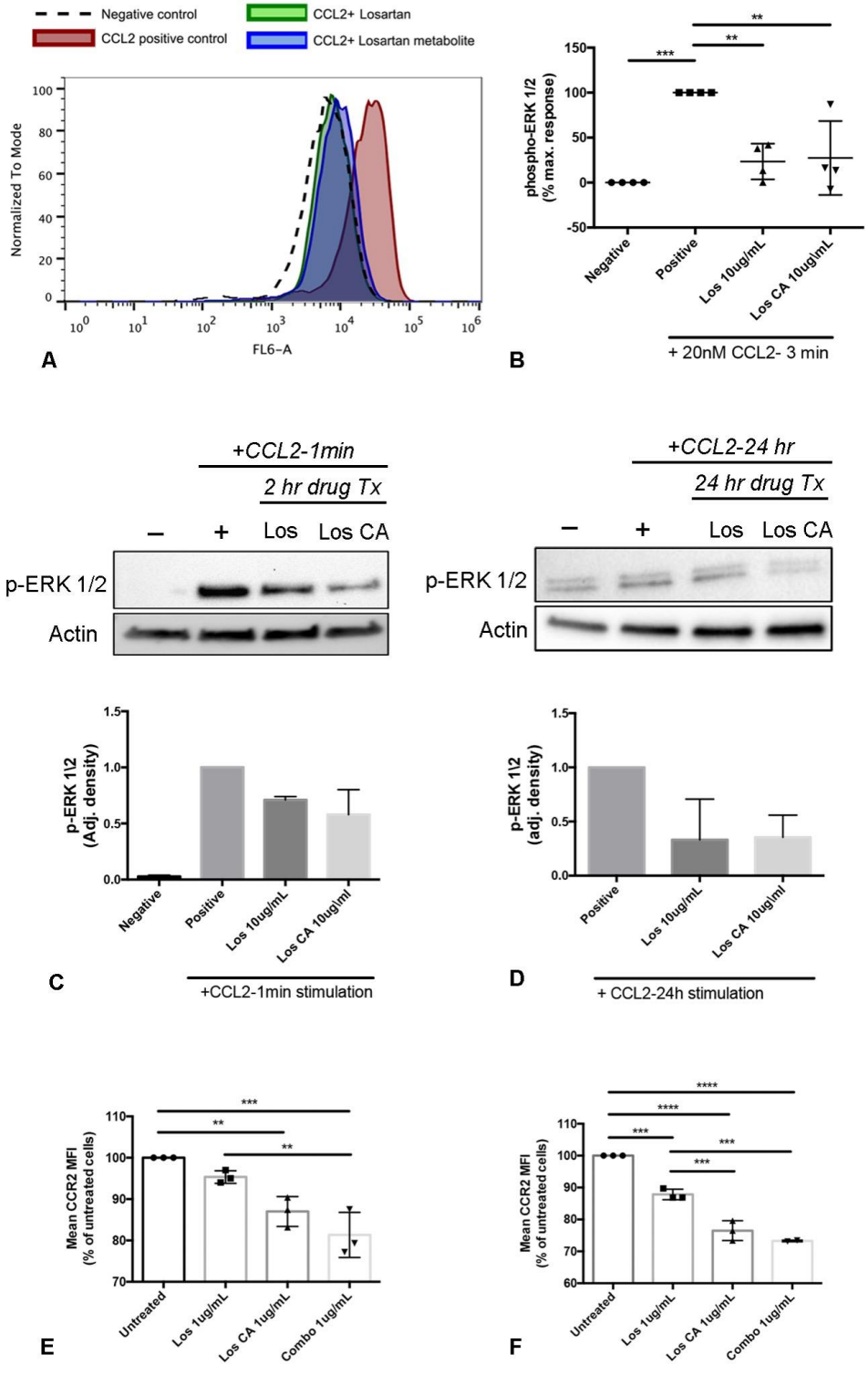

Figure 2.7. Losartan and its EXP3174 metabolite inhibit *CCL2*-mediated *ERK 1/2* phosphorylation in THP-1 monocytes. (A) Histogram overlay of phospho-*ERK 1/2* expression in THP-1 cells which were either untreated (negative control), or stimulated

for 3 min with 20nM *CCL2,* +/- 1hr pre-treatment with losartan or losartan EXP3174 metabolite at 10 μg/mL. (B) Graph demonstrating the % inhibition of *CCL2*-induced *ERK 1/2* phosphorylation. The maximum *CCL2*-induced response was determined as the mean difference in p-*ERK1/2* geometric mean fluorescence intensity (MFI) between unstimulated and *CCL2*-stimulated THP-1 cells. (C and D) Western blots and graphs quantifying the effects of losartan and losartan EXP3174 metabolite treatment on inhibition of *ERK1/2* activation in THP-1 cells following acute (C) or prolonged (D) *CCL2* agonist stimulation. (E and F) Effects of losartan, EXP3174 metabolite, or combination therapy on *CCR2* cell surface expression, as assessed by flow cytometry, in THP-1 cells following short (E) and long-term (F) drug treatment at clinically relevant concentrations. Data expressed as means ± SD, and were analyzed by One-way ANOVA, with Tukey's post-test comparison (n=2-4 independent experiments, each performed in duplicate or triplicate, independent experiments, **p < 0.01, ***p < 0.001, ****p<0.0001).

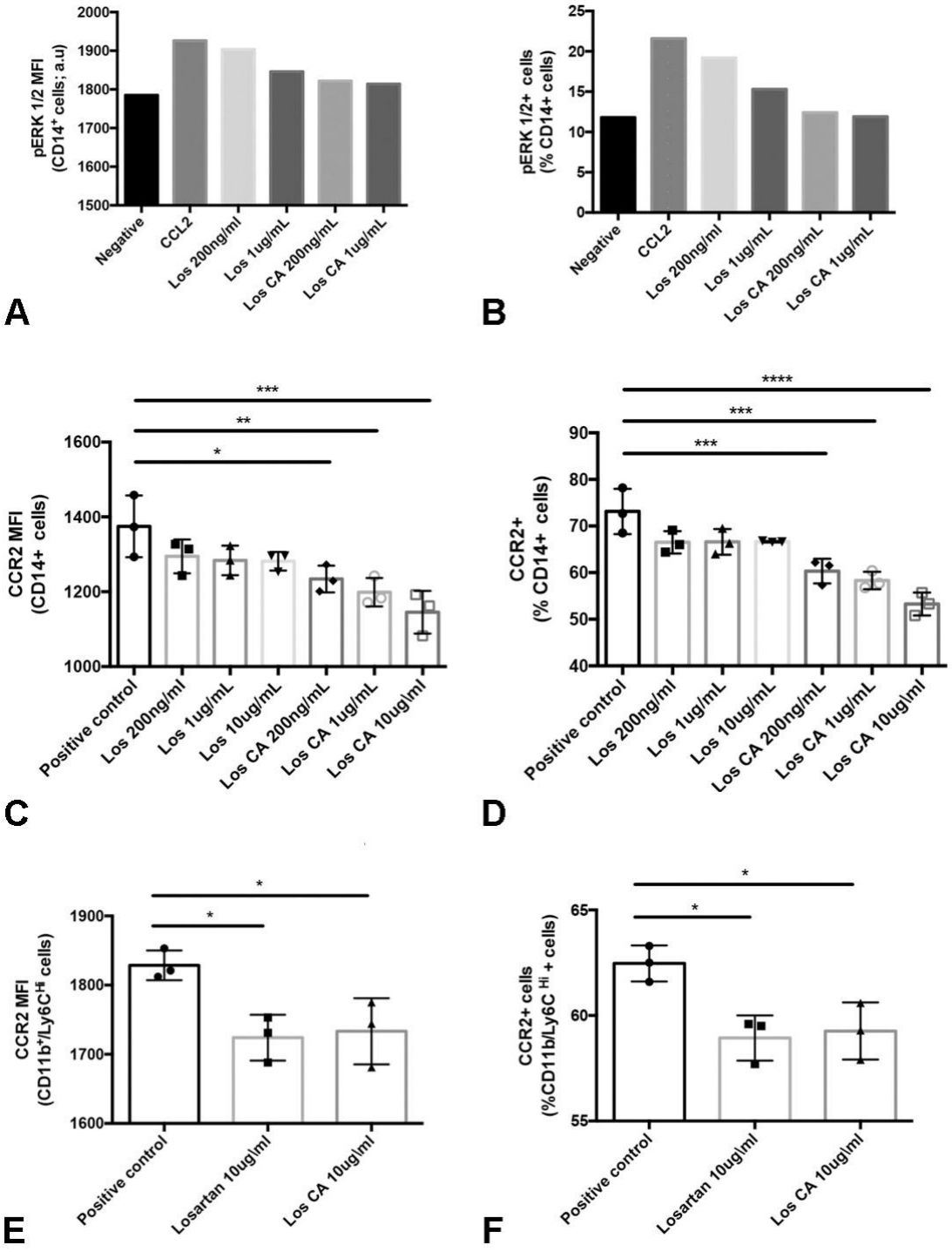

Figure 2.8. Losartan and it's EXP3174 metabolite also reduce *CCL2*-mediated *ERK1/2* activation and decrease *CCR2* cell surface expression in primary human monocytes and murine bone marrow monocytes**.** (A, B) Graphs showing flow cytometric quantification of *CCL2*-mediated *ERK1/2* activation in human peripheral blood $CD14^{+}$

monocytes, +/- pre-treatment with losartan or losartan EXP3174 metabolite. (A) *pERK1/2* geometric MFI in $CD14^+$ monocytes, and (B) *pERK1/2*$^+$ cells as % of total gated $CD14^+$ monocytes. (C, D) Graphs of flow cytometric quantification of cell surface *CCR2* expression in human peripheral blood $CD14^+$ monocytes following 4 hour treatment with a range of clinically relevant concentrations of losartan and EXP3174 metabolite. (C) *CCR2* geometric MFI of CD14+ cells, and (D) *CCR2*$^+$ cells as % of total gated $CD14^+$ cells. (E, F) Flow cytometric quantification of cell surface *CCR2* expression in $Ly6G^-/CD11b^+/Ly6C^+$ murine bone marrow monocytes. Data expressed as *CCR2* geometric MFI (E) and *CCR2*+ as % of total gated monocytes (F). Cells were treated with 10 μg/mL losartan or EXP3174 for 4 hours prior to analysis, mirroring drug exposure levels observed in vivo with once daily 60mg/kg losartan dosing (Fig. S6). Data expressed as means ± SD, and were analyzed by One-way ANOVA, with Tukey's post-test comparison, and represents one independent experiment performed in triplicate (C-F), **p<0.05, **p < 0.01, ***p < 0.001, ****p<0.0001*.

evaluated the effects of losartan and EXP-3174 metabolite on recombinant hCCL2 ligand binding and CCL2-induced intracellular Ca^{2+} release. As a comparison, we used the previously discovered, potent, human CCR2 antagonist INCB3284 as a positive control. Surprisingly, results of the ligand-binding studies demonstrated that while INCB3284 could inhibit 75% of hCCL2 biding at a concentration of 100nM, reaching its maximal inhibitory effect at 1 μM, both losartan and its metabolite completely failed to block CCL2 binding at concentrations ranging from 1 nM to 100 μM (Fig. 2.9 A-C). In contrast, results of the Ca^{2+} flux assays demonstrated that at equimolar concentrations, both losartan and EXP-3174 did indeed block CCL2-stimulated cytosolic calcium release, although in a less potent fashion as compared to INCB3284 (Fig. 2.9 D&E). One hour pre-treatment with 10 μM losartan and EXP-3174 inhibited the CCL2-induced maximal calcium response by 54% and 36%, respectively, while treatment with 10 μM INCB3284 inhibited this response by 92% (Data expressed as % of mean Δ relative fluorescence units, determined as maximum fluorescence observed post CCL2 stimulation minus baseline fluorescence in untreated cells) (Fig. 2.9, E).

Thus, by means of two separate functional assays, we demonstrate that both losartan and EXP-3174 are antagonists of CCR2 signaling at the level of cytosolic Ca^{2+} release and downstream ERK1/2 phosphorylation. Although the results of the Ca^{2+} flux assay suggest only a modest inhibitory activity against the receptor for this functional assay, it should be noted that prior studies by Jimenez-Sainz et al. have elegantly dissected the second messengers required for CCL2-induced activation of ERK1/2, showing that ERK activation was in fact independent of CCR2 receptor internalization or

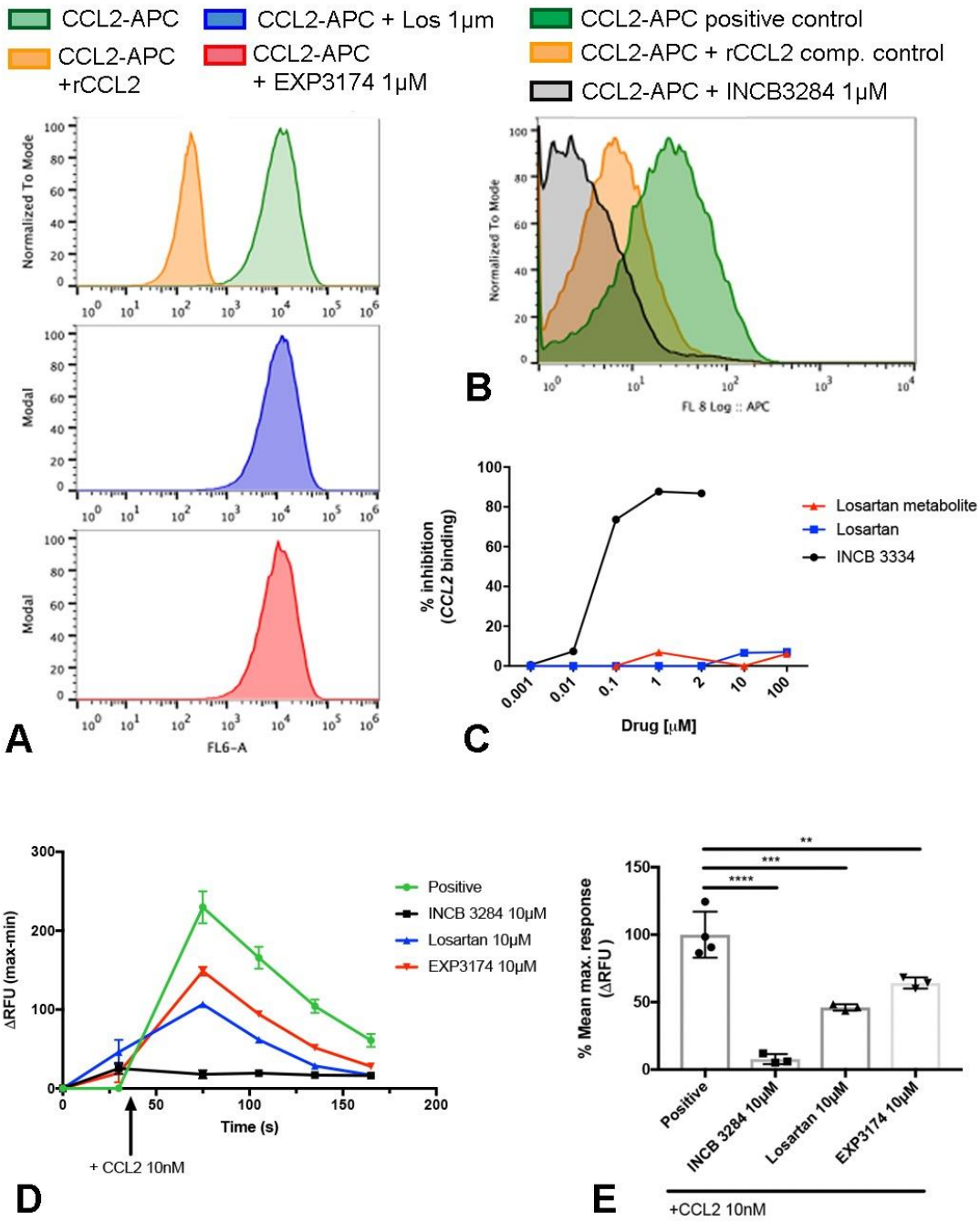

Figure 2.9. Losartan and EXP3174 losartan metabolite do not block *CCL2* ligand binding, but inhibit *CCL2*-induced cytoplasmic Ca^{2+} release in THP-1 monocytes. (A-C) *CCL2* binding was assessed by flow cytometry using fluorescently labeled human r*CCL2* (CCL2-APC). (A, B) Representative histograms showing complete lack of inhibition of *CCL2* ligand binding by losartan or EXP3174 metabolite, which is in striking

contrast to the orthosteric *CCR2* antagonist, INCB3344. (B) Graph depicting flow cytometric measurement of % inhibition of *CCL2* binding for losartan, EXP3174 metabolite, and INCB3344 across a broad range of drug concentrations. (D) Overlay of calcium trace plots for THP-1 cells stimulated with 20nM *CCL2* +/- 1hr pre-treatment with the indicated concentrations of losartan, EXP3174, or the *CCR2* antagonist RS102895. THP-1 cells were loaded with Fluo-3AM to detect *CCL2*-induced calcium flux over time using the kinetics measurement function of a fluorescent plate reader. Data expressed as means ± SEM (D), or SD (E), and were analyzed by One-way ANOVA, with Tukey's post-test comparison, and represents one independent experiment performed in triplicate (C-F), $**p < 0.01$, $***p < 0.001$, $****p<0.0001$.

changes in cytosolic [Ca^{2+}], but required G_i proteins, protein kinase C (PKC), phospho-inositide-3-kinase (PI3K), and RAS. Given that the end consequence of CCL2-CCR2 signaling for monocyte chemotaxis is ERK1/2 activation, and both losartan and EXP-3174 inhibited this process by $\geq$ 75%, these results corroborate the potent in vitro and in vivo inhibition of monocyte recruitment we observed for losartan and EXP-3174. Lastly, as both losartan and EXP-3174 failed to inhibit CCL2 ligand binding over a wide range of concentrations, which was in contrast to the competitive antagonism we observed for INCB3284, these data taken together suggest that both losartan and EXP-3174 appear to function as non-competitive antagonists of CCR2.

Losartan-mediated blockade of inflammatory monocyte recruitment suppresses tumor growth in 4T1 and CT26 experimental pulmonary metastasis models

Given the known role of CCL2-CCR2 recruited IMs in the promotion of tumor metastasis in pre-clinical models of breast and colon cancer, we next sought to determine whether losartan's ability to inhibit CCR2 signaling and monocyte recruitment could suppress metastasis growth in murine 4T1 and CT26 experimental metastasis models. For these experiments, luciferase-transfected 4T1 breast (1×10^5) or CT26

colon carcinoma (2.5 x 10^5) cells were injected in the lateral tail vein of syngeneic BALB/c mice, losartan treatment (60 mg • kg^{-1} • d^{-1} i.p.) was initiated 24 hours post-injection, and metastatic burden was monitored via thrice weekly bioluminescence imaging of mice on the IVIS 100 imager. Daily treatment with losartan significantly reduced both CT26 and 4T1 pulmonary metastatic burden by 64% and 90%, respectively, as quantified by bioluminescent imaging (CT26: Fig. 2.10 A-C, and 4T1; Fig. 2.11 A-B). In the 4T1 model, these results were paralleled by an observed similar reduction in metastatic burden via histopathological evaluation of the lungs at euthanasia (Fig. 2.11 D). In addition, in the 4T1 model, daily losartan treatment also significantly prolonged overall survival, increasing median survival to 23 days in losartan treated mice as compared to 21 days in vehicle treated mice (Fig. 2.11 C, *p=0.04). Importantly, in both the CT26 and 4T1 models, daily losartan treatment resulted in

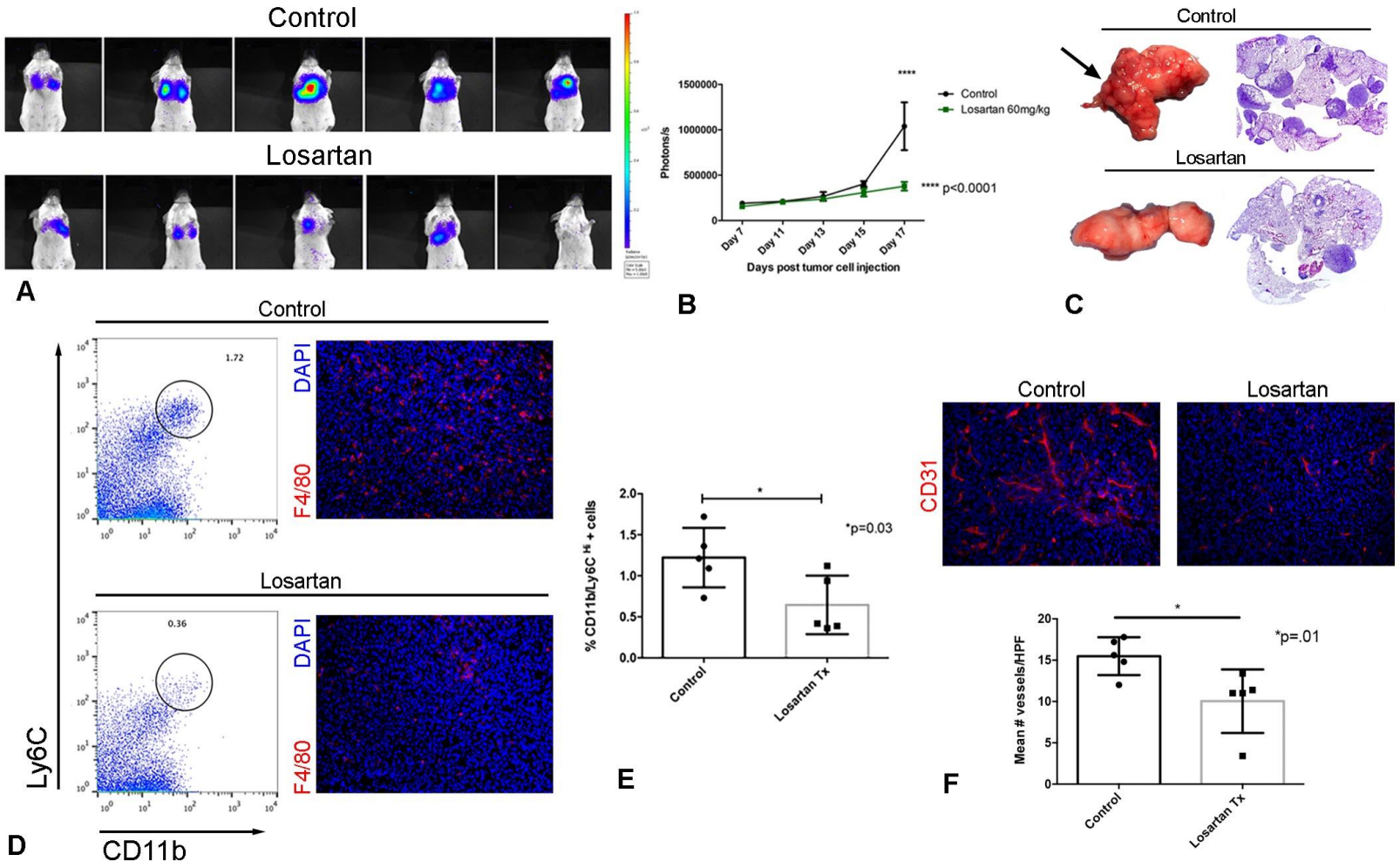

Figure 2.10. Daily treatment with losartan reduces pulmonary metastasis growth in a CT26luc experimental metastasis model**.** (A) IVIS bioluminescent images of CT26luc pulmonary metastases in control and losartan-treated mice on day 17, immediately prior to euthanasia. (B) Graph depicting CT26luc pulmonary metastatic burden over time as quantified by repeated bioluminescent imaging. (C) Representative gross images and sub-gross photomicrographs of the lungs of mice from control and losartan treated groups shown in (A&B). (D) At euthanasia, lung IMs were quantified by flow cytometry,

and MAMs assessed by *F4/80* immunofluorescent staining. Shown are representative dot plots gated on *CD11b*$^{+}$*/Ly6C*^{Hi} cells, and corresponding *F4/80*$^{+}$ immunofluorescent images of pulmonary metastases. (E) Graph depicting flow cytometric quantification of lung IMs at sacrifice for the groups of mice shown in (A-D). (F) Representative CD31 immunofluorescent images and associated graph of quantification of tumor micro-vessel as assessed by CD31 staining of pulmonary metastases. Data expressed as means ± SD, and were analyzed by Two-way ANOVA (B), or two-tailed Student's *t* test (E,F), (n= 5 mice/group, *$p<0.05$, ****$p < 0.0001$).

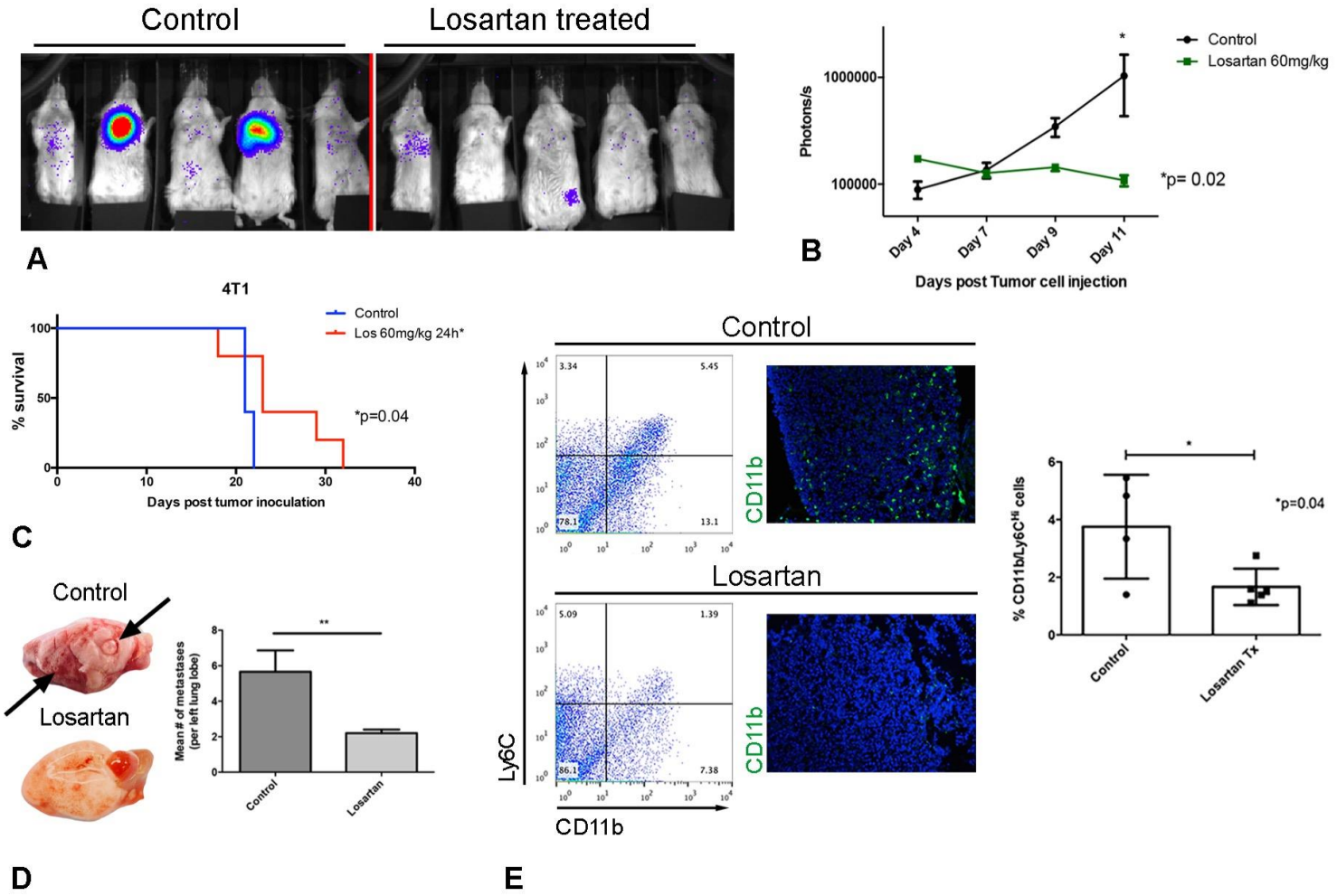

Figure 2.11. Losartan also demonstrates anti-metastatic activity in a 4T1luc experimental pulmonary metastasis model**.** (A) IVIS bioluminescent images of 4T1luc pulmonary metastases in control and losartan-treated mice on day 11, immediately prior to euthanasia. (B) Graph depicting 4T1luc pulmonary metastatic burden over time as quantified by repeated bioluminescent imaging. (C) Kaplan-Meier (KM) survival curves of 4T1luc control or losartan-treated mice. (D) Representative gross images of the lungs of mice from control and losartan treated groups shown in (A&B), and graph of

histological quantification of pulmonary metastatic burden as assessed by H&E staining in these mice. (E) Lung IMs were quantified by flow cytometry at euthanasia, and MAMs assessed by *CD11b* immunofluorescent staining. Shown are representative dot plots gated on *CD11b*$^{+}$/*Ly6C*^{Hi} cells, corresponding *CD11b*$^{+}$ immunofluorescent images of pulmonary metastases, and graph depicting flow cytometric quantification of lung IMs at sacrifice for the groups of mice shown in (A, B, & D). Data expressed as means ± SD, and were analyzed by Two-way ANOVA (B), Log-rank test (C), or two-tailed Student's *t* test (D, E), (n= 5 mice/group, **p<0.05*, ***p* < 0.01).

significant, sustained inhibition of $CD11b^{+}/Ly6C^{Hi}$ IM recruitment to the lungs of metastasis-bearing mice, as flow cytometric analysis of lung IMs at study termination (day 19 for CT26 mice and day 14 for 4T1 mice) showed an ~ 2-fold reduction in the percentage of lung IMs in losartan-treated as compared to vehicle (saline)-treated mice (Fig. 2.10D and Fig. 2.11E). Consistent with the flow cytometry results, immunofluorescent analysis of CT26 and 4T1 pulmonary metastases of from these same mice showed a similar reduction in tumor-infiltrating $F4/80^{+}$ and $CD11b^{+}$ myeloid cells, respectively. As IMs are known to be a rich source of VEGF, we also analyzed CT26 metastatic tumor microvessel density (MVD) in these mice by CD31 immunofluorescence. Quantification of CD31+ vessels within CT26 pulmonary metastases showed a 35% reduction in tumor MVD in losartan-treated as compared to control mice (Fig. 2.10F). Taken together, these results demonstrate that daily losartan treated effectively suppressed breast and colon carcinoma pulmonary colonization and growth, an effect which was associated with a significant reduction in lung IMs in treated vs control animals.

Increasingly, a role for the renin-angiotensin system (RAS) in the promotion of tumor growth via both tumor cell intrinsic and extrinsic (stromal-mediated) actions has been described (32). Specifically, these studies have demonstrated that autocrine angiotensin II-AT1R signaling in tumor cells can stimulate their proliferation, invasion, migration, and growth (33, 34), while AngII-AT1R signaling within the tumor stroma can drive tumor-promoting inflammation (35, 36), as well as tumor angiogenesis (37). Thus, it is plausible that the observed anti-tumor effects of losartan in our metastasis models could be due to direct inhibition of AngII-AT1R signaling, and not secondary to the

observed blockade of IM and tumor-macrophage recruitment. To address this, we first performed CT26luc experimental metastasis assays in BALB/c CCR2$^{-/-}$ mice, as we hypothesized that if losartan had additional anti-tumor effects mediated through AT1R blockade, we should observe enhanced suppression of CT26 metastasis growth in losartan-treated CCR2$^{-/-}$ mice. As expected, CT26 experimental metastasis growth was significantly reduced in CCR2$^{-/-}$ mice; however, the anti-metastatic effect of losartan treatment was not additive in these mice, and in fact was partially abolished in the absence of CCR2$^{-/-}$ (Fig. 2.12 A), suggesting that the presence of CCR2 was required for the anti-tumor mechanism of losartan in this model. To further evaluate the potential role of AngII-AT1R mediated effects in our models, we quantified in vitro 4T1 and CT26 CCL2 and AngII production, as well as in vivo serum AngII levels in CT26 metastasis bearing mice by ELISA. Results of these assays demonstrated that both 4T1 and CT26 cells produced substantially more CCL2 as compared to AngII in vitro (Fig. 2.12 B), and that serum AngII levels were not elevated in CT26 metastasis-bearing control (175.7 $\pm$ 46.8) or losartan-treated mice (143.4 $\pm$ 37.4), as compared to naïve, BALB/c mice (176.1 $\pm$ 9.5) (Fig. 2.12 C, Mean $\pm$ SEM pg/mL). Lastly, a possible direct anti-proliferative/cytotoxic effect of losartan on CT26 and 4T1 cells was assessed in vitro by MTT assay. 72-hour treatment of CT26 or 4T1 cells with a losartan concentration roughly equivalent to overall exposure observed in our in vivo pharmacokinetic studies

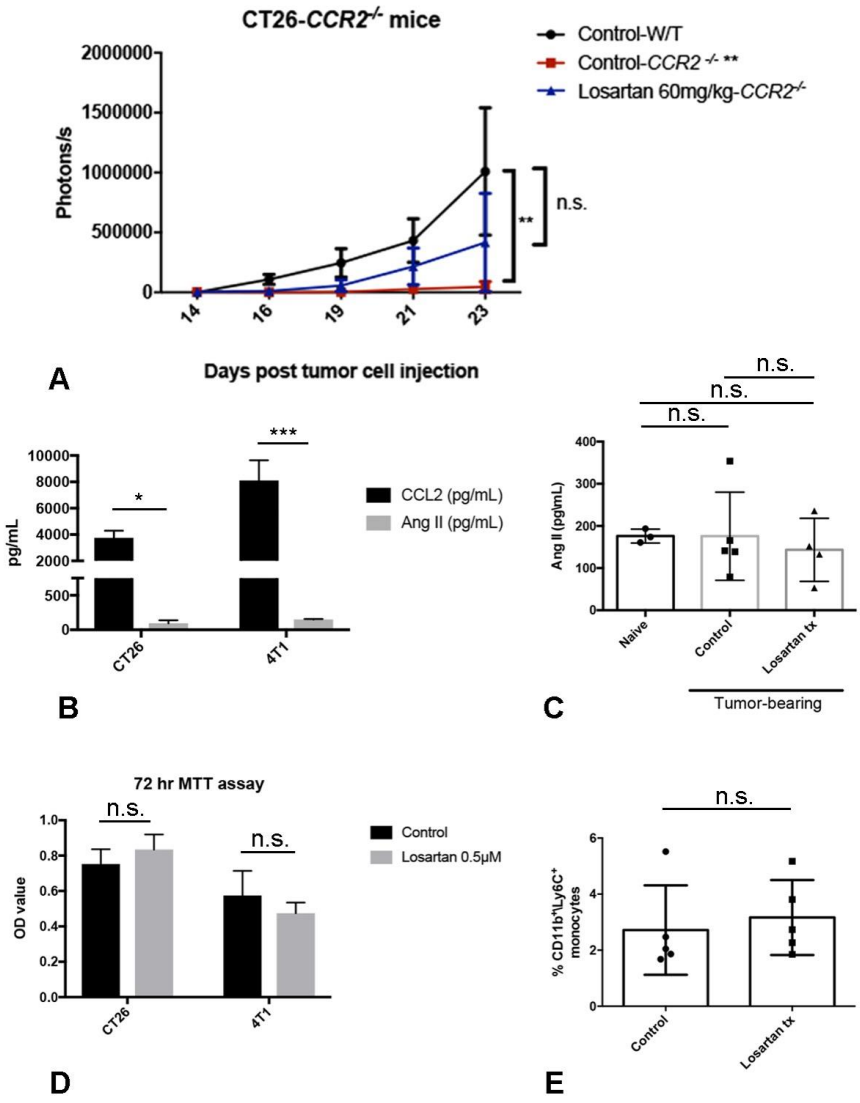

Figure 2.12. Losartan-mediated blockade of IM recruitment and associated anti-tumor effects are not associated with changes in Angiotensin II-AT1R signaling. (A) Graph depicting CT26luc pulmonary metastatic burden over time in control and losartan-treated *CCR2*$^{-/-}$ mice, as quantified by repeated bioluminescent imaging. (B) In vitro *CCL2* and *AngII* production by 4T1 and CT26 cell lines, measured by ELISA assay performed on cell culture supernatants following 24h of culture. (C) Ang II levels in the serum of control and losartan-treated CT26luc pulmonary metastasis-bearing mice vs naïve BALB/c mice, as measured by EIA. (D) Results of MTT assay following 72hr treatment of 4T1 or CT26 cells with losartan at the indicated concentration. (E) Splenic IMs were measured by flow cytometry in CT26luc metastasis-bearing mice on Day 21 post tumor cell injection. Data expressed as means ± SD, and were analyzed by two-way ANOVA (A, B), one-way ANOVA (C) or two-tailed Student's *t* test (D, E), (n= 3-5 mice/group (A, C, & D). (*$p<0.05$, **$p < 0.01$, ***$p<0.001$; not significant, n.s.)

(as determined by AUC0-∞) showed no significant reduction in tumor cell survival/proliferation (Fig. 2.12 D). In addition, treatment of CT26 tumor cells with losartan or losartan EXP-3174 had no effect on CCL2 production by these cells (data not shown).

Cortez-Retamozo et al., have previously demonstrated a unique role for AngII-ATIR signaling in splenic myelopoiesis and subsequent $Ly6C^{Hi}$ monocyte recruitment to the lungs of tumor-bearing mice in the KRAS-p53 (KP) conditional model of NSCLC (38). To determine if a similar signaling axis was present in the CT26 model, we evaluated the percentage of $CD11b^{+}\backslash Ly6C^{+}$ monocytes in the spleens of CT26 metastasis bearing mice on day 21. In contrast to the findings in the KP mouse model, in which disruption of AT1R signaling reduced the number of splenic monocytes, losartan did not significantly alter the percentage of splenic monocytes in treated vs control CT26 metastasis bearing mice (Fig. 2.12 E).

Finally, pharmacokinetic analysis after 14 days of i.p. losartan dosing in mice was performed to determine: 1. If the observed anti-tumor effects in losartan-treated mice were associated with plasma drug levels equivalent to those demonstrated to inhibit CCR2 signaling in our in vitro THP-1 studies, and 2. To assess the clinical relevance and potential to achieve these doses in humans. Fig. 2.13 (A) shows the mean plasma concentration of both losartan and EXP-3174 in mice following a single i.p. dose of 60 $mg \bullet kg^{-1}$ on day 14, and the table in Fig. 2.13 (B) summarizes pertinent pK parameters. Indeed, the maximum plasma concentration (C_{max}) and overall exposure (area under the curve, $AUC_{0-\infty}$) in these mice was well within the range of the demonstrated effective

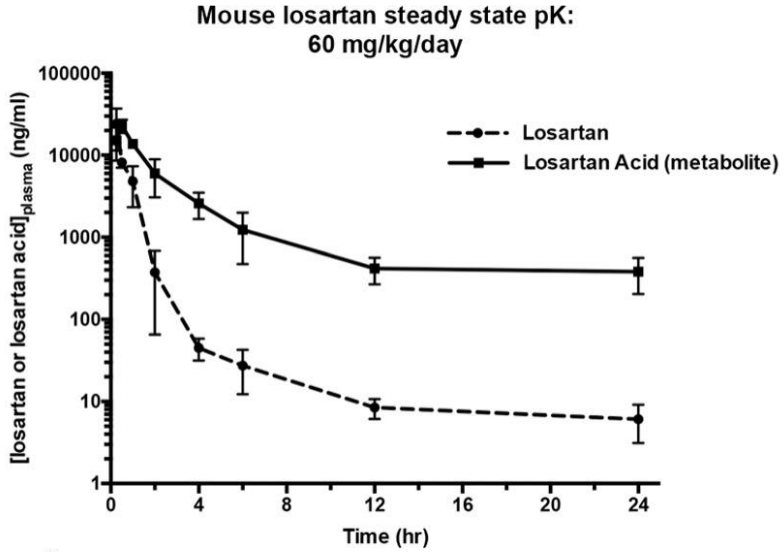

B

Parameters				
	$C_{max\ (\mu g/mL)}$	$AUC_{0-\infty\ (\mu g*hr/mL)}$	$T_{1/2,\ \lambda\ (hr)}$	$C_{24h\ (ng/mL)}$
Losartan	24.3 ± 12.8	13.62	25.8	6.11 ± 2.99
Losartan carboxylic acid metabolite (EXP 3174)	22.9 ± 4.2	47.83	–	382 ± 178

Figure 2.13. Steady-state pharmacokinetics of high dose losartan in mice**.** (A) Mean plasma concentration of losartan and losartan carboxylic acid metabolite (EXP3174) in mice following 14 days of intra-peritoneal dosing at 60mg/kg once daily. Drug levels were measured by LC/MS/MS at the indicated post-dose time points following the last dose on day 14. (B) Table summarizing *pK* parameters from data shown in (A). Data representative of the mean ± SD, n=3 mice per time point.

concentrations in our in vitro CCR2 functional assays. In addition, the half-life ($t_{1/2}$) of both losartan and EXP-3174 at these steady state doses confirmed that 1x per day dosing was sufficient for CCR2 target inhibition. Of important note, EXP-3174 demonstrated significant plasma accumulation with two week once daily dosing, which given the activity of this metabolite against CCR2, suggests a very favorable pK profile for sustained inhibition of CCR2 mediated monocyte recruitment.

Discussion

There is now a substantial amount of data from mouse models of metastasis describing the importance of myeloid cells, and in particular Ly6C$^+$ IMs, in the facilitation of multiple steps of the metastatic cascade (12). Specifically, these studies implicate IMs in conditioning the pre-metastatic site (39) and promoting tumor cell extravasation and growth (16, 40), and have all demonstrated a critical role for CCL2-CCR2 in their recruitment to metastases (13, 39, 41, 42). Validating the relevance of these pre-clinical findings are an increasing number of clinical studies demonstrating the importance of monocytes and/or CCL2 in the prognosis of various human malignancies (18-20, 43), further highlighting the potential of CCL2-CCR2 as a valuable therapeutic target for the treatment of metastasis. Despite this, at present, there are only two ongoing and/or recently completed trials of CCR2 targeted therapies in cancer patients (ClinicalTrials.gov, NCT01015560 and NCT02732938), and prior attempts at targeting CCL2 were unsuccessful (22). Thus, we sought to determine whether the AT1R antagonist losartan, a drug known to modulate monocyte and macrophage responses in

other inflammatory diseases, could be re-purposed as a CCR2 antagonist for the treatment of cancer metastasis.

Using in vitro chemotaxis assays and in vivo models of acute inflammation and experimental pulmonary metastasis, we demonstrate that losartan and its primary metabolite (EXP-3174) effectively inhibit CCL2-CCR2 mediated inflammatory monocyte recruitment. While studies in models of atherosclerosis and auto-immune encephalomyelitis have associated losartan with inhibition of monocyte recruitment via perturbations in CCL2 and/or CCR2, losartan's mechanism of action in these models was shown to be entirely due to a primary inhibition of AngII-AT1R mediated inflammation. Here, via three separate CCR2 functional assays, we provide evidence that losartan and its primary EXP-3174 metabolite can directly antagonize CCL2-CCR2 signaling. We show that losartan and EXP-3174 inhibit CCR2 signaling at the level of cytosolic Ca^{2+} flux and downstream ERK phosphorylation, in a manner that was not associated with inhibition of CCL2-ligand binding, consistent with non-competitive inhibition of CCR2. Interestingly, recent molecular studies on CCR2 have described the presence of a novel, highly druggable, intracellular, allosteric binding site for CCR2 antagonists (44, 45). Based on this observation, we utilized previously published homology models of CCR2 to perform docking studies for both losartan and EXP-3174, which show that indeed, these molecules do bind to CCR2 at this intracellular allosteric site (data unpublished). These preliminary modeling findings are in agreement with the observed lack of inhibition of CCL2-ligand binding, and the overall results of our CCR2 functional studies reported here. Future experiments to verify these modeling results via

assessment of losartan and EXP-3174's effects on CCR2 activation following site-directed mutagenesis of the ortho- and allosteric binding pockets of CCR2 are planned.

Given the continued substantial need for the development of drugs which target metastatic disease, we sought to determine whether losartan, based on its demonstrated inhibition of CCL2-CCR2 signaling, could be re-purposed as an adjunct anti-metastatic therapy. By utilizing experimental metastasis models, we chose to limit our evaluation of losartan's anti-tumor effects to a defined step of the metastatic cascade, removing potential confounding effects of losartan's impact on primary tumor growth or invasion. We demonstrate in these models that tumor cell colonization of the lung was strongly associated with Ly6C^{Hi} IM recruitment, in a process which was dependent on the presence of CCR2, and that losartan therapy prevented this early (72hr) tumor cell colonization, and subsequent IM recruitment and MAM accumulation, to a degree similar to that observed with genetic knockout of CCR2. Using two different tumor cell lines, we show that daily losartan therapy suppresses experimental metastasis growth in a process which was associated with sustained inhibition IM monocyte recruitment and a reduction in metastasis-associated myeloid cells. Lastly, as losartan is an already FDA-approved and known to be same drug, and thus has potential to be rapidly repurposed as an anti-metastatic agent, we felt it was essential to compare the pharmacokinetics of high-dose losartan used in our mouse studies with previously published losartan pK studies in humans. Direct comparison of losartan Cmax and AUC0-∞ observed in our mice suggests that this dose results in ~ 6-fold higher exposure than that published for a single 200 mg dose in humans. However, the drug concentrations evaluated in our in vitro chemotaxis and CCR2 functional assays

were lower than those measured in our in vivo mouse studies, and in the range expected with 2-3 mg • kg^{-1} dosing in humans, doses which are achievable and have already been used in Marfan's syndrome and losartan pK studies in humans, respectively (46, 47).

It is important to note that several other pre-clinical studies in mice have also demonstrated anti-tumor effects associated with losartan monotherapy, albeit using doses 3-5 time greater than used in our studies (48-50). In addition, retrospective analyses of clinical data of patients being treated for hypertension have shown a correlation between the use of losartan, or other ARBs and ACE-inhibitors, with improved outcomes in patients with pancreatic, breast, or lung cancer (33, 51-53). In these models, losartan's anti-tumor mechanism of action was primarily associated with either indirect anti-angiogenic or anti-TGF-β signaling effects, or direct anti-invasive properties, all of which were the downstream result of primary inhibition of AngII-AT1R signaling, and the therapeutic benefit in human cancer patients was presumed to be secondary to these effects. However, it is not without reason to suggest that these previously described anti-angiogenic and TGF-β effects of losartan are not in part the result of its overlapping effects on monocyte/macrophage recruitment, as these cells are known drivers of angiogenesis and TGF-β production in tumors (54, 55). Regardless, the data from our models suggests that this suppression of metastasis is unlikely to be the result of inhibition of AT1R signaling in tumor or stromal cells, as the cell lines used in our models produced significantly less AngII as compared to CCL2, and metastasis-bearing mice did not have elevated serum levels of AngII as compared to naïve, control mice. In addition, losartan therapy did not reduce the tumor-associated macrophage

reservoir of splenic IMs, a previously described effect of AT1R inhibition in the KP mouse model of NSCLC (38). Lastly, it is unlikely that the observed anti-metastatic effects of losartan were due to intrinsic effects on tumor cells, as in our models, losartan therapy was not initiated until 24 hours after tumor cell inoculation and lung colonization, and no direct inhibition of 4T1 or CT26 tumor cell survival/proliferation by losartan was observed in vitro.

In conclusion, our studies demonstrate a unique and previously undescribed mechanism of direct inhibition of CCL2-CCR2 signaling and monocyte recruitment by losartan and its primary EXP-3174 metabolite, and show that daily losartan therapy is effective in suppressing experimental metastasis growth, in a manner which was associated with sustained blockade of inflammatory monocyte mobilization and with suppression of accumulation of metastasis-associated myeloid cells. These results provide another, yet undescribed, anti-tumor mechanism of losartan, in addition to its previously documented effects on angiogenesis and TGF-β signaling. Indeed, this new understanding of losartan's mechanism of action could explain all of the previously described phenomena associated with losartan therapy for cancer. In summary, these data further substantiate the potential clinical utility of losartan in cancer patients, and suggest that this low cost, safe, and already-approved drug, could be rapidly repurposed as an adjuvant therapy for patients at high risk of metastasis.

REFERENCES

1. Mehlen P & Puisieux A (2006) Metastasis: a question of life or death. *Nat Rev Cancer* 6(6):449-458.

2. Monteiro J & Fodde R (2010) Cancer stemness and metastasis: therapeutic consequences and perspectives. *Eur J Cancer* 46(7):1198-1203.

3. Howlader N NA, Krapcho M, Miller D, Bishop K, Altekruse SF, Kosary CL, Yu M, Ruhl J, Tatalovich Z, Mariotto A, Lewis DR, Chen HS, Feuer EJ, Cronin KA (eds). SEER Cancer Statistics Review, 1975-2013, National Cancer Institute. Bethesda, MD, http://seer.cancer.gov/csr/1975_2013/, based on November 2015 SEER data submission, posted to the SEER web site, April 2016.

4. Weigelt B, Peterse JL, & van 't Veer LJ (2005) Breast cancer metastasis: markers and models. *Nat Rev Cancer* 5(8):591-602.

5. O'Shaughnessy J (2005) Extending survival with chemotherapy in metastatic breast cancer. *The oncologist* 10 Suppl 3:20-29.

6. Van Cutsem E & Oliveira J (2009) Advanced colorectal cancer: ESMO clinical recommendations for diagnosis, treatment and follow-up. *Annals of oncology : official journal of the European Society for Medical Oncology* 20 Suppl 4:61-63.

7. Sleeman J & Steeg PS (2010) Cancer metastasis as a therapeutic target. *Eur J Cancer* 46(7):1177-1180.

8. Khanna C*, et al.* (2014) Toward a drug development path that targets metastatic progression in osteosarcoma. *Clin Cancer Res* 20(16):4200-4209.

9. Steeg PS (2016) Targeting metastasis. *Nat Rev Cancer* 16(4):201-218.

10. Hanahan D & Weinberg RA (2011) Hallmarks of cancer: the next generation. *Cell* 144(5):646-674.

11. Liu Y & Cao X (2016) Characteristics and Significance of the Pre-metastatic Niche. *Cancer Cell* 30(5):668-681.

12. Kitamura T, Qian BZ, & Pollard JW (2015) Immune cell promotion of metastasis. *Nat Rev Immunol* 15(2):73-86.

13. Qian BZ*, et al.* (2011) CCL2 recruits inflammatory monocytes to facilitate breast-tumour metastasis. *Nature* 475(7355):222-225.

14. Piao C*, et al.* (2015) Complement 5a Enhances Hepatic Metastases of Colon Cancer via Monocyte Chemoattractant Protein-1-mediated Inflammatory Cell Infiltration. *The Journal of biological chemistry* 290(17):10667-10676.

15. Qian BZ*, et al.* (2015) FLT1 signaling in metastasis-associated macrophages activates an inflammatory signature that promotes breast cancer metastasis. *J Exp Med* 212(9):1433-1448.

16. Chen Q, Zhang XH, & Massague J (2011) Macrophage binding to receptor VCAM-1 transmits survival signals in breast cancer cells that invade the lungs. *Cancer Cell* 20(4):538-549.

17. Mazzieri R*, et al.* (2011) Targeting the ANG2/TIE2 axis inhibits tumor growth and metastasis by impairing angiogenesis and disabling rebounds of proangiogenic myeloid cells. *Cancer Cell* 19(4):512-526.

18. Sanford DE*, et al.* (2013) Inflammatory monocyte mobilization decreases patient survival in pancreatic cancer: a role for targeting the CCL2/CCR2 axis. *Clin Cancer Res* 19(13):3404-3415.

19. Sasaki A*, et al.* (2007) Prognostic value of preoperative peripheral blood monocyte count in patients with colorectal liver metastasis after liver resection. *Journal of gastrointestinal surgery : official journal of the Society for Surgery of the Alimentary Tract* 11(5):596-602.

20. Ni XJ*, et al.* (2014) An elevated peripheral blood lymphocyte-to-monocyte ratio predicts favorable response and prognosis in locally advanced breast cancer following neoadjuvant chemotherapy. *PLoS One* 9(11):e111886.

21. Svensson S*, et al.* (2015) CCL2 and CCL5 Are Novel Therapeutic Targets for Estrogen-Dependent Breast Cancer. *Clin Cancer Res* 21(16):3794-3805.

22. Sandhu SK*, et al.* (2013) A first-in-human, first-in-class, phase I study of carlumab (CNTO 888), a human monoclonal antibody against CC-chemokine ligand 2 in patients with solid tumors. *Cancer chemotherapy and pharmacology* 71(4):1041-1050.

23. Nywening TM*, et al.* (2016) Targeting tumour-associated macrophages with CCR2 inhibition in combination with FOLFIRINOX in patients with borderline resectable and locally advanced pancreatic cancer: a single-centre, open-label, dose-finding, non-randomised, phase 1b trial. *The Lancet. Oncology* 17(5):651-662.

24. DiMasi JA & Grabowski HG (2007) Economics of new oncology drug development. *J Clin Oncol* 25(2):209-216.

25. Kola I & Landis J (2004) Can the pharmaceutical industry reduce attrition rates? *Nature reviews. Drug discovery* 3(8):711-715.

26. Mullard A (2014) New drugs cost US[dollar]2.6 billion to develop. *Nature reviews. Drug discovery* 13(12):877-877.

27. Bertolini F, Sukhatme VP, & Bouche G (2015) Drug repurposing in oncology--patient and health systems opportunities. *Nature reviews. Clinical oncology* 12(12):732-742.

28. Stegbauer J*, et al.* (2009) Role of the renin-angiotensin system in autoimmune inflammation of the central nervous system. *Proc Natl Acad Sci U S A* 106(35):14942-14947.

29. Yang J*, et al.* (2015) Comparison of angiotensin-(1-7), losartan and their combination on atherosclerotic plaque formation in apolipoprotein E knockout mice. *Atherosclerosis* 240(2):544-549.

30. Dai Q, Xu M, Yao M, & Sun B (2007) Angiotensin AT1 receptor antagonists exert anti-inflammatory effects in spontaneously hypertensive rats. *British journal of pharmacology* 152(7):1042-1048.

31. Marshall TG, Lee RE, & Marshall FE (2006) Common angiotensin receptor blockers may directly modulate the immune system via VDR, PPAR and CCR2b. *Theoretical biology & medical modelling* 3:1.

32. George AJ, Thomas WG, & Hannan RD (2010) The renin-angiotensin system and cancer: old dog, new tricks. *Nat Rev Cancer* 10(11):745-759.

33. Rhodes DR*, et al.* (2009) AGTR1 overexpression defines a subset of breast cancer and confers sensitivity to losartan, an AGTR1 antagonist. *Proc Natl Acad Sci U S A* 106(25):10284-10289.

34. Suganuma T*, et al.* (2005) Functional expression of the angiotensin II type 1 receptor in human ovarian carcinoma cells and its blockade therapy resulting in suppression of tumor invasion, angiogenesis, and peritoneal dissemination. *Clin Cancer Res* 11(7):2686-2694.

35. Suzuki Y*, et al.* (2003) Inflammation and angiotensin II. *The international journal of biochemistry & cell biology* 35(6):881-900.

36. Chehl N*, et al.* (2009) Angiotensin II regulates the expression of monocyte chemoattractant protein-1 in pancreatic cancer cells. *Journal of gastrointestinal surgery : official journal of the Society for Surgery of the Alimentary Tract* 13(12):2189-2200.

37. Fujita M*, et al.* (2005) Angiotensin type 1a receptor signaling-dependent induction of vascular endothelial growth factor in stroma is relevant to tumor-associated angiogenesis and tumor growth. *Carcinogenesis* 26(2):271-279.

38. Cortez-Retamozo V*, et al.* (2013) Angiotensin II drives the production of tumor-promoting macrophages. *Immunity* 38(2):296-308.

39. van Deventer HW, Palmieri DA, Wu QP, McCook EC, & Serody JS (2013) Circulating fibrocytes prepare the lung for cancer metastasis by recruiting Ly-6C+ monocytes via CCL2. *J Immunol* 190(9):4861-4867.

40. Qian B*, et al.* (2009) A distinct macrophage population mediates metastatic breast cancer cell extravasation, establishment and growth. *PLoS One* 4(8):e6562.

41. Zhao L*, et al.* (2013) Recruitment of a myeloid cell subset (CD11b/Gr1 mid) via CCL2/CCR2 promotes the development of colorectal cancer liver metastasis. *Hepatology (Baltimore, Md.)* 57(2):829-839.

42. Hoos A, Protsyuk D, & Borsig L (2014) Metastatic growth progression caused by PSGL-1-mediated recruitment of monocytes to metastatic sites. *Cancer Res* 74(3):695-704.

43. Izumi K*, et al.* (2016) Serum chemokine (CC motif) ligand 2 level as a diagnostic, predictive, and prognostic biomarker for prostate cancer. *Oncotarget* 7(7):8389-8398.

44. Zweemer AJ*, et al.* (2014) Discovery and mapping of an intracellular antagonist binding site at the chemokine receptor CCR2. *Molecular pharmacology* 86(4):358-368.

45. Zheng Y*, et al.* (2016) Structure of CC chemokine receptor 2 with orthosteric and allosteric antagonists. *Nature* 540(7633):458-461.

46. Ohtawa M, Takayama F, Saitoh K, Yoshinaga T, & Nakashima M (1993) Pharmacokinetics and biochemical efficacy after single and multiple oral administration of losartan, an orally active nonpeptide angiotensin II receptor antagonist, in humans. *British journal of clinical pharmacology* 35(3):290-297.

47. Brooke BS*, et al.* (2008) Angiotensin II blockade and aortic-root dilation in Marfan's syndrome. *N Engl J Med* 358(26):2787-2795.

48. Arnold SA*, et al.* (2012) Losartan slows pancreatic tumor progression and extends survival of SPARC-null mice by abrogating aberrant TGFbeta activation. *PLoS One* 7(2):e31384.

49. Otake AH*, et al.* (2010) Inhibition of angiotensin II receptor 1 limits tumor-associated angiogenesis and attenuates growth of murine melanoma. *Cancer chemotherapy and pharmacology* 66(1):79-87.

50. Noguchi R*, et al.* (2009) Synergistic inhibitory effect of gemcitabine and angiotensin type-1 receptor blocker, losartan, on murine pancreatic tumor growth via anti-angiogenic activities. *Oncology reports* 22(2):355-360.

51. Chae YK*, et al.* (2011) Reduced risk of breast cancer recurrence in patients using ACE inhibitors, ARBs, and/or statins. *Cancer investigation* 29(9):585-593.

52. Miao L*, et al.* (2016) Impact of Angiotensin I-converting Enzyme Inhibitors and Angiotensin II Type-1 Receptor Blockers on Survival of Patients with NSCLC. *Scientific reports* 6:21359.

53. Nakai Y*, et al.* (2010) Inhibition of renin-angiotensin system affects prognosis of advanced pancreatic cancer receiving gemcitabine. *British journal of cancer* 103(11):1644-1648.

54. Dalton HJ*, et al.* (2014) Monocyte subpopulations in angiogenesis. *Cancer Res* 74(5):1287-1293.

55. Solinas G, Germano G, Mantovani A, & Allavena P (2009) Tumor-associated macrophages (TAM) as major players of the cancer-related inflammation. *J Leukoc Biol* 86(5):1065-1073.

CHAPTER 3

Role of monocyte recruitment in hemangiosarcoma metastasis in dogs

Summary

Canine hemangiosarcoma is a highly malignant tumor, which is associated with poor long-term survival due to the development of early and widespread metastatic disease. Currently, little is known regarding the biology of canine hemangiosarcoma, and the mechanisms accounting for the highly metastatic nature of the tumor are poorly understood. In humans and rodents, monocytes have been shown to play key roles in metastasis through promotion of tumor cell extravasation, seeding, growth, and angiogenesis, as well as suppression of anti-tumor immunity. However, there has been little investigation into the role of monocytes in canine tumor metastasis. Therefore, we investigated the potential role of monocyte infiltration in the regulation of tumor metastasis in dogs. To address this question, we initially performed immunohistochemistry for CD18 to determine the degree of monocyte infiltration in necropsy samples obtained from several common metastatic tumors of dogs, including hemangiosarcoma, osteosarcoma, and various carcinomas. We found that compared to other tumor types, hemangiosarcoma metastases had significantly greater infiltration of CD18+ monocytes. Next, migration assays were used to compare the ability of tumor cell lines to stimulate monocyte migration in vitro. Hemangiosarcoma cell lines were among the strongest at stimulating monocyte migration, and were also found to be the highest producers of the monocyte chemoattractant CCL2. In addition, hemangiosarcoma metastases in vivo were found to produce large amounts of CCL2,

compared to other tumor metastases. These results are consistent therefore with the hypothesis that overexpression of CCL2 and recruitment of large numbers of monocytes may explain in part the aggressive metastatic nature of canine hemangiosarcoma. Moreover, these findings suggest that immunotherapeutic interventions designed to block monocyte recruitment or mobilization may be an effective adjuvant strategy for suppressing tumor metastasis in dogs with hemangiosarcoma.

Introduction

Hemangiosarcoma (HSA) is a malignant vascular neoplasm, which occurs spontaneously in the dog more frequently than any other species (1, 2). Specifically, canine hemangiosarcoma comprises 5-7% of all non-cutaneous malignant canine neoplasms, with the most common primary tumor sites including the right atrium/auricle, spleen, and skin/subcutis (3-10). Based on its histomorphological appearance, the tumor is presumed to arise from transformed endothelial cells; however, the tumors' origins are still under debate, and more recent investigations into the genotypic nature of hemangiosarcoma in dogs and humans show that the tumor likely originates from hematopoietic endothelial progenitor cells (11, 12).

In the dog, hemangiosarcoma is characterized by very aggressive biological behavior and a high rate of rapid and widespread metastasis, with 1-year survival rates following surgery +\- adjuvant chemotherapy reported to be less than 10% (13-16). Current standard of care for canine hemangiosarcoma includes surgical removal of the primary tumor, followed by adjuvant chemotherapy consisting of either a conventional protocol, typically with the anthracycline drug doxorubicin (DOX), or cyclophosphamide-

based metronomic therapy (13-15, 17, 18). However, these adjuvant therapies do little to slow the development and/or growth of metastases, with median survival times for either chemotherapy protocol reported to be 6 months or less in multiple, independent studies (13, 14, 17-19). As such, numerous clinical trials evaluating alternative treatment modalities for canine hemangiosarcoma have been performed, including addition of the anti-angiogenic drug minocycline or the non-specific immune stimulant L-MTP-PE to DOX therapy, doxorubicin dose intensification, and combination metronomic therapy with etoposide, cyclophosphamide, and piroxicam (13, 15, 19-21). However, the majority of these investigative therapies have failed to extend survival times in the post-surgical period, with only L-MTP-PE providing a significant, although still modest, increase in median survival time as compared to DOX therapy alone (162 days vs. 96 days MST, respectively) (15). This lack of efficacious treatments for canine hemangiosarcoma is not surprising however, given the critical knowledge gaps currently present in our understanding of the fundamental biological processes driving the pathogenesis of this tumor.

Inflammatory monocytes (IMs) are one immune cell subset of a heterogeneous population of immature myeloid cells, which have been shown to play key roles in promoting tumor metastasis in both humans and pre-clinical rodent models (22, 23). In contrast to resident monocytes, inflammatory monocytes are defined in part by their high surface expression of the chemokine receptor CCR2 (23). Both tumor and stromal cells at sites of metastases have been shown to produce abundant amounts of the monocyte chemoattractant and CCR2 ligand, CCL2, which efficiently recruits these $CCR2^{+}$ inflammatory monocytes as early as 24 hours following the seeding of

metastatic tumor cells within the lung (23). This CCL2-CCR2 chemotactic axis serves to provide a continual supply of IMs to metastatic sites, whereby these cells can differentiate into metastasis-associated macrophages (MAMs), which function to prepare the metastatic microenvironment for the continued arrival of tumor cells via production of various cytokines and growth factors (22-25). These macrophage-derived soluble factors are critical to the multi-step processes of tumor cell extravasation, survival, growth, and angiogenesis, which are required for the efficient colonization and subsequent outgrowth of tumor cells at the metastatic site. Substantiating these seminal observations in mice, and providing direct clinical evidence supporting a role for inflammatory monocytes in tumor progression in humans are multiple studies demonstrating that pre-treatment elevations in peripheral blood monocyte count and serum CCL2 levels are both negative prognostic indicators for a variety of cancers in people, including melanoma, lymphoma, and carcinomas of the prostate, colon, and kidney, among others (26-32).

Despite rapid gains in our understanding of myeloid cell promotion of tumor growth and metastasis in human oncology, there have been limited investigations into the role of monocytes and other myeloid-derived cells in canine cancer, and currently, their role in tumor metastasis in dogs is poorly defined. Independent results from two retrospective studies performed in tumor-bearing dogs do however provide strong evidence that peripheral blood monocyte counts could have prognostic relevance in canine cancer (33, 34). In one study which evaluated pre-treatment blood monocyte counts in 69 dogs with osteosarcoma, it was demonstrated that higher numbers of circulating monocytes (> $0.4x10^3$ cells/μL) was associated with significantly shorter

disease-free interval, with the proportion of dogs disease free at 1 year being approximately 50% less than dogs with low monocyte counts ($\leq 0.4 \times 10^3$ cells/μL) (34). In a separate but similar study of 26 dogs with lymphoma, Perry et al. demonstrated that serum CCL2 levels, and peripheral blood neutrophil and monocyte counts were significantly elevated in lymphoma-bearing dogs as compared to healthy controls, and that elevations in all three parameters were independently associated with significantly shorter disease free interval (33). In addition, serum CCL2 was also positively and significantly correlated with lymphoma disease stage in these patients.

A handful of other studies have retrospectively characterized the presence of tumor-associated myeloid cells/macrophages (TAMs) in primary canine tumor tissues of various type including melanoma, mammary carcinoma, seminoma, glioma, and nasal carcinoma (35-39). While a single study of canine mammary tumors demonstrated an association between a high density of TAMs and significantly decreased overall survival time (38), the majority of these studies were descriptive in nature and not focused specifically on myeloid cells, but aimed to more broadly characterize the diversity of intra-tumoral immune cell infiltrates. To our knowledge, the characterization of myeloid cells, and specifically monocytes, within metastatic canine tumors of any histo-type has not yet been evaluated, nor have the mechanisms driving the recruitment of these cells been investigated. Therefore, the purpose of this study was to characterize the density of tumor-associated myeloid cells within pulmonary metastases of multiple, common and highly metastatic canine tumor types using immunohistochemistry for CD18. In addition, we sought to determine the potential cellular and molecular mechanisms

responsible for the recruitment of these myeloid cells via in vitro trans well monocyte migration assays, CCL2 ELISA assays, and CCL2 immunohistochemistry.

We found that while all evaluated tumors had some degree of CD18+ myeloid cell infiltration within pulmonary metastases, hemangiosarcoma metastases had a uniquely intense CD18+ monocyte\macrophage infiltrate, which was significantly greater than other evaluated tumor types. In vitro assays demonstrated that hemangiosarcoma cells produce abundant amounts of the monocyte chemoattractant CCL2, and that hemangiosarcoma tumor-conditioned elicited strong canine monocyte migration, which could be significantly inhibited by the addition of CCL2 neutralizing antibody. In addition, hemangiosarcoma pulmonary metastases demonstrated intense positive immunolabeling for CCL2, and hemangiosarcoma tumor-bearing dogs had significantly elevated levels of serum CCL2 as compared to healthy control dogs. These findings demonstrate a potential unique role for CCL2-CCR2 mediated monocyte recruitment in promoting hemangiosarcoma metastasis in dogs, and suggest that recruitment of large numbers of monocytes may explain in part the highly aggressive metastatic nature of canine hemangiosarcoma. Thus, immunotherapeutic interventions designed to inhibit CCL2-CCR2 mediated monocyte recruitment might represent effective adjuvant therapies for suppressing tumor metastasis in dogs with hemangiosarcoma.

Materials and Methods

Tumor tissues

Formalin-fixed, paraffin-embedded (FFPE) tissues of pulmonary metastases of various canine tumor types were obtained from archived cases submitted to the

Colorado State University Veterinary Diagnostic Laboratory (CSU-VDL) for post-mortem evaluation between the years of 2007-2014. Evaluated tumor types included hemangiosarcoma (n=18), osteosarcoma (n=11), transitional cell carcinoma (n=4), melanoma (n=5), and soft tissue sarcoma (n=4). Necropsy reports from the CSU-VDL database were reviewed, and sections were cut and hematoxylin-eosin stained to confirm the previous diagnoses.

Immunohistochemistry

Tissue blocks were sectioned at 5 µm, mounted on Superfrost Plus slides (Fisher Scientific, Pittsburgh, PA) and immunolabeling for the β-2 integrin, pan-leukocyte marker CD18, and chemokine CCL2, was performed using standard methods. Briefly, tissue slides were de-paraffinized in xylenes and re-hydrated using a series of graded-alcohols. Antigen retrieval was performed using either: 1.) A proprietary Leica Bond enzyme-1 (Buffalo Grove, IL) enzymatic retrieval for 10 min (CD18), or 2.) 10mM sodium citrate buffer, pH 6.0, for 20 min at 125 °C in a pressurized chamber (CCL2). Immunolabeling was performed using either a Leica Bond Max autostainer (CD18), or Dako autostainer link 48 (CCL2). Tissues were blocked for endogenous peroxidase by incubation in 3% H_20_2 for 5 minutes. Subsequently, sections were then incubated with the following primary antibodies for 1 hr at room temperature (RT): mouse α canine CD18 (clone CA16.3C10), or rabbit α human CCL2 (Abcam, ab9669, 2.5 µg/ml). For CCL2, detection was performed using the universal labeled streptavidin-biotin2 system (Dako, Carpinteria, CA), which consists of incubation with a mixture of biotinylated goat anti- mouse and rabbit IgG secondary antibodies followed by horseradish peroxidase-

labeled streptavidin. For CD18, detection was performed using the Leica Bond Polymer Red Refine Detection (Buffalo Grove, IL) system, which consists of an alkaline phosphatase-linked rabbit anti-mouse IgG. Positive staining was visualized using either refine red (CD18) or DAB (CCL2) chromogen substrates.

CCL2 immunofluorescence

For intra-cellular CCL2 immunofluorescent staining, canine tumor cells (100,000 cells) in complete MEM media were grown on sterilized glass coverslips (Fisher Scientific, Waltham, MA USA) in 24-well plates for 24 h +\- a protein transport inhibitor (Brefeldin A, 10 ug\ml, BioLegend, San Diego, CA USA) for the last 4 hours of culture. After 24 h, cells were fixed in 1% paraformaldehyde for 10 minutes on ice, and then permeabilized via incubation with 0.1% Triton-X100 in PBS containing 0.5% Tween20 (PBST) for 15 minutes at room temperature. Non-specific binding was blocked by 30 min incubation with 5% donkey serum in 1% bovine serum albumin (BSA) (Calbiochem, San Diego, CA USA). Coverslips were incubated with the primary antibody (rabbit α human CCL2 (Abcam, ab9669, 2.5 µg/ml) diluted in 1% BSA containing 0.1% Triton-X100 for 1 hr at RT. Positive CCL2 labeling was visualized using a FITC-labeled donkey α rabbit IgG secondary antibody (Jackson ImmunoResearch Inc., West Grove, PA USA). Nuclei were counterstained with DAPI, and coverslips mounted onto glass slides using Fluoromount aqueous mounting media (Sigma-Aldrich, St. Louis, MO USA).

Western blot for cross-species validation of the anti-human CCL2 antibody

1 µg of recombinant canine CCL2 (R&D systems Inc., Minneapolis, MN USA) was mixed 1:1 with 2x Laemelli sample buffer containing 5% 2-Mercaptoethanol (BioRad Laboratories, Hercules, CA USA), boiled for 5 minutes, cooled on ice, and then loaded in a 20 µL volume into a Mini-Protean TGX 4-20% pre-cast polyacrylamide gel (BioRad Laboratories, Hercules, CA USA) for sodium dodecyl sulfate polyacrylamide gel electrophoresis (SDS-PAGE). SDS-PAGE was performed at 150 V for approximately 1 h. Protein was then wet transferred to nitrocellulose membranes (95 V, 50 min, at 4 °C), and membranes were blocked for 1 h at RT in a 5% non-fat dry milk in Tris-buffered saline Tween 20 solution (TBST). After washing in TBST, membranes were incubated with the primary antibody (1.25 µg /mL rabbit anti-human CCL2, abcam9669) diluted in 5% non-fat dry milk in TBST, overnight at 4 °C. The following day membranes were rinsed (x3 with TBST), incubated with the secondary antibody (HRP-linked goat anti-rabbit IgG; Thermo Scientific, Waltham, MA USA) diluted 1: 20,000 in 5% milk-TBST for 1 h at RT. Lastly, membranes were imaged with chemiluminescent substrate (Clarity Western ECL, BioRad) using a Chemi Doc XES + system (BioRad, Hercules, CA, USA).

Image analysis and quantification

For quantification of CD18+ immunoreactivity, (5-8) 40x magnification, intra-tumoral independent fields of multiple pulmonary metastases of each tumor were captured using standardized exposure times and either a Nikon 80i microscope and Olympus DP70 camera, or an Olympus IX83 microscope and Olympus SC30 camera.

In order to ensure accurate quantitative assessment of CD18+ cells, we used the color deconvolution algorithm developed for the NIH open-source image analysis software, ImageJ. Using the FastRed and FastBlue vectors for this algorithm, digitized intra-tumoral images of tumor metastases were separated in into 8-bit gray scale images representative of the chromogen color (red) only. A lower threshold limit was then set at a value corresponding to the mean of the isotype control, and universally applied to every single image. Any pixel value falling above this lower threshold value was measured as positive for CD18, and used to determine % area positive within the field. For quality control, image masks of the “thresholded”, positive counted area were also generated and directly visually compared to the originally captured photomicrographs by a board-certified pathologist, to ensure accuracy in representation of CD18+ immunoreactivity (Figure S3). This method was chosen as the most accurate representation of CD18+ immune cell infiltrates within tumor regions, as numerical quantification of single positive cells within tumor fields was impossible due to the marked density and overlap of CD18+ cells within tumor fields.

Tumor cell culture

The DEN-HSA hemangiosarcoma cell line was used for all in vitro monocyte migration and CCL2 immunofluorescence and ELISA assays. The DEN-HSA cell line was provided by Dr. Doug Thamm (Flint Animal Cancer Center), and was originally derived at the University of Wisconsin, Madison, WI from a spontaneous renal hemangiosarcoma of a Golden Retriever (41). Cells were maintained in MEM culture media (Gibco, Grand Island, NY USA) supplemented with 10% fetal bovine serum

(Atlas Biologicals, Fort Collins, CO USA), penicillin (100 U/mL), streptomycin (100 μg/mL), L-glutamine (2 mM), and non-essential amino acids (0.1 mM) (All obtained from Gibco). Cells were grown on standard plastic tissue culture flasks (Cell Treat, Shirley, MA USA), incubated under standard conditions of 37 °C, 5% CO_2, and humidified air.

In vitro monocyte migration assays and CCL2 neutralization

Peripheral Blood Mononuclear Cells (PBMCs) were isolated from fresh, EDTA-treated canine blood and used for in vitro trans-well migration assays to assess the degree to which HSA tumor-conditioned media elicited canine monocyte migration. For generation of tumor conditioned media, 100,000 DEN-HSA tumor cells were plated in a 24-well plate (Falcon) in 1 mL of complete MEM media and grown for approximately 24 hours prior to harvest of the culture supernatant. 600 µL of HSA-conditioned media was placed in the 24-well plate below each migration chamber to serve as the chemoattractant for the PBMCs. The negative control consisted of 600 µL of complete MEM media alone. The positive control consisted of 600 µL of complete MEM media containing 100 ng/mL of recombinant human CCL2 (Peprotech Inc. Rocky Hill, NJ). For CCL2 neutralization experiments, rabbit polyclonal anti-human CCL2 antibody (Abcam, ab9669) or rabbit IgG (Jackson ImmunoReserach, West Grove, PA) was added to the tumor conditioned media at 5 µg/mL immediately prior to addition of PBMCs. 250,000 PBMCs in 100 µL complete MEM were plated in the top well of the migration chamber insert. Subsequently, cells were allowed to migrate for 4 hours under standard conditions of 37 °C, 5% CO_2, and humidified air. Following migration, the non-migrated cells were removed, and membranes were fixed with ice-cold methanol for 10 min on

ice, stained with 3% crystal violet (Sigma-Aldrich, St. Louis, MO USA), rinsed with dH_20, and air-dried overnight. The following day, membranes were cut from the cell culture inserts, and mounted “migrated-side” up on superfrost plus glass slides using immersion oil. A total of (5) 40x fields per membrane were counted to determine the Mean # of monocytes/40x field for each membrane. Only cells displaying the appropriate nuclear and cytoplasmic characteristics consistent with monocytes were counted and included in the analysis. Neutrophils and lymphocytes were rarely observed on the migrated side of the membrane, but if present were excluded based on their segmented nuclear morphology, and nuclear:cytoplasmic ratio, respectively. Each migration assay was run in technical replicates at minimum, and each experiment was repeated at least once.

Serum and cell culture supernatant CCL2 analysis

A commercially available canine CCL2 ELISA kit (R&D Systems Inc., Minneapolis, MN USA) was used to measure the concentration of CCL2 in tumor-conditioned cell culture media and in the serum of healthy control and hemangiosarcoma-bearing dogs. For in vitro assessment of CCL2 production by HSA tumor cells, 200,000 were plated in a 24-well plate in 1 mL of complete MEM media, and grown for approximately 24 hr prior to harvesting the culture supernatants for ELISA assay. Due to the abundant amount of CCL2 produced by tumor cells, culture supernatants were diluted 1:20 (1:10 with MEM media, and 1:1 with the reagent diluent) prior to ELISA measurement, and a 7-point standard curve with a high standard of 4000 pg/mL was used to determine the concentration of CCL2 within the supernatant.

Appropriate controls included cell culture media alone, diluted on a 1:1 ratio with reagent diluent, as well as other canine tumor cell lines (data not shown).

For analysis of serum CCL2 levels in hemangiosarcoma-bearing dogs, archived, frozen, serum samples from dogs with a histologically confirmed diagnosis of hemangiosarcoma (n=24) were obtained from the tissue archive of the Flint Animal Cancer Center. For comparison, serum from "healthy" control dogs (n=6; median age=10 yrs., range 3-12 yrs.) was obtained from personal pets of laboratory personnel or from the Clinical Pathology Laboratory at Colorado State University. These animals were deemed healthy based on their history, medical records, and physical examination, and were not currently receiving any medications at the time of serum sampling.

Statistical analyses

For the comparison of mean values between three or more groups (% CD18+ area analysis, in vitro monocyte migration assays with CCL2 neutralization), a One-way ANOVA with Tukey's post-test was performed. For comparison of means between two groups (in vitro monocyte migration assays, CCL2 ELISA assays of serum samples and tumor-conditioned media) a two-tailed, unpaired *t* test was used. All statistical analyses were performed using Graph Pad Prism software (La Jolla, CA, USA).

Results

Immunohistochemical characterization of CD18^{+} cell infiltrates in pulmonary metastases of various canine tumor types

Positive immunostaining for CD18+ cells within pulmonary metastases was characterized by moderate to intense membranous to cytoplasmic labeling of individualized, round to sometimes slightly polygonal to elongate infiltrating immune cells (Fig. 3.1 A-D). These cells were easily distinguishable from tumor cells by their lack of cellular and nuclear pleomorphism. The CD18+ cells within metastases predominately consisted primarily of monocytes, along with a smaller population of CD18^{+} macrophages). The cellular features of the CD18+ cells included the following: 1) diameter larger than typical lymphocytes, containing a larger nucleus, increased cytoplasm, and a lower nuclear:cytoplasmic ratio, and 2) typical mononuclear morphology, characterized by a round to U-shaped nucleus, lacking the nuclear segmentation typical of neutrophils (Fig. 3.2).

Notably, despite the highly vascular nature of hemangiosarcoma, CD18^{+} cells within hemangiosarcoma metastases were predominately localized to the fibrous connective tissue stroma and connective tissue bundles forming the vascular spaces, and not within vascular spaces (Fig. 3.2). Additionally, hemangiosarcoma pulmonary metastases were often comprised of tumor cells arranged in sheets that resulted in an "epithelioid" appearance, which allowed for easier image capture and analysis of CD18^{+} cell density, as opposed to the highly vascular morphological appearance associated with hemangiosarcoma of the spleen, liver, right atrium, or elsewhere.

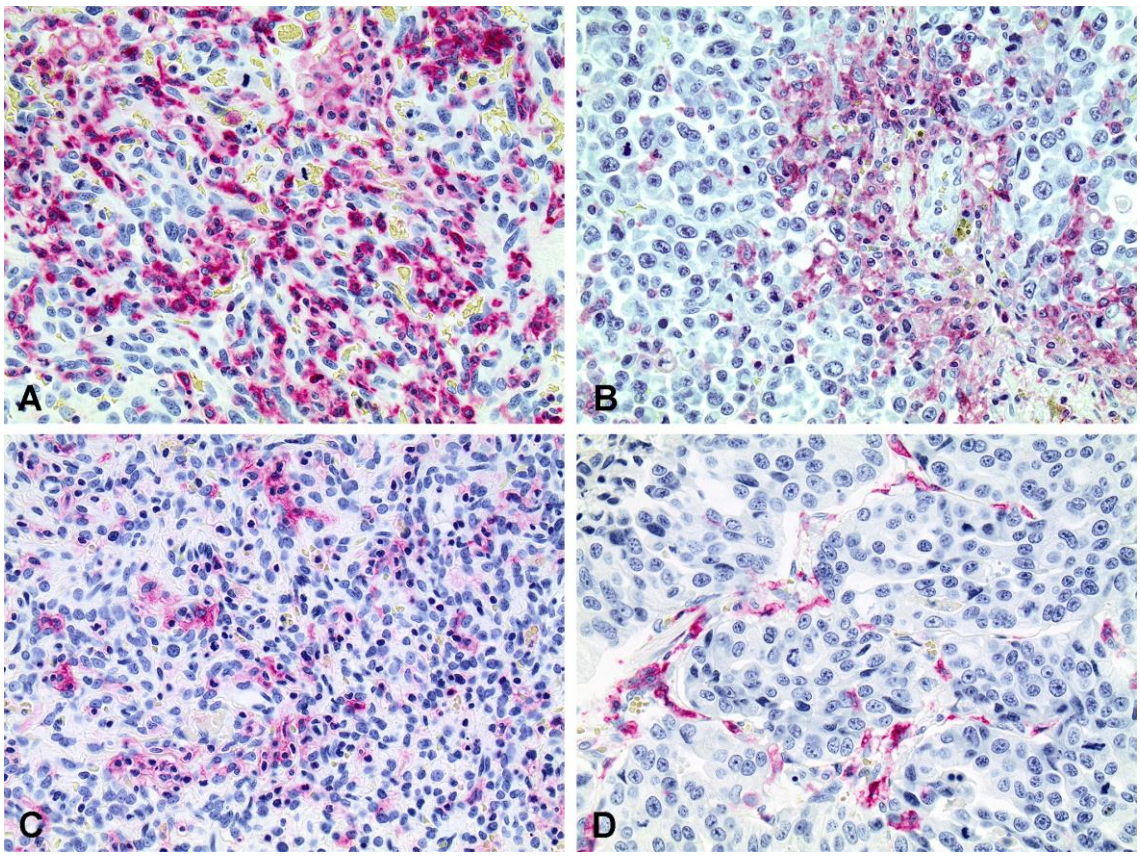

Figure 3.1. Representative photomicrographs of CD18+ myeloid cell infiltrates within pulmonary metastases of various canine tumor types. (A) The greatest density of infiltrating CD18+ cells were typically present within hemangiosarcoma metastases, and was frequently characterized by a very uniform, diffuse, distribution of CD18+ cells infiltrating throughout the tumor stroma. CD18+ cellular infiltrates within osteosarcoma (B), soft tissue sarcoma (C), and transitional cell carcinoma (D) metastases were typically less dense, and more frequently composed of multifocal, small to medium sized nodular clusters present throughout the tumor stroma. All images 40x magnification. Fast red chromogen. Hematoxylin counterstain.

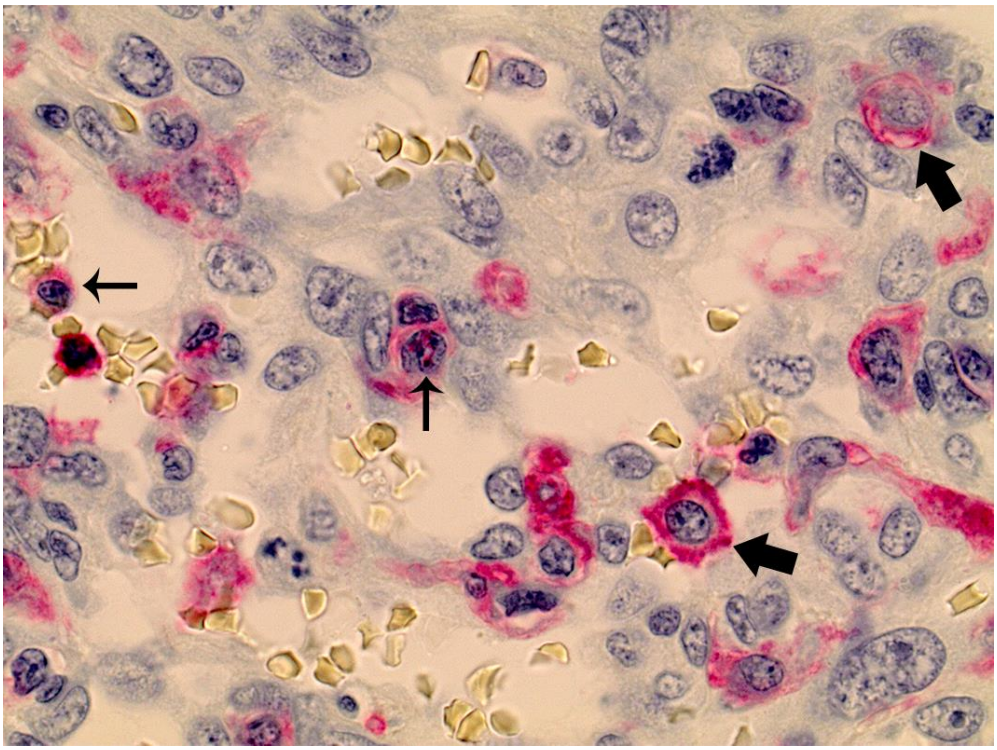

Figure 3.2. Higher magnification image of CD18+ myeloid cell infiltrates within a hemangiosarcoma metastasis. CD18+ cells were typically characterized by a U-shaped to round, mononuclear morphology, consistent with either monocyte (thin arrows) or macrophage (thick arrows) morphology. Importantly, CD18+ cellular infiltrates were localized to the tumor stroma and thin fibrovascular septa forming the vascular spaces, and were not present within the lumens of neoplastic vessels. 100x magnification. Fast red chromogen. Hematoxylin counterstain.

The micro-anatomical distribution and density of $CD18^+$ cellular infiltrates within pulmonary metastases varied between tumor types. For hemangiosarcoma metastases, the CD18+ cells had the greatest density and degree of uniformity in cellular infiltrates (Fig. 3.1A). For example, CD18+ cells were typically uniformly distributed, dense infiltrates throughout the tumor core, as well as forming dense rims 3-5 cell layers thick, which circumferentially surrounded the periphery of metastatic nodules (Fig. 3.3). In contrast, CD18+ cells within soft tissue sarcoma and osteosarcoma metastases were more frequently arranged in small to medium sized nodular clusters, randomly scattered throughout the tumor periphery and within the tumor core. Within melanoma and transitional cell carcinoma metastases, CD18+ cells were typically localized to within thin bands of reactive fibrous connective tissue stroma surrounding packets and nests of tumor cells, and were significantly less dense, individualized, and frequently more polygonal to elongate in appearance (Fig. 3.1 B-D). Lastly, the density of CD18+ cells varied within each tumor type, with some tumors exhibiting markedly high degrees of CD18+ cellular infiltrates, while other cases were almost completely devoid of CD18+ cells.

CD18+ cellular infiltrates are greatest within hemangiosarcoma pulmonary metastases

For accurate quantitative assessment of CD18+ cells, we used the ImageJ color deconvolution algorithm as described in Materials and Methods. For each image, a mask of the positive area as determined by ImageJ was generated and directly compared to its “parent” photomicrograph to ensure accuracy in automated assessment

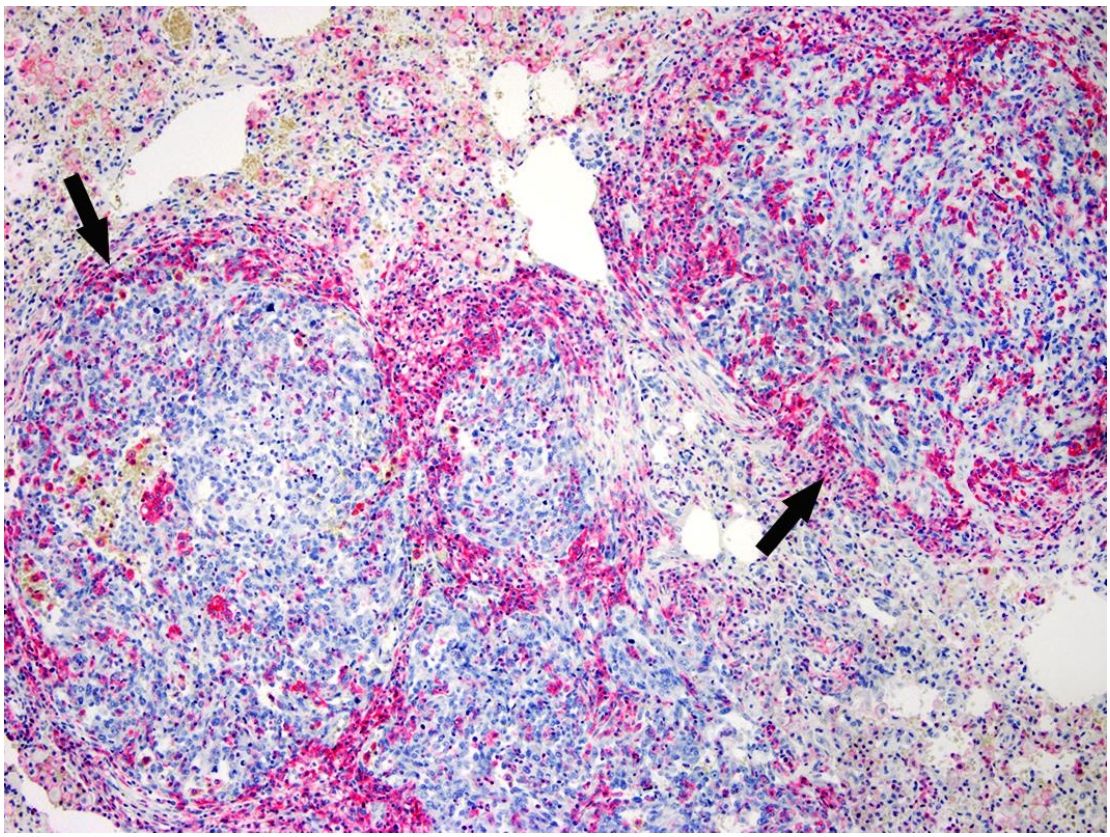

Figure 3.3. Overview of distribution of CD18+ cells within hemangiosarcoma metastases. Low-magnification image demonstrating CD18+ cells localized both circumferentially around the periphery of metastatic nodules (black arrows), as well as diffusely infiltrating through the tumor stroma and core of metastatic nodules. 10x magnification. Fast red chromogen. Hematoxylin counterstain.

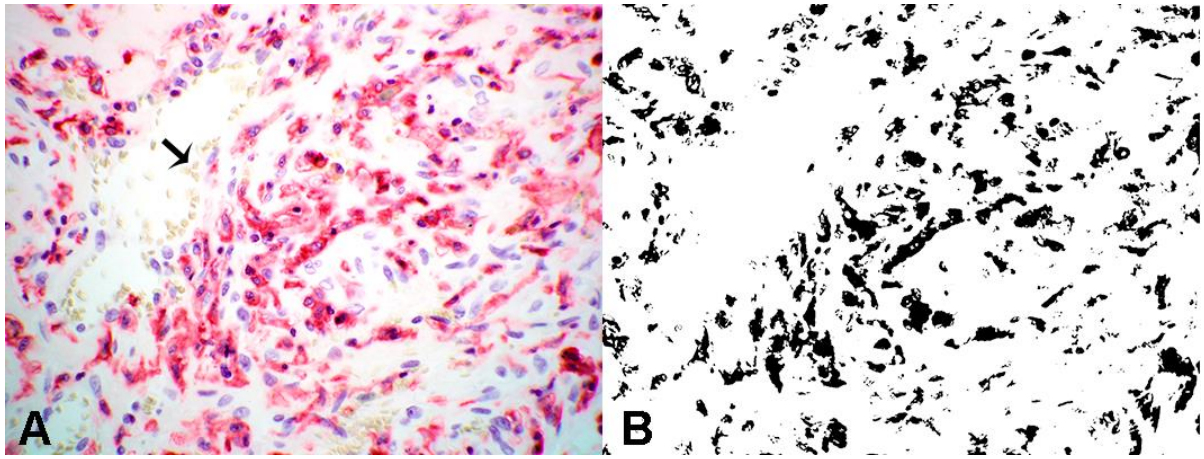

Figure 3.4. Validation of the ImageJ color deconvolution algorithm for quantitative assessment of CD18+ cell density. (A) Original 40x image of CD18+ immunolabeling, and (B) corresponding quality control, thresholded image mask of CD18 positive area as determined in ImageJ using the color deconvolution algorithm. Color deconvolution with the Fast red and Fast blue vectors followed by setting a lower threshold limit at the mean gray value of negative control images generated effective masks for accurate quantitative evaluation of $CD18^{+}$ cellular infiltrates.

of CD18 immunoreactivity. As shown in Figure 3.4, the color deconvolution algorithm was accurate in identifying CD18+ immunoreactivity, accurately selecting the Fast red chromogen signal localized to cellular membranes and cytoplasm, but at the same time excluding pigment, hyperchromatic nuclei, or other artifacts. Importantly, this algorithm was also effective in discriminating the Fast red positive chromogen from the red hue of erythrocytes, thus preventing false positives resulting from the vascular nature of hemangiosarcoma (black arrow, Fig. 3.4). The percentage of CD18+ area within tumor metastases was significantly greater within hemangiosarcoma, which had a mean of 11.75 % (± 2.913 % positive area), as compared to transitional carcinoma metastases (6.229 ± 2.746 %), and melanoma metastases (6.623 ± 3.245 %) (Fig. 3.5A; One-way ANOVA, Tukey's post-test, *$p<0.05$). While the mean % CD18+ area within hemangiosarcoma metastases was numerically greater than for osteosarcoma (9.164 ± 4.168 %) and soft tissue sarcoma metastases (8.924 ± 3.788 %), but did not reach the level of statistical significance ($p = 0.28$, and 0.56, respectively). Importantly, the mean % CD18+ area within hemangiosarcoma metastases was significantly greater than the mean of the other tumor types combined (11.75 ± 0.69 % vs. 8.11 ± 0.76 %, respectively) ($p=0.001$).

CCL2 secreted by canine hemangiosarcoma cell line elicits strong monocyte migration.

A canine hemangiosarcoma cell line (DEN-HSA) was used to investigate the immunological mechanisms responsible for monocyte infiltrates observed in

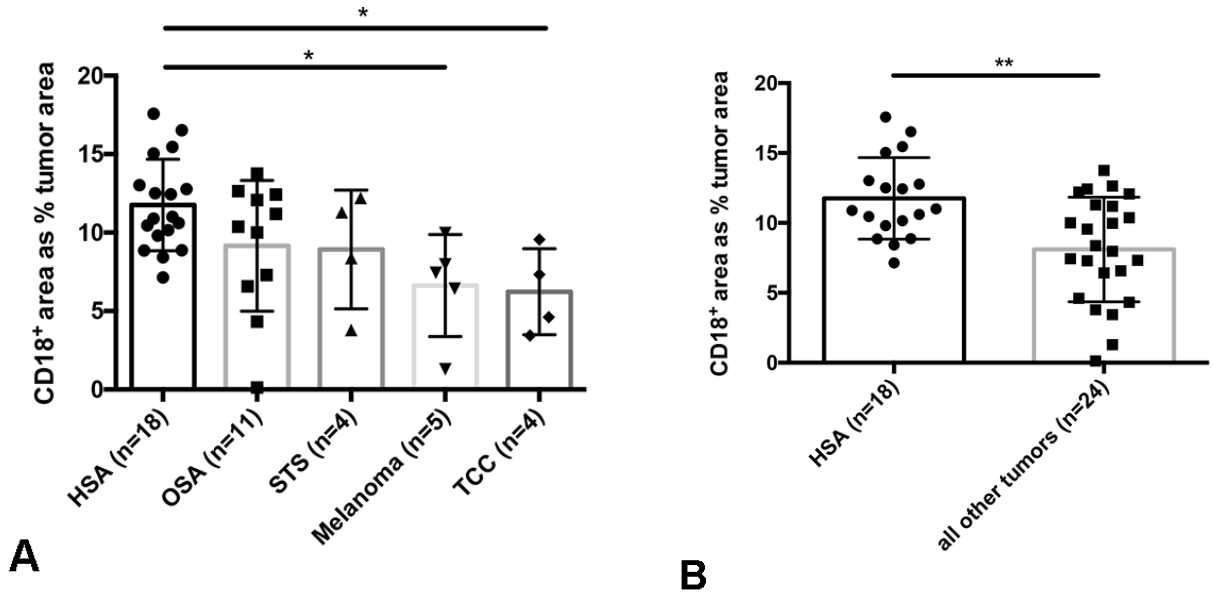

Figure 3.5. Quantification of CD18+ cell density within pulmonary metastases using ImageJ color deconvolution. (A) The density of C18+ cells, expressed as CD18+ area as percentage of tumor area, was greatest within hemangiosarcoma metastases, and was significantly greater than that observed in transitional cell carcinoma and melanoma metastases. (B) Furthermore, the percentage of CD18+ cells were even more significantly greater in hemangiosarcoma metastases, when compared to all other evaluated tumor types combined. HSA=hemangiosarcoma, OSA=osteosarcoma, STS=soft tissue sarcoma, and TCC=transitional cell carcinoma. Data representative of Mean ± SD. *p=0.03 (HSA vs. melanoma) and *p=0.04 (HSA vs TCC); One-way ANOVA, Tukey's post-test; **p=0.001; unpaired, two-tailed *t* test.

hemangiosarcoma metastases. A monocyte migration assay was used to evaluate the effects of DEN-HSA conditioned medium on monocyte recruitment, using canine peripheral blood mononuclear cells (PBMC) from healthy control dogs and transwell plates (Fig. 3.6 A-C). Following exposure of PBMC to HSA-conditioned medium, the mean number of migrated monocytes per HPF (24.7 ± 10.02) was significantly increased compared to control medium (1.6 ± 2.054) ($p<0.05$ (Fig. 3.6). In addition, as CD18+ monocyte infiltrates were also observed in pulmonary metastases of other canine tumor types evaluated by IHC (although not the same significant degree as canine hemangiosarcoma), we decided to quantify in vitro PBMC migration to tumor-conditioned media from a panel of other canine tumor cell lines. As shown in Figure 3.7, cell lines of other metastatic canine tumor histotypes, including histiocytic sarcoma (Nike), transitional cell carcinoma (Bliley), and osteosarcoma (Abrams) also elicited strong in vitro PMBC migration; however, hemangiosarcoma cells (DEN-HSA) demonstrated the greatest mean number of monocytes migrated in greater than 4 independent experiments performed in duplicate.

Given the known role of the CCL2-CCR2 chemotactic axis in monocyte recruitment in mouse and human tumor models, we hypothesized that the observed monocyte recruitment by canine tumor cell lines could also be mediated by CCL2. Thus, CCL2 secretion by DEN-HSA tumor cells was quantified in the same conditioned media utilized in the above PBMC migration assays using a canine CCL2 ELISA, as described previously (42). DEN-HSA conditioned media contained very high concentrations of CCL2 (Fig. 3.8A), with a mean concentration of 22,830 pg/mL. Furthermore, a second canine hemangiosarcoma cell line (SB-HSA) was evaluated for CCL2 production by

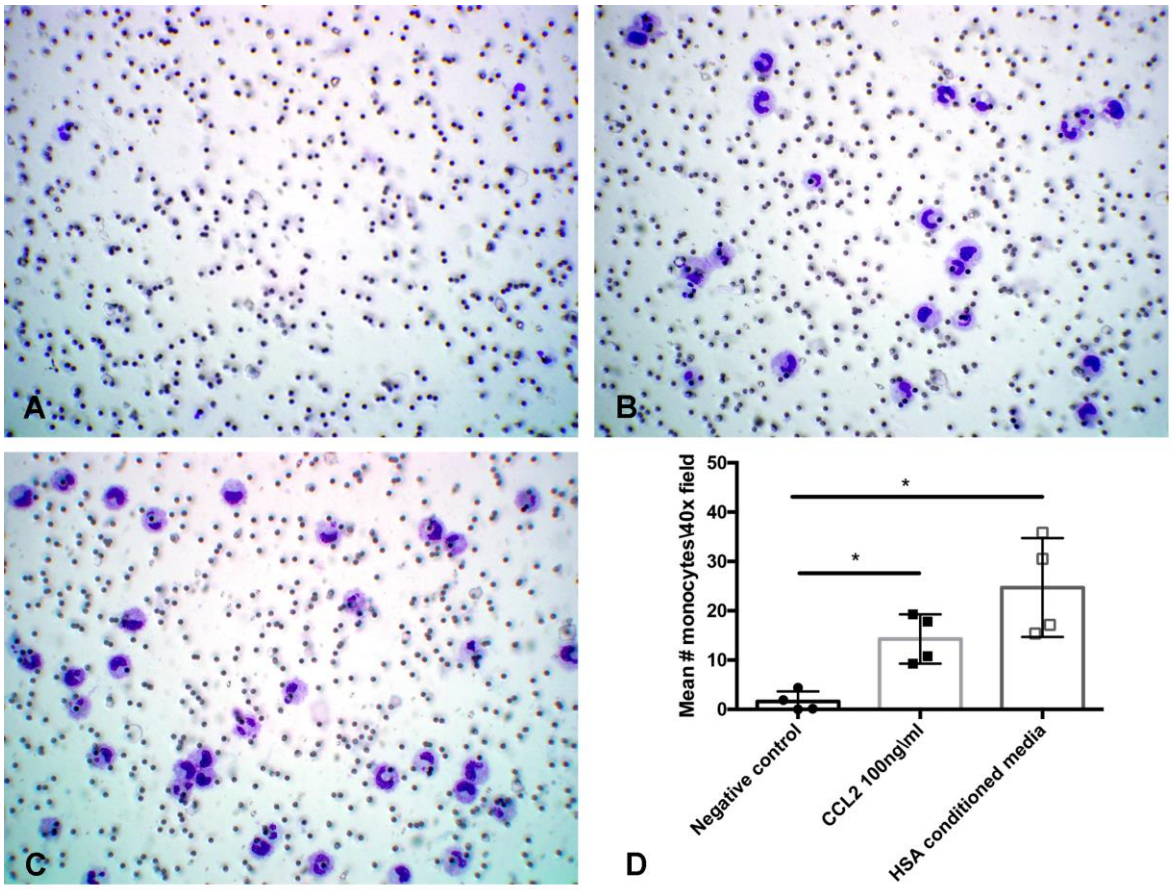

Figure 3.6. Canine hemangiosarcoma tumor-conditioned media stimulates strong monocyte migration in vitro. Representative photomicrographs of crystal violet stained membranes of the cell culture inserts used for quantification of in vitro monocyte migration. Complete MEM media stimulated little to no monocyte migration (A); however, conditioned-media from canine DEN-HSA cells stimulated strong monocyte migration (C), which was significantly greater than the negative control, and at minimum equivalent to the positive control of 100 ng/mL recombinant human rCCL2 (B). Only migrated cells displaying a mononuclear morphology consistent with monocytes were counted and included in the analysis. (D) Quantitative assessment of monocyte migration to media alone (negative control), 100 ng/mL recombinant human CCL2 (positive control), or HSA-conditioned media. Each data point represents the mean (± SD) number of monocytes per 40x field for duplicate membranes as determined by counting (5) independent 40x fields per membrane. *$p<0.05$, repeated measures One-way ANOVA, Tukey's post-test. All images are 40x magnification and crystal violet stained.

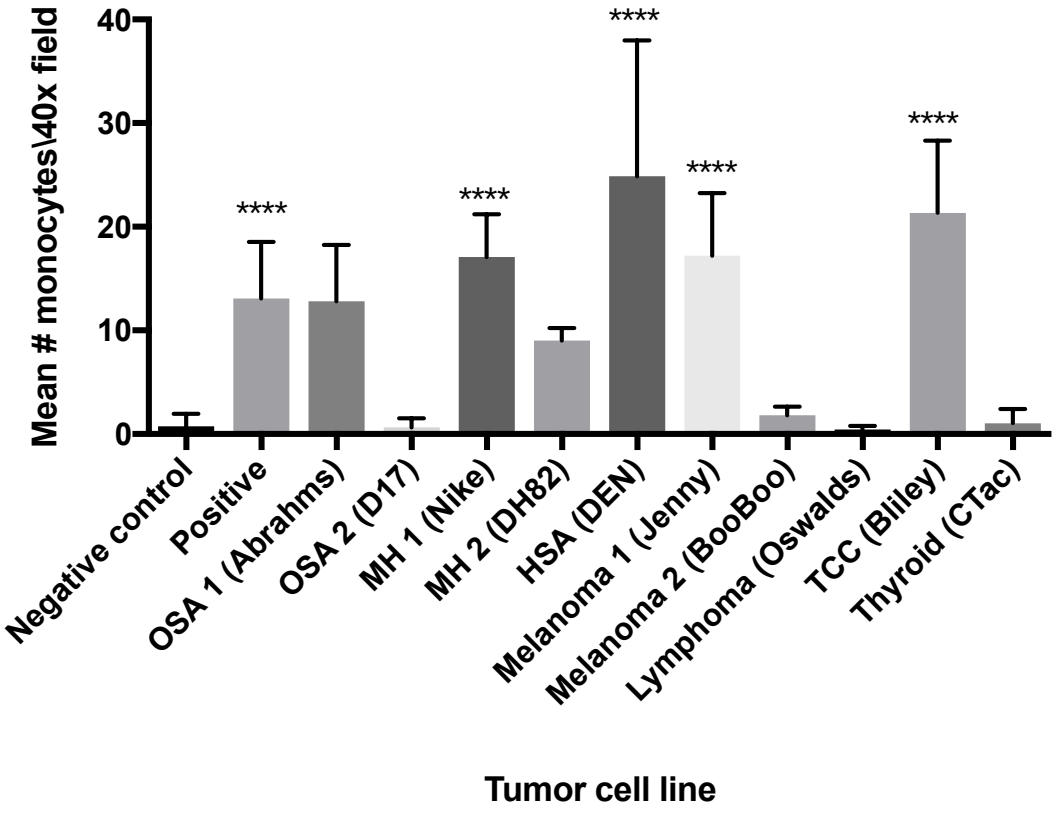

Figure 3.7. Conditioned media of other highly metastatic canine tumor cell lines also stimulates strong monocyte migration in vitro*.* Graph showing quantitative assessment of monocyte migration to media alone (negative control), 100 ng/mL recombinant human CCL2 (positive control), or tumor-conditioned media form the indicated cell line. Each data point represents the mean (± SD) number of monocytes per 40x field for duplicate membranes as determined by counting (5) independent 40x fields per membrane. ****$p<0.0001$ as compared to negative control, One-way ANOVA, Tukey's post-test.

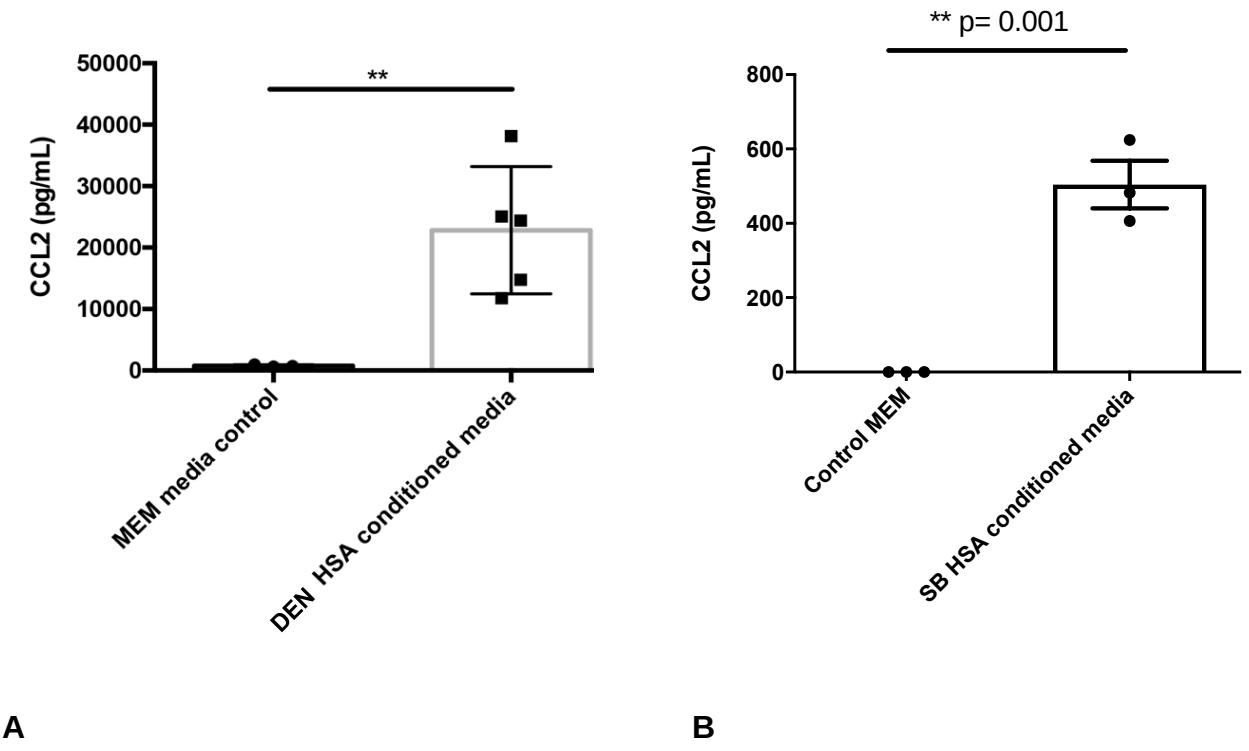

A **B**

Figure 3.8. Canine hemangiosarcoma cells produce abundant amounts of CCL2 in vitro. Significant amounts of CCL2 was detected via ELISA assay of conditioned media from both the DEN and SB canine hemangiosarcoma cell lines. 2 x 10^5 tumor cells were seeded in 24-well plates and allowed to grow for 24h prior to harvesting the supernatant for CCL2 measurement via ELISA assay. **p<0.01; unpaired, two-tailed *t* test. Data representative of Mean ± SD.

ELISA assay, and was found to also produce significant amounts of the chemokine (Fig. 3.8B).

To determine the potential chemokine responsible for the observed in vitro PBMC migration elicited by the other evaluated canine tumor cells lines, CCL2 production by these cells was also quantified by ELISA assay, again which was performed on the same conditioned media utilized in the above PBMC migration assays. Similar to hemangiosarcoma cells, the other canine tumor cell lines which also elicited strong in vitro monocyte migration (Abrams, Bliley, and Nike), were significant producers of CCL2 (Fig. 3.9A). In addition, the amount of CCL2 produced by canine tumor cell lines strongly correlated with the mean number of migrated monocytes for all evaluated canine tumor cell lines (Fig. 3.9B; *r=0.87, **p=0.001*). In summary, these results suggest that of all evaluated canine tumor cell lines in our panel, those derived from tumor histotypes which are known to be more clinically aggressive and highly metastatic (hemangiosarcoma, osteosarcoma, and histiocytic sarcoma) produced abundant amounts of CCL2. Of interesting note, the Jenny melanoma cell line elicited strong in vitro monocyte migration, yet was found to produce minimal to no CCL2, suggesting another monocyte chemoattractant is likely responsible for the observed monocyte recruitment for this cell line.

To further confirm the results of the CCL2 ELISA assays, immunofluorescence staining was used to localize tumor cell production of CCL2. Initially, cross-reactivity of a polyclonal CCL2 antibody for canine CCL2 was confirmed via western blotting against recombinant canine CCL2 (Fig. 3.10 C). The antibody detected a band of approximately 15 kDa, consistent with the predicted molecular weight of canine CCL2 (8-12 kDa).

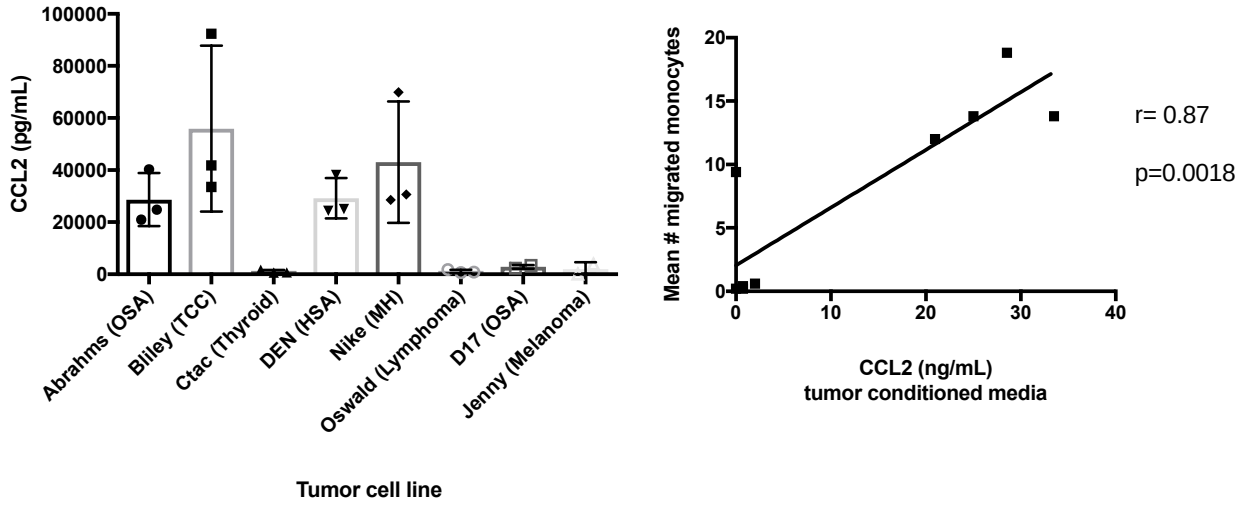

A **B**

Figure 3.9. Other highly metastatic canine tumor cell lines also produce abundant amounts of CCL2, which correlates with in vitro monocyte migration. (A) Graph showing quantitative assessment of CCL2 production by tumor cell lines via ELISA assay of conditioned media. Again, 2 x 10^5 tumor cells were seeded in 24-well plates and allowed to grow for 24h prior to harvesting the supernatant for ELISA. (B) Graph demonstrating a strong positive correlation between CCL2 concentration within tumor conditioned media and mean number of migrated monocytes for all cell lines evaluated in (A). Each data point in (A) represents the mean (± SD) number of monocytes per 40x field for duplicate membranes as determined by counting (5) independent 40x fields per membrane. Pearson correlation = 0.87, **p=0.0018.

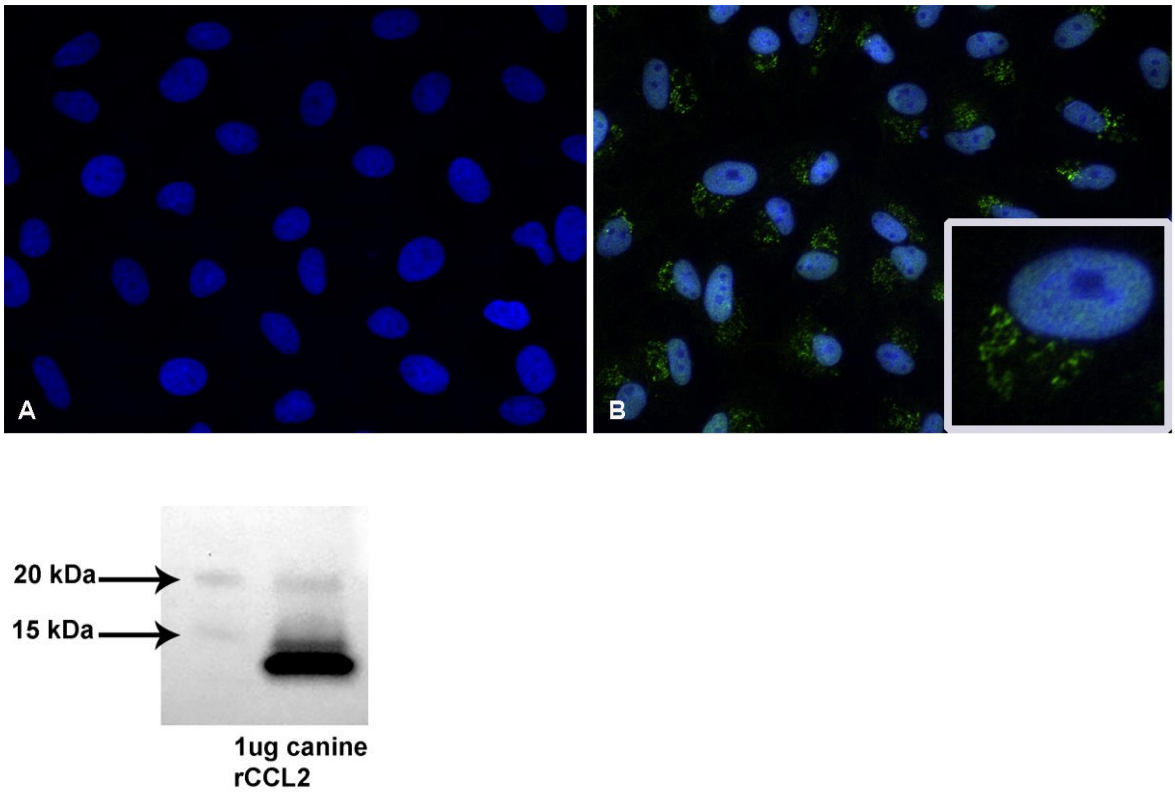

Figure 3.10. Immunofluorescent localization of CCL2 within canine hemangiosarcoma cells. Immunolabeling of DEN-HSA cells for CCL2 required pre-treatment with a protein transport inhibitor (Brefeldin A). Un-treated cells (A) displayed no immunoreactivity for CCL2, whereas cells pre-treated with Brefeldin A (B), demonstrated, strong, punctate, peri-nuclear immunoreactivity for CCL2, which is more clearly demonstrated in the enlarged single cell image inset. 40x magnification. CCL2=FITC (green). Nuclei=DAPI (blue) (C) Cross-reactivity of the anti-human CCL2 antibody was confirmed via western blot against canine recombinant CCL2 (R&D systems Inc. Minneapolis, MN), which detected a band of ≈ 15 kDa (predicted M.W. of 8-12 kDa).

DEN-HSA cells were pre-incubated with the protein transport inhibitor Brefeldin A (10 µg/mL) for 4 hours prior to staining. DEN-HSA cells exhibited strong CCL2 positive immunoreactivity, characterized by punctate to granular staining which discretely localized to the peri-nuclear golgi zone of the cytoplasm (Fig. 3.10 A, B).

Lastly, while these assays confirmed the ability of DEN-HSA cells to make abundant amounts of the monocyte chemokine CCL2, they still did not directly implicate this CCL2 production with the observed in vitro monocyte migration. In order to investigate this relationship, monocyte migration assays were repeated using DEN-HSA conditioned media +/- treatment with a CCL2 neutralizing antibody, or irrelevant IgG control antibody. Addition of the CCL2 neutralizing antibody to the tumor-conditioned media significantly reduced the mean number of migrated monocytes to approximately 60-80% lower than that observed for the positive control of HSA-conditioned media alone (***p=0.0002) (Fig. 3.11). This result verifies that DEN-HSA in vitro elicited monocyte migration is in fact dependent to a significant degree on the CCL2-CCR2 chemotactic axis.

Immunohistochemical localization of CCL2 in hemangiosarcoma and other canine tumor pulmonary metastases

To corroborate our in vitro results of CCL2 mediated monocyte migration by hemangiosarcoma and other canine tumor cell lines, we performed CCL2 immunohistochemistry on the same cases of canine pulmonary metastases evaluated for CD18+ infiltrates in Figure 3.1. Within hemangiosarcoma metastases, expression of CCL2 in all evaluated cases was almost entirely restricted to neoplastic cells, with

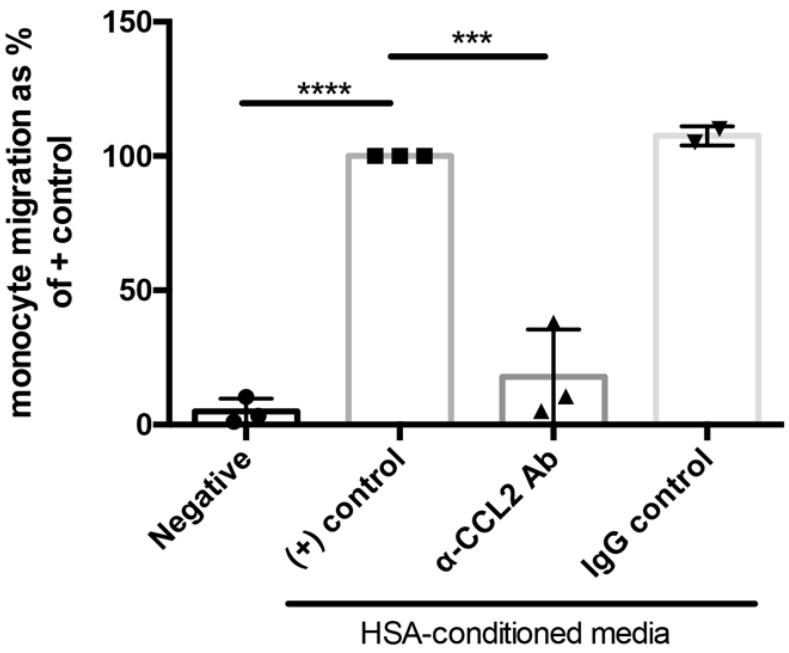

Figure 3.11. In vitro monocyte migration elicited by canine hemangiosarcoma cells (DEN-HSA) is primarily mediated by CCl2. Neutralization of CCL2 in HSA-conditioned media using an anti-human CCL2 antibody (5 µg/mL) resulted in a significant (~60-80%) reduction in in vitro monocyte migration as compare to the positive control of HSA-conditioned media only. Data representative of Mean ± SD. ***p=0.0002, ****p<0.0001. One-way ANOVA, Tukey's post-test.

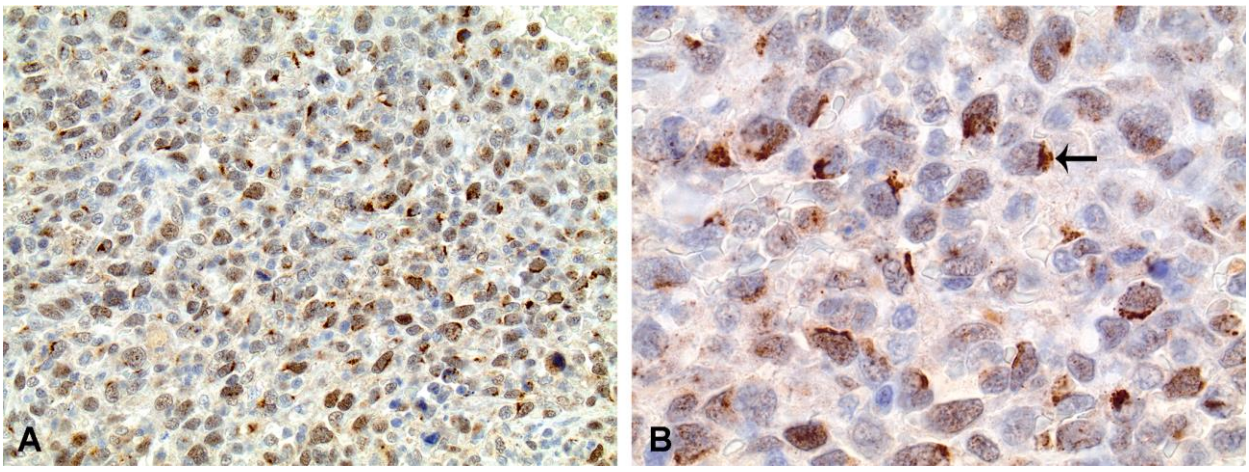

Figure 3.12. Tumor cells within hemangiosarcoma metastases demonstrate positive immunolabeling for CCL2. All evaluated cases (n=5) demonstrated strong, positive immunolabeling for CCL2. (A) In all cases, greater than 50-75% of tumor cells within hemangiosarcoma pulmonary metastases demonstrated moderate to strong immunoreactivity for CCL2. 20x magnification. DAB chromogen. Hematoxylin counterstain. (B) Higher magnification image of the same case in (A), which demonstrates the strongly positive, intra-cytoplasmic, peri-nuclear (golgi zone) localization for CCL2 within tumor cells. 50x magnification.

between 50% and 100% of cells within metastatic nodules demonstrating moderate to strong labeling intensity for CCL2 (Fig. 3.12 A). Within tumor cells, the localization of CCL2 immunoreactivity varied from diffuse and intra-cytoplasmic, to focal, intense, and peri-nuclear (Fig.3.12 B). Metastatic transitional cell carcinoma tumors demonstrated diffuse, intense, cytoplasmic labeling for CCL2, which was present in 75-100% of tumor cells (Fig. 3.12 B). Additionally, most osteosarcoma pulmonary metastases also displayed positive CCL2 labeling (Fig. 3.12 C), though the pattern of immunoreactivity was typically characterized by weaker cytoplasmic labeling for CCL2 as compared to hemangiosarcoma metastases (Fig. 3.12 A). Lastly, only one of three metastatic melanoma biopsies demonstrated positive immunolabeling of tumor cells for CCL2 (Fig. 3.12 D). Thus, while there was a wide range of CCL2 expression by all evaluated tumor types, hemangiosarcoma metastases were most consistently strongly CCL2 positive.

Serum CCL2 levels elevated in the blood of dogs with splenic hemangiosarcoma

CCL2 concentrations in the pre-treatment serum of 24 dogs with a histopathologically confirmed diagnosis of hemangiosarcoma, were measured using an ELISA assay as described above. For comparison, CCL2 concentrations were also measured in the serum of 6 age-matched, healthy control dogs. The median age of hemangiosarcoma-bearing dogs was 9.8 years (range of 7-15 years), and consisted of 12 males and 12 females. The median age of the healthy control dogs was 10 years (range of 3-12 years), and consisted of 3 males and 3 females. The mean concentration of CCL2 in the serum of hemangiosarcoma-bearing dogs (267.4 ± 56.64 pg/mL) was

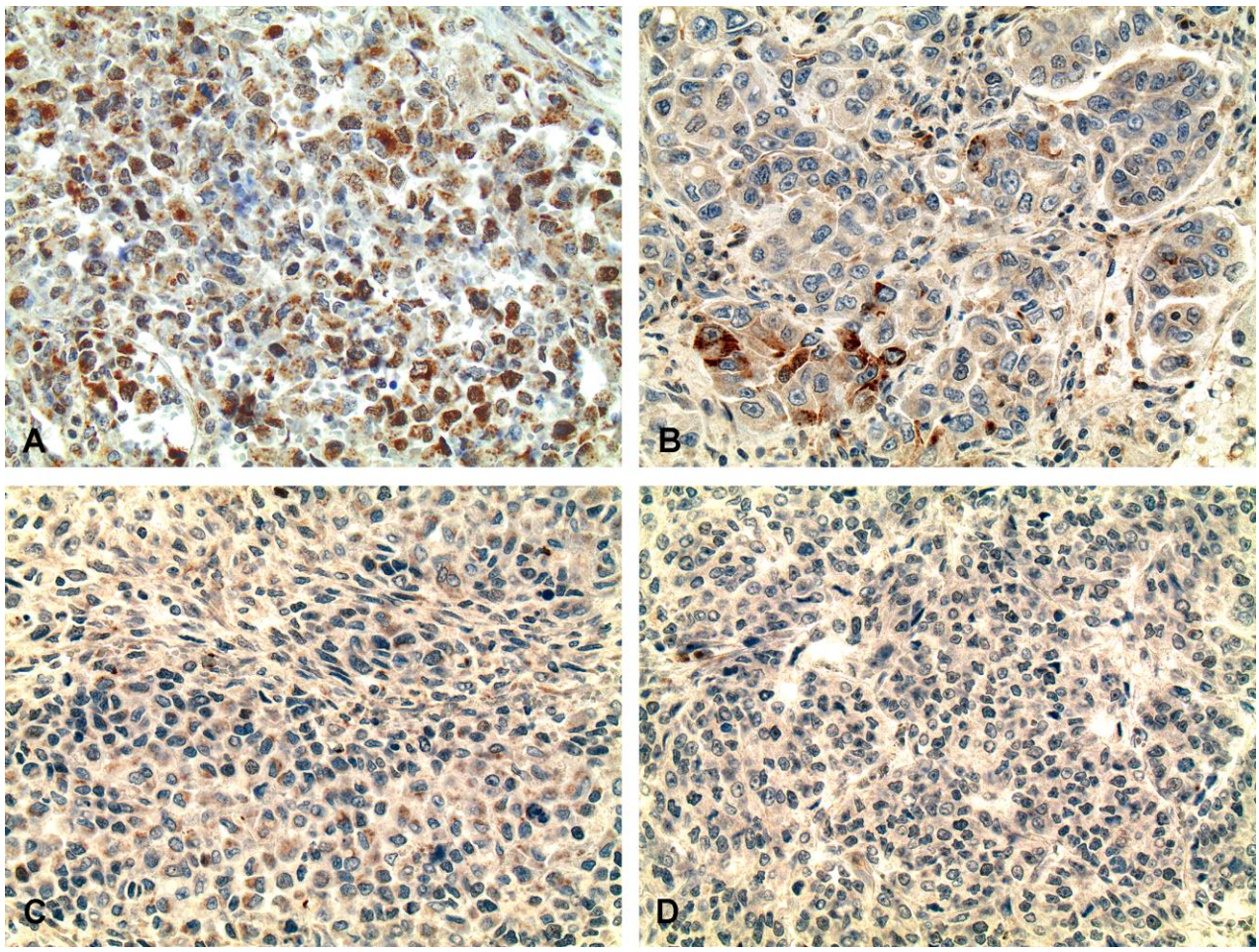

Figure 3.12. CCL2 positive immunolabeling within other pulmonary metastatic canine tumors. (A) Another case of hemangiosarcoma demonstrating strong CCL2 cytoplasmic immunoreactivity in the majority (>75%) of tumor cells. (B) A transitional cell carcinoma metastasis demonstrating multifocal, strong CCL2 cytoplasmic immunoreactivity in focal clusters of tumor cells. (C) Diffuse, weak to moderate positive immunolabeling for CCL2 within an osteosarcoma metastasis. (D) A melanoma metastasis that was negative for CCL2. 40x magnification. DAB chromogen. Hematoxylin counterstain.

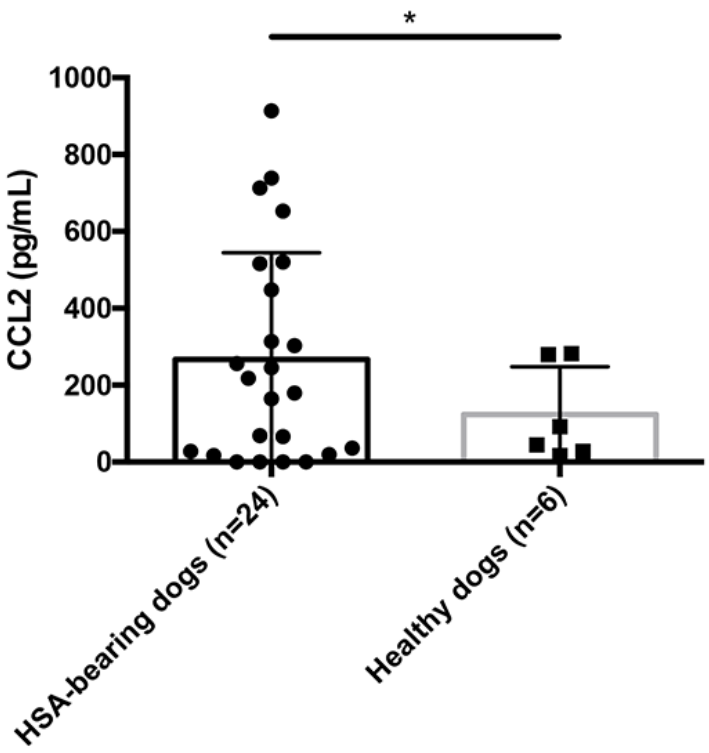

Figure 3.13. Serum CCL2 levels are elevated in dogs with hemangiosarcoma vs. "healthy" controls. Serum samples from dogs with HSA (n=24) were obtained at the time of surgical removal of the primary tumor, performed at the CSU Veterinary Teaching Hospital. Samples were frozen and maintained in the tissue archive of the Flint Animal Cancer Center until analysis. Serum CCL2 concentrations were measured using a commercially available canine CCL2 ELISA. Data representative of Mean ± SD. *p=0.03. unpaired, one-tailed *t* test with Welch's correction.

significantly elevated (Fig. 3.13) compared to healthy control dogs (123.9 ± 50.68 pg/mL). Values for serum CCL2 concentration were significantly elevated compared to control dogs, whether evaluating dogs with hemangiosarcoma of any primary location, or only dogs with primary splenic hemangiosarcoma (data not shown).

Discussion

While experimental and clinical evidence strongly suggests that monocytes promote tumor metastasis in humans and rodent tumor models, there remains a considerable knowledge gap in our understanding of the role of monocytes in canine tumor metastasis. A primary goal of this study was to immunohistochemically characterize the degree of monocyte infiltration within pulmonary metastases of common and highly metastatic canine tumors of multiple histo-types. One of the most important findings that emerged from these studies was that hemangiosarcoma pulmonary metastases appear to have a unique propensity in their ability to recruit monocytes, as these tumors demonstrated a significantly greater degree of CD18+ monocyte infiltration as compared to all other evaluated canine tumor metastases (Figs. 1-3). In order to build on this observation and expand the translational relevance of this finding, we performed CCL2 immunostaining of tumor metastases, as well in vitro migration and ELISA assays to determine the mechanism responsible for this recruitment. As the CCL2-CCR2 axis is known to recruit metastasis-promoting monocytes in multiple tumors types in humans and mouse models, we specifically focused on this chemotactic axis. CCL2 immunostaining of hemangiosarcoma metastases as well as measurement of serum CCL2 levels in hemangiosarcoma-

bearing dogs confirmed an overproduction of CCL2 by hemangiosarcoma cells in vivo (Figs. 6 & 7). In vitro assays utilizing a HSA tumor cell line demonstrated that this CCL2 production correlated with the ability for in vitro recruitment of canine peripheral blood derived monocytes by HSA tumor-conditioned media (Figs. 4 & 5). As hemangiosarcoma is an endothelial-derived tumor, and monocytes are known to be a rich source of the endothelial growth factor VEGF (23), these findings may be reflective of a unique dependence between this specific canine tumor type, and monocyte-derived endothelial growth factors. Future studies aimed at assessing changes in the cytokine profile of canine blood-derived monocytes following exposure to HSA-conditioned media could begin to shed light on this phenomenon.

Interestingly, hematopoietic stem/progenitor cells of a CD11b+ myelo-monocytic phenotype are also one of multiple cell types which preferentially accumulate at metastatic sites even *before* the arrival of tumor cells, a phenomenon known as the pre-metastatic niche (41-43). This phenomenon has been demonstrated experimentally in syngeneic mouse models of lung carcinoma and melanoma, as well as a human xenograft breast cancer model (41-43). In addition, elevated levels of these cells have been detected in human cancer patients and correlate with increased risk for metastatic progression (41). Once present at metastatic sites, these cells function to establish a permissive niche for incoming tumor cells through mechanisms involving immune suppression, up-regulation of tumor cell chemoattractants, and promotion of tumor cell survival, both directly via secretion of molecules like S100A8 and A9, and indirectly via matrix metalloproteinase-mediated release of VEGF and c-KIT (41-43). Furthermore, the functional impact of these cells on metastatic progression has been confirmed

experimentally, as antibody-mediated depletion of these cells completely prevented metastasis in mice bearing well-established tumors [43]. Obvious inherent limitations of the canine spontaneous cancer model limit our study to the evaluation of canine tumor metastases not in a pre-metastatic setting, but in a wide temporal spectrum encompassing established metastatic tumors at various stages of growth. Nonetheless, our results suggest that the rapid and widespread visceral metastasis characteristic of hemangiosarcoma could be due to a distinctive ability of this tumor type to efficiently prime the soil of distant metastatic sites through efficient CCL2-CCR2 monocyte recruitment.

The role of inflammatory monocytes and macrophages in the regulation of tumor responses to chemotherapeutic drugs is also beginning to be defined. Recently, it has been demonstrated that conventional cytotoxic therapies such as doxorubicin can induce tumor and stromal cell production of CCL2 as well as other monocyte and macrophage chemoattractants such as M-CSF (44, 45). This therapy-induced inflammatory response was shown to lead to enhanced recruitment of CCR2+ monocytes and macrophage infiltration of primary tumors in a murine breast cancer model and in human breast cancer patients treated with neoadjuvant chemotherapy (44, 45). Importantly, the functional role of these myeloid-derived cells in mediating chemoresistance was demonstrated via concurrent macrophage depletion with chemotherapy, which significantly improved overall survival in mammary tumor bearing mice (44, 45). In addition, clinical evidence supporting a role for macrophages in chemoresistance comes from human breast cancer patients, in which patients having a high tumor gene expression ratio of CD68+ macrophages to CD8+ T cells had a

significantly lower rate of pathological complete response to neoadjuvant chemotherapy, and significantly reduced overall survival (44). As our study compared the degree of myeloid cell infiltration within metastatic canine tumors in the post-therapeutic setting, these observations could have significant implications regarding the interpretation of the results of our study. It is plausible then that our findings suggest that canine hemangiosarcoma may be unique in its ability to elicit a counter regulatory, CCL2-driven myeloid response following cytotoxic therapy. This could in part, potentially explain the poor response of this tumor type to conventional cytotoxic therapies, and suggest that combination of chemotherapy with a monocyte blocking drug could have a synergistic effect in treating this tumor. To more fully investigate these findings and potential associations, future studies could be aimed at comparing pre- and post-chemotherapy treatment serum CCL2 levels and peripheral blood monocyte counts in dogs with hemangiosarcoma.

In conclusion, these studies demonstrate that canine hemangiosarcoma, as compared to other common and highly metastatic canine tumors types, is unique in its ability to recruit large numbers of monocytes to sites of metastasis. Moreover, through CCL2 immunostaining as well as serum ELISA and in vitro assays, we provide substantial mechanistic data which strongly suggests that monocyte recruitment to hemangiosarcoma metastases is at least in part dependent on the CCL2-CCR2 chemotactic axis. These observations provide important insights into the biology and immunopathogenesis of hemangiosarcoma, and are consistent with the hypothesis that overexpression of CCL2 and recruitment of large numbers of monocytes may explain in part the aggressive metastatic nature of canine hemangiosarcoma. Thus, drugs

designed at blocking monocyte recruitment through disruption of the CCL2-CCR2 axis might represent a novel immunotherapeutic approach for slowing the growth and/or development of metastasis in dogs with hemangiosarcoma.

REFERENCES

1. Priester WA and McKay FW. The occurrence of tumors in domestic animals. *Natl Cancer Inst Monogr*. 1980; (54): 1-210.

2. Spangler WL and Culbertson MR. Prevalence, type, and importance of splenic diseases in dogs: 1,480 cases (1985-1989). *J Am Vet Med Assoc*. 1992; 200(6): 829-34.

3. Bastianello SS. A survey on neoplasia in domestic species over a 40-year period from 1935 to 1974 in the Republic of South Africa. VI. Tumours occurring in dogs. *Onderstepoort J Vet Res*. 1983; 50(3): 199-220.

4. Brown NO, Patnaik AK and MacEwen EG. Canine hemangiosarcoma: retrospective analysis of 104 cases. *J Am Vet Med Assoc*. 1985; 186(1): 56-8.

5. Kleine LJ, Zook BC and Munson TO. Primary cardiac hemangiosarcomas in dogs. *J Am Vet Med Assoc*. 1970; 157(3): 326-37.

6. MacVean DW, Monlux AW, Anderson PS, Jr., Silberg SL and Roszel JF. Frequency of canine and feline tumors in a defined population. *Vet Pathol*. 1978; 15(6): 700-15.

7. Pearson GR and Head KW. Malignant haemangioendothelioma (angiosarcoma) in the dog. *J Small Anim Pract*. 1976; 17(11): 737-45.

8. Schultheiss PC. A retrospective study of visceral and nonvisceral hemangiosarcoma and hemangiomas in domestic animals. *J Vet Diagn Invest*. 2004; 16(6): 522-6.

9. Srebernik N and Appleby EC. Breed prevalence and sites of haemangioma and haemangiosarcoma in dogs. *Vet Rec*. 1991; 129(18): 408-9.

10. Vail DM and MacEwen EG. Spontaneously occurring tumors of companion animals as models for human cancer. *Cancer Invest*. 2000; 18(8): 781-92.

11. Lamerato-Kozicki AR, Helm KM, Jubala CM, Cutter GC and Modiano JF. Canine hemangiosarcoma originates from hematopoietic precursors with potential for endothelial differentiation. *Exp Hematol*. 2006; 34(7): 870-8.

12. Liu L, Kakiuchi-Kiyota S, Arnold LL, Johansson SL, Wert D and Cohen SM. Pathogenesis of human hemangiosarcomas and hemangiomas. *Hum Pathol*. 2013; 44(10): 2302-11.

13. Sorenmo K, Duda L, Barber L, Cronin K, Sammarco C, Usborne A, Goldschmidt M and Shofer F. Canine hemangiosarcoma treated with standard chemotherapy and minocycline. *J Vet Intern Med*. 2000; 14(4): 395-8.

14. Sorenmo KU, Jeglum KA and Helfand SC. Chemotherapy of canine hemangiosarcoma with doxorubicin and cyclophosphamide. *J Vet Intern Med*. 1993; 7(6): 370-6.

15. Vail DM, MacEwen EG, Kurzman ID, Dubielzig RR, Helfand SC, Kisseberth WC, London CA, Obradovich JE, Madewell BR, Rodriguez CO, Jr. and et al. Liposome-encapsulated muramyl tripeptide phosphatidylethanolamine adjuvant immunotherapy for splenic hemangiosarcoma in the dog: a randomized multi-institutional clinical trial. *Clin Cancer Res*. 1995; 1(10): 1165-70.

16. Wendelburg KM, Price LL, Burgess KE, Lyons JA, Lew FH and Berg J. Survival time of dogs with splenic hemangiosarcoma treated by splenectomy with or without adjuvant chemotherapy: 208 cases (2001-2012). *J Am Vet Med Assoc*. 2015; 247(4): 393-403.

17. Hammer AS, Couto CG, Filppi J, Getzy D and Shank K. Efficacy and toxicity of VAC chemotherapy (vincristine, doxorubicin, and cyclophosphamide) in dogs with hemangiosarcoma. *J Vet Intern Med*. 1991; 5(3): 160-6.

18. Ogilvie GK, Powers BE, Mallinckrodt CH and Withrow SJ. Surgery and doxorubicin in dogs with hemangiosarcoma. *J Vet Intern Med*. 1996; 10(6): 379-84.

19. Lana S, U'Ren L, Plaza S, Elmslie R, Gustafson D, Morley P and Dow S. Continuous low-dose oral chemotherapy for adjuvant therapy of splenic hemangiosarcoma in dogs. *J Vet Intern Med*. 2007; 21(4): 764-9.

20. Sorenmo KU, Baez JL, Clifford CA, Mauldin E, Overley B, Skorupski K, Bachman R, Samluk M and Shofer F. Efficacy and toxicity of a dose-intensified doxorubicin protocol in canine hemangiosarcoma. *J Vet Intern Med*. 2004; 18(2): 209-13.

21. U'Ren LW, Biller BJ, Elmslie RE, Thamm DH and Dow SW. Evaluation of a novel tumor vaccine in dogs with hemangiosarcoma. *J Vet Intern Med*. 2007; 21(1): 113-20.

22. Kitamura T, Qian BZ and Pollard JW. Immune cell promotion of metastasis. *Nat Rev Immunol*. 2015; 15(2): 73-86.

23. Qian BZ, Li J, Zhang H, Kitamura T, Zhang J, Campion LR, Kaiser EA, Snyder LA and Pollard JW. CCL2 recruits inflammatory monocytes to facilitate breast-tumour metastasis. *Nature*. 2011; 475(7355): 222-5.

24. Kitamura T, Qian BZ, Soong D, Cassetta L, Noy R, Sugano G, Kato Y, Li J and Pollard JW. CCL2-induced chemokine cascade promotes breast cancer metastasis by

enhancing retention of metastasis-associated macrophages. *J Exp Med*. 2015; 212(7): 1043-59.

25. Qian BZ, Zhang H, Li J, He T, Yeo EJ, Soong DY, Carragher NO, Munro A, Chang A, Bresnick AR, Lang RA and Pollard JW. FLT1 signaling in metastasis-associated macrophages activates an inflammatory signature that promotes breast cancer metastasis. *J Exp Med*. 2015; 212(9): 1433-48.

26. Feng J, Zhang W, Wu J, Gao S, Ye H, Sun L, Chen Y, Yu K and Xing CY. Effect of initial absolute monocyte count on survival outcome of patients with de novo non-M3 acute myeloid leukemia. *Leuk Lymphoma*. 2016: 1-7.

27. Izumi K, Mizokami A, Lin HP, Ho HM, Iwamoto H, Maolake A, Natsagdorj A, Kitagawa Y, Kadono Y, Miyamoto H, Huang CK, Namiki M and Lin WJ. Serum chemokine (CC motif) ligand 2 level as a diagnostic, predictive, and prognostic biomarker for prostate cancer. *Oncotarget*. 2016; 7(7): 8389-98.

28. Lu X, Qian CN, Mu YG, Li NW, Li S, Zhang HB, Li SW, Wang FL, Guo X and Xiang YQ. Serum CCL2 and serum TNF-alpha--two new biomarkers predict bone invasion, post-treatment distant metastasis and poor overall survival in nasopharyngeal carcinoma. *Eur J Cancer*. 2011; 47(3): 339-46.

29. Nishijima TF, Muss HB, Shachar SS, Tamura K and Takamatsu Y. Prognostic value of lymphocyte-to-monocyte ratio in patients with solid tumors: A systematic review and meta-analysis. *Cancer Treat Rev*. 2015; 41(10): 971-8.

30. Sasaki A, Kai S, Endo Y, Iwaki K, Uchida H, Tominaga M, Okunaga R, Shibata K, Ohta M and Kitano S. Prognostic value of preoperative peripheral blood monocyte count in patients with colorectal liver metastasis after liver resection. *J Gastrointest Surg*. 2007; 11(5): 596-602.

31. Schmidt H, Bastholt L, Geertsen P, Christensen IJ, Larsen S, Gehl J and von der Maase H. Elevated neutrophil and monocyte counts in peripheral blood are associated with poor survival in patients with metastatic melanoma: a prognostic model. *Br J Cancer*. 2005; 93(3): 273-8.

32. Vassilakopoulos TP, Dimopoulou MN, Angelopoulou MK, Petevi K, Pangalis GA, Moschogiannis M, Dimou M, Boutsikas G, Kanellopoulos A, Gainaru G, Plata E, Flevari P, Koutsi K, Papageorgiou L, Telonis V, Tsaftaridis P, Sachanas S, Yiakoumis X, Tsirkinidis P, Viniou NA, Siakantaris MP, Variami E, Kyrtsonis MC, Meletis J, Panayiotidis P and Konstantopoulos K. Prognostic Implication of the Absolute Lymphocyte to Absolute Monocyte Count Ratio in Patients With Classical Hodgkin Lymphoma Treated With Doxorubicin, Bleomycin, Vinblastine, and Dacarbazine or Equivalent Regimens. *Oncologist*. 2016; 21(3): 343-53.

33. Perry JA, Thamm DH, Eickhoff J, Avery AC and Dow SW. Increased monocyte chemotactic protein-1 concentration and monocyte count independently associate with a poor prognosis in dogs with lymphoma. *Vet Comp Oncol*. 2011; 9(1): 55-64.

34. Sottnik JL, Rao S, Lafferty MH, Thamm DH, Morley PS, Withrow SJ and Dow SW. Association of blood monocyte and lymphocyte count and disease-free interval in dogs with osteosarcoma. *J Vet Intern Med*. 2010; 24(6): 1439-44.

35. Boozer LB, Davis TW, Borst LB, Zseltvay KM, Olby NJ and Mariani CL. Characterization of immune cell infiltration into canine intracranial meningiomas. *Vet Pathol*. 2012; 49(5): 784-95.

36. Gregorio H, Raposo TP, Queiroga FL, Prada J and Pires I. Investigating associations of cyclooxygenase-2 expression with angiogenesis, proliferation, macrophage and T-lymphocyte infiltration in canine melanocytic tumours. *Melanoma Res*. 2016.

37. Grieco V, Rondena M, Romussi S, Stefanello D and Finazzi M. Immunohistochemical characterization of the leucocytic infiltrate associated with canine seminomas. *J Comp Pathol*. 2004; 130(4): 278-84.

38. Raposo T, Gregorio H, Pires I, Prada J and Queiroga FL. Prognostic value of tumour-associated macrophages in canine mammary tumours. *Vet Comp Oncol*. 2014; 12(1): 10-9.

39. Vanherberghen M, Day MJ, Delvaux F, Gabriel A, Clercx C and Peeters D. An immunohistochemical study of the inflammatory infiltrate associated with nasal carcinoma in dogs and cats. *J Comp Pathol*. 2009; 141(1): 17-26.

40. Thamm DH, Dickerson EB, Akhtar N, Lewis R, Auerbach R, Helfand SC and MacEwen EG. Biological and molecular characterization of a canine hemangiosarcoma-derived cell line. *Res Vet Sci*. 2006; 81(1): 76-86.

41. Giles AJ, Reid CM, Evans JD, Murgai M, Vicioso Y, Highfill SL, Kasai M, Vahdat L, Mackall CL, Lyden D, Wexler L and Kaplan RN. Activation of Hematopoietic Stem/Progenitor Cells Promotes Immunosuppression Within the Pre-metastatic Niche. *Cancer Res*. 2016; 76(6): 1335-47.

42. Hiratsuka S, Watanabe A, Aburatani H and Maru Y. Tumour-mediated upregulation of chemoattractants and recruitment of myeloid cells predetermines lung metastasis. *Nat Cell Biol*. 2006; 8(12): 1369-75.

43. Kaplan RN, Riba RD, Zacharoulis S, Bramley AH, Vincent L, Costa C, MacDonald DD, Jin DK, Shido K, Kerns SA, Zhu Z, Hicklin D, Wu Y, Port JL, Altorki N, Port ER, Ruggero D, Shmelkov SV, Jensen KK, Rafii S and Lyden D. VEGFR1-positive haematopoietic bone marrow progenitors initiate the pre-metastatic niche. *Nature*. 2005; 438(7069): 820-7.

44. DeNardo DG, Brennan DJ, Rexhepaj E, Ruffell B, Shiao SL, Madden SF, Gallagher WM, Wadhwani N, Keil SD, Junaid SA, Rugo HS, Hwang ES, Jirstrom K, West BL and Coussens LM. Leukocyte complexity predicts breast cancer survival and functionally regulates response to chemotherapy. *Cancer Discov*. 2011; 1(1): 54-67.

45. Nakasone ES, Askautrud HA, Kees T, Park JH, Plaks V, Ewald AJ, Fein M, Rasch MG, Tan YX, Qiu J, Park J, Sinha P, Bissell MJ, Frengen E, Werb Z and Egeblad M. Imaging tumor-stroma interactions during chemotherapy reveals contributions of the microenvironment to resistance. *Cancer Cell*. 2012; 21(4): 488-503.

CHAPTER 4

Phase I/II clinical trial and pharmacodynamic evaluation of combination losartan and toceranib in dogs with spontaneous, metastatic osteosarcoma

Summary

Further progress in the field of immuno-oncology would be greatly accelerated by the ability to assess immune-based therapies in the more translationally relevant spontaneous canine cancer model. Inflammatory monocytes (IMs) and regulatory T cells (Tregs) are two immune cell subsets which have been shown to plays keys roles in tumor growth and metastasis through mechanisms involving promotion of tumor cell extravasation and angiogenesis, and suppression of anti-tumor immune responses, respectively. Recruitment of CCR2+ IMs to sites of metastasis is mediated primarily via tumor and stromal cell production of the monocyte chemokine CCL2. We have previously demonstrated that losartan, an angiotensin II type 1 receptor (AT1R) antagonist, can suppress tumor growth in murine metastasis models through inhibition of CCL2-CCR2 signaling and suppression of monocyte recruitment. In addition, prior studies have shown that the tyrosine kinase inhibitor (TKI) toceranib, has immunomodulatory effects on Tregs in tumor-bearing dogs. Thus, we hypothesized that combination losartan and toceranib therapy could exert significant anti-metastatic activity based on their combined immunomodulatory effects on monocytes and Tregs. We performed initial studies in a murine osteosarcoma (OS) experimental metastasis model (K7M2), which demonstrated synergistic anti-tumor activity of losartan when combined with the TKI sunitinib, a drug which shares significant functional homology to

toceranib. Immunohistochemical analyses of canine OS pulmonary metastases, as well as in vitro assays utilizing a canine OS tumor cell line, suggested a potential role for CCL2-CCR2 monocyte recruitment in the pathogenesis of OS in dogs. Utilizing in vitro monocyte chemotaxis assays, we identified a target losartan dose that significantly inhibited CCL2-mediated canine monocyte migration. This dose was therefore used as a target plasma drug concentration for dosing of losartan in PK/PD studies in dogs with OS metastases.

Thus, trials were designed in which we sought to determine the safety and efficacy of losartan plus toceranib as a novel immunotherapy combination in a Phase I/II trial in dogs with spontaneous osteosarcoma (OS) pulmonary metastases. We performed losartan pharmacokinetic analysis for 3 separate dose cohorts of dogs treated with 1mg/kg, 2.5mg/kg, and 10mg/kg losartan (given BID) in normal and tumor bearing dogs, as well as assessed pharmacodynamics (PD) responses via ex-vivo monocyte chemotaxis assays, changes in plasma CCL2 concentrations, and flow cytometric evaluation of pre- and post-treatment changes in peripheral blood Tregs and monocytes. Results of these studies identified a safe and well tolerated dose of losartan in dogs which effectively inhibited CCL2-mediated monocyte migration in blood samples collected from treated dogs. In the 10 mg/kg losartan cohort, objective tumor responses included 2/8 dogs experiencing a partial response (PR) for an overall response rate of 25%, while 1 additional dog experienced clinically meaningful stable disease (>8 weeks), for an overall biologic response rate of 37.5% (3/8 dogs). No objective responses were observed in the 1mg/kg cohort (0/8), while the biologic response rate in this dose cohort was 37.5% (3 dogs with SD). The Median PFS was 42.5 days in

10mg/kg cohort, and 61 days in the 1mg/kg cohort. The ORR observed for combination losartan and toceranib therapy in this small pilot study of dogs with OSA metastasis suggests that a larger, randomized, placebo-controlled trial may be warranted to assess the true potential efficacy of this novel immunotherapy combination.

Introduction

Successful progress in oncology research has led to improvements in the treatment of primary tumors, with advances in molecular therapeutics such as drugs targeting receptor tyrosine kinases helping to make substantial gains in the treatment of patients whose tumors harbor specific mutations (1, 2). Despite this, the inevitable clinical reality is that tumor metastasis remains the single greatest contributor to cancer patient mortality (1, 2). Independent analyses of clinical trial data for certain tumor types, such as those of the breast or pancreas, demonstrate that in the established metastatic setting, survival of these patients has been unchanged for over 30 years (3-5). This lack of therapeutic advancement in the metastatic setting is alarming, given that up to 50% of patients with certain malignancies, such as those of the breast, colon, or bone, will eventually develop metastasis despite successful first line therapy of their localized disease (2, 6, 7). Thus, there remains a critical need for continued clinical development of anti-metastatic therapies, in both the context of preventing metastasis formation and treating established metastatic lesions.

Tumor metastasis is a complex multi-step process governed by intricate, overlapping interactions between tumor cells, immune cells, and their surrounding host environment (8). The G-protein coupled chemokine receptor CCR2 and its ligand,

CCL2, represent a signaling axis which has been demonstrated to play numerous vital roles in both tumor cell intrinsic and extrinsic processes of the metastatic cascade (9). CCL2 is produced by both tumor and stromal cells in primary tumors and metastatic sites (10, 11) Autocrine CCL2-CCR2 signaling in tumor cells has been shown to stimulate their migration and invasion, either directly through CCR2 signaling, or indirectly through the induction of matrix metalloproteinase (MMP) production by tumor cells (12, 13). More well documented are the extrinsic tumor-promoting effects of CCL2-CCR2 signaling in the tumor microenvironment. CCL2 production by tumor cells has been associated with the recruitment of CCR2-expressing inflammatory monocytes to primary tumors, as well as their subsequent polarization into a growth promoting (M2) tumor-associated macrophage (TAM) phenotype associated with immune suppression and promotion of angiogenesis and tumor cell intravasation (14, 15). In addition, the CCL2-CCR2 axis has been heavily implemented in the process of metastatic colonization. In pre-clinical mouse models of metastasis, CCR2 expressing IMs are preferentially recruited early on to metastatic sites via tumor and stromal cell-mediated production of CCL2 (10, 16). Once present at metastases, these monocytes can differentiate into metastasis-associated macrophages (MAMs), which have been shown to play essential roles in metastatic colonization via promotion of tumor cell extravasation, growth, and angiogenesis (10, 17-19). Thus, the combined tumor promoting effects of CCL2-CCR2 signaling in both tumor and stromal-immune cells suggest that this chemotactic axis represents an attractive target for metastasis-directed therapies.

A significant therapeutic advancement in human oncology over the last decade has been the use of immunotherapy as a new treatment modality (20). In the case of certain patients, such as those with melanoma, lung, or renal cancer, immunotherapeutic interventions have resulted in unprecedented responses in patients with advanced stage/metastatic disease that would have otherwise been fatal (21, 22) . These clinical responses have been primarily observed with the use of monoclonal antibodies targeting checkpoint molecules such as programmed cell-death protein 1 (PD-1), or cytotoxic T-lymphocyte associated protein 4 (CTLA-4) (22, 23). However, the magnitude and durability of responses observed for certain tumor types suggest that therapies designed to target other conserved and tightly-regulated immune cell processes, such as those involved in metastasis, likely hold great promise if applied to the right patient subsets.

While these recent developments in human oncology have dramatically increased the relevance of immunotherapy as a new treatment modality, further progress in immuno-oncology and anti-metastatic drug development would be greatly accelerated by the ability to assess immune-based therapies in the more translationally relevant spontaneous canine cancer model (24, 25). While murine cancer models remain an invaluable tool for understanding basic cancer biology, the continued low rate of successful translation of therapies from pre-clinical studies to human cancer patients calls into question their predictive value (26). Spontaneously occurring tumors in pet dogs represent a highly valuable intermediary animal model for evaluation of novel therapeutics and validation of pre-clinical findings, prior to assessment in expensive human clinical trials. Naturally occurring tumors in dogs co-evolve in the presence of an

intact host immune system and complex tumor microenvironment, and share striking similarities on a clinical, biological, genetic, and histological basis (26, 27).

Canine osteosarcoma (OSA) is a prime example of a naturally occurring canine cancer with the potential to inform oncology drug development (2, 28). Dogs with OSA share many clinical similarities with human pediatric OSA including primary tumor location, response to conventional therapies, the presence of microscopic metastases at diagnosis, and unfortunately, a lack of significant improvement of survival times over the past 15 years (2, 28). Yet one significant hurdle to fully leveraging this drug development pathway is that even a basic knowledge of the immune landscape of common canine tumor types, including osteosarcoma, is currently lacking, and to date, there has been little investigation into the role of monocytes and the CCL2-CCR2 axis in the regulation of canine OSA metastasis. Our lab has previously demonstrated an increased infiltrate of CD18+ myeloid cells in canine OSA metastases(29), and have shown that elevated peripheral blood monocyte counts as well as a decrease in the ratio of CD8+ T cells to regulatory T cells are independently associated with decreased survival in dogs with OSA (30, 31). In addition, a substantial amount of clinical data from dogs with OSA suggest that this canine tumor type is not immunologically ignorant, and indeed appears primed for response to immunotherapy. For example, some of the earliest immunotherapy trials in veterinary medicine were conducted in dogs with OSA, and demonstrated that administration of non-specific innate immune stimulants such as Bacillus Calmette-Geurin (BCG) or liposomal muramyl tripeptide (L-MTP) resulted in the activation and induction of tumoricidal activity of monocytes and macrophages, and significantly improved median survival times and disease free intervals in these dogs

(32-36). These data suggest that patient immune responses likely play a significant role in the progression of canine OSA, and that dogs with spontaneous OSA likely represent a valuable model for the assessment of novel immunotherapy combinations.

Losartan, an angiotensin II type 1 receptor (AT1R) antagonist, has been previously reported by our laboratory to suppress tumor growth in murine metastasis models through mechanisms associated with blockade of CCL2-CCR2 monocyte recruitment and inhibition of angiogenesis (Regan et al. in review). In addition, our laboratory has previously shown that the tyrosine kinase inhibitor, toceranib phosphate (Palladia), has immunomodulatory properties, including reduction in peripheral blood Tregs (37). Thus, we sought to assess the safety and tolerability of combined losartan and toceranib therapy, as well as its potential anti-tumor activity and immunomodulatory effects on canine Tregs and monocytes, in dogs with naturally occurring osteosarcoma. Here we provide preliminary evidence for a role of CCL2-CCR2 mediated monocyte recruitment in canine OSA metastasis, and report the results of a Phase I/II clinical trial of continuous losartan/toceranib combination therapy in dogs with spontaneous pulmonary metastatic osteosarcoma.

Materials and Methods

Patient enrollment

All patients enrolled in this trial were client-owned dogs presenting to either the Colorado State University Veterinary Teaching Hospital (Fort Collins, CO), or VRCC Veterinary Specialty and Emergency Hospital (Englewood, CO). Owners of dogs were offered enrollment for treatment with losartan plus toceranib under compliance with the

Clinical Review Board and Animal Care and Use Committee of Colorado State University, and signed informed consent was obtained from all owners prior to enrollment. For consideration of study inclusion, all patients were required to have a previous histopathologically confirmed diagnosis of osteosarcoma, with measurable pulmonary metastasis documented via thoracic radiographs. Prior treatment of the primary tumor with surgical resection was also required. Previous cytotoxic chemotherapy or other antineoplastic treatment was acceptable with a 2-week washout period. Dogs receiving concurrent homeopathic/alternative therapies, or that had received chemotherapy within 2 weeks of enrollment were excluded. In addition, animals that had other concurrent malignancies, or were <1 year of age on Day 0 were also excluded. Prior to study entry, dogs were assessed by physical examination, and standard laboratory tests including complete blood count (CBC), serum chemistry, urinalysis, urine protein:creatinine ratio (UPCR) and systolic blood pressure to ensure that inclusion criteria were met. Dogs were included in the study if the above clinical criteria were met, were deemed to have adequate organ function (as determined by the standard laboratory tests), and had a modified Eastern Comparative Oncology Group (ECOG) score of 0 or 1. Baseline 3-view thoracic radiographs were obtained and evaluated by a board-certified radiologist. Target lesions (up to 5) were identified and measurements (longest diameters) were recorded. For study immune endpoints, baseline serum, plasma and whole blood samples were also obtained, processed accordingly and banked for subsequent analysis.

Drug treatments

For clinical trial dogs and healthy dogs who participated in losartan pharmacokinetic studies, 50mg losartan potassium tablets (Cozaar) were obtained from the Veterinary Teaching Hospital pharmacy and administered orally at doses of 1mg/kg, 2.5mg/kg or 10mg/kg BID. For losartan, doses were rounded up to the nearest tablet size/number. In addition, clinical trial dogs also received Palladia (toceranib phosphate) P.O at a dose of 2.75mg/kg every other day (EOD). Palladia for study dogs was generously supplied by Zoetis Animal health Inc. For dogs enrolled in the 1mg/kg dose cohort, losartan and palladia therapy was started concurrently on Day 0. For the first 5 dogs enrolled in the 10mg/kg dose cohort, dogs received losartan monotherapy only for the first two weeks to allow for accurate collection of losartan pK samples and assessment of pharmacodynamics response via ex vivo monocyte migration. Subsequently, remaining dogs enrolled in this high dose cohort (n=3) initiated losartan and palladia therapy concurrently on day 0.

For in vitro assays and animal experiments, losartan tablets were ground using a mortar and pestle, and dissolved in water and sterile-filtered to obtain a stock concentration of 10mg/mL. Sunitinib maleate was obtained from Sigma-Aldrich (St. Louis, MO), and dissolved in dimethyl sulfoxide (DMSO) to a concentration of 2.5mg/mL. All drug stocks were aliquoted and stored at -20°C. For animal experiments, losartan and sunitinib drug stocks were further diluted in PBS, and administered in 100 μL at the following doses: 1.) Once daily intra-peritoneal (i.p.) injection of 60 mg/kg for the losartan single agent study, or 2.) Twice daily i.p. injection of 3 mg/kg losartan plus

once daily i.p. sunitinib at 0.015 mg/mouse (previously reported to be the mouse equivalent of the 50mg human daily dose) for the combination study.

Patient monitoring and treatment evaluations

Dogs enrolled in the losartan toceranib OSA trial were re-assessed at weeks 1, 2, and 4 post-initiation of therapy, and every 4 weeks thereafter for the duration of the study. At each visit, owner history, physical examination, and systolic blood pressure were recorded. In addition, a CBC, serum chemistry, urinalysis, and UPCR were performed at week 4 and every 4 weeks thereafter. Adverse events (AEs) were recorded and graded according to the Veterinary Cooperative Oncology Group Common Terminology for Adverse Events v1.1 (VCOG CTAE; Vail et al.) based on owner history, physical examination, CBC, serum chemistry, urinalysis, and UPCR. AEs were recorded on day 0, 7, and 14, and every visit thereafter. Reductions in dosage and/or frequency were permitted to manage AEs which were attributed to losartan and/or Palladia. Treatment response was evaluated according to the published modified Response Evaluation Criteria in Solid Tumors (RECIST) and VCOG criteria and were based on measurements obtained for target lesions identified at baseline thoracic radiographs. Responses were monitored via repeat thoracic radiographs performed at week 8 and every 8 weeks thereafter. In addition, dogs in the 10mg/kg losartan dose cohort were also evaluated by thoracic radiographs at week 2. Dogs experiencing stable disease, or a partial or complete response at week 2 (10mg/kg cohort) or week 8 were allowed to remain on study. At each recheck examination, EDTA treated whole blood, as well as serum and plasma were collected for immune endpoints. Serum and plasma

were aliquoted and stored at -80C for batch cytokine analysis by ELISA. Blood was processed within 1 hour of collection by ACK lysis, and freshly isolated PBMCs were immediately assayed for CCL2-directed ex vivo monocyte migration (as described below) at weeks 0, 1, 2, and 4. Remaining PBMCs were immediately frozen and stored in liquid nitrogen until processing for flow cytometry and immune cell subset analysis.

Flow cytometry

Previously processed, frozen PBMCs were thawed, washed into cell culture medium, re-suspended in FACS buffer (PBS with 2% fetal bovine serum and 0.05% sodium azide), counted, and plated at ~ 2.5 x 10^5 cells/well in 96 well round bottom plates for immunostaining. For analysis of T cell subsets, cells were stained with the following directly conjugated antibodies directed against canine CD4 (clone YKIX302.9, conjugated to Pacific Blue, AbD Serotec, Kidlington, UK), canine CD8 (clone YCATE55.9, Alexa 647, AbD Serotec) and canine CD5 (clone YKIX322.3, PE, eBioscience, San Diego, CA, USA) diluted in FACS buffer and incubated for 20 min at RT in the dark. Following cell surface labeling, PBMCs were then stained for intracellular FoxP3 expression, performed as previously described with a cross-reactive, PE-conjugated murine FoxP3 antibody (clone FJK-16s, eBioscience).

For assessment of CD4 and CD8 T cells, cells were gated initially by forward and side-scatter properties, then $CD5^+$ cells were gated and separated into $CD5^+CD4^+$ and $CD5^+CD8^+$populations to determine relative percentages. Gates for analysis of $FoxP3^+$ regulatory T cells (Tregs) were determined based on binding of a FoxP3 matched isotype control antibody to the CD5+/CD4+ T cell population. Tregs were

considered $CD5^+/CD4^+/FoxP3^+$, and relative percentages of Tregs were expressed as the percentage of CD4+ T cells expressing FoxP3. Absolute numbers of Treg, CD4+ and CD8+ T cells in peripheral blood were calculated based on the total lymphocyte count determined from a CBC performed with an automated cell counter on a matched blood sample.

For analysis of CCL2+ peripheral blood monocyte populations, PBMCs were immunostained with the following panel of directly conjugated antibodies: anti canine CD11b (clone Mac-1, PeCy7, Beckman Coulter, Indianapolis, IN, USA), anti canine CD4 (clone YKIX302.9, conjugated to Pacific Blue, AbD Serotec, Kidlington, UK), anti canine MHCII (clone YKIX334.2, FITC, BioRad, Hercules, CA), cross-reactive anti human CD14 (clone TüK4, APC, Invitrogen, Carlsbad, CA), and cross-reactive AlexaFluor-647 conjugated human rCCL2 (CAF-2, Almac, Souderton, PA). Myeloid cell populations were gated first on forward and side scatter properties, then gated on $CD11b^+$/CCL2+ cells, which were further delineated based on their expression of CD4 and MHCII. The cell populations analyzed included $MHCII^-/CD4^+$ granulocytic (based on side scatter properties) myeloid cells and $MHCII^+/CD4^-$ monocytes. All (100%) of CD11b+/CCL2+ cells co-expressed CD14. Flow cytometry was conducted using a Beckman Coulter Gallios flow cytometer (Indianapolis, IN). Analysis was performed with FlowJo software (Ashland, OR).

Losartan pharmacokinetics

For initial assessment of losartan trough concentrations in the 1mg/kg dose cohort, weekly blood samples were collected via jugular venipuncture approximately 6

hours following oral administration of losartan. Blood samples were treated with EDTA anticoagulant, centrifuged, and plasma removed and stored at -80°C prior to batch analysis. For pharmacokinetic analysis of high dose losartan, healthy dogs or dogs with osteosarcoma metastasis enrolled in the clinical trial received losartan (2.5mg/kg or 10mg/kg PO BID.) for 14 days. On day 14, a catheter was placed in the lateral saphenous vein to allow for ease with repeated sampling, and blood was collected at 0.25, 0.5, 1, 2, 4, 6, and 12 hours post dosing. Samples were treated with EDTA anticoagulant, centrifuged, and plasma removed and stored at -80°C prior to analysis. Standard curve and QCs were prepared in the following manner: Initial 10mg/ml stocks of losartan and losartan EXP3174 carboxylic acid metabolite were prepared in 1:1 acetonitrile(ACN)/Milli-Q water (1 mg/mL). A standard curve of losartan and EXP3174 metabolite was then prepared ranging from 5 to 25000 ng/mL in 1:1 ACN/Milli-Q water. 10µl of each appropriate standard was then added to 100 µL of blank plasma collected from naïve ICR mice fortified with 10 µL internal standard (ENMD-2076 at 1000 ng/mL). 10 µL internal standard, 10 µL 1:1 ACN/Milli-Q water, and 100 µL ACN were then added to 100 µL of each unknown plasma sample in 1.5mL micro centrifuge tubes. All samples were then vortexed for 5 min, centrifuged @ 13,300 rpm for 20 min, and 200 µL of the organic phase was transferred to fresh 2-mL micro-centrifuge tubes. Samples were concentrated to dryness on a speed vacuum then reconstituted in 200 µL of 85:15 [v:v], 0.1% formic acid: 50/50 ACN/methanol. Finally, samples were transferred to glass autosampler vials for injection onto the HPLC system. Mass spectra were obtained with a MDS Sciex 3200 Q-TRAP triple quadrupole mass spectrometer (Applied Biosystems, Inc., Foster City, CA) with a turbo ionspray source (operating in positive ion mode)

interfaced to an Agilent 1200 Series Binary Pump SL HPLC system (Santa Clara, CA). Samples were chromatographed with Kinetix 2.6 □ C18 100 Å (Size 50 mm X 4.6 mm) Phenomenex, Torrance, CA). An LC gradient was employed with mobile phase A consisting of 0.1% formic acid and mobile phase B consisting of 50/50 ACN/methanol. Chromatographic resolution was achieved by increasing mobile phase B linearly from 15 to 98% from 1 to 1.5 min, maintaining at 98% from 1.5 to 3.75 min, decreasing linearly from 98 to 215% from 3.75 to 4 min, followed by re-equilibration of the column at 15% B from 4 to 5 min. The LC flow rate was 1.25 mL/min, the sample injection volume was 30 µL, and the analysis run time was 5 min.

Losartan pharmacokinetic data analysis

Quantitation of losartan was based on linear standard curves in spiked blank canine plasma using the ratio of losartan peak area to ENMD-2076 peak area and $1/x^2$ weighting of linear regression. Noncompartmental modeling was used for the calculation of pharmacokinetic (PK) parameters using Phoenix® WinNonlin® software, version 6.3 (Pharsight Corp., Cary, NC, USA).

Ex vivo monocyte migration assays for assessment of losartan pharmacodynamics

Peripheral Blood Mononuclear Cells (PBMCs) were isolated from fresh, EDTA-treated blood of healthy dogs, tumor bearing dogs, or dogs enrolled in the clinical trial and used for in vitro trans-well migration assays by lysing erythrocytes (x2) with ACK buffer solution (150 mM NH_4Cl, 10 mM $KHCO_3$, and 0.1 mM Na_2EDTA). PBMCs were

washed into serum-free Dulbecco Modified Eagle Medium (sf-DMEM), and re-suspended at 1 x 10^6 cells/ml. For in vitro losartan dose titrations, 10mg/mL losartan drug stocks were diluted to 2x treatment concentrations in sf-DMEM. PBMCs were diluted 1:1 in media alone (positive and negative controls) or in media containing 2x drug dilutions. Cells were pre-treated @ 37°C in the incubator for 1 hour prior to plating. The chemotactic stimulus for positive control and drug treated wells consisted of 50 ng/ml recombinant canine CCL2 (R&D Systems, Minneapolis, MN). Negative control wells consisted of sf-DMEM only. For these assays as well as ex-vivo PBMC migration assays of clinical trial patients, 96 well chemotaxis plates (Corning, Corning, NY) with an 8 μM pore diameter were used, and 150μl of media +/- CCL2 was plated in the lower compartment of the plate, while 50μl (5 x 10^4) PBMCs in media +/- drug were plated in the upper compartment of the cell culture insert. Cells were allowed to migrate for 4 h. Following migration, non-migrated cells were removed, wells washed, and remaining adherent PBMCs in the bottom wells were fixed with 4% paraformaldehyde for 10 min on ice, stained with 3% crystal violet (Sigma-Aldrich, St. Louis, MO USA), rinsed with dH_20, and air-dried overnight. For analysis and quantification of migration, 4x4-tiled 10x magnification overviews of 96 well plates were obtained for each individual well, and total monocytes per/well counted using ImageJ (NIH). To normalize data for comparison between clinical trial patients and dose cohorts, the chemotactic index for each patient was calculated, which was determined to be the mean fold-change in CCL2-directed migration (positive control) over mean spontaneous migration observed in negative control wells.

Mice

6-8 week old, female BALB/c mice were purchased from Harlan laboratories (Denver, CO). All animals were housed in microisolator cages in the laboratory animal facility at Colorado State University, and all procedures were approved by the Institutional Animal Care and Use Committee at Colorado State University.

Cell lines

The Abrams osteosarcoma (OSA) cell line was used for all in vitro monocyte migration and CCL2 ELISA assays. The Abrams-OSA cell line was provided by…… The parent K7M2 and luciferase-transfected K7M2 murine osteosarcoma cell lines were generously provided by the laboratory of Dr. Chand Khanna (National Cancer Institute, Bethesda, MD). Both cell lines were maintained in MEM media (Gibco, Grand Island, NY USA) supplemented with 10% fetal bovine serum (FBS; Atlas Biologicals, Fort Collins, CO USA), penicillin (100 U/mL), streptomycin (100 μg/mL), L-glutamine (2 mM), and non-essential amino acids (0.1 mM) (All obtained from Gibco). Cells were grown sterilely on standard plastic tissue culture flasks (Cell Treat, Shirley, MA), under standard conditions of 37 °C, 5% CO_2, and humidified air.

Experimental lung metastasis models

Wild-type BALB/c mice were inoculated by I.V. tail vein injection of 2.5 x 10^5 to 1 x 10^6 K7M2-luc cells in 100 μL PBS. Treatment with losartan (60 mg/kg SID or 3 mg/kg BID, i.p.) ± sunitinib (0.015 mg per mouse i.p.) was initiated 24h after tumor cell inoculation and continued until study completion. To monitor the development and

growth of luciferase-positive pulmonary metastases, bioluminescence imaging was performed thrice weekly using an IVIS100 imager (Perkin-Elmer, Waltham, MA). For imaging, mice were injected i.p. with 100 μL of 30mg/mL luciferin (GoldBio, St. Louis, MO), followed by isoflurane anesthesia and imaging 12 minutes post-luciferin injection (2 minute exposure, medium binning). For the single agent high dose (60 mg/kg) losartan study, metastatic burden was determined by dissecting the heart and lungs and measuring the total pluck weight at study termination, which was compared to age and sex-matched naïve control BALB/c mice.

Canine tumor tissues

Formalin-fixed, paraffin-embedded (FFPE) tissues of osteosarcoma primary tumors and pulmonary metastases were obtained from the Flint Animal Cancer Center tissue archive, or archived cases submitted to the Colorado State University Veterinary Diagnostic Laboratory (CSU-VDL) for post-mortem evaluation between the years of 2007-2014. Necropsy reports from the CSU-VDL database were reviewed, and slides were cut and hematoxylin-eosin stained to confirm the previous diagnoses.

CCL2 and MAC387 Immunohistochemistry

Tissue blocks were sectioned at 5 μm, mounted on Superfrost Plus slides (Fisher Scientific, Pittsburgh, PA) and immunolabeling for the myeloid antigen MAC387, and chemokine CCL2, was performed using standard methods. Briefly, tissue slides were de-paraffinized in xylenes and re-hydrated using a series of graded-alcohols. Antigen retrieval was performed using either: 1.) A proprietary Leica Bond enzyme-1 (Buffalo

Grove, IL) enzymatic retrieval for 10 min (MAC387), or 2.) 10mM sodium citrate buffer, pH 6.0, for 20 min at 125C in a pressurized chamber (CCL2). Immunolabeling was performed using either a Leica Bond Max autostainer (MAC387), or Dako autostainer link 48 (CCL2). Primary antibodies were incubated for 1 hr at room temperature (RT), and included the following clones mouse α human myeloid/histiocyte antigen(Dako, clone MAC 387), or rabbit α human CCL2 (Abcam, ab9669). For CCL2, detection was performed using the universal labeled streptavidin-biotin2 system (Dako, Carpinteria, CA), which consists of incubation with a mixture of biotinylated goat anti- mouse and rabbit IgG secondary antibodies followed by horseradish peroxidase-labeled streptavidin. For MAC387, detection was performed using the Leica Bond Polymer Red Refine Detection (Buffalo Grove, IL) system, which consists of an alkaline phosphatase-linked rabbit anti-mouse IgG. Positive staining was visualized using either refine red (CD18) or DAB (CCL2) chromogen substrates.

Image Analysis

For quantification of MAC387+ immunoreactivity, 10x magnification, whole slide images were captured using standardized exposure times and an Olympus IX83 microscope and Olympus SC30 camera. For analysis, regions of interest (tumor tissue) was outlined in ImageJ (NIH) by a board-certified veterinary pathology (DPR). To ensure accurate quantitative assessment of MAC387+ cells, we used the color deconvolution algorithm developed for the NIH open-source image analysis software, ImageJ. Using the FastRed and FastBlue vectors for this algorithm, whole slide images contained outlined ROIs of primary tumors and metastases were separated in into 8-bit

gray scale images representative of the chromogen color (red) only. A lower threshold limit was then set at a value corresponding to the mean of the isotype control, and universally applied to every single image. Any pixel value falling above this lower threshold value was measured as positive for MAC387, and used to determine the total area of MAC387+ positive within the ROI. This number was the divided by the mean area of a single MAC387+ cell (determined in previous experiments in our lab) to get a total MAC387+ cell count, which then the expressed as cells/mm^2 based on the area of the entire outlined ROI of tumor tissue. For quality control, image masks of the "thresholded", positive counted area were also generated and directly visually compared to the originally captured photomicrographs by a board-certified pathologist, to ensure accuracy in representation of MAC387+ immunoreactivity.

In vitro monocyte migration to OSA tumor-conditioned media and CCL2 neutralization assays

Peripheral Blood Mononuclear Cells (PBMCs) were isolated from fresh, EDTA-treated blood of healthy dogs and used for in vitro trans-well migration assays to assess the degree to which Abrams OSA tumor-conditioned media elicited canine monocyte migration. For generation of tumor conditioned media, 1x 10^5 Abrams OSA tumor cells were plated in a 24-well plate (Falcon) in 1 mL of complete MEM media and grown for approximately 24 hours prior to harvest of the culture supernatant. 600 µL of OSA-conditioned media was placed in the 24-well plate below each migration chamber to serve as the chemoattractant for the PBMCs. The negative control consisted of 600 µL of complete MEM media alone. The positive control consisted of 600 µL of complete

MEM media containing 100 ng/mL of recombinant human CCL2 (Peprotech Inc. Rocky Hill, NJ). For CCL2 neutralization experiments, rabbit polyclonal anti-human CCL2 antibody (Abcam, ab9669) or rabbit IgG (Jackson ImmunoReserach, West Grove, PA) was added to the tumor conditioned media at 5 µg/mL immediately prior to addition of PBMCs. 250,000 PBMCs in 100 µL complete MEM were plated in the top well of the migration chamber insert. Subsequently, cells were allowed to migrate for 4 hours under standard conditions of 37°C, 5% CO_2, and humidified air. Following migration, the non-migrated cells were removed, and membranes were fixed with ice-cold methanol for 10 min on ice, stained with 3% crystal violet (Sigma-Aldrich, St. Louis, MO USA), rinsed with dH_20, and air-dried overnight. The following day, membranes were cut from the cell culture inserts, and mounted “migrated-side” up on superfrost plus glass slides using immersion oil. A total of (5) 40x fields per membrane were counted to determine the Mean # of monocytes/40x field for each membrane. Only cells displaying the appropriate nuclear and cytoplasmic characteristics consistent with monocytes were counted and included in the analysis. Neutrophils and lymphocytes were rarely observed on the migrated side of the membrane, but if present were excluded based on their segmented nuclear morphology, and nuclear:cytoplasmic ratio, respectively. Each migration assay was run in technical replicates at minimum, and each experiment was repeated at least once.

Cytokine analysis of patient samples and cell culture supernatant

A commercially available canine CCL2 ELISA kit (R&D Systems Inc., Minneapolis, MN USA) was used to measure the concentration of CCL2 in pre- and

post treatment patient plasma samples and in osteosarcoma tumor-conditioned cell culture media. In addition, IFN-γ and VEGF was also quantified in pre- and post treatment patient plasma samples also by commercially available ELISA kits (R&D Systems Inc.). For in vitro assessment of CCL2 production by Abrams OSA tumor cells, 1×10^5 cells were plated in a 24-well plate in 1 mL of complete MEM media, and grown for approximately 24 hr prior to harvesting the culture supernatants for ELISA assay. Due to the abundant amount of CCL2 produced by tumor cells, culture supernatants were diluted 1:20 (1:10 with MEM media, and 1:1 with the reagent diluent) prior to ELISA measurement, and a 7-point standard curve with a high standard of 4000 pg/mL was used to determine the concentration of CCL2 within the supernatant. Appropriate controls included cell culture media alone, diluted on a 1:1 ratio with reagent diluent, as well as other canine tumor cell lines (data not shown).

Statistical analyses

For the comparison of mean values between three or more groups, a One-way ANOVA with Tukey's post-test was performed. For comparison of means between two groups, or comparison of repeated measures between two groups, a two-tailed, unpaired Students' *t* test or Wilcoxon matched-pairs t test was used, respectively. All statistical analyses were performed using Graph Pad Prism software (La Jolla, CA, USA).

Results

Immunohistochemical quantification of MAC387^{+} myeloid cell infiltrates and localization of CCL2 expression in canine osteosarcoma primary tumors and pulmonary metastases

For accurate quantitative assessment of MAC387+ cells, we used the ImageJ color deconvolution algorithm as described in Materials and Methods. For each image, regions of interest (tumor tissue only) were defined by a blinded veterinary pathologist, and then masks of the MAC387+ cell area and total tumor area analyzed were generated by intensity thresholding in ImageJ and directly compared to its "parent" photomicrograph to ensure accuracy in the image analysis. Strikingly, the number of MAC387+ cells per mm^2 of tumor tissue was significantly greater in osteosarcoma pulmonary metastases (n=10, 869.8 ± 358.5 cells) as compared to primary tumors (n=26, 191.5 ± 57.2 cells), suggesting a preferential recruitment of monocytes and macrophages to OSA pulmonary metastases (Fig. 4.1 A-C; **$p<0.01$). Importantly, immunohistochemistry for the monocyte chemokine CCL2, performed on matched OSA pulmonary metastases, demonstrated strong, peri-nuclear, cytoplasmic positive immunolabeling of tumor cells for CCL2 (Fig. 4.1D), suggesting a potential relationship between CCL2 expression and monocyte and macrophage recruitment to OSA metastases.

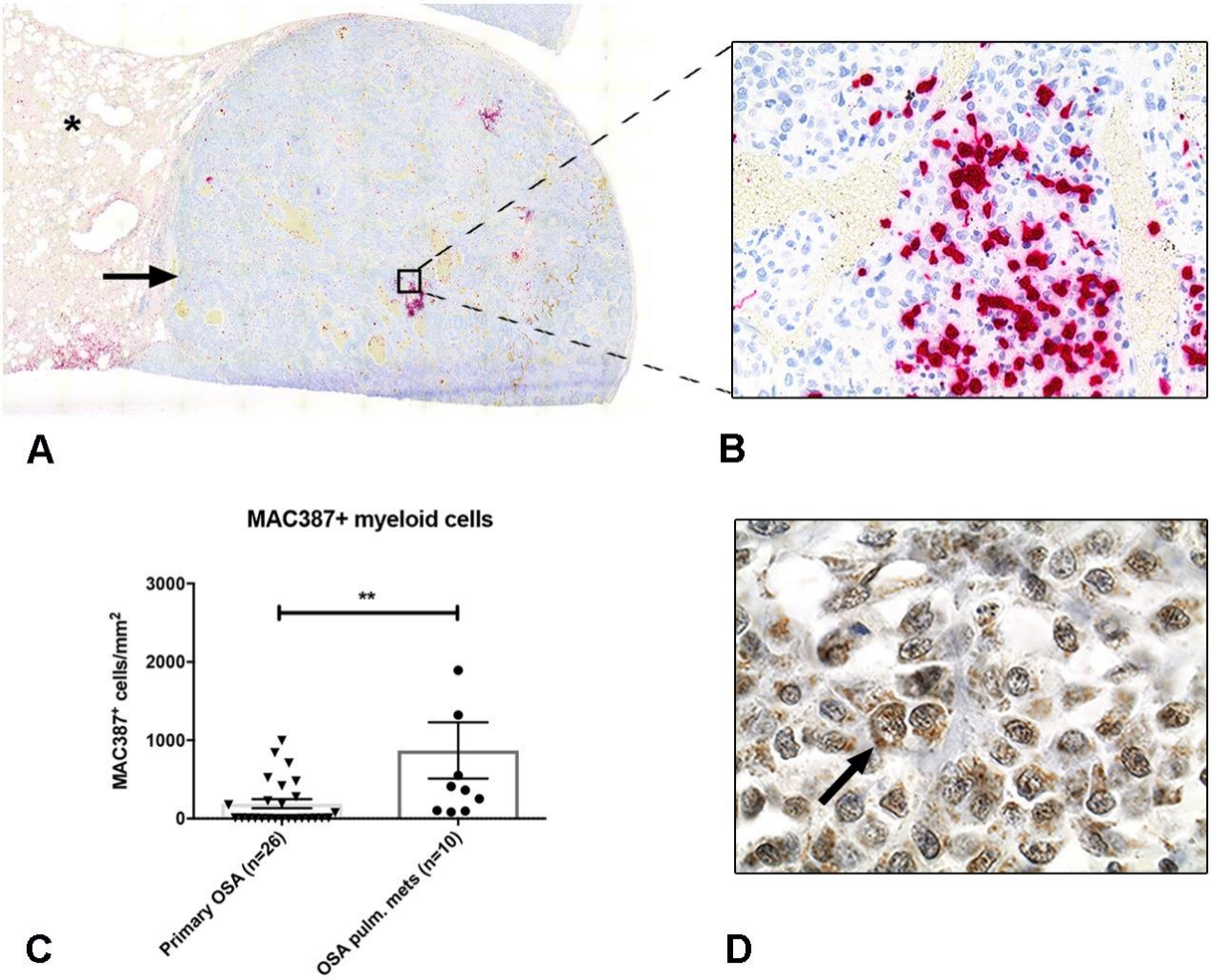

Figure 4.1. MAC387+ myeloid cells are increased in canine osteosarcoma pulmonary metastases vs. primary tumors and are associated with tumor cell production of the monocyte chemoattractant CCL2. (A) 10x magnification overview of an osteosarcoma pulmonary metastasis (arrow) demonstrating extensive peripheral and intratumoral infiltrates of MAC387+ monocytes and macrophages (red) (Asterisk denotes normal lung parenchyma). (B) 40x higher magnification of the metastatic lesion in (A) demonstrating the density of intratumoral MAC387+ myeloid cells (red). (C) Graph showing immunohistochemical quantification of MAC387+ myeloid cells in osteosarcoma pulmonary metastases as compared to primary tumors. (D) 100x magnification image of the same metastatic lesion shown in (A & B) demonstrating strong intracytoplasmic, peri-nuclear positive immunolabeling of OSA tumor cells for CCL2 (arrow; brown). Fast Red (MAC387) or DAB (CCL2) chromogens. Hematoxylin counterstain. Data expressed as means ± SEM, and was analyzed by two-tailed Student's *t* test (C), (n=10-26 animals per group, ***p<0.01*).

Canine osteosarcoma tumor-conditioned media elicits strong ex vivo monocyte migration in a CCL2 dependent manner

A canine osteosarcoma cell line (Abrams-OSA) was used to further investigate the potential immunological mechanisms responsible for the MAC387+ monocyte infiltrates observed in osteosarcoma metastases. First, we performed trans-well monocyte migration assays to evaluate the effects of Abrams-OSA conditioned medium on ex vivo monocyte recruitment, using canine peripheral blood mononuclear cells (PBMC) from healthy control dogs. After 4 hours, Abrams OSA tumor-conditioned media strongly elicited canine monocyte migration (13.3 ± 4.1 cells per hpf), which was significantly greater than the random migration observed in negative control wells (1.5 ± 1.8 cells per hpf), and similar to that observed for the 100ng/mL CCL2 positive control wells (14.3 ± 5.0 cells per hpf) (Fig. 4.2 A-D, **$p<0.01$, ***$p<0.001$). To determine if CCL2 production by Abrams-OSA cells was potentially responsible for this ex vivo monocyte recruitment, CCL2 secreted by Abrams-OSA cells was quantified using a canine CCL2 ELISA, as described previously (38). Abrams-OSA conditioned media contained very high concentrations of CCL2, with a mean concentration of 24.5 ± 11.8 ng/mL (Fig. 4.2E).

While these assays confirmed the ability of Abrams-OSA cells to make abundant amounts of the monocyte chemokine CCL2, they still did not directly implicate this CCL2 production with the observed ex vivo monocyte migration. In order to investigate this, monocyte migration assays were repeated using Abrams-OSA conditioned media +/- treatment with a CCL2 neutralizing antibody (previously demonstrated to bind canine CCL2), or irrelevant IgG control antibody. Addition of the CCL2 neutralizing antibody to

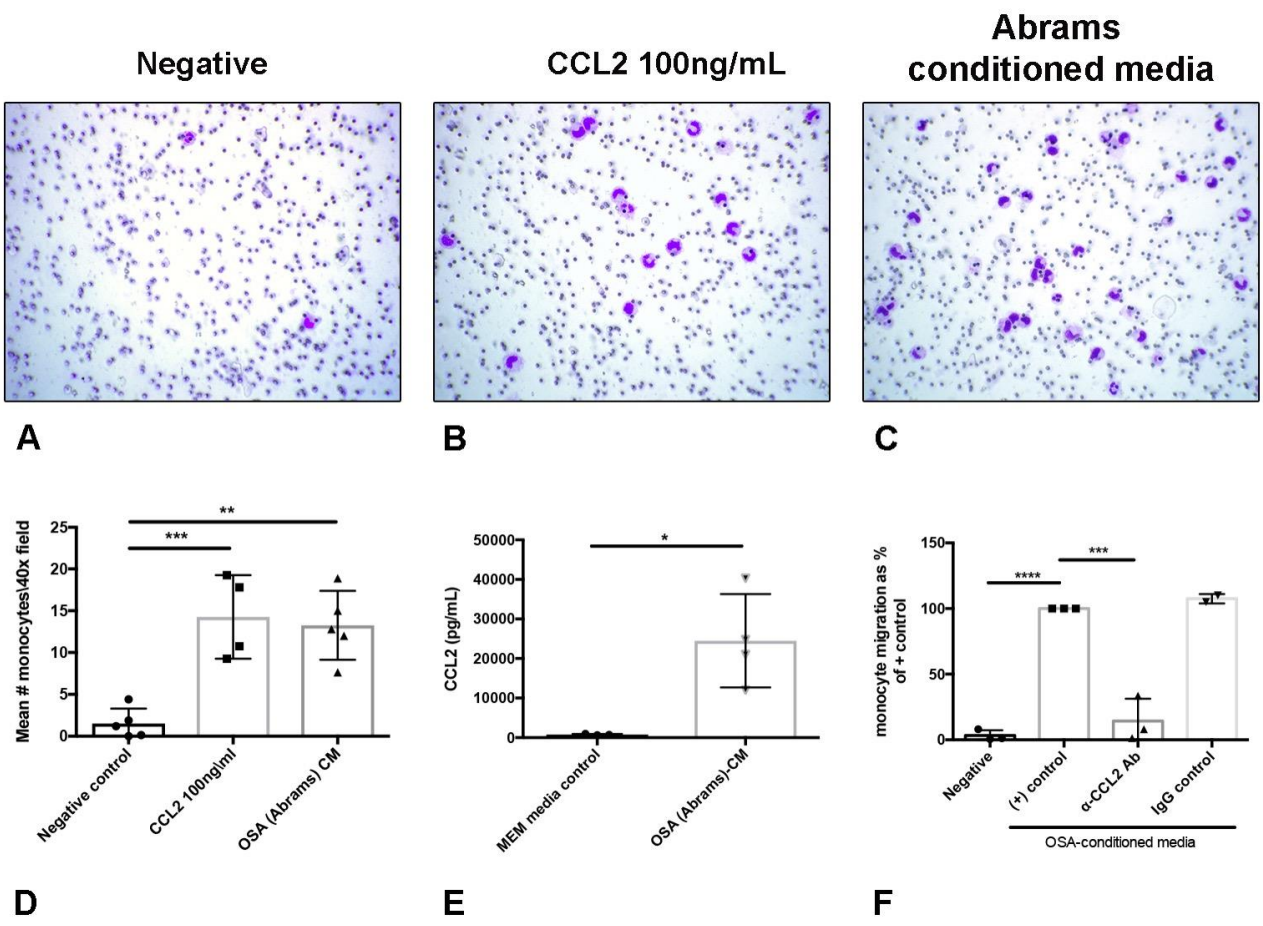

Figure 4.2. Canine osteosarcoma cells produce abundant amounts of CCL2 in vitro and elicit canine monocyte migration in a CCL2-CCR2 dependent manner. (A-C) Representative photomicrographs of crystal violet stained membranes of the cell culture inserts used for quantification of in vitro monocyte migration to OSA tumor-conditioned media. Complete MEM media stimulated little to no monocyte migration (A), while conditioned-media from canine Abrams OSA cells stimulated strong monocyte migration (C), which was significantly greater than the negative control, and similar in magnitude to the positive control of 100ng/mL recombinant human CCL2 (B). (D) Graph showing quantification of in vitro canine monocyte migration assays depicted in (A-C). (E) Graph showing CCL2 production by Abrams OSA cells, quantified via ELISA performed on the same tumor-conditioned media utilized in the monocyte migration assays shown in (A-D). (F) Neutralization of CCL2 in Abrams OSA-conditioned media using a cross-reactive anti-human CCL2 antibody (5 µg/mL) resulted in a significant (~60-80%) reduction in in vitro monocyte migration as compare to the positive control of HSA-conditioned media only. Data expressed as means ± SD, and were analyzed by One-way ANOVA, with Tukey's post-test comparison (n=3-5 independent experiments, each performed in duplicate or triplicate, *p < 0.05**p < 0.01, ***p < 0.001, ****p<0.0001).

Abrams tumor-conditioned media significantly reduced the mean number of migrated monocytes by ~85% as compared to that observed for the positive control of Abrams OSA-conditioned media alone (Fig. 4.2F, ***p=0.0001). This result verifies that the ex vivo monocyte migration elicited by Abrams-OSA cells is in fact dependent to a significant degree on tumor cell production of CCL2.

Evidence of synergistic anti-tumor activity of losartan plus sunitinib therapy in a mouse K7M2 osteosarcoma experimental metastasis model

We have previously demonstrated that the angiotensin receptor blocker drug, losartan, demonstrates significant anti-metastatic activity in murine breast and colon cancer experimental metastasis models through its ability to inhibit CCL2-CCR2 monocyte recruitment and reduction in angiogenesis. Initially, we evaluated the anti-metastatic activity of single agent losartan in the K7M2 model at a dose of 60 mg • kg^{-1} • d^{-1} i.p., which is the same dose we have previously demonstrated to have anti-tumor activity in other mouse metastasis models. As assessed by gross visualization of lung metastases and total lung weights, high dose losartan monotherapy showed a trend towards reduction in experimental metastasis growth in the K7M2 model; however, this trend was not significant (Fig. 4.3 A, B). Previous work by Ozao-Choy and others have shown that the tyrosine kinase inhibitor, sunitinb, also exhibits anti-angiogenic activity, and can reverse tumor immune suppression in mice via decreasing the number of myeloid-derived suppressor cells and Tregs. Thus, we hypothesized that the combined immunomodulatory and anti-angiogenic effects of losartan and sunitinib would exert

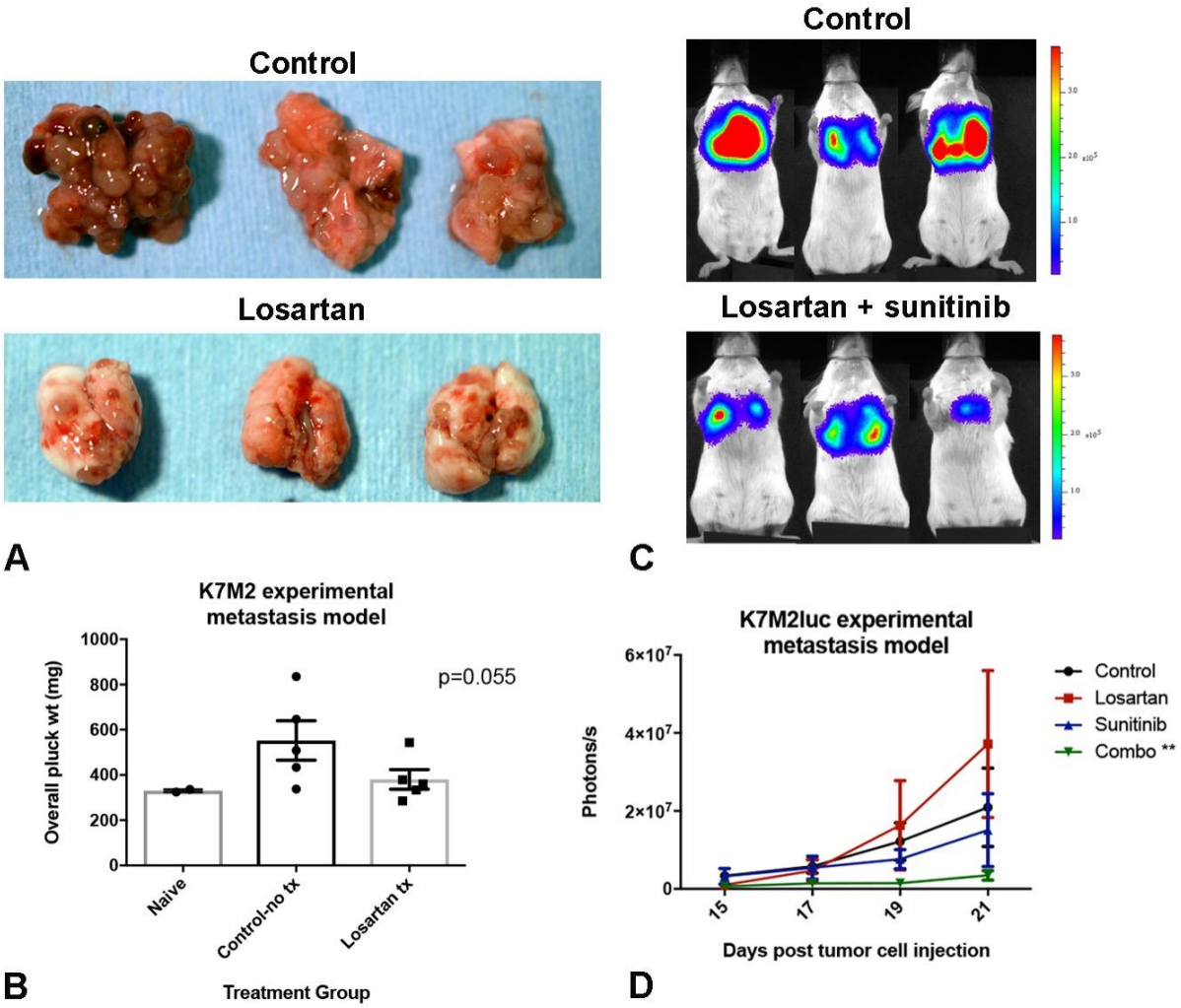

Figure 4.3. Losartan demonstrates anti-metastatic activity in a mouse K7M2 osteosarcoma experimental metastasis model which is synergistic when used in combination with the tyrosine-kinase inhibitor sunitinib. (A) Representative gross images of lung metastases in control and high dose losartan-treated (60 mg • kg^{-1} • d^{-1}) mice on day 21 post tail vein injection of 1 x 10^6 K7M2 cells. (B) Graph showing quantification of lung metastatic burden in control vs. high-dose losartan treated mice, as determined by overall pluck weight. (C) IVIS bioluminescent images of K7M2-luciferase positive pulmonary metastases on day 22 in control mice and mice treated with low dose losartan in combination with sunitinib. (D) Graph depicting quantification of K7M2luc pulmonary metastasis growth over time in control, single agent losartan or sunitinib-treated mice, and combination losartan + sunitinib treated mice, expressed as photons/second, and quantified by repeated bioluminescent IVIS imaging. Data expressed as means ± SD, and were analyzed by two-tailed Student's *t* test (B) or Two-way ANOVA (D), (n= 3-5 mice/group, **p<0.01).

more significant anti-metastatic activity in the K7M2 metastasis model as compared to that observed for losartan monotherapy.

Our previous work evaluating the pharmacokinetics of 60 mg • kg^{-1} • d^{-1} losartan dosing in mice suggested that the maximum plasma drug levels and exposure seen at this dose would not be biologically achievable in dogs. Thus, for these studies, mice were treated with losartan at a significantly lower and more clinically relevant dose of 3 mg • kg^{-1} every 12 hours, and sunitinib was administered at 0.015 mg per mouse, a dose previously published to be equivalent to the 50mg daily human dose. While neither losartan nor sunitinib alone demonstrated any significant anti-metastatic activity at these lower doses, the combination of the two drugs resulted in a robust reduction in pulmonary metastatic burden as compared to control and losartan only treated mice, by ~ 83% and 91%, respectively, as quantified by repeated bioluminescent imaging (Fig. 4.3 C, D, **$p<0.01$ control vs combination therapy, and losartan vs. combination therapy). As sunitinib bears significant structural and functional similarity to toceranib phosphate (55), a tyrosine kinase inhibitor approved for the treatment of canine mast cell tumor, we felt this data provided additional strong rationale for a clinical trial assessing losartan plus toceranib immunotherapy for the treatment of pulmonary metastatic osteosarcoma in dogs.

Losartan inhibits in vitro CCL2-mediated canine monocyte migration at pharmacologically relevant concentrations

Prior to initiating clinical studies in OSA-bearing dogs, we first sought to determine the therapeutic range of losartan required for inhibition of CCL2-directed in

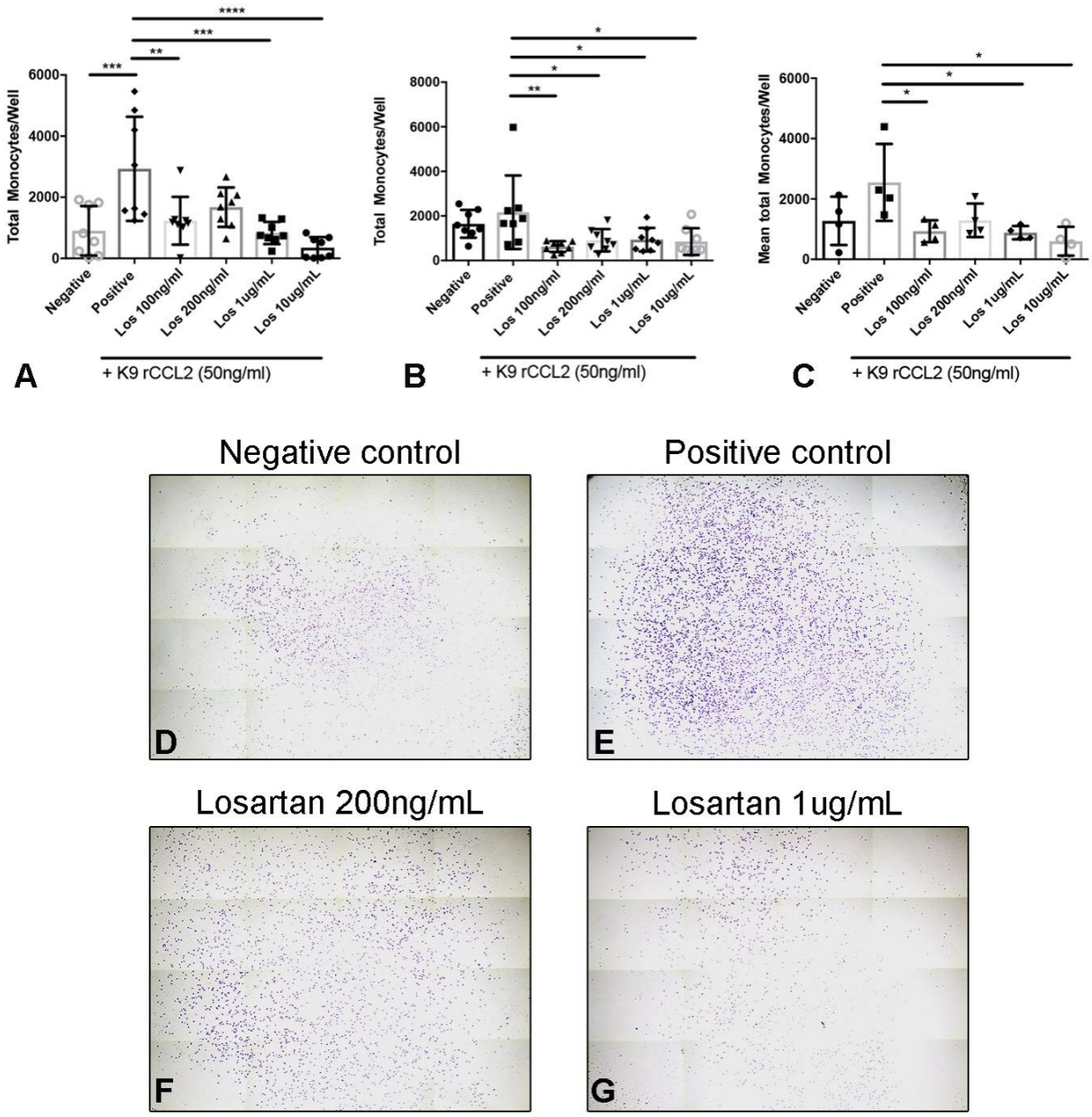

Figure 4.4. Losartan inhibits *CCL2-CCR2* mediated canine monocyte migration in vitro at pharmacologically relevant concentrations. (A-C) Graphs showing quantification of ex vivo CCL2-directed monocyte migration of PBMCs obtained from tumor-bearing dogs (A), healthy control dogs (B), or the pooled-results of both healthy and tumor-bearing dogs (C). PBMCs were pre-treated with losartan for 1h at the indicated concentrations. (D-G) Representative whole well images (10x magnification) of the canine PBMC

migration assays quantified in (A). Data expressed as means ± SD, and were analyzed by One-way ANOVA, with Tukey's post-test comparisons (n= 2 (tumor-bearing and healthy dogs) or 4 (tumor and healthy) dogs, 8 (A, B) to 20 (C) technical replicates per condition, each replicate being the mean number of migrated monocytes determined in (16) 10x fields (*p <0.05, **p < 0.01, ***p < 0.001, ****p<0.0001).

vitro canine monocyte migration. To determine this, we again performed trans-well migration assays, this time utilizing a 96 well format for more high throughput screening, and canine rCCL2 for the chemotactic stimulus instead of tumor-conditioned media. For these assays, PBMCs were isolated via ACK lysis of EDTA-treated whole blood obtained from both tumor-bearing dogs (n=2, OSA and grade III soft tissue sarcoma) and healthy control dogs (n=2). In tumor bearing dogs, in vitro losartan treatment of PBMCs significantly reduced CCL2 mediated migration in a dose-dependent manner to levels ranging from 42% (100ng/mL) to 12% (10 μg/mL) of those observed for untreated PBMCs in CCL2 positive control wells (Fig. 4.4 A, D-G **p<0.01, ***p<0.001, and ****p<0.0001). Similar results were also observed for PBMCs obtained from healthy control dogs, with losartan inhibiting PBMC migration to ~ 29% (100ng/mL) to 39% (10 μg/mL) of the levels observed in CCL2 positive control wells (Fig. 4.4B, *p<0.05, **p<0.01). When analyzing the pooled results for both tumor-bearing and healthy control dogs, losartan treatment reduced CCL2-directed ex vivo monocyte migration to 36-24% (100ng/mL to 10 μg/mL) of those observed for untreated CCL2 positive control wells (Fig. 4.4C, *p<0.05). Based on the results of these in vitro assays, we determined that our target therapeutic range for in vivo inhibition of canine monocyte migration was a maximum plasma concentration (Cmax) of at least ~ 200 ng/mL, with a minimum exposure (AUC) of 60 $\mu g \bullet min \bullet mL^{-1}$. Previous work by Christ et al. determined the pharmacokinetics of losartan in healthy dogs following single p.o doses of 5 mg/kg to 20 mg/kg (39). These studies demonstrated a strong linear relationship between losartan dose and plasma concentration (Cmax) and systemic exposure (AUC). Based on this data, we were able to extrapolate the predicted Cmax and AUC for a losartan dose of 1

mg/kg, as this is the dose previously published for the treatment of proteinuria in dogs (40). Based on this extrapolation, a p.o losartan dose of 1 mg/kg was predicted to result in a Cmax of 285 ng/mL and an AUC of 5.9 $\mu g \bullet min \bullet mL^{-1}$. While the Cmax was within the range identified by our in vitro migration assays, the overall exposure was significantly lower; however, as this dose of losartan was known to be safe for repeated daily administration to dogs, we chose 1 mg/kg as our initial target dose for treatment of OSA metastasis-bearing dogs. Overall, these results demonstrate that similar to our prior studies with human and murine monocytes, losartan can significantly inhibit CCL2-mediated canine PBMC migration at a dose which is likely to be clinically achievable.

Patient characteristics

Sixteen dogs that met eligibility criteria were enrolled in the study between December 2014 through February 2017, with 8 dogs enrolled in the initial 1 mg/kg dose cohort, and a subsequent 8 dogs enrolled in the 10 mg/kg cohort. All but two of the dogs in the study were treated at the Colorado State University Veterinary Teaching Hospital (Fort Collins, CO), while the other two dogs (1 in each cohort) were treated by Dr. Robyn Elmslie at the VRCC-Veterinary Specialty and Emergency Hospital (Englewood, CO). Data from all 16 dogs was available for assessment of toxicity associated with combined losartan and toceranib therapy. In addition, data for single agent high dose losartan (10mg/kg) toxicity assessment was available for 5 dogs treated with losartan only for 2 weeks prior to initiation of toceranib therapy. Progression-free survival was evaluable for all dogs; however, measurable responses were only evaluable in 5/8 dogs in the 1 mg/kg trial and 7/8 dogs in the 10 mg/kg trial, as the remaining dogs did not

remain on study long enough for repeat thoracic radiographs. Samples for pharmacokinetic analysis were available for all 8 dogs in the 1 mg/kg cohort, and the initial 5 dogs treated with single agent losartan in the 10 mg/kg cohort. All patients had prior surgical removal of their primary tumor, which included amputation for 14 cases of appendicular OSA, amputation and hemi-pelvectomy for a single case of axial (right ischium) OSA (10mg/kg cohort), and hemi-mandibulectomy for a single case of mandibular OSA (1mg/kg cohort). Prior adjuvant chemotherapy was administered in 14 of 16 patients, and consisted primarily of carboplatin-based protocols. Two patients did not receive prior therapy due to the presence of pulmonary metastases at time of diagnosis. All patients underwent pre-treatment evaluation including physical exam, blood pressure measurement, serum chemistry and CBC, and baseline thoracic radiographs. Baseline characteristics for all patients, including information on primary tumor and prior therapies, are presented in Table 4.1.

Losartan pharmacokinetics and pharmacodynamic responses in peripheral blood

Pharmacodynamic responses to 1 mg/kg losartan therapy were evaluated via quantification of ex vivo PBMC migration to CCL2 and ELISA measurement of plasma CCL2 levels, performed on day 14. Compensatory elevations in plasma CCL2 levels has been previously shown to be a valid, mechanism of action-based pharmacodynamic endpoint for CCR2 antagonists in human clinical trials (ClinicalTrials.gov NCT01215279). Monocyte migration data was expressed as the chemotactic index, as described in materials and methods. Samples from all 8 dogs in this cohort were

Table 4.1		
Baseline characteristics	**Losartan 1mg/kg** *(+ toceranib phosphate 2.75mg/kg EOD)*	**Losartan 10 mg/kg** *(+ toceranib phosphate 2.75 mg/kg EOD)*
Median age, years (range)	8.5 (3-11)	10 (7-11.5)
Sex (no., %)		
Male castrated	2 (25)	5 (62.5)
Female spayed	6 (75)	3 (37.5
Breed (no., %)		
Purebred	6 (75)	5 (62.5)
Mixed breed	2 (25)	3 (37.5
Primary tumor location (no., %)		
Forelimb	5 (62.5)	5 (62.5)
Hind limb	2 (25)	2 (25)
Other	1 (12.5)	1 (12.5)
Adjuvant chemotherapy		
Carboplatin	6 (75)	5 (62.5)
Alt. Carbo/DOX	□	1 (12.5)
Other[a]	□	2 (25)
None[b]	2 (25)	□
[a]Carboplatin +/- rapamycin clinical trial		
[b]Pulmonary metastases present at time of diagnosis		

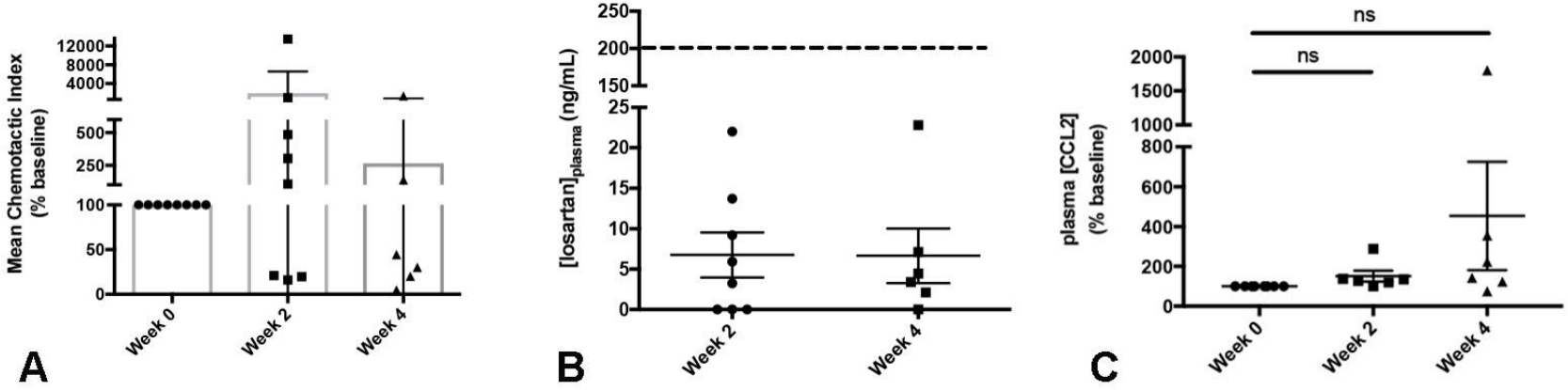

Figure 4.5. Assessment of losartan drug levels and pharmacodynamic responses of dogs in the 1 mg/kg cohort. (A) Graph showing quantification of ex-vivo CCL2 directed migration of PBMCs obtained from dogs following 2 and 4 weeks of oral losartan dosing at 1 mg/kg BID. Data depicted is the mean chemotactic index (fold-change of CCL2-directed migration over negative control wells) as a percentage of week 0 baseline. (B) Plasma levels of losartan, determined in matched blood samples collected concurrently (~ 4-6h post dose) with the same blood utilized for migration assays in (A). The dotted line indicates the 200 ng/mL level, the target concentration identified for inhibition of monocyte migration by the in vitro chemotaxis assays shown in Fig S2. (C) Graph showing plasma CCL2 concentration at week 0 and following 2 and 4 weeks of losartan 1 mg/kg dosing, as measured by ELISA (expressed as % of week 0 baseline). Data expressed as means ± SD (migration assay) or SEM (losartan and CCL2 plasma concentrations), and were analyzed by two-tailed paired *t* test (Wilcoxon signed rank test), (n=6-8 dogs/time point, ns, not significant).

available for evaluation of monocyte migration and losartan pharmacokinetics, while 6 of 8 dogs had plasma samples available for CCL2 measurement.

Unexpectedly, quantification of CCL2-mediated ex vivo monocyte migration demonstrated an overall increase in the mean (± SD) chemotactic index as a percentage of baseline at both week 2 (1,924 ± 4,677 %, n=8) and week 4 (266 ± 537%, n=6) post losartan therapy (Fig. 4.5 A, B). While 3 of 8 dogs in this cohort did experience a 79-85% reduction in their mean chemotactic index, the other 5 dogs demonstrated increased monocyte migration ranging from 106% to 13,469% of their baseline measurements. Determination of losartan levels in plasma collected concurrently with the peripheral blood utilized for migration assays (~ 4-6h post dose) demonstrated significantly low levels of the drug, and substantial inter-individual variation, with a plasma concentration (mean ± SD) of 6.8 ± 7.9 ng/mL at week 2 (n=8) and 6.7 ± 8.3 ng/mL at week 4 (n=6) (Fig. 5B). In fact, 1 to 3 dogs in this cohort had drug levels below the lower limit of quantification (<1 ng/mL) at each time point. For the 6 dogs in which post-treatment plasma CCL2 concentrations could be measured, 5 of these 6 dogs demonstrated increases in plasma CCL2 at both weeks 2 and 4 post treatment, ranging from 20 to 1800% above pre-treatment baseline values (Fig. 4.5C, p=0.06, week 2, and p=0.09 week 4). No significant correlations were observed between changes in monocyte migration or plasma CCL2 concentrations and losartan blood levels (data not shown). Although 2 weeks would be considered a relatively short time period for a significant enough increase in tumor burden to account for elevations in plasma CCL2, it is not without reason. However, 2 of the 5 dogs demonstrating

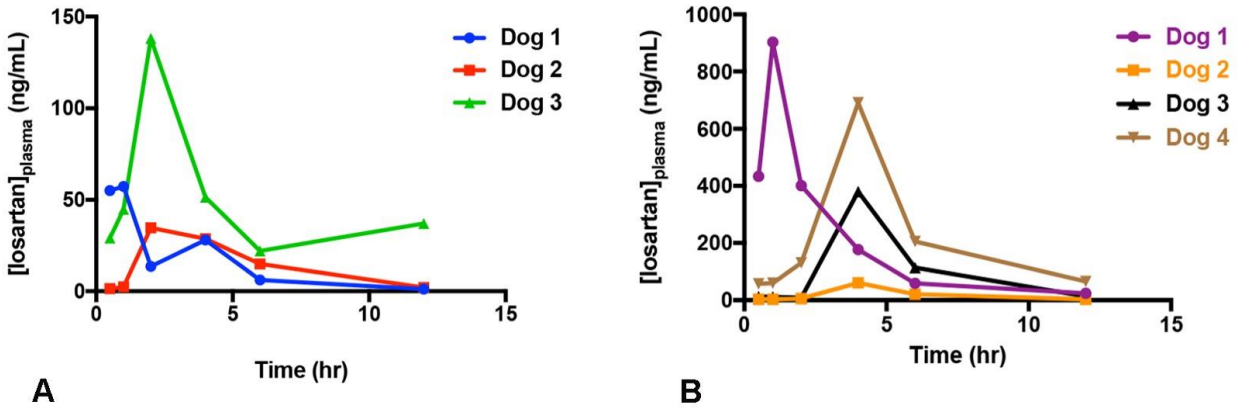

Figure 4.6. Losartan drug concentration curves for individual dogs in the 2.5 mg/kg and 10 mg/kg cohorts (A) Losartan plasma concentration over time for individual healthy dogs following 14 days consecutive oral dosing at 2.5 mg/kg BID. (B) Losartan plasma concentration over time for individual osteosarcoma-bearing dogs following 14 days consecutive oral dosing at 10 mg/kg BID.

increases in plasma CCL2 experienced stable disease of 12 and 16 weeks, while the 1 dog in which the plasma CCL2 concentration did not increase had progressive disease (grossly detectable subcutaneous metastasis) by week 4, suggesting that progression of disease is an unlikely mechanism accounting for this increase.

However, given the significantly low plasma levels of losartan and lack of robust pharmacodynamic responses on ex vivo monocyte migration in these patients, we decided to perform an interim dose escalation study of losartan to 2.5 mg/kg BID in a cohort (n=3) of healthy control dogs. Again, losartan pharmacokinetics and pharmacodynamics were assessed after 14 days of losartan therapy, at six defined time points post dose. Drug concentration curves over time for individual dogs are shown in Figure 4.6. In these dogs, the mean ($\pm$ SD) C_{max} for losartan was 76.7 $\pm$ 54.3 ng/mL, while the mean $\pm$ SD $AUC_{0\text{-}12h}$ was 18.2 $\pm$ 13.2 $\mu g \bullet min \bullet mL^{-1}$ (Fig. 4.7 A, B). The mean $\pm$ SD chemotactic index (expressed as % of baseline) for CCL2-mediated ex vivo monocyte migration following 2 weeks of losartan dosing in these dogs was 73 $\pm$ 51% (range of 42 - 132%) (Fig. 4.7C). These data demonstrated that while the effects of losartan on CCL2-mediated monocyte pharmacodynamic responses were significantly more robust as compared to the 1mg/kg cohort, still only 2 of 3 dogs demonstrated a reduction in monocyte migration below baseline, and maximum losartan plasma concentrations and exposure levels were still significantly below the therapeutic levels determined from our prior in vitro migration assays. Based on these results, we decided to enroll an additional 8 dogs in the clinical trial at an escalated losartan dose of 10mg/kg BID.

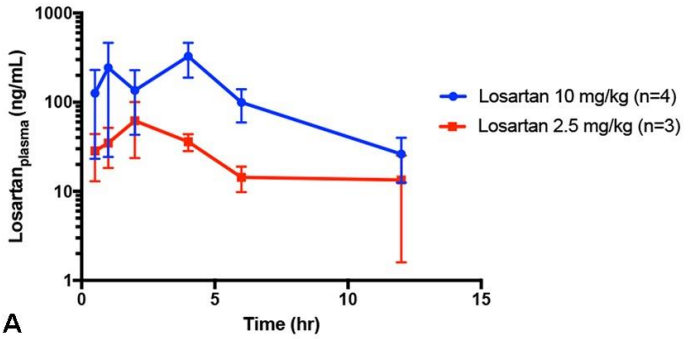

A

Dose	Parameter	
	Cmax (ng/mL)	*AUC (µg*min/mL)*
2.5 mg/kg	76.7 (± 54.3)	18.2 (± 13.2)
10 mg/kg	508.6 (± 368.1)	94.9 (± 64.2)

B

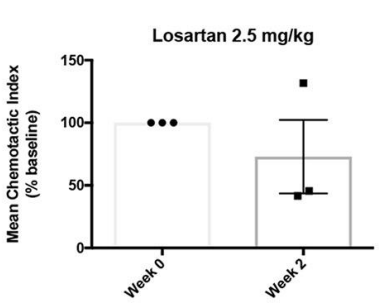

C

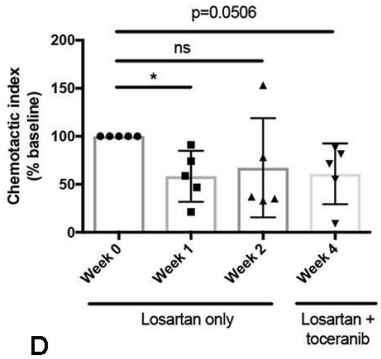

D

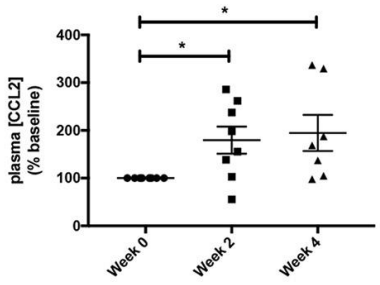

E

Figure 4.7. Pharmacokinetics and pharmacodynamic responses of losartan dose-escalation in healthy and osteosarcoma metastasis-bearing dogs. (A) Mean (± SEM) plasma losartan concentration over time following oral administration of losartan at 2.5 mg/kg or 10 mg/kg BID for 14 consecutive days (n=3 or 4 dogs/group). (B) Table summarizing pertinent pK parameters of losartan maximum concentration (Cmax) and concentration over time (AUC) for the two dose cohorts. (C) Pharmacodynamic assessment of ex vivo CCL2-directed monocyte migration pre- and 14 days post dosing of losartan at 2.5 mg/kg BID in healthy dogs (D) Pharmacodynamic assessment of ex vivo CCL2-directed monocyte migration pre- and post 7, 14, and 28 days oral dosing of either losartan only (10 mg/kg BID, days 7 and 14), or losartan (10mg /kg BID) plus toceranib (2.75 mg/kg EOD; day 28) in osteosarcoma-bearing dogs. (E) Graph showing plasma CCL2 concentration at week 0 and weeks 2 and 4 post losartan 10 mg/kg dosing, as measured by ELISA (expressed as % of week 0 baseline). For graphs (C & D), data depicted is the mean chemotactic index (fold-change of CCL2-directed migration over negative control wells), as percentage of week 0 baseline. Data expressed as means ± SD (C, D) or SEM (A, E) and were analyzed by a two-tailed paired *t* test (Wilcoxon signed rank test), (n=3-8 dogs/group/time-point. *p < 0.05).

The first 5 dogs enrolled in this cohort were treated with losartan only for an initial two-week period to eliminate the effects of potential pharmacokinetic interactions between losartan and palladia. Blood samples were collected from these five dogs for assessment of monocyte migration at week 1 and week 2 post losartan treatment, and again at week 4 following addition of toceranib therapy. In addition, repeated blood samples at six time points post day 14 dosing were collected in 4 of the 5 dogs for pharmacokinetic analysis. The other dog was enrolled at an outside veterinary hospital (VRCC) and did not have a complete set of blood samples available for pK analysis. Plasma samples were collected from all 8 dogs in this cohort at Weeks 0, 2, and 4 for quantification of CCL2 via ELISA. Mean (± SEM) plasma losartan concentration over time for the 10 mg/kg cohort vs. 2.5 mg/kg cohort is shown in Fig. 4.7A, with drug concentration curves for individual dogs presented in Fig. 4.6 B. A comparison of pertinent pK parameters between the two cohorts is summarized in Fig. 4.7B. Again, significant inter-individual variation was observed in this 10mg/kg cohort, and the mean concentration curves for individual dogs presented in Fig. 4.6 B. A comparison of pertinent pK parameters between the two cohorts is summarized in Fig. 4.7B. Again, (± SD) C_{max} for losartan was 508.6 ± 368.1 ng/mL, while the mean ± SD $AUC_{0\text{-}12h}$ was 94.9 ± 64.2 μg • min • mL^{-1} (Fig. 4.7B). Most importantly however, the observed mean maximum losartan concentration and exposure over time were significantly above the target therapeutic levels determined from our prior in vitro migration assays.

Pharmacodynamic assessment of ex vivo CCL2-mediated monocyte migration showed a significant reduction in the mean (± SD) chemotactic index (expressed as % of baseline) at week 1 post losartan therapy in all 5 dogs (58.3 ± 26.6%; range of 21.3 -

91%) (Fig. 4.7D, *p<0.05). However, this reduction was not statistically significant at week 2 (67.3 ± 51.6 %, mean ± SD), as a single dog experienced an increase in monocyte chemotaxis above baseline (Fig. 4.7D, *p<0.05). Of note, addition of toceranib therapy at week 2 resulted in restored inhibition of monocyte migration in this dog at week 4, with a reduction in the mean (± SD) chemotactic index of all patients to 60.9 ± 31.6% of baseline, although this effect was not significant (Fig. 4.7D, p=0.056). Post losartan treatment increases in plasma CCL2 levels were observed in 7 of 8 dogs at week 2, and 6 of 7 dogs at week 4, with mean (± SD) increases of 79.4 ± 80.4% and 94.6 ± 99.9% above baseline, respectively (Fig. 4.7E, *p<0.05). However, similar to the 1mg/kg cohort, no statistically significant correlations were observed between changes in plasma CCL2 levels, ex vivo monocyte migration, and blood losartan concentrations (data not shown). Nonetheless, these significant elevations in plasma CCL2 levels and consistently lower ex vivo monocyte migration at week 2 and 4 post losartan therapy provide strong evidence for greater CCR2 target inhibition by this higher (10 mg/kg) dose of losartan, as compared to results for the 1 mg/kg cohort.

Toxicity and treatment response

Concurrent oral administration of losartan and toceranib was well tolerated by dogs in both the 1mg/kg and 10mg/kg losartan dose cohorts (Table 4.2). Of important note, no dogs experienced any significant degree of hypotension associated with losartan treatment, and repeated blood pressure measurements for dogs in the 10mg/kg losartan cohort are shown in Fig. 4.8. Toxicities observed in the 1mg/kg losartan plus toceranib cohort were predominately grade 1 and 2 and consisted

Table 4.2: Treatment-related adverse events by dose cohort

Losartan 1mg/kg + toceranib phosphate 2.75mg/kg EOD

Adverse event	*Grade*	*n (events/dogs)*
Lethargy		3/2
	1	2/2
	2	1/1
Generalized muscle weakness	2	1/1
Anorexia		4/2
	1	3/2
	2	1/1
Vomiting	1	2/2
Diarrhea	1	2/2
Neutropenia	1	3/2
Thrombocytopenia	1	2/2
Metabolic: Increase ALT		2/1
	2	1/1
	3	1/1
Metabolic: Increased AST		5/3
	1	3/3
	2	1/1
	3	1/1
Metabolic: Increased ALP		2/1
	1	1/1
	2	1/1
Dermatologic; Hypopigmentation (nasal planum)	1	1/1
Cutaneous ulceration	1	1/1
Otitis	1	1/1
Dyspnea	2	1/1
Cough	2	1/1
Fever	1	1/1

Losartan 10 mg/kg[a]

Adverse event	*Grade*	*n (events/dogs)*
Vomiting	1	1/1
Diarrhea	1	3/1
Lethargy	3	1/1
Fore-/hind limb weakness	2	1/1
Anorexia		3/2

	1	2/2
	2	1/1
Metabolic: Increased ALT	2	1/1
Metabolic: Increased AST	1	1/1
[a] Losartan toxicities for the 10mg/kg cohort were determined for the first 5 dogs enrolled in the trial during a 2 week losartan only dosing period prior to initiation of toceranib		
Losartan 10 mg/kg + toceranib phosphate 2.75 mg/kg EOD		
Adverse event	*Grade*	*n (events/dogs)*
Ocular		3/1
	2	1/1
	3	1/1
Lethargy	1	3/2
Fore-/hind-limb weakness		3/3
	1	2/2
	3	1/1
Anorexia		2/2
	1	1/1
	2	1/1
Diarrhea	2	1/1
Cough	1	2/2
Seizure	2	2/1
Increased urine protein:creatinine (UPC) ratio[b]	3	1/1
Other[c]	1	3/3
[b]Pre-existing condition but increased severity post-enrollment [c]Other toxicities include adverse events of unknown etiology (elevated creatinine kinase)		

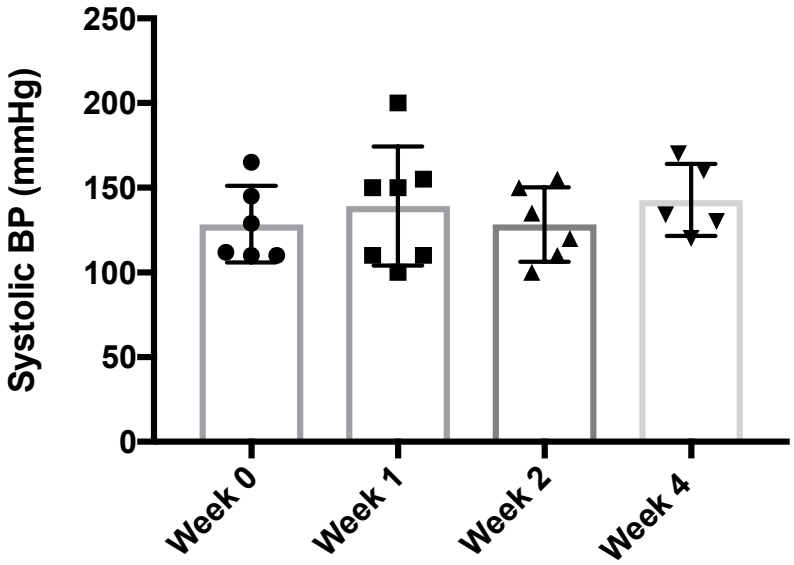

Figure 4.8. Weekly mean systolic blood pressure measurements for osteosarcoma-bearing dogs receiving 10 mg/kg losartan BID.

primarily of gastrointestinal (anorexia, vomiting, diarrhea), hematologic (neutropenia, thrombocytopenia), metabolic (liver enzyme elevations), or lethargy. Grade 3 toxicities were experienced by one dog in this cohort and included elevated AST and ALT liver enzymes; however, these abnormalities were diagnosed pre-enrollment, and the only increases of these enzymes observed on study were for AST at 1 week post-initiation of therapy. In addition, one dog experiencing grade 2 lethargy was withdrawn from the study based on the owner's request. For the entire study duration, lethargy, gastrointestinal toxicities of vomiting and diarrhea, and hematologic abnormalities of neutropenia and thrombocytopenia were all transient and observed at a frequency of 25% (2 out of 8 dogs), while transient increases in serum AST levels were observed in 37.5% of dogs (3/8).

In addition, toxicities directly attributable to high dose losartan therapy were assessed in a subset of 5 dogs treated with single agent losartan (10mg/kg) for two weeks prior to initiation of toceranib therapy (Table 4.2). Again, losartan toxicities observed during this period were limited and primarily grade 1 or 2 gastrointestinal (anorexia, vomiting, diarrhea), neuromuscular, or metabolic toxicities, with anorexia being the most frequently observed toxicity (25%; 2/8 dogs). However, a single dog in this cohort did experience grade 3 lethargy directly attributed to losartan therapy, which resolved within 7 days following a 25% dose reduction. No significant increases in frequency, severity, or duration of toxicities were observed with concurrent administration of toceranib in the 10mg/kg losartan dose cohort (Table 4.2). Observed grade 1 and 2 toxicities were similar to those reported for the 1mg/kg dose combination therapy cohort and the 10mg/kg single agent losartan cohort, and most commonly

included neuromuscular weakness (37.5 %, 3/8 dogs), anorexia (25%, 2/8 dogs), cough (25%, 2/8 dogs), and lethargy (25%, 2/8 dogs). The grade 3 toxicities observed in this cohort included one dog which experienced bilateral ocular discharge, which progressed to grade 3 episcleral injection and 3rd eyelid swelling, another dog with transient grade 3 weakness of the right hind limb, and one dog experiencing a persistently increased urine protein:creatinine (UPC) ratio above baseline. This dog had an elevated UPC ratio of 1.6 on pre-enrollment evaluation, but which increased to 4.2 over the 16-week course of therapy. The dog who experienced grade 3 hind limb weakness, also experienced grade 2 focal and generalized seizures; however, this is likely attributable to tumor progression, as calvarial metastases were identified on necropsy.

Treatment responses were evaluated by repeat thoracic radiographs according to the revised Response Evaluation Criteria in Solid Tumors (RECIST) (41). For the 1mg/kg losartan cohort, repeat thoracic radiographs were performed every 8 weeks, while for the 10 mg/kg cohort, radiographs were performed at 2 weeks, 8 weeks, and every 8 weeks thereafter. Measurements of target lesions were compared to those obtained at baseline radiographs performed within 2 weeks of enrollment. Response data for all dogs is summarized in Table 4.3 and presented in Figure 4.9A. Best responses in the 1mg/kg cohort included stable disease in 3 of 8 dogs (of 11, 16, and 17 weeks duration) for an overall biologic response rate of 37.5%. In the 10mg/kg dose cohort, partial responses occurred in 2 of 8 dogs, with stable disease (of 16 weeks duration) in 1 of 8 dogs, for an overall response rate of 25% and a biologic response rate of 37.5%. Baseline and 16 week thoracic radiographs are presented in Figure 4.10

Table 4.3: Treatment responses by dose cohort

Best Response (no., %)	LOS 1mg/kg + TOC 2.75mg/kg EOD (n=8)	LOS 10mg/kg + TOC 2.75mg/kg EOD (n=8)
Complete response	0 (0)	0 (0)[a]
Partial response	0 (0)	2 (25)
Stable disease (> 8 weeks)	3 (37.5)	1 (12.5)
Progressive disease	5 (62.5)	5 (62.5)
Overall response rate (PR and CR; %)	0	25
Biologic response rate (SD, PR, and CR; %)	37.5	37.5
Progression-free survival (days)	61	42.5
[a]*Radiographic assessment consistent with a PR, but no evidence of pulmonary metastasis was observed at necropsy*		

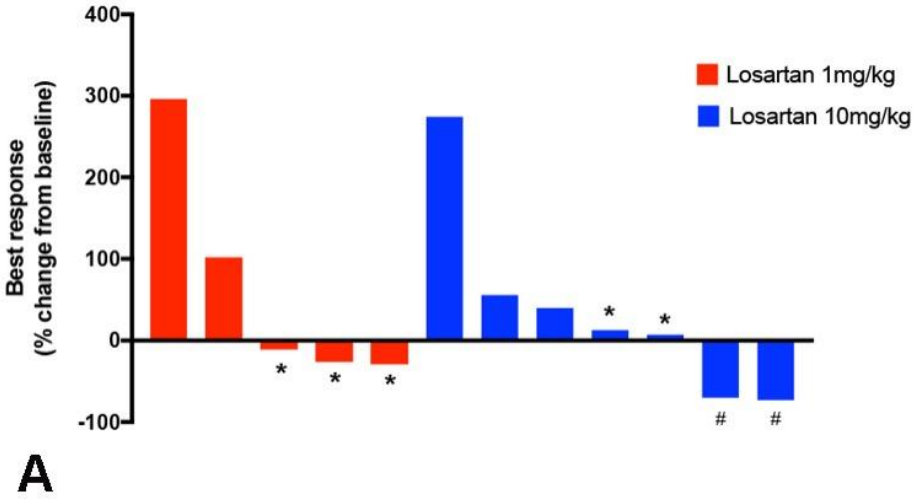

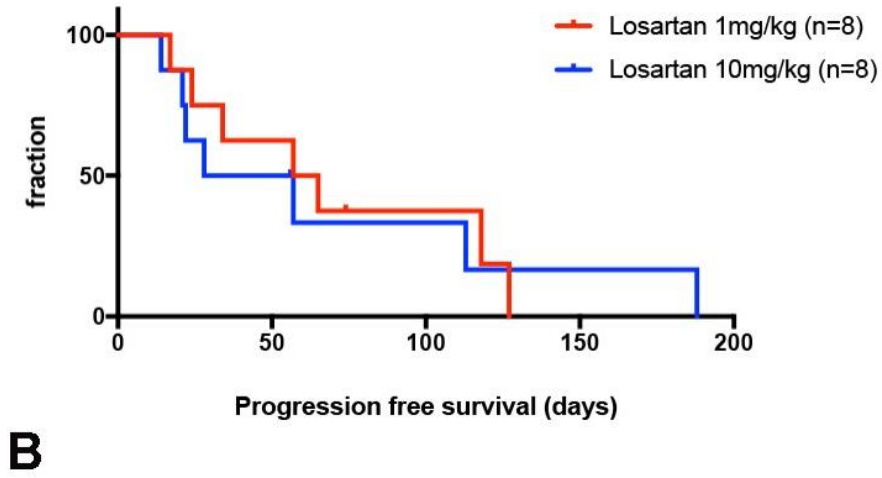

Figure 4.9. Progression-free survival and objective responses. (A) Graph depicting objective tumor responses, as determined by RECIST criteria (shown as % change from baseline) for dogs which survived long enough for at least one cycle of repeat thoracic radiographs. (B) Kaplan-Meier curve showing progression-free survival for osteosarcoma-metastasis bearing dogs receiving either 1 mg/kg or 10 mg/kg losartan BID in combination with toceranib. There was no significant difference between dose cohorts (log rank test, p=0.83) and median time to progression was 61 days (1 mg/kg) vs. 42.5 days (10 mg/kg). * Denotes dogs with stable disease, and # denotes dogs experiencing a partial response.

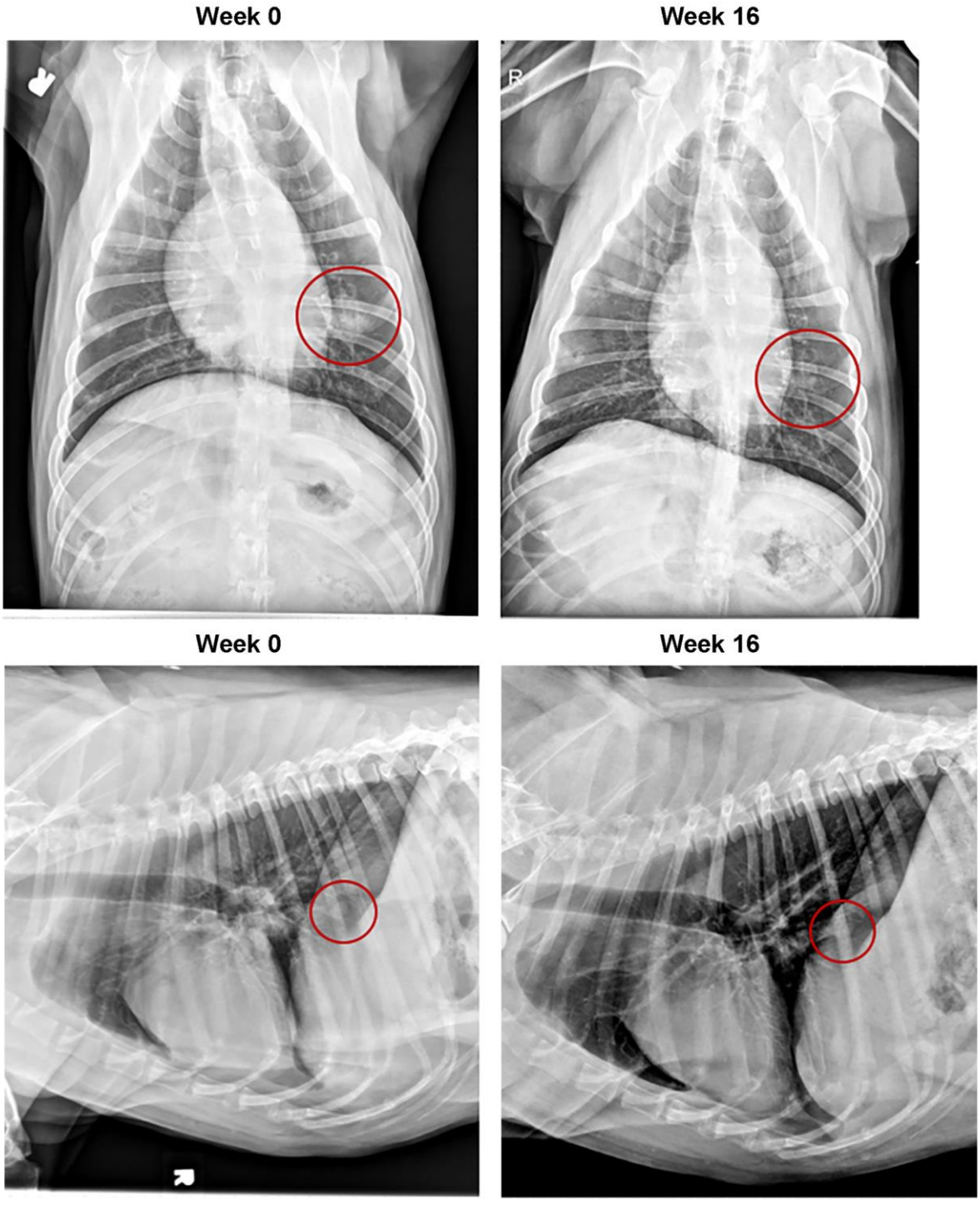

Figure 4.10. Baseline and week 16 thoracic radiographs of patient 005 in the 10 mg/kg cohort demonstrating regression of pulmonary metastases after losartan plus toceranib therapy. Right lateral and ventrodorsal views of week 0 thoracic radiographs depicting

two separate target lesions (red circles) are shown on the left. Repeat thoracic radiographs of these same nodules at week 16 are shown on the right (red circles), which demonstrated an ~ 70 % size reduction in these lesions (based on RECIST criteria). This response was initially noted at week 8, and remained present to slightly increased at week 16. Regression of grossly visible OSA pulmonary metastases were confirmed on necropsy of this patient, with only minimal microscopic metastases observed in the lung.

for one of the dogs who experienced a partial response. Median progression-free survival (PFS) was 61 days (17-127 days) for the 1mg/kg cohort, and 42.5 days (14-188 days) for the 10 mg/kg cohort, and was not statistically different between the two groups (Fig. 4.9B, p=0.82). For PFS analysis, one dog with SD in the 1mg/kg cohort was censored at 74d due to owner's request for withdrawal from the study (due to grade 2 lethargy). Of note, one of the dogs in the 10mg/kg cohort who experienced a partial response eventually died secondary to OSA metastases to the right scapula and distal ulna; however, on necropsy only microscopic evidence of pulmonary metastasis was identified, with no grossly visible lung metastases observed.

Evidence for reversal of tumor immune suppression in the peripheral blood of dogs treated with toceranib and losartan

Immune parameters associated with evidence of Treg and inflammatory monocyte modulation by combined toceranib and losartan therapy, and secondary enhancement of anti-tumor immune responses, were evaluated in the peripheral blood of dogs at various post-treatment time points. Samples were available from 7 of 8 dogs who also had matched CBC data for the same time points for determination of absolute cell numbers. Similar to previously published results of the immunomodulatory effects of toceranib therapy on Tregs in dogs, there was a decrease in the mean absolute number of Tregs at week 4 post therapy (85 $\pm$ 56.1 cells/μL), as compared to baseline (105.3 $\pm$ 68.3 cells/μL), with absolute Treg numbers decreased in 6 of 7 evaluable dogs; however, this trend was not significant (Fig. 4.11A, p=0.13). Absolute numbers of CCR2+ peripheral blood monocytes were quantified by flow cytometry at weeks 1 and 2

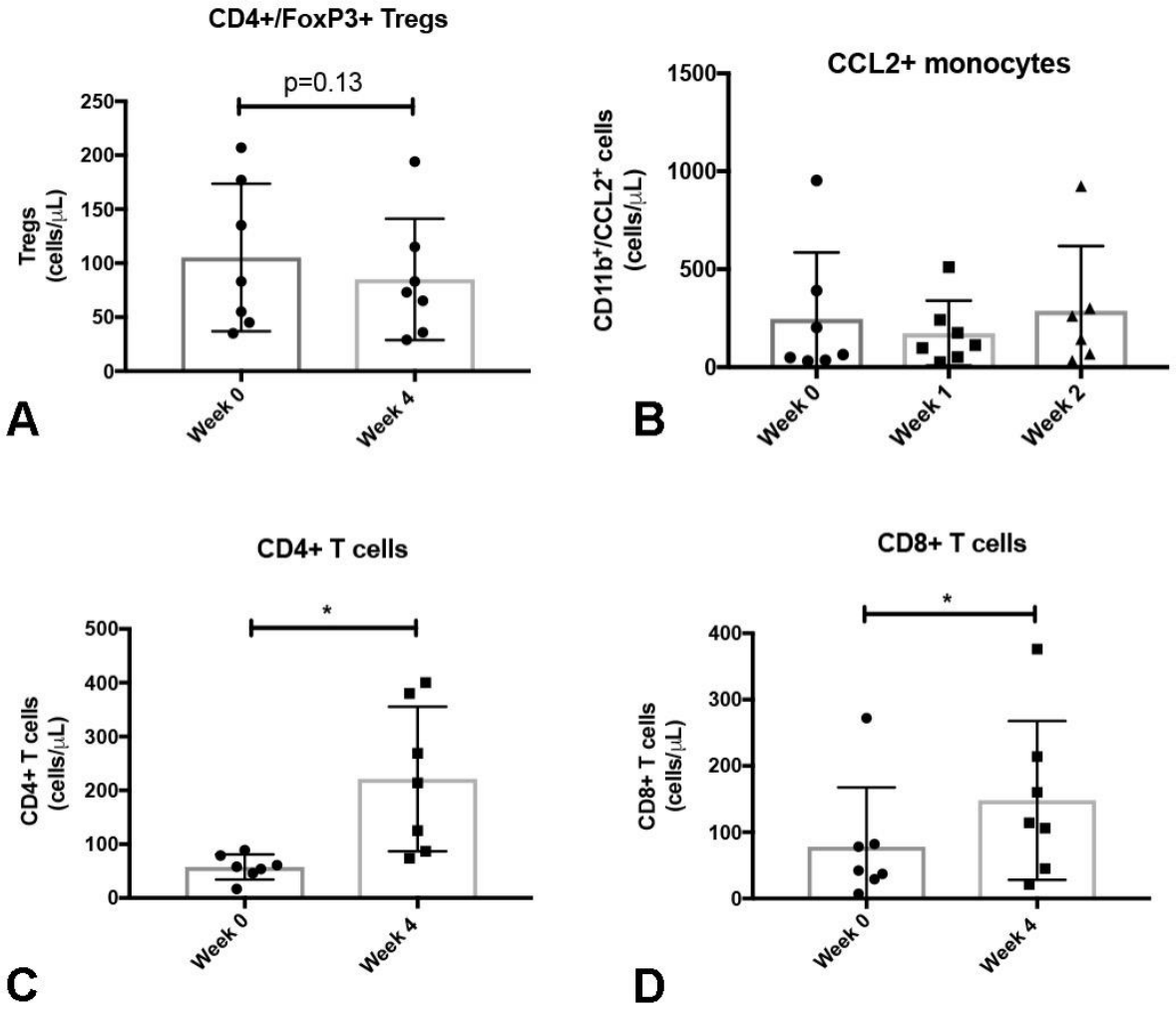

Figure 4.11. Effects of high dose losartan and Palladia combination therapy on immune cell subpopulations in the peripheral blood of dogs with metastatic osteosarcoma**.** (A) Absolute numbers of CD4+/FoxP3+ regulatory T cells (Tregs) in the peripheral blood of dogs with metastatic osteosarcoma at baseline and following 1 month combination therapy with losartan (10mg/kg BID) and Palladia (2.75 mg/kg EOD). (B) Absolute numbers of CD11b+/CCL2+ monocytes in the blood of dogs at baseline and 1 and 2 weeks post losartan (n=5) ± toceranib (n=2) combination therapy. (C) Absolute numbers of CD5+/CD4+ T cells, and CD5+/CD8+ T cells (D). Data expressed as means ± SD and analyzed by Wilcoxon signed rank test (n=7 dogs per time point, * $p < 0.05$).

post treatment. CCR2 expression was determined indirectly using a fluorescently-labeled human CCL2 ligand, as to our knowledge, no commercially available species-specific or cross-reactive antibody exists for canine CCR2. However, we suspect thisligand to be specific for canine CCR2 as its binding is completely competed off by pre-incubation with unlabeled canine rCCL2 (data not shown). No significant decreases in absolute numbers of CD11b+/CCL2+ peripheral blood monocytes were observed with losartan treatment (Fig. 4.11B). In addition, a broader analysis of peripheral blood monocytes at these time points, by various permutations of CD11b, MHCII, CD4, and CD14 expression, revealed no statistically significant decrease in these cell populations at weeks 1 and 2 post losartan therapy (data not shown).

Interestingly, however, we observed a statistically significant negative correlation between week 4 neutrophil or total myeloid (neutrophil and monocyte) cell counts (as a percentage of baseline), and progression-free survival, when analyzing all dogs in the study (1 mg/kg and 10 mg/kg cohorts) (Fig. 4.12A, Spearman r = -0.59, *p = 0.02). Additionally, when values for week 4 neutrophil and total myeloid cell counts (as % decrease from baseline) were dichotomized based on the median for all evaluable dogs (n=14), dogs experiencing a decrease of week 4 neutrophil or total myeloid cell counts greater than the median value of 32% had significantly longer PFS (median PFS = 74 days), as compared to dogs experiencing a decrease below the median value (median PFS = 28 days) (Fig. 4.12B, log rank test, *p=0.02, HR 2.8, 95% confidence intervals; CI, 0.853 – 9.21).

Lastly, we sought to determine if losartan plus toceranib therapy had immunomodulatory effects on other T cell subsets that might be reflective of an

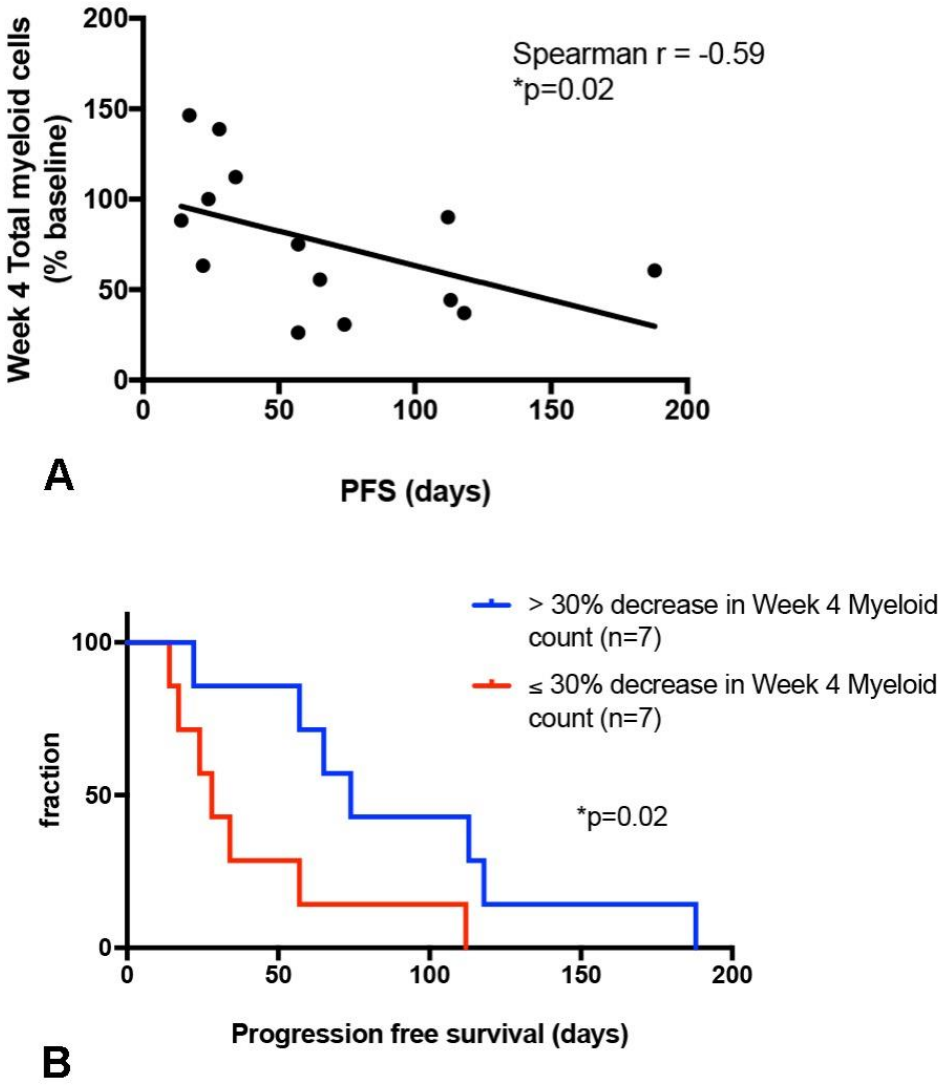

Figure 4.12. Effects of losartan and toceranib combination therapy on changes in total myeloid cell counts and association with progression-free survival. (A) Linear regression plot depicting the correlation between % change in total myeloid cell counts at 4 weeks post treatment and progression-free survival (n=14 dogs). (B) Kaplan-Meier curve comparing progression free survival in dogs experiencing a greater than 30% decrease in week 4 total myeloid cell counts below baseline (n=7), vs. those that did not (n=7). (Spearman correlation = -0.59, *p=0.02; log rank test *p=0.02).

enhanced anti-tumor immune response. For this, we measured absolute numbers of peripheral blood CD4+ and CD8+ T cells by flow cytometry. We observed significant increases in the mean number of CD4+ and CD8+ T cells at week 4 as compared to baseline. The mean number of CD4+ cells pre-treatment was 57.7 (±23.3 cells/μL), as compared to 221 (±134 cells/μL) at week 4, while the mean number of CD8+ cells pre-treatment was 78.1 (±89.5 cells/μL), as compared to 148 (±119.8 cells/μL) at week 4 (Fig. 4.11 C, D, *$p<0.05$). To determine if the observed increases in peripheral blood CD4+ and CD8+ T cells were associated with restoration of an IFN-γ mediated T cell response, we quantified plasma IFN-γ concentrations at these same time points via ELISA assay. However, no significant elevations in plasma IFN-γ as compared to baseline were observed in these dogs (data not shown).

Discussion

The last decade has seen significant advances in the utility of immunotherapy as a new treatment modality in human oncology. These responses have primarily been observed with the use of monoclonal antibodies (mAbs) targeting T cell checkpoint molecules in tumors such as melanoma and non-small cell lung cancer, or genetically engineered autologous T cells for the treatment of hematologic malignancies (20, 45). Yet, glaringly absent from the growing tool box of currently approved immunotherapies are small molecule drugs, a class of compounds which have previously been a mainstay in molecularly targeted cancer therapeutics (45). However, it is likely that processes such as infiltration of immune suppressive cells into the tumor microenvironment and immune cell promotion of metastasis would be best targeted by

small molecule drugs, and that the combination of currently approved biologic immune therapies with small molecule antagonists of these processes could result in substantial improvement of patient responses.

The CCL2-CCR2 axis represents an attractive therapeutic target for the treatment of tumor progression and metastasis, as a significant amount of experimental and clinical evidence now exists implicating CCL2-CCR2 signaling in multiple, over-lapping, pro-tumorigenic functions (9). In tumor-bearing hosts, CCL2 mediates the recruitment of CCR2+ inflammatory monocytes from the bone marrow into the peripheral blood, subsequently facilitating macrophage population of both primary and metastatic sites (10, 46). These primary tumor- and metastasis-associated macrophages promote tumor growth and metastasis through multiple mechanisms involving stimulation of angiogenesis, induction of an immune suppressive microenvironment, and activation of intrinsic tumor cell survival pathways (17-19). Regulatory T cells (Tregs) represent another immune cell subset known to promote tumor growth and metastasis, primarily through mechanisms associated with suppression of anti-tumor NK and CD8+ T cell responses (47, 48). As such, immunotherapeutic strategies designed to target both Tregs and the CCL2-CCR2 axis represent a rational combination for the reversal of tumor immune suppression and treatment of cancer metastasis.

We have previously demonstrated that the small molecule drug losartan, an angiotensin II type 1 receptor (AT1R) antagonist, can suppress tumor growth in murine metastasis models through mechanisms associated with blockade of CCL2-CCR2 monocyte recruitment and inhibition of angiogenesis (Regan et al. in review). Sunitinb, a

multi-kinase inhibitor approved for the treatment gastrointestinal stromal tumors and renal cell carcinomas, has also been shown to have potent immunomodulatory effects on the tumor microenvironment, including prevention of Treg and myeloid-derived suppresser cell (MDSC) accumulation (49). Furthermore, previous clinical studies in tumor bearing dogs have demonstrated that the veterinary-approved tyrosine kinase inhibitor toceranib (Palladia), a drug which shares significant functional homology to sunitinib, has similar immunomodulatory properties, including reduction in peripheral blood Tregs (37). Therefore, we sought to evaluate the potential anti-tumor effects of combination losartan and sunitinb/toceranib immunotherapy in a pre-clinical murine osteosarcoma metastasis model, and a phase I/II clinical trial in dogs with spontaneous osteosarcoma pulmonary metastasis.

We initially choose canine osteosarcoma, as 1.) Previous clinical data has implicated a prognostic role for both monocytes and regulatory T cells in the progression of this disease(30, 31), 2.) The high incidence of canine OSA provides for rapid patient accrual (28), and 3.) The predilection for canine OSA to metastasize to the lungs allows for ease and reproducibility in monitoring metastatic tumor progression via thoracic radiographs (28). Additionally, we simultaneously undertook descriptive immunohistochemical studies aimed at characterizing the immune landscape, including the role of CCL2-CCR2 monocyte recruitment, in canine OSA primary tumors and metastases. Results of these analyses demonstrated that OSA pulmonary metastases contained a significantly greater number of MAC387+ monocytes and macrophages as compared to primary tumors, and that neoplastic cells within OSA metastases produced abundant amounts of CCL2, suggesting a potential role for CCL2-CCR2 signaling in

monocyte recruitment to metastatic sites of canine OSA. These results were further corroborated by a series of in vitro assays utilizing a canine OSA tumor cell line, which demonstrated the ability of this cell line to elicit strong ex vivo canine monocyte migration, in a mechanism primarily dependent on tumor cell production of CCL2.

While losartan has been used in the treatment of glomerular disease and proteinuria in dogs, formal pharmacokinetic and pharmacodynamic assessment for inhibition of CCL2 mediated canine monocyte migration has not been performed (50). As such, our primary objective for the clinical study in tumor-bearing dogs was to determine the pharmacokinetics of losartan dosing for canine monocyte migration inhibition, as well as assess its safety and tolerability when combined with toceranib. In addition, data on treatment responses as well as immune parameters associated with monocyte and Treg modulation and enhancement of effector T cell responses were collected. For the clinical trial, we initiated losartan dosing at 1 mg/kg BID orally, as while no specific data exists for the use of losartan in dogs, this was the anecdotal dose recommended for the treatment of proteinuria (50). Assessment of pharmacodynamic activity in PBMCs and plasma obtained from the 8 dogs enrolled in this 1 mg/kg cohort demonstrated equivocal results for CCR2 target inhibition by losartan, with an overall increase in the mean chemotactic index as a percentage of baseline at both weeks 2 and 4 post losartan therapy. Concordantly, determination of losartan concentration in plasma collected concurrently with the peripheral blood utilized for PBMC pharmacodynamic responses demonstrated levels of losartan which were significantly below the therapeutic target of 200 ng/mL identified by our in vitro canine monocyte migration studies. Of note, these plasma samples were collected around the time

predicted for observation of losartan trough concentrations (~4-6h post dose), thus it is possible that the maximum plasma concentrations for 1mg/kg dosing in these dogs could have reached levels near the 200ng/mL target. Supporting this notion, increased plasma CCL2 concentrations, a pD response observed in human clinical trials of the CCR2 mAbs and small molecule antagonists (42, 43), were observed in 5 of 6 evaluable dogs, suggesting potential CCR2 inhibition; however, these increases were not statistically significant, and combined with the equivocal results of the PBMC migration assays, prompted us to perform losartan dose escalation studies in additional cohorts of healthy and tumor-bearing dogs.

Pharmacokinetic and pharmacodynamic assessment of losartan at doses of 2.5 mg/kg and 10 mg/kg demonstrated increasing maximum plasma and overall drug exposure levels, which at the 10 mg/kg dose met or exceeded the in vitro predicted therapeutic target for Cmax and exposure (AUC). More importantly, significant inhibition of ex vivo CCL2-directed monocyte migration was observed in 5 of 5 evaluated dogs at weeks 1 and 4, and 4 of 5 dog at week 2 in this 10 mg/kg cohort. Additionally, statistically significant elevations in mean plasma CCL2 concentrations above baseline were observed at both 2 and 4 weeks post treatment in this cohort. Overall, these results demonstrated increasing CCR2 target inhibition at increasing doses of losartan, and identified an oral losartan dose (10 mg/kg BID) effective for the inhibition of CCL2-mediated monocyte migration in tumor-bearing dogs.

Despite this, it is important to note that these results highlight the potential difficulty in assessing peripheral blood pharmacodynamic responses for chemokine receptor antagonists, especially in terms of drugs, such as losartan, which are predicted

to be non-competitive antagonists (Regan et al. in review). Pharmacodynamic results of previously published clinical trials of chemokine receptor antagonists have primarily relied on either the evaluation of drug receptor occupancy, indirectly through measuring the inhibition of chemokine-induced receptor internalization, or assessment of inhibition of fluorescently-labeled chemokine ligand binding (51, 52). In the case of losartan, neither of these approaches were feasible, as we have previously demonstrated that losartan itself induces CCR2 internalization, and in human monocytes does not inhibit CCL2 binding, and is predicted to be a non-competitive antagonist of CCR2 (Regan et al. in review). Thus, we relied on assays of ex vivo monocyte migration and assessment of changes in plasma CCL2 levels. One problem with our method of evaluation of ex vivo monocyte migration was that blood was processed via erythrocyte lysis followed by repeated washes, thus removing PBMCs from the patients' plasma containing free losartan drug. Inherently, this assumes that losartan's effects on CCR2 signaling remain active during the 4-hour duration of the migration assay, despite a likely free losartan drug concentration of essentially zero. While out of the scope of these studies, this hypothesis could be easily tested in vitro utilizing data from our in vivo pK studies. One possibility for improving this pD endpoint in future studies could be the optimization of ex vivo migration assays using leukocyte-rich plasma instead of blood processed via Ficoll separation or ACK lysis. Alternatively, in line with results of CCR2 antagonist trials in people we consistently observed post-treatment elevations in plasma CCL2 levels in both the 1 mg/kg and 10 mg/kg dose cohorts, suggesting that ELISA measurement of plasma CCL2 likely represents a more reliable and high-throughput means for monitoring target inhibition by CCR2 antagonists.

For all 19 dogs (including 3 healthy control dogs), losartan therapy was well tolerated at doses up to 10 mg/kg BID. Toxicities observed during a 2-week period of 10 mg/kg losartan monotherapy were generally mild and self-limiting and most commonly included gastrointestinal disturbance (anorexia, vomiting, diarrhea). Addition of toceranib therapy was well tolerated in dogs in both the 1 mg/kg and 10 mg/kg cohorts and resulted in no significant increases in toxicity, with the most commonly reported adverse events consistent with those previously reported for toceranib, including gastrointestinal disturbance, lethargy, and neuromuscular (fore-/hind-limb) weakness. In terms of observed clinical responses, combination losartan and toceranib therapy produced objective responses in 2 of 16 dogs (12.5%) with metastatic osteosarcoma, both which occurred in the high dose 10 mg/kg cohort. In addition, stable disease of meaningful duration (>8 weeks) was observed in 4 of 16 dogs (25%).

In this study, the mechanisms accounting for the observed tumor growth stabilization/regression are not known. Besides inhibition of monocyte migration, losartan has been previously demonstrated to exert anti-tumor effects associated with mechanisms of blockade of angiogenesis or TGF-β signaling, secondary to primary AT1R inhibition (53, 54). Likewise, toceranib can directly suppress the proliferation of neoplastic cells with activating KIT mutations, and also has potential to inhibit angiogenesis based on its activity against other kinases including VEGFR and PDGFR (55). Thus, it is plausible that the observed tumor responses could be the result of blockade of tumor angiogenesis and/or direct inhibition of KIT signaling in tumor cells. However, in contrast to this notion, we observed a statistically significant negative correlation between week 4 neutrophil or total myeloid (neutrophil and monocyte)

counts (as % of baseline), and progression-free survival for all study dogs. Additionally, PFS was significantly prolonged in those dogs experiencing a greater than 30% decrease of their week 4 neutrophil or total myeloid cell counts below baseline, as compared to those that did not. While it is possible that these results are reflective of dogs receiving a greater biologically effective dose of toceranib, given the known role of KIT signaling in hematopoiesis, we feel this is an unlikely scenario. Toceranib has not been reported to result in significant myelotoxicity, and thus variations in the degree of myelosuppression are not likely to be a good surrogate marker for dose intensity as they are with traditional cytotoxic therapies (55, 56). In fact, only 1 dog in our study experienced neutropenia, which was grade 1 in severity, and based on the phase I trials for toceranib in dogs (55), more significant variations in gastrointestinal toxicities than those observed in our study would be predicted, if true differences in dose intensity were present. Interestingly, similar results have been observed in humans with advanced stage melanoma treated with the checkpoint inhibitor ipilimumab (57). In these patients, an elevated neutrophil to lymphocyte ratio (NLR) at baseline or a >30% increase during ipilimumab treatment was significantly associated with worse overall and progression free survival, while changes in the NLR in patients receiving BRAF inhibitors were not consistently associated with outcome (57).

Lastly, we observed statistically significant increases in absolute numbers of CD4+ and CD8+ T cells in the peripheral blood of dogs in the 10 mg/kg cohort; an effect evaluated in but not previously reported for dogs receiving toceranib (37), suggesting this observation is the result of the addition of losartan to toceranib therapy. Interestingly, previous studies characterizing canine myeloid-derived suppressor cells

(MDSCs), an immune cell subset known to suppress T cell responses in tumor-bearing humans and mice, have demonstrated that these cells are of granulocytic (neutrophilic) phenotype in dogs (58). Thus, based on the observed changes in total neutrophil and myeloid cell counts, in conjunction with the observed increases in peripheral CD4+ and CD8+ T cells, we feel these results support our hypothesis of potential reversal of the systemic tumor immune suppression by combination losartan and toceranib therapy.

In conclusion, these studies provide preliminary evidence implicating a role for CCL2-CCR2 signaling in canine OSA metastases, and are the first to evaluate losartan pharmacokinetics for the pharmacodynamic endpoint of inhibition of CCL2-mediated monocyte migration in any species. Here, we demonstrate that 10 mg/kg BID oral dosing of losartan is a safe and well-tolerated dose which can effectively inhibit CCL2-mediated monocyte migration in dogs with spontaneous osteosarcoma metastasis. In addition, results of this pilot Phase I/II trial demonstrate that these drugs can be co-administered at their respective recommended dosages on a continuous basis with minimal toxicity. Furthermore, the biological response rate observed in these dogs with advanced, established metastases, in conjunction with the observed modulation of systemic immune suppression, support further clinical evaluation and validation of this novel immunotherapeutic combination and potential mechanisms of action in larger, randomized, placebo controlled studies.

REFERENCES

1. Steeg PS (2016) Targeting metastasis. *Nat Rev Cancer* 16(4):201-218.

2. Khanna C*, et al.* (2014) Toward a drug development path that targets metastatic progression in osteosarcoma. *Clin Cancer Res* 20(16):4200-4209.

3. Tevaarwerk AJ*, et al.* (2013) Survival in Metastatic Recurrent Breast Cancer after Adjuvant Chemotherapy: Little Evidence for Improvement Over the Past Three Decades. *Cancer* 119(6):1140-1148.

4. Bernards N*, et al.* (2013) No improvement in median survival for patients with metastatic gastric cancer despite increased use of chemotherapy. *Annals of Oncology* 24(12):3056-3060.

5. Worni M*, et al.* (2013) Modest improvement in overall survival for patients with metastatic pancreatic cancer: a trend analysis using the surveillance, epidemiology, and end results registry from 1988 to 2008. *Pancreas* 42(7):1157-1163.

6. O'Shaughnessy J (2005) Extending survival with chemotherapy in metastatic breast cancer. *The oncologist* 10 Suppl 3:20-29.

7. Van Cutsem E & Oliveira J (2009) Advanced colorectal cancer: ESMO clinical recommendations for diagnosis, treatment and follow-up. *Annals of oncology : official journal of the European Society for Medical Oncology* 20 Suppl 4:61-63.

8. Valastyan S & Weinberg RA (2011) Tumor metastasis: molecular insights and evolving paradigms. *Cell* 147(2):275-292.

9. Lim SY, Yuzhalin AE, Gordon-Weeks AN, & Muschel RJ (2016) Targeting the CCL2-CCR2 signaling axis in cancer metastasis. *Oncotarget* 7(19):28697-28710.

10. Qian BZ*, et al.* (2011) CCL2 recruits inflammatory monocytes to facilitate breast-tumour metastasis. *Nature* 475(7355):222-225.

11. Nakasone ES*, et al.* (2012) Imaging tumor-stroma interactions during chemotherapy reveals contributions of the microenvironment to resistance. *Cancer Cell* 21(4):488-503.

12. Chiu HY*, et al.* (2012) Autocrine CCL2 promotes cell migration and invasion via PKC activation and tyrosine phosphorylation of paxillin in bladder cancer cells. *Cytokine* 59(2):423-432.

13. Tang CH & Tsai CC (2012) CCL2 increases MMP-9 expression and cell motility in human chondrosarcoma cells via the Ras/Raf/MEK/ERK/NF-kappaB signaling pathway. *Biochemical pharmacology* 83(3):335-344.

14. Roca H*, et al.* (2009) CCL2 and interleukin-6 promote survival of human CD11b+ peripheral blood mononuclear cells and induce M2-type macrophage polarization. *The Journal of biological chemistry* 284(49):34342-34354.

15. Low-Marchelli JM*, et al.* (2013) Twist1 induces CCL2 and recruits macrophages to promote angiogenesis. *Cancer Res* 73(2):662-671.

16. Piao C*, et al.* (2015) Complement 5a Enhances Hepatic Metastases of Colon Cancer via Monocyte Chemoattractant Protein-1-mediated Inflammatory Cell Infiltration. *The Journal of biological chemistry* 290(17):10667-10676.

17. Qian BZ*, et al.* (2015) FLT1 signaling in metastasis-associated macrophages activates an inflammatory signature that promotes breast cancer metastasis. *J Exp Med* 212(9):1433-1448.

18. Chen Q, Zhang XH, & Massague J (2011) Macrophage binding to receptor VCAM-1 transmits survival signals in breast cancer cells that invade the lungs. *Cancer Cell* 20(4):538-549.

19. Mazzieri R*, et al.* (2011) Targeting the ANG2/TIE2 axis inhibits tumor growth and metastasis by impairing angiogenesis and disabling rebounds of proangiogenic myeloid cells. *Cancer Cell* 19(4):512-526.

20. Khalil DN, Smith EL, Brentjens RJ, & Wolchok JD (2016) The future of cancer treatment: immunomodulation, CARs and combination immunotherapy. *Nature reviews. Clinical oncology* 13(5):273-290.

21. Robert C*, et al.* (2015) Pembrolizumab versus Ipilimumab in Advanced Melanoma. *N Engl J Med* 372(26):2521-2532.

22. Rizvi NA*, et al.* (2015) Activity and safety of nivolumab, an anti-PD-1 immune checkpoint inhibitor, for patients with advanced, refractory squamous non-small-cell lung cancer (CheckMate 063): a phase 2, single-arm trial. *The Lancet. Oncology* 16(3):257-265.

23. Hodi FS*, et al.* (2010) Improved survival with ipilimumab in patients with metastatic melanoma. *N Engl J Med* 363(8):711-723.

24. Khanna C, London C, Vail D, Mazcko C, & Hirschfeld S (2009) Guiding the Optimal Translation of New Cancer Treatments From Canine to Human Cancer Patients. *Clinical Cancer Research* 15(18):5671.

25. LeBlanc AK*, et al.* (2016) Perspectives from man's best friend: National Academy of Medicine's Workshop on Comparative Oncology. *Science translational medicine* 8(324):324ps325.

26. Gordon I, Paoloni M, Mazcko C, & Khanna C (2009) The Comparative Oncology Trials Consortium: using spontaneously occurring cancers in dogs to inform the cancer drug development pathway. *PLoS medicine* 6(10):e1000161.

27. Paoloni M & Khanna C (2008) Translation of new cancer treatments from pet dogs to humans. *Nat Rev Cancer* 8(2):147-156.

28. Fenger JM, London CA, & Kisseberth WC (2014) Canine osteosarcoma: a naturally occurring disease to inform pediatric oncology. *ILAR journal* 55(1):69-85.

29. Regan DP, Escaffi A, Coy J, Kurihara J, & Dow SW (2016) Role of monocyte recruitment in hemangiosarcoma metastasis in dogs. *Vet Comp Oncol*.

30. Biller BJ, Guth A, Burton JH, & Dow SW (2010) Decreased ratio of CD8+ T cells to regulatory T cells associated with decreased survival in dogs with osteosarcoma. *J Vet Intern Med* 24(5):1118-1123.

31. Sottnik JL*, et al.* (2010) Association of blood monocyte and lymphocyte count and disease-free interval in dogs with osteosarcoma. *J Vet Intern Med* 24(6):1439-1444.

32. Wycislo KL & Fan TM (2015) The immunotherapy of canine osteosarcoma: a historical and systematic review. *J Vet Intern Med* 29(3):759-769.

33. Owen LN & Bostock DE (1974) Effects of intravenous BCG in normal dogs and in dogs with spontaneous osteosarcoma. *Eur J Cancer* 10(12):775-780.

34. Betton GR, Gorman NT, & Owen LN (1979) Cell mediated cytotoxicity in dogs following systemic or local BCG treatment alone or in combination with allogeneic tumour cell lines. *Eur J Cancer* 15(5):745-754.

35. Kurzman ID*, et al.* (1995) Adjuvant therapy for osteosarcoma in dogs: results of randomized clinical trials using combined liposome-encapsulated muramyl tripeptide and cisplatin. *Clin Cancer Res* 1(12):1595-1601.

36. Kurzman ID, Shi F, & MacEwen EG (1993) In vitro and in vivo canine mononuclear cell production of tumor necrosis factor induced by muramyl peptides and lipopolysaccharide. *Vet Immunol Immunopathol* 38(1-2):45-56.

37. Mitchell L, Thamm DH, & Biller BJ (2012) Clinical and immunomodulatory effects of toceranib combined with low-dose cyclophosphamide in dogs with cancer. *J Vet Intern Med* 26(2):355-362.

38. Duffy AL, Olea-Popelka FJ, Eucher J, Rice DM, & Dow SW (2010) Serum concentrations of monocyte chemoattractant protein-1 in healthy and critically ill dogs. *Veterinary clinical pathology / American Society for Veterinary Clinical Pathology* 39(3):302-305.

39. Christ DD*, et al.* (1994) The pharmacokinetics and pharmacodynamics of the angiotensin II receptor antagonist losartan potassium (DuP 753/MK 954) in the dog. *The Journal of pharmacology and experimental therapeutics* 268(3):1199-1205.

40. Brown S, Elliott J, Francey T, Polzin D, & Vaden S (2013) Consensus recommendations for standard therapy of glomerular disease in dogs. *J Vet Intern Med* 27 Suppl 1:S27-43.

41. Wang Y*, et al.* (2009) CCR2 and CXCR4 regulate peripheral blood monocyte pharmacodynamics and link to efficacy in experimental autoimmune encephalomyelitis. *Journal of inflammation (London, England)* 6:32.

42. Gilbert J*, et al.* (2011) Effect of CC chemokine receptor 2 CCR2 blockade on serum C-reactive protein in individuals at atherosclerotic risk and with a single nucleotide polymorphism of the monocyte chemoattractant protein-1 promoter region. *The American journal of cardiology* 107(6):906-911.

43. Vergunst CE*, et al.* (2008) Modulation of CCR2 in rheumatoid arthritis: a double-blind, randomized, placebo-controlled clinical trial. *Arthritis and rheumatism* 58(7):1931-1939.

44. Eisenhauer EA*, et al.* (2009) New response evaluation criteria in solid tumours: revised RECIST guideline (version 1.1). *Eur J Cancer* 45(2):228-247.

45. Adams JL, Smothers J, Srinivasan R, & Hoos A (2015) Big opportunities for small molecules in immuno-oncology. *Nature reviews. Drug discovery* 14(9):603-622.

46. Kitamura T*, et al.* (2015) CCL2-induced chemokine cascade promotes breast cancer metastasis by enhancing retention of metastasis-associated macrophages. *J Exp Med* 212(7):1043-1059.

47. Smyth MJ*, et al.* (2006) CD4+CD25+ T regulatory cells suppress NK cell-mediated immunotherapy of cancer. *J Immunol* 176(3):1582-1587.

48. Olkhanud PB*, et al.* (2009) Breast cancer lung metastasis requires expression of chemokine receptor CCR4 and regulatory T cells. *Cancer Res* 69(14):5996-6004.

49. Ozao-Choy J*, et al.* (2009) The novel role of tyrosine kinase inhibitor in the reversal of immune suppression and modulation of tumor microenvironment for immune-based cancer therapies. *Cancer Res* 69(6):2514-2522.

50. Harley L & Langston C (2012) Proteinuria in dogs and cats. *The Canadian veterinary journal = La revue veterinaire canadienne* 53(6):631-638.

51. Rosario MC*, et al.* (2008) Population pharmacokinetic/ pharmacodynamic analysis of CCR5 receptor occupancy by maraviroc in healthy subjects and HIV-positive patients. *British journal of clinical pharmacology* 65(Suppl 1):86-94.

52. Dairaghi DJ*, et al.* (2011) Pharmacokinetic and pharmacodynamic evaluation of the novel CCR1 antagonist CCX354 in healthy human subjects: implications for selection of clinical dose. *Clinical pharmacology and therapeutics* 89(5):726-734.

53. Arnold SA*, et al.* (2012) Losartan slows pancreatic tumor progression and extends survival of SPARC-null mice by abrogating aberrant TGFbeta activation. *PLoS One* 7(2):e31384.

54. Otake AH*, et al.* (2010) Inhibition of angiotensin II receptor 1 limits tumor-associated angiogenesis and attenuates growth of murine melanoma. *Cancer chemotherapy and pharmacology* 66(1):79-87.

55. London CA*, et al.* (2003) Phase I dose-escalating study of SU11654, a small molecule receptor tyrosine kinase inhibitor, in dogs with spontaneous malignancies. *Clin Cancer Res* 9(7):2755-2768.

56. Vaughan A, Johnson JL, & Williams LE (2007) Impact of chemotherapeutic dose intensity and hematologic toxicity on first remission duration in dogs with lymphoma treated with a chemoradiotherapy protocol. *J Vet Intern Med* 21(6):1332-1339.

57. Cassidy MR*, et al.* (2017) Neutrophil to Lymphocyte Ratio is Associated With Outcome During Ipilimumab Treatment. *EBioMedicine* 18:56-61.

58. Goulart MR, Pluhar GE, & Ohlfest JR (2012) Identification of myeloid derived suppressor cells in dogs with naturally occurring cancer. *PLoS One* 7(3):e33274.

CHAPTER 5

Final conclusions and future directions

G protein-coupled receptors (GPCRs) have traditionally been a cornerstone of drug discovery in the pharmaceutical industry. Thus, the initial discovery of chemokine receptors functioning as GPCRs stimulated great excitement at the prospects of small molecule drug development for the treatment of a variety of immune-related diseases, ranging from inflammatory conditions such as atherosclerosis, chronic obstructive pulmonary disease, and rheumatoid arthritis, to cancer and HIV (1). However, almost two decades after the discovery of many of these receptors, only two small molecule chemokine receptor antagonists are approved for clinical use in humans, including the CCR5 antagonist maraviroc for treatment of HIV, and the CXCR4 antagonist plerixafor (AMD3100) for hematopoietic stem cell mobilization (1).

While numerous large pharmaceutical companies continue to maintain active programs for the development of small molecule chemokine receptor antagonists, including against CCR2, their therapeutic targets appear to be predominately focused on inflammatory diseases and not cancer (2). Indeed, a search of “chemokine receptor AND cancer” on ClinicalTrials.gov demonstrates that only 3 small molecule chemokine receptor antagonists, including one CCR2 antagonist, are currently in trials for treatment of human cancer patients (the other two being the aforementioned CCR5 and CXCR4 antagonists) (ClinicalTrials.gov identifiers: NCT01736813, NCT02737072, NCT02732938). Although drug development is a lengthy process, these results are surprising, given the well-documented role of chemokine receptor signaling in tumor

progression and control of metastasis, both through direct signaling on tumor cells, as well as indirectly through the recruitment of tumor-promoting immune cells (3). As one example, it has been demonstrated that signaling between the chemokine SDF-1 (CXCL12) and CXCR4 expressed on breast cancer cells promotes both primary tumor growth, as well as breast tumor cell invasion and recruitment to metastatic sites (4, 5).

In contrast, biological therapies targeting immune-related proteins and their associated processes have driven major clinical advancements in human oncology over the last decade (6). These immunotherapeutic advancements have primarily been observed with the use of monoclonal antibodies targeting T cell checkpoint molecules such as programmed cell-death protein 1 (PD-1), or cytotoxic T-lymphocyte associated protein 4 (CTLA-4) (6-8), predominately in patients with certain tumor types such as melanoma, lung, or renal cancer. Yet, it is likely that certain processes such as infiltration of immune suppressive cells into the tumor microenvironment and immune cell promotion of metastasis would be best targeted by small molecule drugs, and that the combination of currently approved biologic immune therapies with small molecule antagonists of these processes could result in substantial improvement of patient responses.

Small molecule immunotherapies could offer distinct advantages over currently approved biologics. These include: 1.) oral bioavailability, 2.) their small size, which potentially lends itself to greater intratumoral distribution and ability to cross physiological barriers (such as the blood-brain barrier), and 3.) the ability to access intracellular drug targets which are otherwise unachievable by large biological therapies (9). As has been extensively outlined and documented throughout this thesis, the CCL2-

CCR2 chemokine plays a significant role in the promotion of tumor metastasis, and thus likely holds great promise as an immunotherapeutic target. Despite this, at the onset of the studies presented in this thesis, only a single drug targeting the CCL2-CCR2 axis, the anti-CCL2 monoclonal antibody Carlumab, was in early phase clinical development for human cancer patients (10). Given that current estimations for the time and cost invested in new drugs is now a staggering 10 years and $2.6 billion dollars (11), alternative drug development programs which focus on re-purposing already approved drugs as potential anti-cancer therapies might offer greater promise, in terms of reduced cost and time, for getting more effective treatment options to patients with cancer (12). Thus, we initially sought to identify potential CCR2 antagonists via in silico screening of a library of > 300 FDA approved small molecule drugs against a CCR2 homology model. We chose this approach in hopes of identifying an already approved, known to be safe, cost effective drug which could be rapidly repurposed as a CCR2 antagonist.

An identified lead compound from these in silico studies was the angiotensin receptor blocker, losartan. We initially chose losartan out of a list of predicted CCR2 antagonists, among other things, based on its previously published reports of immunomodulatory activity on monocytes and macrophages in other inflammatory diseases such as atherosclerosis (13, 14). In the studies presented in chapter 2, we pharmacologically characterize losartan as a potential CCR2 antagonist, and assess its ability to inhibit CCL2-CCR2 mediated monocyte recruitment. Results of these studies demonstrated that both losartan and its primary metabolite (EXP-3174) potently inhibit CCL2-CCR2 dependent human and murine monocyte recruitment at clinically relevant doses, and in a manner which appears most consistent with non-competitive

antagonism of CCR2. In addition we also assessed the potential of losartan to be re-purposed as an anti-metastatic therapy in experimental metastasis models of breast and colon cancer, which showed that losartan significantly slowed metastatic progression in a process that was associated with blockade of inflammatory monocyte recruitment and reduction in metastasis-associated macrophages. Taken together, these studies suggest that losartan and its primary metabolite might represent a novel class of safe and already-FDA approved, noncompetitive CCR2 antagonists, with potential to be rapidly repurposed for the treatment of metastatic disease.

While the results presented in Chapter 2 provide strong evidence that losartan functions as a non-competitive CCR2 antagonist, full confirmation of these findings require additional CCR2 functional studies. As such, we have already collaborated with a group of molecular pharmacologists at the University of California-San Diego (UCSD), which have re-evaluated the in silico modeling of losartan and EXP-3174, now using the recently solved molecular structure of CCR2 (15) instead of a CCR2 homology model. Results of these assays have confirmed that both losartan and EXP-3174 bind with moderate potency to the CCR2 receptor, and at a novel, recently described intracellular allosteric binding site(15, 16); however, these results must be further substantiated by additional molecular pharmacology assays. Specifically, we are collaborating with this same group at UCSD as they have fully automated, high-throughput fluidic capabilities to more completely evaluate and generate a full dose-response curve for changes in CCL2-induced intracellular calcium release for both increasing concentration of losartan and CCL2 ligand. The response and shape of this curve will provide significant further insight as to the ortho or allosteric nature of losartan in terms of inhibition of CCR2.

Furthermore, we plan to repeat the CCR2 signaling studies shown in chapter 2, this time using cell lines which have been transfected with plasmids containing human CCR2 mutants with specific mutations in both the orthosteric and allosteric binding site. It would be hypothesized that the functional impact of losartan CCL2 signaling would be lost with mutation of its binding site (whether the ortho or allosteric pocket of CCR2), and thus results of these studies will definitively confirm to which portion of the CCR2 molecule losartan binds.

In addition, the in silico CCR2 modeling work by this same group of collaborators have demonstrated that double-antagonist bound CCR2, that is CCR2 bound by both orthosteric and allosteric (intracellular) antagonist drugs, represents the most highly inactive conformation of a G-protein coupled receptor observed to date (15). Thus, if losartan is determined to be a true intracellular allosteric inhibitor of CCR2, we plan to perform additional pre-clinical metastasis studies in mice assessing the combination of losartan (an allosteric inhibitor), with an orthosteric CCR2 antagonist, such as INCB3344 (17).

While only a single small molecule CCR2 antagonist is currently in human clinical trials for the treatment of cancer; other small molecule CCR2 drugs have been evaluated in clinical trials for a variety of other diseases including rheumatoid arthritis and neuropathic pain (2, 18). In both of these trials however, CCR2 antagonist drugs failed to provide a clinical benefit greater than that observed in placebo-treated individuals (18, 19). It has previously been assumed that redundancy of the chemokine system was the likely cause for these failures, but more recent insights suggest that instead, inappropriate target selection and sub-therapeutic dosing might be the most

likely barriers to the success of these drugs (18). In chapters 3 and 4, we address both of these potential hurdles in the continued development and assessment of losartan as a CCR2 antagonist.

In chapter 3, we demonstrate that canine hemangiosarcoma (HSA), as compared to other common and highly metastatic canine tumors types, is unique in its ability to recruit large numbers of monocytes to sites of metastasis. Moreover, we provide substantial mechanistic data which strongly suggests that monocyte recruitment to hemangiosarcoma metastases is at least in part dependent on the CCL2-CCR2 chemotactic axis. These observations provide important insights into the biology and immunopathogenesis of hemangiosarcoma, and are consistent with the hypothesis that overexpression of CCL2 and recruitment of large numbers of monocytes may explain in part the aggressive metastatic nature of canine hemangiosarcoma. Future studies building on the foundational work we present here are currently underway. Specifically, we are collaborating to conduct a prospective, randomized, double blinded placebo-controlled clinical trial evaluating the effects of oral losartan (10mg/kg) plus intravenous doxorubicin vs. intravenous doxorubicin (plus placebo) in 40 dogs that had splenectomy for splenic HSA.

Finally, the studies presented in chapter 4 provide preliminary evidence also implicating a role for CCL2-CCR2 signaling in canine OSA metastases, and are the first to evaluate losartan pharmacokinetics for the pharmacodynamic endpoint of inhibition of CCL2-mediated monocyte migration in any species. Here, we demonstrate that 10 mg/kg BID oral dosing of losartan is a safe and well-tolerated dose which can effectively inhibit CCL2-mediated monocyte migration in dogs with spontaneous osteosarcoma

metastasis. In addition, results of this pilot Phase I/II trial demonstrate that these drugs can be co-administered at their respective recommended dosages on a continuous basis with minimal toxicity. Furthermore, the biological response rate observed in these dogs with advanced, established metastases, in conjunction with the observed modulation of systemic immune suppression, support further clinical evaluation and validation of this novel immunotherapeutic combination and potential mechanisms of action in larger, randomized, placebo controlled studies.

Future directions for the studies in chapter 4 will be focused on increasing our understanding of the immune response to canine tumors, and specifically of the role of CCL2-CCR2 in canine tumor metastasis. To this end, we plan to immunohistochemically evaluate larger numbers of osteosarcoma metastases for both MAC387 and CCL2, so that we can assess if there is a statistically significant positive correlation between CCL2 production and macrophage infiltration of canine OSA metastases.

In addition, we plan to evaluate the immunotherapeutic effects of both losartan monotherapy, and in combination with toceranib, in a larger, better powered Phase II clinical trial in dogs with osteosarcoma. Furthermore, we plan to assess the monocyte migration inhibiting and anti-tumor effects of other drugs within the class of angiotensin receptor blockers. Informative studies on the comparative pharmacokinetics of ARBs have already been performed in both humans and rodents (20). Based on the results of these studies, it appears that other second and third generation ARBs, such as telmisartan may have a potentially more favorable pK profile for daily dosing and maintenance of therapeutic levels effective at inhibiting monocyte migration (20).

Specifically, telmisartan has a higher oral bioavailability than losartan, as well as a significantly greater half-life, which could facilitate once a day dosing in humans and dogs that still maintains the same or greater drug levels that we demonstrate here in our studies of losartan (20).

In addition, besides the potential for losartan to inhibit CCL2-CCR2 signaling, we feel it is important not to ignore the other potential anti-tumor effects of this drug or other members of the class of ARBs. Pre-clinical studies in mice have demonstrated losartan to have potent anti-fibrotic effects through inhibition of TGF-B signaling (21-24). It is now well documented that radiation induces increased TGF-β signaling, the effects of which contribute to the activation of carcinoma-associated fibroblasts and myofibroblasts in the tumor microenvironment, inducing the post-radiation fibrotic response often observed (25, 26). In addition, it has been shown that a pre-existing or induced fibrotic microenvironment provides a protective niche for the survival of tumor cells, as well as potentially accounting for radio-resistance through enhanced integrin signaling between tumor cells and ECM (25, 27). Additionally, radiation therapy is known to induce a significant inflammatory response, which in some regards is hypothesized to be beneficial due to enhanced immunogenic cell death of tumor cells, release of tumor antigens, and recruitment of T cells (27). However, this radiation-induced inflammation also leads to the production of chemokines and recruitment of myeloid cells which are likely to have deleterious effects on anti-tumor immune responses as well as serve to promote regrowth of tumor cells via their known roles in angiogenesis (28).

Given that we and others have demonstrated in mouse models that losartan has significant anti-inflammatory properties (via inhibition of CCL2-CCR2 signaling) and anti-

fibrotic properties (via inhibition of TGF-β signaling), it is likely that this drug, or potentially other drugs in the ARB class might represent successful adjuvant therapies for tumor radiation, especially in cases of stereotactic radiation therapy for individuals with oligometastatic lung tumors. We feel that the clinical effects of the addition of losartan to radiotherapy could be easily assessed in dogs with oligometastatic osteosarcoma in a randomized, placebo controlled trial. While one potential hypothesis is that inhibition of myeloid cell recruitment could have a negative impact through dampening recruitment of cells required for presentation of newly liberated tumor antigens following radiation, we hypothesize that the negative impact of myeloid cell recruitment would far outweigh the potential role of these cells in stimulating an immune response. Thus, we feel that adjuvant losartan therapy for patients undergoing radiation could have significant potential clinical benefits in terms of enhancement of radiosensitization and/or suppression of tumor recurrence through suppression of pro-fibrotic signaling, as well as the mitigation and/or prevention of radiation-induce counter-regulatory immune responses. Inadvertently, losartan may also possess the potential to mitigate radiation induced side effects such as pulmonary fibrosis (26).

In addition, the anti-fibrotic effects of losartan have already been co-opted by others for the enhancement of therapeutic effects of other traditional anti-cancer therapies, such as doxorubicin (24). Multiple studies from the laboratory of Rakesh Jain demonstrate that inhibition of TGF-β induced collagen synthesis via daily losartan treatment can result in the decompression of tumor blood vessels, allowing enhanced chemotherapeutic drug delivery and improved survival above chemotherapy alone in mouse tumor models (24, 29). We feel that the dog model of osteosarcoma is well-

aligned for the further validation of this pre-clinical result. Following amputation, dogs with osteosarcoma are often treated with adjuvant single agent platinum drugs (carboplatin) (30). When these dogs either fail during platinum-based chemotherapy, or eventually develop metastasis post-completion of adjuvant chemotherapy, they are often times offered experimental drugs, or other traditional cytotoxic therapies; however, these have been woefully ineffective in this established metastatic setting (31-33). Thus, we feel there is promise and opportunity in assessing, in a randomized, placebo controlled trial, the effect of losartan therapy on improving doxorubicin efficacy in dogs with grossly evident metastatic osteosarcoma which have been previously treated with single agent platinum-based chemotherapy.

In summary, these studies describe the pharmacological and pre-clinical characterization of losartan as a repurposed CCR2 antagonist and potential anti-metastatic therapy in both pre-clinical mouse models and in companion dogs with spontaneous cancer. This work demonstrates a unique and previously undescribed mechanism of direct inhibition of CCL2-CCR2 signaling and monocyte recruitment by losartan and its primary EXP-3174 metabolite, and show that in pre-clinical models, daily losartan therapy is effective in suppressing experimental metastasis growth, in a manner which is associated with sustained blockade of inflammatory monocyte mobilization and accumulation of metastasis-associated myeloid cells. These results provide another, yet undescribed, anti-tumor mechanism of losartan, in addition to its previously documented effects on angiogenesis and TGF-β signaling

Furthermore, through retrospective histopathological and immunohistochemical analyses, as well as in vitro assays utilizing canine tumor cell lines, we provide

foundational descriptive data which provides a rational basis for the evaluation of monocyte-targeted therapies in distinct canine tumor types. In addition, we highlight the importance of pharmacokinetics and pharmacodynamics for dose optimization in translational chemokine antagonist drug development, and utilized pK/pD studies to optimize losartan dosing for inhibition of canine monocyte migration and evaluation as a novel immunotherapy, in combination with the tyrosine kinase inhibitor toceranib, in dogs with spontaneous metastatic disease. In this pilot Phase I/II clinical trial, the biological response rate, in conjunction with the observed modulation of systemic immune suppression, support further clinical evaluation of losartan and toceranib as a novel immunotherapeutic combination, with greater focus on secondary endpoints of their immunomodulatory mechanism(s) of action, in a larger, randomized, placebo controlled study. In conclusion, these data further substantiate the potential clinical application of losartan in cancer patients, and suggest that this low cost, safe, and already-approved drug, could be rapidly repurposed as an adjuvant therapy for both dogs and humans at high risk of metastasis.

REFERENCES

1. Garin A & Proudfoot AE (2011) Chemokines as targets for therapy. *Experimental cell research* 317(5):602-612.

2. Xia M & Sui Z (2009) Recent developments in CCR2 antagonists. *Expert opinion on therapeutic patents* 19(3):295-303.

3. Chow MT & Luster AD (2014) Chemokines in Cancer. *Cancer immunology research* 2(12):1125-1131.

4. Smith MC*, et al.* (2004) CXCR4 regulates growth of both primary and metastatic breast cancer. *Cancer Res* 64(23):8604-8612.

5. Muller A*, et al.* (2001) Involvement of chemokine receptors in breast cancer metastasis. *Nature* 410(6824):50-56.

6. Khalil DN, Smith EL, Brentjens RJ, & Wolchok JD (2016) The future of cancer treatment: immunomodulation, CARs and combination immunotherapy. *Nature reviews. Clinical oncology* 13(5):273-290.

7. Hodi FS*, et al.* (2010) Improved survival with ipilimumab in patients with metastatic melanoma. *N Engl J Med* 363(8):711-723.

8. Rizvi NA*, et al.* (2015) Activity and safety of nivolumab, an anti-PD-1 immune checkpoint inhibitor, for patients with advanced, refractory squamous non-small-cell lung cancer (CheckMate 063): a phase 2, single-arm trial. *The Lancet. Oncology* 16(3):257-265.

9. Adams JL, Smothers J, Srinivasan R, & Hoos A (2015) Big opportunities for small molecules in immuno-oncology. *Nature reviews. Drug discovery* 14(9):603-622.

10. Sandhu SK*, et al.* (2013) A first-in-human, first-in-class, phase I study of carlumab (CNTO 888), a human monoclonal antibody against CC-chemokine ligand 2 in patients with solid tumors. *Cancer chemotherapy and pharmacology* 71(4):1041-1050.

11. Mullard A (2014) New drugs cost US[dollar]2.6 billion to develop. *Nature reviews. Drug discovery* 13(12):877-877.

12. Bertolini F, Sukhatme VP, & Bouche G (2015) Drug repurposing in oncology--patient and health systems opportunities. *Nature reviews. Clinical oncology* 12(12):732-742.

13. Dai Q, Xu M, Yao M, & Sun B (2007) Angiotensin AT1 receptor antagonists exert anti-inflammatory effects in spontaneously hypertensive rats. *British journal of pharmacology* 152(7):1042-1048.

14. Yang J*, et al.* (2015) Comparison of angiotensin-(1-7), losartan and their combination on atherosclerotic plaque formation in apolipoprotein E knockout mice. *Atherosclerosis* 240(2):544-549.

15. Zheng Y*, et al.* (2016) Structure of CC chemokine receptor 2 with orthosteric and allosteric antagonists. *Nature* 540(7633):458-461.

16. Zweemer AJ*, et al.* (2014) Discovery and mapping of an intracellular antagonist binding site at the chemokine receptor CCR2. *Molecular pharmacology* 86(4):358-368.

17. Brodmerkel CM*, et al.* (2005) Discovery and pharmacological characterization of a novel rodent-active CCR2 antagonist, INCB3344. *J Immunol* 175(8):5370-5378.

18. Schall TJ & Proudfoot AEI (2011) Overcoming hurdles in developing successful drugs targeting chemokine receptors. *Nat Rev Immunol* 11(5):355-363.

19. Kalliomaki J*, et al.* (2013) A randomized, double-blind, placebo-controlled trial of a chemokine receptor 2 (CCR2) antagonist in posttraumatic neuralgia. *Pain* 154(5):761-767.

20. Burnier M & Maillard M (2001) The comparative pharmacology of angiotensin II receptor antagonists. *Blood pressure. Supplement* 1:6-11.

21. Habashi JP*, et al.* (2006) Losartan, an AT1 antagonist, prevents aortic aneurysm in a mouse model of Marfan syndrome. *Science* 312(5770):117-121.

22. Nyström A*, et al.* (2015) Losartan ameliorates dystrophic epidermolysis bullosa and uncovers new disease mechanisms. *EMBO Molecular Medicine* 7(9):1211-1228.

23. Arnold SA*, et al.* (2012) Losartan slows pancreatic tumor progression and extends survival of SPARC-null mice by abrogating aberrant TGFbeta activation. *PLoS One* 7(2):e31384.

24. Diop-Frimpong B, Chauhan VP, Krane S, Boucher Y, & Jain RK (2011) Losartan inhibits collagen I synthesis and improves the distribution and efficacy of nanotherapeutics in tumors. *Proceedings of the National Academy of Sciences of the United States of America* 108(7):2909-2914.

25. Barker HE, Paget JTE, Khan AA, & Harrington KJ (2015) The Tumour Microenvironment after Radiotherapy: Mechanisms of Resistance and Recurrence. *Nature reviews. Cancer* 15(7):409-425.

26. Flechsig P*, et al.* (2012) LY2109761 attenuates radiation-induced pulmonary murine fibrosis via reversal of TGF-beta and BMP-associated proinflammatory and proangiogenic signals. *Clin Cancer Res* 18(13):3616-3627.

27. Zhang C*, et al.* (2016) Fibrotic microenvironment promotes the metastatic seeding of tumor cells via activating the fibronectin 1/secreted phosphoprotein 1-integrin signaling. *Oncotarget* 7(29):45702-45714.

28. Connolly KA*, et al.* (2016) Increasing the efficacy of radiotherapy by modulating the CCR2/CCR5 chemokine axes. *Oncotarget* 7(52):86522-86535.

29. Chauhan VP*, et al.* (2013) Angiotensin inhibition enhances drug delivery and potentiates chemotherapy by decompressing tumour blood vessels. *Nature communications* 4:2516.

30. Selmic LE, Burton JH, Thamm DH, Withrow SJ, & Lana SE (2014) Comparison of carboplatin and doxorubicin-based chemotherapy protocols in 470 dogs after amputation for treatment of appendicular osteosarcoma. *J Vet Intern Med* 28(2):554-563.

31. Ogilvie GK*, et al.* (1993) Evaluation of single-agent chemotherapy for treatment of clinically evident osteosarcoma metastases in dogs: 45 cases (1987-1991). *Journal of the American Veterinary Medical Association* 202(2):304-306.

32. Poirier VJ*, et al.* (2004) Efficacy and toxicity of paclitaxel (Taxol) for the treatment of canine malignant tumors. *J Vet Intern Med* 18(2):219-222.

33. Batschinski K, Dervisis NG, & Kitchell BE (2014) Evaluation of ifosfamide salvage therapy for metastatic canine osteosarcoma. *Vet Comp Oncol* 12(4):249-257.